FUNCTIONAL LAMINAR ARCHITECTURE OF RAT PRIMARY AUDITORY CORTEX FOLLOWING ACOUSTIC TRAUMA

Tansi Jamshed Khodai

University of Strathclyde

Strathclyde Institute of Pharmacy and Biomedical Sciences

Submitted in partial fulfilment of the requirements for the degree of

Doctor of Philosophy

2014

Candidate's Declaration

I, Tansi Jamshed Khodai, certify that this thesis is the result of my original research and has been written by me. This research which is approximately 50,000 words long is the record of the work carried out by me and has not been previously submitted for examination which has led to the award of a degree.

Tansi Jamshed Khodai

23th September 2014

To my father and late mother for believing in me.....

Acknowledgement

With no prior background in auditory research, in vivo electrophysiology or even the most basic levels of programming skills, my doctoral studies has been a fascinating challenge. A task, I don't think I could have achieved without the love, support and care of family, friends and colleagues.

I would like to thank my supervisor Dr Shuzo Sakata, for giving me this opportunity and providing supervision and training throughout my studies, helping me evolve into a better scientist. I would also like to thank Prof Judith Pratt my second supervisor and Dr Benjamin Pickard for their advice and much needed motivation and vote of confidence. Special thanks to Dr Josue Yague for his immense contribution to helping me understand and interpret my data.

Furthermore, I would like to thank my friends and colleagues, Dr Morag Farquhar, Dr Nadine Gut, Martin Wernoski, Dr Ivo Kretzers and all my fourth floor SIPBS colleagues for their help and support throughout my studies. I would also like to thank Dr Helen Bright, Dr Mike Westby and Dr Peter Loudon for their advice during my studies.

Finally, a big thank you to my family especially daddy for his love, support and understanding. I am grateful to my partner Rav Sharma for being my strength and support, coping with my frustrations and for simply being there, you got me through!

Table of Contents

Abstract

Exposure to loud sound can cause a series of hearing problems, the most common being tinnitus or hearing loss (temporary or permanent). Furthermore, tinnitus caused due to acoustic trauma may be observed with or without hearing loss, making it harder for tinnitus researchers to understand the pathology of this condition. Despite extensive studies in both animal and human subjects, it is still not fully understood how acoustic trauma can change neuronal activity in the auditory cortex. Several animal studies suggest changes in auditory tuning properties and increase in spontaneous activity after exposure to acoustic trauma. However, there are several discrepancies in observed changes. One possible explanation for this could be that these findings represent an average response across cortical depths which could mask the layer specific alteration in neural activity following acoustic trauma because previous studies have shown laminar specific evoked and spontaneous activity. In this study we tested the hypothesis that acoustic trauma alters neural activity in a layer-specific manner**.** Rats were anesthetised with urethane anaesthesia and recordings were obtained using multichannel linear silicon probes inserted vertically into the primary auditory cortex. The animals were exposed (bilaterally) to one octave white noise centred at 16 kHz, at 110 dB SPL for 1 hour. Spontaneous and auditory-evoked activity was measured before trauma and then one and two hour time-points after the acoustic trauma.

We quantified laminar specific and average changes in different tuning curve parameters such as threshold, characteristic frequency, bandwidth, sparseness, spontaneous firing rate and burst like activity after trauma exposure in three different frequency regions of primary auditory cortex. We observed laminar-specific changes in auditory tuning properties such as increase in threshold and spontaneous activity mainly in layer V of the primary auditory cortex following acoustic trauma. Furthermore, we also observed increase in burst-like spiking in the superficial layers. These findings support the hypothesis that acute effects of

acoustic trauma on auditory cortical population activity is laminar-specific. These findings provide essential information regarding the changes in circuit mechanisms that develop following acoustic trauma which are critical for enhancing our knowledge about the pathology of these conditions and also to identify new potential targets to treat them.

List of Tables

List of Figures

Abbreviations

AI	Primary auditory cortex
AII	Secondary auditory cortex
ABR	Auditory brain-stem response
AC	Auditory cortex
AAF	Anterior auditory field
AN	Auditory nerve
AVCN	Anteroventral cochlear nucleus
BW	Bandwidth at 10 dB above threshold
CF	Characteristic frequency
CN	Cochlear nucleus
CSD	Current source density
EToS	Efficient technology of spike sorting
fMRI	Functional magnetic resonance imaging
IC	Inferior colliculus
IHC	Inner hair cells
ISI	Inter-spike interval
LL	Lateral lemniscus
LFP	Local field potential
MGB	Medial geniculate body
msec	Milliseconds

MU	Multi-unit
MUA	Multi-unit activity
NIHL	Noise induced hearing loss
OHC	Outer hair cells
oct	Octave
PAF	Posterior auditory field
PBS	Phosphate buffered saline
PO	Posterior nucleus of thalamus
RE	Auditory section of Reticular nucleus
SA	Spontaneous activity(spikes/second)
SD	Sprague Dawley
SOC	Superior olivary complex
SPL	Sound pressure level
T	Temporal auditory field
TC	Tuning Curve
TDT	Tucker-Davis Technologies
vMGB	Ventral Medial geniculate body
VPAF	Ventro-posterior auditory field

Nomenclature

Acoustic stimuli	Short pips, long tones
Background	SA measure 50 msec before stimulus onset
Long tones	500 msecs long, rate of 1.2 Hz
Pre	Acoustic stimuli before trauma induction
Post 1	Acoustic stimuli after trauma induction
Post 2	Acoustic stimuli after Post 1
SA before	SA measured before 5 min before stimuli presentation
SA after	SA measured 5 mins after stimuli presentation
Short pips	50 msecs long, rate of 2.5 Hz
Threshold	Minimum intensity of evoked response
Trauma induction	One oct band centred at 16 kHz, 110 dB SPL

Chapter 1

Introduction

1.1 Summary

This chapter provides a general introduction for the research context of the subsequent chapters. Section 1.2 provides a summary of the general structure of the thesis followed by section 1.3 which gives a general background for the present research context. The chapter is summarised in Section 1.4.

1.2 Structure of thesis

The thesis is organised into five chapters. Chapter 1 Introduction: is the current chapter, Chapter 2 Literature review and analysis: Details critical analysis of the research with regards to the scope of the present research and philosophy behind the hypothesis, Chapter 3 Materials and Methods: details the materials and procedures used for the present investigation, Chapter 4 Baseline: which is the first results chapter discusses the observed results during normal auditory processing, Chapter 5 Acoustic trauma: is the second results chapter which discusses the observed results with regards to shift in auditory processing following acoustic trauma. Finally Chapter 6, Discussions and Conclusion: is the final chapter of the thesis and discusses novel findings and limitations of the present research concluding with the results in relation to past literature and future work in context of the presented research.

1.3 Research overview

The auditory system is considered to be the most sensitive and versatile sensory system which enables the sense of hearing, allowing us to experience and adapt to our surroundings through sound. However, this system is also extremely vulnerable to damage by a wide range of factors such as, loud noise (Sliwinska-Kowalska and Davis, 2012), medicines (Schacht, 1986), diseases (Dierks et al., 1999), genetic factors(Anderson and Wedenberg, 1968) and age (Huang, 2007).

Until fairly recently it was believed that the pathology of auditory disorders induced by the above mentioned factors were confined to the peripheral auditory

system. Now it is understood that this is not always true. This shift in approach towards auditory disorders came with the realisation that damage only to the peripheral system (ear to cochlea) could not account for all types of auditory related disorders such as the ones in which no obvious peripheral damage is observed e.g. auditory hallucinations or phantom auditory perceptions. According to the World Health Organisation (WHO) about 360 million people world-wide suffer from disabling hearing loss alone (WHO, 2012). Furthermore, adult onset hearing impairment is considered as the third leading cause of disability (Mathers et al., 2008). Phantom auditory perception or tinnitus is also an increasing cause of concern with an estimate 278 million people suffering from this condition worldwide (WHO)(Geocze et al., 2013). Treatments such as cochlear implants have contributed immensely to hearing loss related disorders, however they still have their limitations (Moore and Shannon, 2009). Furthermore cochlear implants have limited applications in other auditory disorders like tinnitus highlighting a compelling need for newer treatments for such disorders.

One possible reason for the limited treatments available to date is our limited knowledge about auditory processing, especially central auditory processing. Such missing pieces of information make it harder to understand pathologies that develop during auditory disorders. Furthermore, the different internal and environmental factors that are implicated in the development and progression of auditory disorders can affect one or more components of the auditory pathway which may be involved at any level of auditory processing making it harder to decipher the pathologies of the resulting disorders.

Recent advances in electrophysiological and imagining techniques now allow investigations in the central auditory systems which were difficult to achieve in the past. For example, functional magnetic resonance imaging (fMRI) studies showed cortical activation in tinnitus sufferers compared to non-sufferers (Muhlnickel et al., 1998). Also in another class of auditory pathologies which involved abnormal perception of sound such as individuals suffering with schizophrenia and experiencing auditory hallucinations, fMRI investigations showed decreases responsiveness of temporal cortex to external stimuli only during episodes of

hallucinations (David et al., 1996). Such investigations in humans can now allow better interpretation of animal model investigations, greatly enhancing possibilities of developing newer effective treatments.

By understanding the neural basis of normal and abnormal auditory processing novel targets for treatment of auditory related disorders could be achieved. These identified targets could then be modified using newly available treatment strategies, a few of which are discussed in the subsequent paragraphs.

Stem cell research has opened doors to fascinating possibilities for treating a wide range of diseases such as neurodegenerative diseases (Lindvall and Kokaia, 2010) and metabolic diseases (Peters and Steward, 2003). The promising opportunities offered by this approach in the above mentioned disease areas has spurred interest in using this novel approach in treating sensory disorders. Recent attempts have been made to regenerate damaged hair cells in the cochlea using embryonic stem cells (Koehler et al., 2013; Li et al., 2003a), stem cells isolated from the inner ear (Li et al., 2003b) or other organs such as the brain (Rietze et al., 2001), and skin (Toma et al., 2001). Stem cell replacement has also shown some promise in possibilities of repair and regeneration of damaged auditory nerve (Hu et al., 2004). This approach can also be used for identified gene targets in the central auditory system, which has the added advantage of overcoming issues with target gene delivery. In spite of all the advances this treatment strategy is still in its infancy (Brigande and Heller, 2009) and much more knowledge and understanding about the auditory system would aid in the development of better effective treatments. Another approach for treating auditory disorders emerges from the field of optogenetics which combines the fields of optics and genetics to control activities of individual cells or tissues. Even though this field is relatively new, it has already shown exciting possibilities of gene targeted therapies in the visual system by demonstrated exciting possibilities of gene targeted therapy for restoring blindness (Cronin and Bennett, 2011; LaLumiere, 2011). Such prospects show possibilities for similar advancements that could be achieved in treating auditory disorders using optogenetics (Hernandez et al., 2014). Furthermore,

there is the exciting possibility of combining the advantages of stem cell research and optogenetics which has shown promising advances in treating a range of diseases (Byers et al., 2012; Piña-Crespo et al., 2012; Weick et al., 2011). Such evidence offers hope that combining these two techniques would also facilitate the identification of relevant circuits and novel treatments of auditory pathologies (Moser, 2015).

All of the above mentioned approaches show possibilities for the development of better treatments of auditory processing disorders. However, the success of such approaches in providing effective treatments not only depends on the technical aspects of these approaches but also on a better understanding of the auditory system and the changes that occur during abnormal pathologies which is the main focus of the current research.

The inspiration for the current research could be considered to be derived from three areas within auditory research:

1) Normal auditory processing: The present investigation could contribute towards the current knowledge in this area. The focus is on central mechanism of auditory processing with emphasis on the laminar processing within the auditory cortex (AC).

   The neocortex consist of six well defined layers, each containing different cell types and forming unique neuronal connections (Mountcastle, 1957). However, it is seen that neurons in the different layers share similar response properties to neurons in layers above and below them, showing some kind of vertical organisations, termed as cortical columns (Mountcastle, 1957, 1997). It is believed that the neocortex is made up of several such columns, each representing a computational model (Mountcastle, 1997). Hence, understanding the principles that determine these organisational models would provide vital information regarding the functioning of the neocortex. Such organising features have been extensively studied in the visual and somatosensory system. However, our knowledge in the auditory system is still limited (Linden and Schreiner,

2003) and the present investigation aims to contribute towards such understanding.

2) Abnormal auditory processing: As discussed previously in this chapter, several factors can affect normal auditory processing resulting in several auditory pathologies. The current investigation focuses on pathologies resulting from exposure to loud noise (acoustic trauma), a factor that has been implicated in auditory pathologies such as hearing loss and tinnitus. Several studies have studied changes in different areas of the auditory pathway including the AC (Abbott et al., 1999; Brozoski et al., 2012b; Bruce et al., 2003; Clark and Pickles, 1996; Mulders and Robertson, 2009; Noreña and Eggermont, 2003b, 2005). However, little is known about how exposure to loud noise affects the lamination of the AC in particular, which is the main focus of the present research.

3) Newer treatments: Finally, the current research aims to help identify newer, novel targets involved in noise induced pathologies. Such identified targets could be evaluated for potential treatments using some of the above mentioned approaches, allowing for the development of better treatments for auditory disorders.

1.4 Conclusion

In this chapter a general background and the motivation behind the present thesis is provided.

In the following chapter an in-depth analysis of the literature in context to the present research and the origin of the hypothesis will be discussed in detail.

Chapter 2

Literature review

2.1 Summary

In first part of this chapter literature analysis about various aspects of anatomy and physiology of the auditory system is summarised in Section 2.2. Furthermore, details regarding various aspects of acoustic trauma are discussed in Section 2.3. Section 2.4 details the history and development of Electrophysiology. Finally, the chapter concludes with the proposed hypothesis in Section 2.5.

2.2 Auditory system

The auditory system is an extremely versatile and sensitive sensory modality which serves a range of purpose such as sound localisation and communication Auditory perception involves a series of steps which begins with the encoding of the acoustic information in the ear and ends with the interpretation of the encoded signals (Neff, 1995). This process is complex and involves a series of interconnected structures(Ryugo, 1992), sub-cortical nuclei (Oliver, 1987; Winer, 1992; Young et al., 1992) and cortical areas (Kaas and Hackett, 2000), each playing a crucial role in auditory processing. The following sub-sections discuss the anatomy and physiology of the auditory pathway in more detail.

2.2.1 Auditory Pathway:

Anatomically, the auditory pathway can be divided into two components 1) Peripheral Auditory System which includes the ear and auditory nerve (AN) connecting the peripheral auditory system to the central auditory system, and 2) Central Auditory system which includes the auditory centres in the brain and connecting pathways in the brainstem. This is a very simplistic (classic) classification and does not take into account the several ascending (Winer, 2005b) and descending (Winer, 2005a) pathways that run in parallel (Lee and Sherman, 2010). Nevertheless, it gives a clear understanding of the basis of auditory processing.

2.2.1.1 Peripheral Auditory System; Ear

The peripheral auditory system is involved in the stepwise, linear transmission of the auditory information to the auditory nerve where mechanical energy is converted to electrical energy which then progresses towards the ascending connections of the auditory pathway (Ades and Engström, 1974).

Functionally the ear is divided into three parts: a) outer ear ,b) middle ear, & c) inner ear (Figure 2.1).

The *outer ear* consists of the Pinna (visible part) and Ear canal. The pinna has a vital role in median plane localisation (Brumberg et al., 1999; Gardner, M.B. and Gardner, 1973; Kazuhiro Iida, 1998). Furthermore, the outer ear collects the sound waves and directs it towards the middle ear and also helps protect the deeper structures in the ear.

The anatomical and functional aspects of the *middle ear* have been well studied (Henson.O.W, 1974). The middle ear (tympanic cavity) is an air-filled cavity. The lateral wall of the middle ear consists of the tympanic membrane (ear drum) whereas the medial wall is formed by a bony wall that separates the middle ear from the inner ear. This wall contains two membranous windows called the oval window and round window. Within this cavity are three tiny bones (malleus, incus and stapes (Figure 2.1A) collectively called ossicles which form an 'ossicular chain' that connects the tympanic membrane with the oval window. Two striated muscles tensor tympani and the stapedial muscle are also found in the middle ear. The tensor tympani muscle (innervated by the trigeminal nerve) is attached to the malleus and the stapedial muscle (innervated by the stapedial branch of the facial nerve) to the stapes. These muscles are believed to serve a wide range of functions such as providing rigidity to the ossicular chain by muscle contraction on exposure to sounds exceeding 80 dB SPL, thus protecting the cochlea from acoustic damage (Torben Brask, 1978). These muscles are also believed to contribute to the blood supply of the chain , and play a vital role in high frequency

sound by attenuating low frequency high intensity sounds (E. Borg and J. E. Zakrisson, 1974).

To summarise, the main purpose of the middle ear is to amplify and transfer the tympanic membrane vibrations to the inner ear by converting energy that is air borne to fluid borne (Møller.A.R, 1974)

The *inner ear* is the most complex part of the ear. Understanding of the anatomy and physiology of the inner ear came fairly late in auditory research history mainly due to the difficulty in accessing the inner ear tissue. It was predominantly the work of Retzius (Retzius, 1881)in the second half of the eighteenth century that gave us a good understanding of the anatomy of the inner ear (Hawkins, 2005).The inner ear is anatomically divided into three parts: a) Semicircular canals, b) Vestibules & c) Cochlea.

Functionally the inner ear is divided into the Cochlea and Vestibular system:

Cochlea: The cochlea is a fluid filled snail like structure that is divided along its entire length by a partition (membranous labyrinth) and contains the receptor organ for hearing i.e. the organ of Corti. The two channels formed by the partition is filled with a fluid called perilymph (high concentration of sodium ions, low potassium ions). The membranous labyrinth on the other hand is filled with a fluid called endolymph (high concentration of potassium ions and low sodium ions), the chemical composition of which is very different from that of the perilymph. The endolymph provides the correct ionic concentration required for the proper function of the hair cells. The perilymph on the other hand conveys the pressure waves (discussed later in this section). The organ of Corti (named after Alfonso Corti for his immense contribution in this area (Hawkins, 2004)) sits on a basilar membrane and is made up of sensory (hair) cells and supporting cells. Another membrane called the tectorial membrane floats on top of these hair cells and is held in place by a hinge like mechanism on the side of organ of Corti. There are two types of hair cells lining the organ of Corti: three rows of outer hair cells (OHC) and one row of inner hair cells (IHC). Each hair cell has a number of small hair-like projections called stereocilia and the group of stereocilia on top of each hair cell

are called a stereocilia bundle. The stereocilia bundles are arranged in in a 'W' and 'V' shape for the outer hair cells and shallow U shape for the IHC (Roth and Bruns, 1992).

The organ of Corti plays the important role of converting mechanical energy into electrical energy that travel through the AN to the central auditory system. Sound waves cause the Basilar membrane to be displaced and set off a travelling wave that moves from the apex to the base of the cochlea (Georg von Békésy in the XIX century)(von Békésy, 1960). This travel wave causes the tectorial membrane to move laterally over the steriocilia located on top of the hair cells (Russell, 1987). These hair cells are innervated by several efferent and afferent nerve endings act as receptor cells (Dallos, 1976) that convert mechanical energy into electrical energy. Mechanical fluctuations caused by the lateral movement of the tectorial membrane cause potassium channels to open, resulting in an influx of potassium ions, depolarising the hair cells (Zdebik et al., 2009). This in turn activates voltage gated calcium ion channels which promote neurotransmitter release from the basal end of the hair cells which then stimulate the auditory nerve endings, marking the end of peripheral auditory processing.

2.2.1.2 Anatomy and Physiology of Auditory Nerve and Sub-cortical structures

2.2.1.2.1 Anatomy of Auditory Nerve

The auditory nerve (AN) is responsible for transferring the acoustic information from organ of Corti to the central nervous system. It is made up of two distinct types of primary AN that innervate the IHC and OHC of the inner ear; Type I and Type II (Liberman and Kiang, 1984). The dendrite of the type I (large, bipolar, myelinated, 90-95% population) primary AN innervates the IHC of the Organ of Corti and type II (small, pseudo-unipolar, unmyelinated, 5-10% of population) innervates the OHC (Rouiller.E.M, 1997). Each type I neuron innervates only one IHC (Spoendlin, 1969) whereas each IHC is innervated by 10-20 type I primary AN (Liberman, 1980). On the contrary, one type II primary AN innervates several OHC

(Kiang et al., 1982; Liberman, 1988; Spoendlin, 1972) and each OHC also receives input from different type II primary AN (Figure 2.1). The axons of the primary AN project to the cochlear nucleus in the brainstem. Here they form synapses with the second-order AN (Strominger et al., 1977). These afferent fibres then form two branches innervating different parts of the cochlear nucleus (Liberman, 1991, 1993; Ryugo et al., 1991).

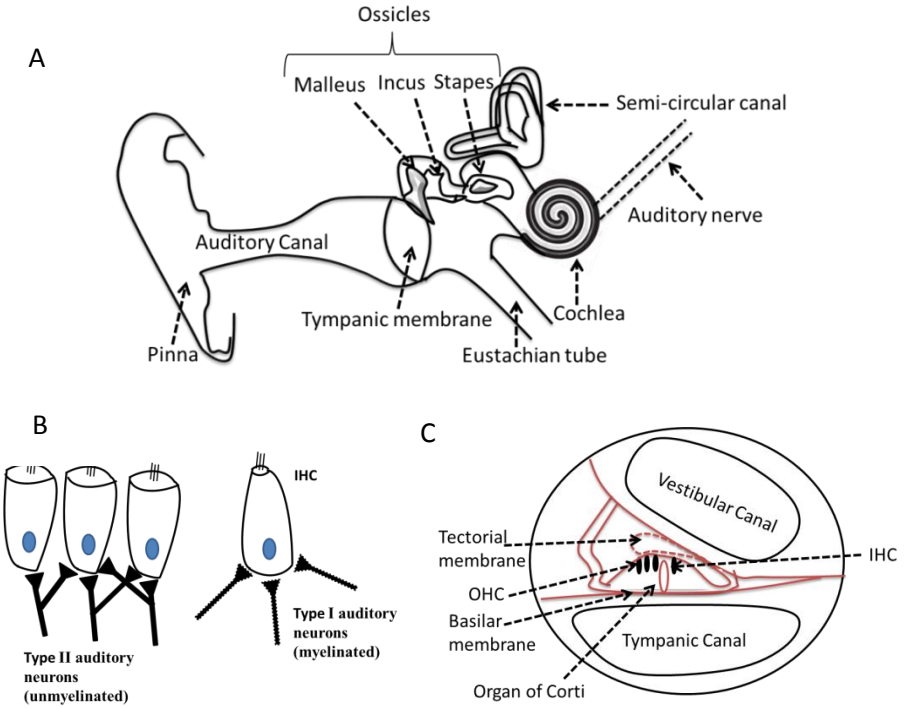

Figure2.1 Peripheral Auditory System; A. Schematic representation of various parts of the peripheral auditory system, B. Illustration of innervation patterns of IHC and OHC. Each type I primary AN innervates only one IHC whereas the ramified dendrites of a single type II AN innervates more than one OHC, C. Cross-Section of the cochlea.

2.2.1.2.2 Anatomy of Sub-cortical structures

The ascending pathway of the central auditory (Figure 2.2) nervous system consists of several nuclei (group of cell bodies) and fibre tracts that carry information in between them. These nuclei act as a relay centre for sending neural information from one nuclei to another.

Cochlear Nucleus (CN) - After the initial processing of sound information in the cochlea it reaches the CN in the brainstem (Cant, 1992; Lee, 2014). The CN contain

several types of neuronal cell types (globular bushy, pyramidal, spherical bushy, giant granule, octopus cells) that allow the CN to be divided into different subdivisions (Brawer et al., 1974; Cant, 1992; Evans et al., 1980; Mugnaini E et al., 1980; Rouiller.E.M, 1997). The CN is divided into the Dorsal CN and the Ventral CN, which is further divided into two subdivisions the anteroventral CN (AVCN) and the posteroventral CN (PVCN) (Feldman and Harrison, 1969; Osen, 1969). AVCN receives most of the anterior ascending AN innervations and the posteroventral CN receives inputs from the posterior AN (Moller, 1982).

From the CN most of the ascending fibres cross over (contralateral) to another region in the brainstem called the superior olivary complex (SOC) (Lee and Sherman, 2010; Oliver, 1987; Schwartz, 1992). Some fibres continue ipsilaterally. Here the ascending fibres travel through the lateral lemniscus (LL) (Schwartz, 1992) and converge into the IC (IC)(Wenstrup JJ, 2005) in the midbrain.

SOC- This region receives ascending afferents from both the CNs, thus forming the first point of integration of information from both ears (Rouiller.E.M, 1997; Schwartz, 1992) and plays a vital role in directional hearing (Moller, 2006). Anatomically the SOC represents three distinct nuclei: the lateral superior olivary nucleus, the medial superior olivary complex, and the trapezoid body each receiving innervations from distinct regions of the Ventral CN (Rouiller.E.M, 1997; Schwartz, 1992).

Similar to the nerve fibres travelling to the SOC from the CN, the fibres arising from the SOC either cross over or connect with IC on the same side(Osborne et al., 1988).

IC-Similar to the CN, the IC is an obligatory relay nucleus in the auditory pathway (Aitkin and Phillips, 1984a) which receives innervation from CN (Oliver, 1987; Oliver et al., 1999), SOC (Saldaña et al., 2009) and LL(Winer, 2005b).

The IC can be anatomically divided into several nuclei (Faye-Lund and Osen, 1985; Morest and Oliver, 1984). In rats, based on cytoarchitecture and electrophysiological findings, these can be broadly classified into three sub-

divisions which are defined based on the spatial organization of the dendrites and axons (Faye-Lund and Osen, 1985). Similar IC divisions are observed across species including man (Geniec and Morest, 1971), monkey (KA., 1975), cat (Morest, 1965; Morest and Oliver, 1984). These are the central nucleus which receives most of the ascending inputs (Winer, 2005b), the external cortex (also known as the external nucleus) and the dorsal cortex (also known as peri-central nucleus. The main nucleus of the IC is the central nucleus. In rats this nucleus is relatively smaller as compared to that observed in carnivores. This subdivision shows laminar organization (Faye-Lund and Osen, 1985; Malmierca et al., 2005) representing spatial representation of neurons tuned to different frequencies (Malmierca et al., 2008; Ress and Chandrasekaran, 2013) and is part of the fast frequency tuned and threshold sensitive ascending auditory pathway. The external cortex and the dorsal cortex on the other hand are mainly involved in the feedback loops and the polysensory component of the auditory pathway (Syka et al., 2000). The auditory information is then carried to the auditory thalamus(Aitkin and Phillips, 1984b).

Auditory thalamus- The auditory thalamus is the relay centre of the auditory pathway. This region can be divided into: the medial geniculate body (MGB) (principal division of the thalamus), the posterior nucleus of the thalamus (PO) and the auditory section of the reticular nucleus (RE)(Morest, 1965; Raman and Cajal, 1955). The primary afferents from the IC mainly project to the MGB (Aitkin and Phillips, 1984b; Lee and Sherman, 2010; Winer, 1992) in the thalamus. A lamination corresponding to the spatial arrangement of frequencies observed in the principal nuclei of IC is also observed in the MGB (Allon et al., 1981; Bartlett and Smith, 1999; Cetas et al., 2001; Imig and Morel, 1985). The MGB can be further divided into the ventral (vMGB), medial and dorsal segments which are involved in different aspects of auditory processing (Calford, 1983; Clerici and Coleman, 1990). Projections from the IC also stimulate the PO and the RE (Calford and Aitkin, 1983).

Finally, these projections arising from the different parts of the thalamus together carry information to and receive information from different areas of the auditory

cortex(AC)(Diamond et al., 1969; Lee, 2014; Lee and Sherman, 2011; Winer et al., 2005)(mainly ipsilateral) located in the transverse temporal gyrus of Heschl (Morosan et al., 2001).

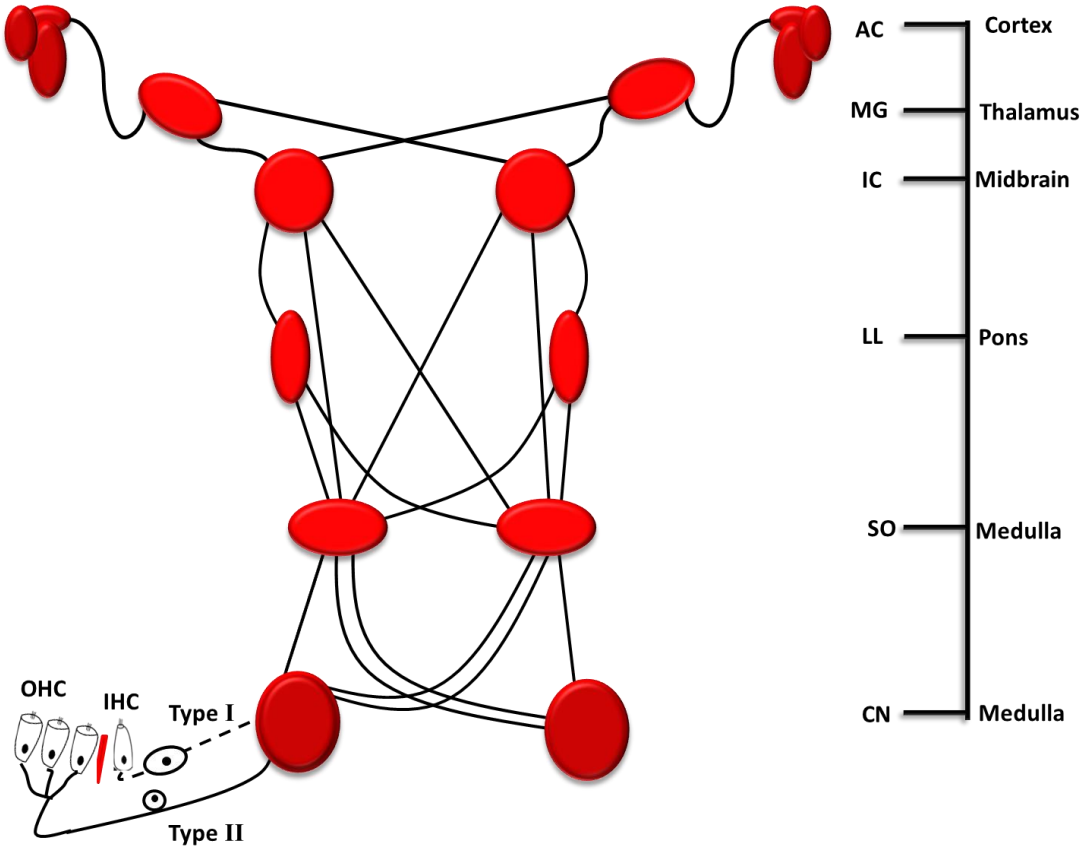

Figure 2.2 Schematic representation of the ascending auditory pathway. The main nuclei and bilateral connections are shown (except for cochlea).

2.2.1.2.3 Physiology of Auditory nerve and Sub-cortical structures

The auditory system has the complex task of extracting spectral, temporal and spatial aspects of the presented sound stimuli. To understand how such an arduous task is efficiently managed by the system a combination of electrophysiological and morphological techniques have been used to correlate anatomical and functional properties of the auditory system. With the help of electrophysiology, multi-unit and single-unit functional properties of the AN (Kiang, 1965), sub cortical structures such as the CN (Bourk, 1976; Evans, 1972), SOC (Tsuchitani, 1967; Tsuchitani and Boudreau, 1966), LL (Aitkin et al., 1970), IC

(HIND et al., 1963), MGB (Winer et al., 2005) and cortical structures(Kaas and Hackett, 2000; Lee and Sherman, 2010, 2011; Winer, 2005a; Winer and Lee, 2007) have been extensively researched, details of which will be provided in the following sub-sections.

2.2.1.2.3.1 Tonal selectivity

Several studies have explored the discharge property of neurons to simple acoustic stimuli at various anatomical levels of the auditory pathway CN (Bourk, 1976), SOC (Irvine, 1986), IC (Merzenich and Reid, 1974). In response to an acoustic stimuli, neuronal discharge rate is higher than that during spontaneous activity (Kiang, 1965). Furthermore, it is noticed that individual neuronal cells respond only to a small fraction of the total frequency range. This property is inherited from the cochlea where mechanical energy is split into narrow frequency bands by the basilar membrane and preserved by the IHC (Kanold et al., 2014).The representation of selectivity is via tuning curves (TC) (frequency response area) (Figure 2.3) which represents the tone evoked response at different intensities for a range of frequencies (Rouiller.E.M, 1997). The minimum intensity at which a response is recorded is termed as the 'threshold' and the frequency to which the neuron is most sensitive is called the characteristic frequency (CF). The shape of the TC varies in the different location and even within a single nuclei of the auditory pathway e.g. CN (Bourk, 1976; Godfrey et al., 1975).

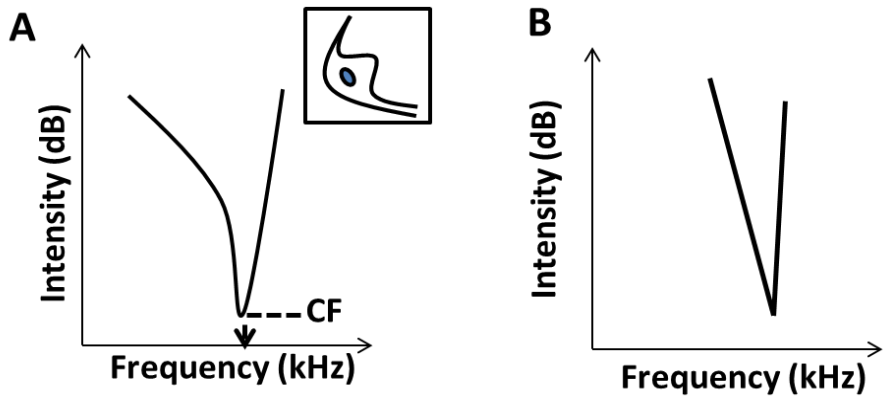

Figure 2.3 Schematic sketch of example single-unit TC seen in auditory pathway nuclei. **A.** Typical TC of an octopus cell type (inset) in CN. **B.** Typical TC seen in IC.

2.2.1.2.3.2 Tonotopic organisation

This characteristic of the auditory pathway is the fundamental organising principle of auditory processing and is preserved at all anatomical levels of the auditory pathway starting at the cochlea and ending at the core cortical auditory areas(Kanold et al., 2014). In this organization referred to as tonotopic organisation, neurons tuned to similar CF are grouped together and arranged in increasing order of frequency along one axis (Figure 2.4) i.e. a preferential spatial arrangement based on their CF (Rouiller.E.M, 1997).

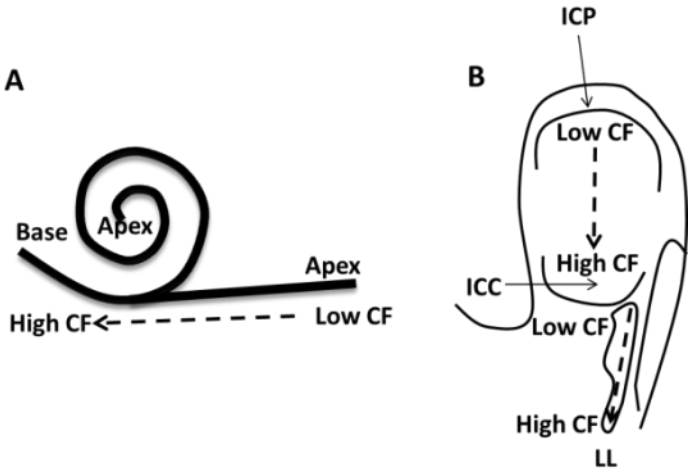

Figure 2.4 Schematic representation of **A.** Cochlea and **B.** IC in cat and their respective tonotopic organisation. ICC- Central nucleus, ICP-the peri-central nucleus (adapted from Rouiller.E.M, 1997).

2.2.1.2.3.3 Response type

The peri-stimulus time histograms (PSTH) depict the discharge patterns of single units across the auditory pathway in response to pure tone bursts or white noise; before, during and after sound exposure. The large variety of cell types in the different auditory nuclei are correlated with a wide range of responses characteristic of the cell type and auditory structures such as CN (Bourk, 1976; Kiang et al., 1965), AN (Kiang, 1965), IC (HIND et al., 1963), MGB (Rouiller.E.M,

1997). These response properties are further modified depending on the intensity and frequency of the presented stimulus (Rouiller.E.M, 1997).

2.2.1.2.3.4 Spontaneous activity (SA)

The AN show irregular SA in the absence of an external stimuli (Kiang, 1965; Rouiller.E.M, 1997) which is then carried through the auditory pathway. The SA activity of the AN (Figure 2.5) before hearing onset involves an ATP-induced neurotransmitter release by IHC (Tritsch et al., 2007, 2010). Before onset of hearing, SA activity is believed to play a vital role in the refinement, development of tonotopic organisation (Leao et al., 2006) and the overall maturation of the auditory circuit (Friauf and Lohmann, 1999). However, the origin of SA activity after the age of onset hearing is not clearly understood (Tritsch et al., 2007). For example, in anesthetised cats, ablation of the cochlea abolishes single-unit SA activity in the ventral cochlear nucleus whereas no changes in single-unit SA were observed in the dorsal cochlear nucleus, suggesting complex control of SA in the auditory pathway (Koerber et al., 1966). Furthermore, there is emerging evidence of the importance of SA activity in adult auditory plasticity (Gold and Bajo, 2014; Syka, 2002).

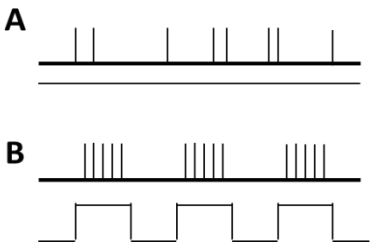

Figure 2.5 Schematic representation of **A.** SA and **B.** toneburst response of type I AN. The time intervals in the SA are irregular

2.2.1.2.3.5 Temporal properties

The auditory system extracts relevant information such as intensity of the presented stimuli or relative levels of frequencies in a complex sound stimulus (Heinz et al., 2001) by measuring the temporal pattern of neuronal firing. By gauging the synchronization of discharges with the phase of presented stimuli, termed as phase-locking (Brian C. J. Moore, 2003) the auditory system estimates the period of the presented waveform hidden in the temporal discharge pattern.

Furthermore, for complex stimuli (e.g. speech), phase-locking which is well preserved for frequencies below 4-5 kHz (Brian C. J. Moore, 2003) (the range slightly varies from one nuclei to another (Lavine, 1971; Rouiller.E.M, 1997)) can help estimate the relative levels of different components of the sound (Blackburn and Sachs, 1990).

Heinz further suggested that the neural firing patterns across an array of neurons can give an estimation of phase changes which in turn are altered due to changes in sound level of the presented stimuli, providing a possible code of sound intensity (Heinz et al., 2001).

2.2.1.3 Anatomy and physiology of Auditory cortex

2.2.1.3.1 Anatomy of Auditory Cortex

Our initial knowledge of the location and anatomy of the AC is from the elaborate work done by Monakow and Cajal in the early nineteenth century (Jones, 2011). Since then significant advances have been made in our understanding about the role of the AC in sound perception (Moore et al., 2007). Most of the initial findings were primarily in cats through electrophysiological recordings (Doron et al., 2002; Genis et al., 1974; Mendelson and Cynader, 1985; Merzenich et al., 1975; Rouiller.E.M, 1997; Winer, 2005a). However, with the development of new techniques such as positron emission tomography (PET), magnetic resonance imaging (MRI) in recent times, the investigation of the non-human primate and human AC has now become possible (Humphries et al., 2010; Petkov et al., 2006; Tanji et al., 2010; Wessinger et al., 1997; Zatorre, 2001).

The AC can be divided functionally (Figure 2.6, discussed in details in Section 2.4.2.) into a primary core area (AI and AAF) surrounded by a belt of secondary areas, which in turn is surrounded by a lateral parabelt AC (PAF and vPAF)(Kaas and Hackett, 2000; Lee et al., 2004). The number of identified primary core areas vary from one species to another; three in monkey (Kaas and Hackett, 2000), five in cat (Reale and Imig, 1980), two in ferrets (Kelly et al., 1986) two in mouse (Stiebler et al., 1997), three in rats (Horikawa et al., 1988; Sally and Kelly, 1988).

However, newer evidence suggests more than three functional core areas (possibly five) are seen in rats (Kalatsky et al., 2005; Polley et al., 2007). The one-dimensional gradient of CF is preserved across different species. However, the sub-region within the CF varies for e.g. in cats the 2-16 kHz regions is nearly three times greater than that seen in rats (Sally and Kelly, 1988). The laminar cytoarchitecture of AC shows the classical six layered organization similar to that seen in other cortical areas (Rose, 1949). Furthermore, each layer has a unique neuronal architecture (Table 2.1) and functional connections (Winer, 2011).These layers can be further grouped into supragranular, granular and infragranular layers (Barth and Di, 1990; Kaur et al., 2005; Stolzberg et al., 2012) .

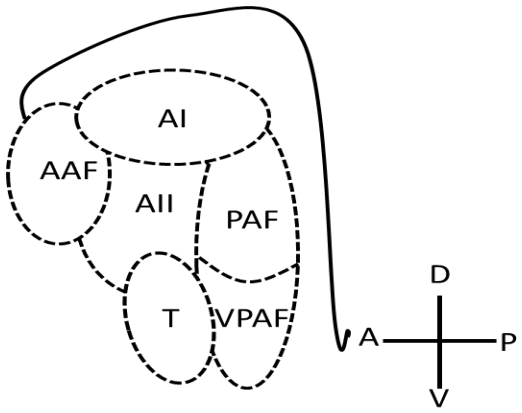

Figure 2.6 Schematic representation of the spatially distributed auditory cortical areas in the cat. AI-Primary auditory cortex, AAF- Anterior auditory field, AII-Secondary auditory cortex, PAF- Posterior auditory field, VPAF- Ventro-Posterior auditory field, T- Temporal auditory field. There are several more identified areas and the numbers vary from one species to another.

Table 2.1 Laminar, morphological details of the AI. The layers differ in the type of cells and the cell density each playing a vital role in AC processing.

Layer	Classification	Neuronal type	Cell density	Reference
I	Supragranular	Apical dendrites, Axon terminals , GABAergic neurons	Sparse	(Huang and Winer, 2000; Sousa-Pinto, 1973)
II		Small pyramidal neurons GABAergic neurons	Less sparse than Layer I	(Winer, 1985)
III	Granular	Medium Pyramidal neurons GABAergic neurons	Dense	(Winer, 1984a, 1984b)
IV		Pyramidal neurons GABAergic neurons	Dense	(Smith and Populin, 2001; Winer, 1984c)
V	Infragranular	Thickest AC layer, Large Pyramidal neurons GABAergic neurons	Medium dense	(Prieto et al., 1994)
VI		Small Pyramidal neurons Horizontal cells GABAergic cells	Less dense than layer V	(Radnikow et al., 2002)

These different layers of AC receive afferents from different divisions of the thalamus (Figure 2.7). The vMGB send afferent primarily to the core AC areas primarily layer III and layer IV as well as branches to supragranular and infragranular layers (Huang and Winer, 2000; Imaizumi and Lee, 2014; Lee and Imaizumi, 2013). In the rat barrel cortex, it has been suggested that instead of a single major branch from the thalamus received by layers III/IV, a second similar innervation is received by the layers V/VI cortical layers, indicating similar possible innervations in the AI (Constantinople and Bruno, 2013).

The medial MGB send afferents to all AC areas and end mainly in layers I and VI . Finally, the dorsal MGB extend to all cortical layers preferentially in non-tonotopic areas (Winer and Lee, 2007).

The two main neuronal types found in the auditory cortex are the excitatory glutamatergic neurons (80%) and the inhibitory GABAergic interneurons (20%)(DeFelipe et al., 1993; Martinez et al., 2002)(see Table 2.1). Furthermore, 20 different subtypes of interneurons have been identified e.g. Somatostatin, cholecystokinin, vasoactive intestinal peptide (VIP), neuropeptide Y (Ascoli et al., 2008). Several of these markers co-localise with GABA across layers to varying degrees. For example in layer VI of the cortex all neurons that show VIP mark positive for GABA. A similar trend was observed in all the other layers except layer I (Bayraktar et al., 1997).

2.2.1.3.2 Physiology of Auditory Cortex

All the functional properties discussed for the sub cortical structures in the auditory pathway also apply to the AC. The ascending projections from IC to AC are arranged functionally into parallel projections similar to that seen in the visual cortex (Rauschecker, 1998). These systems can be classified into three categories (Andersen et al., 1980; Morest, 1965; Winer and Lee, 2007): projections from ventral MGB (vMGB) (Raczkowski et al., 1976) and PO (Morel and Imig, 1987) to the core AC areas (tonotopic), projections from dorsal MGB secondary cortical areas (non-tonotopic)(Calford and Aitkin, 1983) and projections from other sensory modalities and medial MGB to both core and secondary cortical areas (multi-modal systems)(Rouiller.E.M, 1997; Winer and Lee, 2007).

2.2.1.3.2.1 Tuning properties and Tonotopy

The tonotopic organisation seen in the MGB is preserved in the projections to the A1, AAF and PAF. These projections are further divided into two branches, one from the anterior vMGB (to AAF and AI) (Morel and Imig, 1987) and the other from the posterior vMGB (to PAF)(Rodrigues-Dagaeff et al., 1989). These two

projections contribute to two in mouse (Stiebler et al., 1997), five in cats (Imig and Reale, 1980)and three in monkeys (Kaas and Hackett, 2000) tonotopic maps (Winer and Lee, 2007), arranged as mirror reversals(Kanold et al., 2014).

Measurements in the AI showed a wide range of tuning curve shapes such as 'V' shaped, 'U' shaped and multi-peak in varying proportions(Sutter et al., 2014). Electrophysiological studies in rats have also shown sharp tuning properties of AI neurons, the responsiveness of which increase with intensity. However, unlike other species, the rat shows a single model of spectral tuning(Polley et al., 2007; Sutter and Schreiner, 1995).

The cortical neurons receive innervations from afferent nerve fibres tuned to several different CF (Noreña and Eggermont, 2002; Wang et al., 2000). The fine tuning of the cortical neurons in spite of receiving innervations from a broad frequency band is maintained by selective intracortical masking in the form of inhibition (GABA mediated (Wang et al., 2000)) of innervations tuned to frequencies different from that expected of the tonotopic organisation (Noreña and Eggermont, 2002; Rajan, 1998; Wang et al., 2000).

2.2.1.3.2.2 Laminar physiology of AI

As mentioned in the Sections 2.4.2 and Section 2.4.2.3, the AI receives strong auditory input mainly from vMGB forming the first stage of auditory processing. The information processing within a cortical column follows a vertical microcircuitry (Mountcastle, 1997). Information from the thalamorecipient is first processed in the superficial layers followed by deep layers (Atencio and Schreiner, 2010a; Winer, 2011) (but see(Constantinople and Bruno, 2013; Sakata and Harris, 2009)). Horizontal projections to other cortical columns arise in layer II/III whereas feedback to the thalamus arise from layer V and layer VI respectively (Linden and Schreiner, 2003).

The tonotopic arrangement in AI varies among different species e.g. in rats is progresses from low towards high in posterior to anterior direction (Sally and Kelly, 1988). Laminar profile of CF is more or else preserved across the six cortical

layers (Abeles and Goldstein, 1970; Atencio and Schreiner, 2010a). However, recent two photon imaging studies in mouse suggests a more heterogeneous organisation of CF properties in the different cortical layers (Kanold et al., 2014; Rothschild et al., 2010). These studies indicate that the CF is more preserved in the thalamo-recepient layers as compared to the superficial and deep layers (Winkowski and Kanold, 2013), suggesting a non-homogenous distribution of tuning properties across the different layers. These findings however are not on par with findings in rats where a smooth tonotopy was observed across the different layers using continuous-periodic stimulation combined with continuous data acquisition (Kalatsky et al., 2005). The lack in consensus with the observed findings may possibly be due to the difference in resolution offered by the different techniques.

Threshold values as well seemed to be preserved in the middle layers as compared to the superficial layers (Sugimoto et al., 1997) however there seem to be some discrepancies with regards to this observation (Linden and Schreiner, 2003).

Tuning profiles in the AC show the typical 'V' shaped curve. However, there are some discrepancies regarding the laminar specific tuning sharpness in the AI where some have noticed increased sharpness with depth (Sugimoto et al., 1997) and whereas others reported no laminar specific differences (Abeles and Goldstein, 1970) in the primary auditory cortex. However recent evidence show that the tuning profiles of the thalamorecepient layers (layer III/IV) is sharper than the ones observed in layers V and VI (Atencio and Schreiner, 2010a; Harris et al., 2011; Sakata and Harris, 2009).

Laminar profiles of temporal properties show a variation across the different layers (Atencio and Schreiner, 2010b). The minimum response latencies in the layers receiving the thalamic input are shortest compared to superficial and deep layers (Linden and Schreiner, 2003) in cats. However in rodents, shortest latency is observed in layer V (Sakata and Harris, 2009; Sugimoto et al., 1997). SA in the AI show laminar specific change with denser activity in the layers V as compared to the superficial layers (Sakata and Harris, 2009).

How the above mentioned laminar specific organisations affect overall auditory processing is not clear. Laminar investigations of evoked responses and SA in the AC could possibly explain the relative dynamics between these layer specific organisations and their contribution to auditory processing. Furthermore, how these dynamics change following exposure to trauma intensities could provide insight into the pathologies of the resulting auditory disorders such as noise-induced hearing loss.

2.2.1.4 Core-belt-parabelt axis

The different cortical areas are also interconnected which similar to that seen in the visual cortex define the hierarchical organisation of the various cortical fields. Based on the criteria used to determine the hierarchical cortical levels in the visual cortex (Van Essen and Maunsell., 1983; Felleman and Van Essen, 1991), the auditory cortical areas are divided into four hierarchical levels (Kaas and Hackett, 2000; Kaas et al., 1999; Lee and Sherman, 2010; Rouiller.E.M, 1997; Rouiller et al., 1991).

The origin of some of the interconnections are in cortical layers II and III, which then project into layer IV of the target area. Other interconnections take their origin in the infragranular layers and terminate outside the cortical layers providing a feedback loop. There are several other interconnections across all layers that project to areas at a similar hierarchical level.

Level 1: Core auditory areas, especially AI and AAF provide the first level of auditory processing. They send projections to the AII (Lee and Sherman, 2010)sub cortically, and to similar core areas in the other hemisphere (Luethke et al., 1989). Furthermore they also send projections to other core auditory areas and adjoining belt areas (Rouiller et al., 1991). Finally these areas send feedback projections to vMGB (Lee and Sherman, 2010; Winer and Lee, 2007).

Level 2: AII forms the second level of auditory processing where it receives feed forward input from AI and operates feedback control on AI (Hackett, 2011; Lee

and Sherman, 2010). AII feeds forward to PAF and VPAF and receives feedback control from the same (Rouiller et al., 1991).

Level 3: Involves processing at the level of the parabelt region. Here the information processing extends beyond auditory processing with major inputs to fourth level of processing (Hackett, 2011; Rouiller et al., 1991).

Level 4: Finally PAF receives input from all other cortical areas and is primarily involved in multisensory processing (Kaas and Hackett, 2000).

The core auditory area is functionally divided into two main segments, AI, AAF (Figure 2.3) in rodents and cats (see review (Kanold et al., 2014)) ; AI, rostral area (R) and a more rostral temporal field (RT) in non-human primates (Kaas and Hackett, 2000). Imaging studies have confirmed similar areas in human AC (Humphries et al., 2010).

2.2.1.5 Descending Auditory Pathway

For a long time research of the ascending auditory pathway has dominated the field of auditory system. However, interest in the descending auditory pathway has magnified as the abundance of this pathway was realised (Winer, 2005a).

The auditory pathway is reciprocal and the descending pathway can be viewed as a descending chain embedded with feedback loops in various regions of the pathway (Warr, 1992). Feedback control of the lower level structures is maintained via a profuse supply of descending projections (Bajo et al., 1995; Malmeirca and Ryugo, 2011; Winer et al., 1998). The first link of the pathway is the efferent projections originating from the AC (Figure 2.7). The vMGB receives reciprocal projections, mainly ipsilateral from layer VI of AI and AII whereas the dorsal MGB receive non reciprocal projections from Layer V of AI (Corticothalamic)(Lee and Sherman, 2010; Ojima, 1991; Winer et al., 2001). Efferent projections from Layer V of all cortical areas bypass the thalamus and extend to IC (corticocollicular) (Figure 2.7), the region of the IC receiving these inputs vary from one species to another (Bajo et al., 2007; Druga et al., 1997;

Winer, 2005c).AC efferents from layer V also extend to other regions of the auditory pathway LL(Feliciano et al., 1995; Heffner), SO (Feliciano et al., 1995; Kuypers and Lawrence, 1967)and the CN (Feliciano et al., 1995; Meltzer and Ryugo, 2006).

The second link of the pathway starts at the level of the IC (Malmeirca and Ruygo, 2011). These are the colliculiolivary where the efferents terminate in the medial olivocochlear cells (Schofield and Cant, 1999) that are located in the periphery of principal SO nuclei (Warr, 1975) and the colliculocochlear circuits which terminate in the cochlear nucleus (Schofield, 2001).

Finally a third link of more peripheral systems exist; Olivocochlear system, where the hair cells of the cochlea are innervated by the olivocochlear neurons in the SO (Bredberg, 1977; Ciuman, 2010; Dannhof and Bruns, 1993). The morphology, origin and projection patterns of these neurons entering the cochlear nucleus were investigated in rats by Warr and his group using axonal transport of horseradish peroxidase (White and Warr, 1983). The two distinct sets of olivocochlear neurons are observed; medial and lateral where the lateral neurons were seen to project ipsilaterally (White and Warr, 1983). The reflex pathway originating from this system is believed to play an important role in sound protection(Brown et al., 2003). The other peripheral system; Middle ear muscle reflexes (Moller, 1975) which involve the combined influence primary AN, inputs from CN, SO (Rouiller et al., 1986)and motor neurons (Shaw and Baker, 1983). This arc is believed to play a protective role during acoustic over stimulations by causing middle ear muscle contraction (Borg, 1973; Kanold et al., 2014)

In the following sections, the functional properties of the sub cortical and auditory cortex will be discussed in more detail.

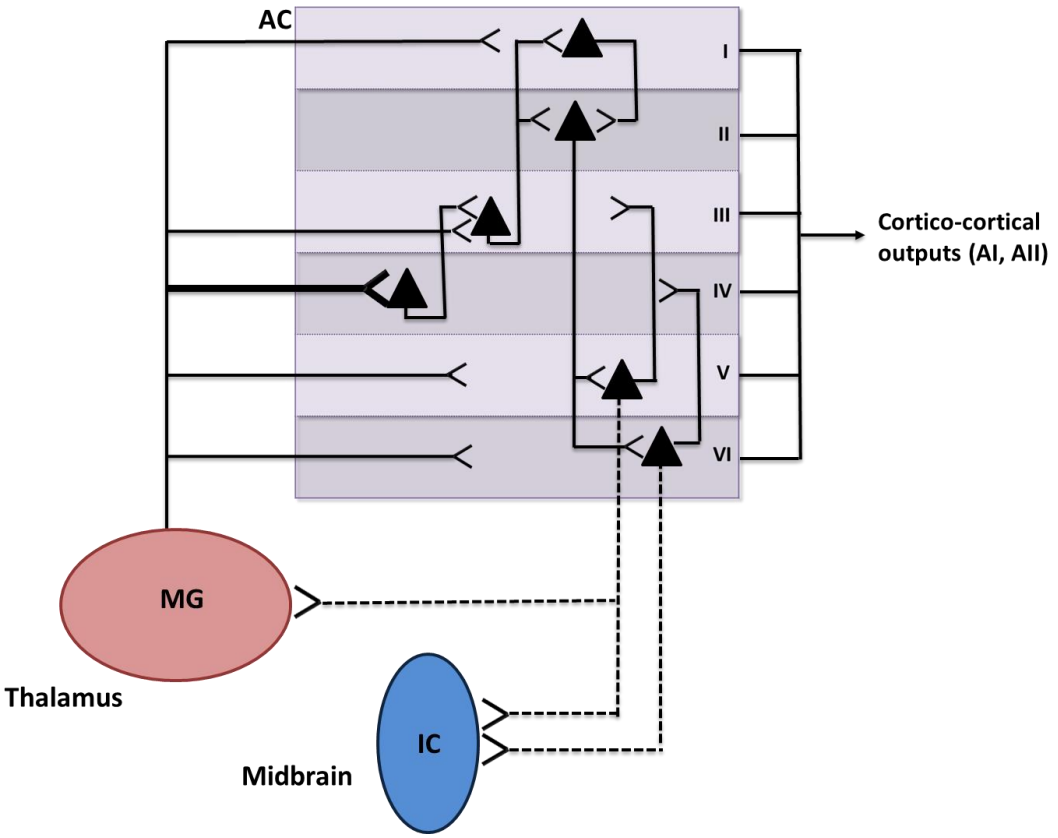

Figure 2.7 Schematic representation of the major anatomical connections in an AC circuit. Solid lines represent feed-forward connections and broken lines represent feedback connections.

2.3 Noise-induced hearing impairment

Based on the anatomical level of auditory pathway involved in auditory pathology hearing impairment can be divided into two categories: Conductive; pathology confined to peripheral ear i.e. the sound waves are not able to freely travel to the inner ear(Raz, 2004)and Sensorineural; pathology involving any structure in the ascending auditory pathway beyond the cochlea (Chau et al., 2010). Conductive hearing loss mainly occurs due to a blockage or infection and mainly affects the intensity of the sound. This form of hearing loss can be either temporary or permanent depending on the cause and can be usually rectified with medical treatment or surgery (Raz, 2004). Sensorineural hearing loss on the other hand not only affects the intensity but also affects the quality of the sound. This form of hearing loss is almost always irreversible as permanent damage to the hair cells is usually observed (Epstein and Reilly, 1989).

Sudden brief (Yankaskas, 2013) or cumulative exposure (Daniel, 2007) to very loud noise levels can cause sensorineural auditory pathologies such as acoustic trauma that further lead to conditions such as noise induced hearing loss (NIHL) and tinnitus(Eggermont, 2013). Unlike previous times where exposure to loud noise was confined to limited occupational settings, technology in the modern age exposes us to constant levels of traumatic noise(Hawkins and Schacht, 2005).

2.3.1 Implications and Current treatments

Adult onset hearing loss is considered as the third leading cause of disability (Mathers et al., 2008). The World Health Organisation (WHO) estimates that about 10 percent of the world population is exposed daily to injurious levels of sounds (Hawkins and Schacht, 2005) and is the leading cause of adult onset of hearing loss accounting for approximately 16 percent of hearing loss cases reported worldwide (Nelson et al., 2005).

Unfortunately, to date treatment options to manage acoustic trauma pathologies are extremely limited. This is partly due to the fact that depending on the intensity frequency and length of trauma exposure, the extent of acoustic trauma in the auditory system can be varied making it hard to assess level recovery using medications in man (D'Aldin et al., 1999).

Traditional therapies for avoiding acoustic trauma induced hearing loss were carbogen inhalation (Brown et al., 2009; Hatch et al., 1991), Dextran infusion, a combination of both Carbon dioxide and Dextran, Oxygen therapy (Hatch et al., 1991)and corticoid therapies (D'Aldin et al., 1999; Lesoine, 1983). However, these treatments are peripheral : increase vascular blood flow (Carbogen), Oxygen supply to damaged cochlea (Oxygen therapy), inflammatory responses (Corticoid therapies) and animal studies show conflicted results in terms of managing acoustic trauma (D'Aldin et al., 1999) and very limited clinical applications. These treatments options could possibly provide mild relief from acoustic trauma but cannot reverse hearing loss.

Other options to manage acoustic trauma related hearing loss are hearing aids and cochlear implants (Lasak et al., 2014). The traditional hearing aids would aid in coping with hearing loss by amplifying sounds and hence have limited use in acoustic trauma pathologies which have progressed into the central auditory system.

Cochlear implants greatly overcome the limitations of hearing aids as they can generate electrical signals that stimulate the AN directly. Even though these implants provide significant relief from hearing loss, they have their limitations. Apart from the design limitation which requires a functional auditory nerve, other factors such as the time of cochlear implant is critical i.e. younger children would benefit more from these implant, the duration of hearing loss limit the functionality of cochlear implants. Nevertheless, these implants show promise and based on the potential benefits observed with these implants, prostheses with targeting higher auditory structures such as the IC have been developed (Moore and Shannon, 2009). These are called Inferior colliculus implants (Colletti et al., 2007)or auditory midbrain implants (Lim et al., 2008)and have been tested in up to six patients with neurofibromatosis type 2. Even though, the results were not as expected i.e. reversal of hearing loss, moderate improvement in sound awareness was observed indicating potential benefits of such implants in the future.

With the increasing demand of efficient interventions, coupled with the stark limitation of available treatments, there is an urgent need to develop new and novel treatments to treat hearing loss (Moore and Shannon, 2009).

The following section discuss animal models used to understand the mechanisms of acoustic trauma related pathologies.

2.3.2 Animal models of noise-induced hearing impairment

Effects of noise induced hearing loss on different components of the auditory

pathway have been investigated in different species: mouse (Hakuba et al., 2000), rats(Milbrandt et al., 2000), cats (Noreña and Eggermont, 2003a), hamsters (Brozoski et al., 2012b). Animals exposed to acoustic trauma often show behavioural signs of tinnitus (phantom perception of sound), hyperacusis 9increased sensitivity to a certain frequency) and hearing loss (Eggermont, 2013) making them an attractive model to measure the neural correlates of these disorders. Tinnitus and hyperacusis may exist on their own or may be associated with hearing loss. However, parameters of induction of trauma such as intensity, frequency, duration need to be modified depending on species (Table 2.2). For e.g. in rats, a one to two hour unilateral or bilateral exposure to an octave band noise with peak intensity at 110 dB SPL and frequency centre at 16 kHz is commonly used (Zhang and Kaltenbach, 1998) whereas for cats a 6 kHz trauma frequency is often selected (Noreña and Eggermont, 2005). Furthermore, the exposure time may vary from as little as 10 milliseconds (blast induced tinnitus) (Mao et al., 2012) to almost 9 hours (Abbott et al., 1999) of continuous exposure.

For studies evaluating acute changes following acoustic trauma, factors such as evoked response spontaneous firing, synchronous activities are evaluated in animals immediately after exposure to loud noise (Noreña and Eggermont, 2003a) whereas more chronic effect measurements of acoustic trauma involves evaluation of the above mentioned parameters several weeks after exposure (Brozoski et al., 2012a; Eggermont and Komiya, 2000; Noreña and Eggermont, 2005; Seki and Eggermont, 2003). To measure evoked response, several different combinations of frequency and intensity are presented before and after induction of trauma. The parameters of these stimuli are based on the hearing frequency range of the different species (Table 2.2) to ensure that the measured responses are measured in the audible range of the species. As seen in Table 2.2, the trauma frequency is modified based on the hearing frequency that varies between different species. The trauma signal information is extracted from the audiogram which reflects the most sensitive frequency/intensity combination e.g. 10 or 16 dB SPL for rats and 6 dB SPL for cats.

Anaesthesia can induce variation in the results obtained using this model. For example, isoflurane seems to block temporary tinnitus after acoustic trauma (Norman et al., 2012) and also shows a smaller degree of hearing loss in mice as compared to control (Chung et al., 2007). Under anaesthesia, enhancement of

Table2.2. Parameters for induction of acoustic trauma in different species. References for the auditory hearing range for the different species are: Rats(Heffner and Heffner, 2007) , Cats(Heffner and Heffner, 2007), Guinea pigs(Heffner et al., 1971), Hamsters(Heffner et al., 2001), Chinchillas(Heffner and Heffner, 1991).

Species	Hearing range at 60 dB SPL	Frequency of trauma (kHz)	Intensity of Trauma	Duration of exposure	Tone	References
Rats	500 Hz- 64 kHz	10, 12,16, 20	100-130	4 hours 1 hour 10 minutes	Pure tone Band noise, Pure tone	(Zhang and Kaltenbach, 1998;Bauer et al., 2007; Scholl and Wehr, 2008; Sun et al., 2012)
Guniea pigs	32 Hz- 50 kHz	10	124	1 hour	Pure tone	(Mulders and Robertson, 2009)
Cats	48 Hz- 64 kHz	6	100-130	30 minutes 2 hours	Pure tone, 1/3 Octave Band noise	(Kimura and Eggermont, 1999; Noreña and Eggermont, 2005; Seki and Eggermont, 2003)
Hamsters	63 Hz- 50 kHz	10	125- 130	4 hours	Pure tone	(Kaltenbach et al., 2004)
Chinchillas	50 Hz-33 kHz	4	80-85	~ 1 hour	Pure tone	(Bauer and Brozoski, 2008; Brozoski et al., 2002)

inhibitory responses have been reported. This enhanced inhibition results in evoked and spontaneous responses which are different from that seen in awake rats(Behrens, 2014; Gaese and Ostwald, 2001). Therefore, caution should be used

while interpreting results from studies which measure acute changes in acoustic trauma in anesthetised animals.

Quantification of peripheral threshold shifts in animals exposed to acoustic trauma and its comparison to behavioural correlates of hearing loss or tinnitus is achieved by measuring auditory evoked brainstem responses (ABR) under anaesthesia before and after induction of acoustic trauma (Chen et al., 2003; Dehmel et al., 2012; Seki and Eggermont, 2003). These are the earliest auditory evoked potentials (Escera et al., 2014) which comprise of synchronous firing of cochlea, AN, and brainstem (Hill, 2011) and can be picked up by scalp electrodes. These potentials show a sustained phase-locked response to periodic stimulus (Skoe and Kraus, 2010) and provide an interpretation of behavioural threshold at different intensities (Skoe and Kraus, 2010) in individuals with sensorineural hearing (Stapells, 2011). Usually, a series of pure tones or pips at varying intensities are presented to estimate the minimum intensity at which an evoked response is observed (Hill, 2011).

The objective, non-invasive method of ABR recording have resulted in its utilisation to asses hearing loss in Humans allowing a direct translation of animal model interpretation (Heffner et al., 2008; Jewett and Willinston, 1971).

2.3.3 Behavioural models of acoustic trauma induced pathologies

As mentioned in the Chapter 1 and Section 2.3, exposure to traumatic noise can cause a range of auditory pathologies such as hearing loss or tinnitus. Several animal models have been developed which can measure behavioural specific co-ordinates of such auditory disorders; hearing loss (Heffner et al., 2008; Hill, 2011) or frequency dependant pathologies (tinnitus)(Eggermont, 2013) .

2.3.3.1 Behavioural models of hearing loss

The commonly used measure to quantify an animal's hearing ability is a pure-tone audiogram, which measures an animal's behavioural response to pure tone(Hill,

2011). The audiogram is composed of the threshold intensity that the animal identifies in more than half the total number of trails within the hearing frequency range of the species (Heffner et al., 2001).

The animals are trained and conditioned in different ways to respond to a tone after which the above mentioned audiogram is derived based on the animals ability to detect and respond to various intensity/frequency combinations (Heffner et al., 2006).

One commonly used conditioning protocol based on conditioned response suppression (Estes and Skinner, 1941) is used to measure the above mentioned behavioural thresholds. In this model, water deprived animals are placed in a chamber and trained to get water by making contact with the spout. If the animal is in contact with the spout when a sound is played it is presented with a mild shock. With time, the animal learns to break contact with the spout when the stimulus that signals a shock is presented (Heffner et al., 2006). To optimise the performance of the animals, and minimise the number of false positives, the reward frequency and intensity of shock can be accordingly modified (Heffner and Heffner, 2003).

2.3.3.2 Behavioural models of tinnitus

Several animal models have been developed to measure the behavioural correlates of tinnitus (Kaltenbach, 2011; Moody, 2004). They are similar (Jastreboff et al., 1988a, 1988b) to or are a modification of the above mentioned conditioned response suppression model. As tinnitus is perception of phantom sounds and it is believed to occur at specific frequencies (Eggermont and Roberts, 2004), the aim of tinnitus animal models is to evaluate the inability to detect silence at a particular frequency rather than the ability to detect a sound which is the case in animal models of hearing loss.

One major concern with the conditioned response suppression task is in that food or water deprivation, along with the aversive stimulus may involve the limbic or other cognitive systems (Turner, 2007) making it harder to evaluate the more

direct factors involved in tinnitus development. Also, these models use tasks which rely on memory, motivation, etc., making them less relevant in evaluating the sensory components of tinnitus. Another caveat with the technical aspects of the above mentioned models is that the animals require intense training to learn the response paradigm.

All of the above issues are overcome with the recently validated and developed Turner's gap detection model (Turner et al., 2006). This model requires minimal animal training and allows the generation of a large amount of data from a single animal making it a powerful screening tool for tinnitus (Turner, 2007; Turner et al., 2006). This model utilises a modification of pre-pulse inhibition of acoustic startle reflex which is the decrease in startle reflex when the startling stimulus is shortly preceded with a non-startling sensory stimulus (pre-pulse) (Li et al., 2009). The behavioural coordinates are then evaluated by calculating the ratio of the peak-to-peak value of the startle waveform in startle inducing versus non startle inducing trials across several repetitions (Li et al., 2009). Furthermore, the startle-reflex can be made more sensitive by fear conditioning on the pre-pulse (Du et al., 2011; Eggermont, 2013; Li et al., 2009). Another behavioural model that can be used to measure correlates of tinnitus is the Preyer reflex model (Berger et al., 2012). The Preyer reflex measures the pinna reflex and like the startle response in Turner's model is an unconscious reflex (Bohmer, 1988). Furthermore, unlike Turners model it is less prone to habituation (decrease in response to a frequently presented stimulus. This is different from adaptation where change in sensitivity of receptors occur to an unchanging stimuli) and can be a more reliable measure of behavioural correlates of tinnitus in animals such as guinea pigs where habituation is a concern (Berger et al., 2012).

This model is now routinely used to evaluate noise induced tinnitus (Dehmel et al., 2012; Stuber et al., 2011; Wang et al., 2011). However, caution should be followed while evaluating data generated using this model as there is a risk of false positive or negative interpretations (Lobarinas et al., 2013).

2.3.4 Neurophysiology of noise-induced hearing impairment in animal models

One key observation that can be derived from auditory anatomy and physiology discussed in section 2.2 is that each component of the auditory system is a vital link to process of auditory integration, and that it is very likely that damage to any part of the auditory system would affect subsequent structures of the auditory pathway causing abnormalities in the overall auditory processing (Butler and Lomber, 2013). Hence, to understand the pathology caused by induction of acoustic trauma on auditory processing, the effect of acoustic trauma has been measured on most components of the auditory pathway, starting at the peripheral cochlear cells (Chen et al., 2003) right up to the AC (Noreña and Eggermont, 2003a) in a wide range of species (Abbott et al., 1999; Noreña and Eggermont, 2005; Salvi et al., 1990).

Exposure to trauma noise levels can cause temporary or permanent shift in threshold. In instances where acoustic trauma causes permanent hearing loss morphological and metabolic damage to IHC (Chen et al., 2003; Clark and Pickles, 1996) and mechanical damage to OHC (Saunders, 1985) are noticed at the cochlear level. Damage to IHC and OHC results in increased peripheral glutamatergic over excitation at hair cell (Giraudet et al., 2002), AN synapses causing pathological changes in the stereocelia. These pathologies further cause an elevation of AN threshold and broadening of AN tuning curves (Dallos and Harris, 1978; Schmiedt et al., 1980).

Electrophysiological recordings in peripheral AN show decreased SA following acoustic trauma (Kiang et al., 1970). Contrary to decreased SA in peripheral system, acute and long term increase in SA is observed in central auditory structures such as cochlear nucleus (Zhang and Kaltenbach, 1998) and the IC (Mulders and Robertson, 2009; Zhang and Kaltenbach, 1998). It is hypothesized that this increase in central SA is to compensate for the reduced peripheral input (Noreña, 2011).

At the cortical level acute changes of trauma induction show increase in spontaneous firing rate in the AI and AII following acoustic trauma (Eggermont and Roberts, 2004; Engineer et al., 2011; Kimura and Eggermont, 1999; Noreña and Eggermont, 2003a; Noreña and Farley, 2013; Roberts et al., 2010). However, the increase in SA is delayed and is only seen a few hours after induction of trauma (Noreña and Eggermont, 2003a). Another acute change in neuronal activity associated with acoustic trauma is increase in synchronous firing. However, unlike SA, an immediate increase in synchronous firing and bursting activity is observed in cat auditory cortex following acoustic trauma (Engineer et al., 2011; Noreña and Eggermont, 2003b; Seki and Eggermont, 2003).

In AI, acute changes following trauma induction not only effects SA activity but also alter evoked response such as threshold and CF (Engineer et al., 2011; Noreña and Farley, 2013; Noreña et al., 2003; Roberts et al., 2010). The reduced peripheral input to the central auditory system causes an expansion of the receptive fields in the low frequency range of the AC (Noreña et al., 2003; Scholl and Wehr, 2008). This observed modification of the CF tuning property is believed to be a consequence of a shift in the ratio of inhibitory (GABA mediated) and excitatory balance control of fine-tuned AC neuronal population (See Section 2.2.2.2.1). Following induction of trauma an enhanced unmasking of these inputs is observed due to the increased inhibition of the intracortical GABA mediated inhibitory control at the low frequency half of the receptive field. On the contrary an increase in these inhibitory controls is observed at the high frequency region at the periphery of the threshold shift (Scholl and Wehr, 2008). These alterations in the inhibitory intracortical controls with little or no change in the excitatory response of cortical neurons result in the observed alterations of cortical receptive fields following trauma induction. Similar changes in receptive fields are observed in subcortical structures such as the IC (Basta and Ernest, 2004; Milbrandt et al., 2000; Willott and Lu, 1982) and CN (Kaltenbach and Zhang, 2007) following acoustic trauma. This indicates that the changes in the receptive fields of the cortical neurons following trauma is due to the combination of altered input from

the trauma altered sub cortical structures and modified intracortical control (Scholl and Wehr, 2008).

A long term consequence of exposure to trauma intensities is tonotopic re-organisation in the AI observed several weeks after noise induced high frequency hearing loss (Noreña and Eggermont, 2003b, 2005; Willott et al., 1993). The CF within the frequency region of the hearing loss acquires the CF of the edge frequency of the hearing loss range causing an over representation of that CF in the AC (Eggermont and Komiya, 2000). This reorganisation may possibly contribute to acoustic trauma related disorders like tinnitus (phantom perception of sound) (Eggermont, 2013; Engineer et al., 2011).

2.3.5 Critical analysis with emphasis on AC

In the last fifty years immense progress has been made in the field of noise induced auditory pathologies (Gold and Bajo, 2014; Knipper et al., 2013). However, the fact that the treatments available to date to treat these disorders are limited suggests a gap in our understanding about the neural pathologies of these disorders. As seen in the previous section each component of the auditory pathway is possibly involved in the origin and progression of these disorders. However, in recent times the AC has gained interest in the investigation of these pathologies and will be the focus of this discussion.

Growing evidence from animal models and human subjects suffering from noise-induced auditory disorders suggests a major involvement of AC in the pathology of these disorders.

In cats, cortical measurements following long term exposure to loud noise showed hearing loss and tonotopic reorganisation in primary cortical areas (Eggermont and Komiya, 2000). However, if these animals were maintained in an acoustic rich environment after exposure to similar trauma intensities, no reorganisation of the cortical tonotopy was observed. Interestingly, these animals unlike those in which tonotopic reorganisation was observed, showed hearing loss to a lesser extent suggesting the role of AC in such pathologies (Noreña and Eggermont, 2005).

Using chronic recording techniques similar changes in cortical plasticity have also been reported in awake guinea pigs following acoustic trauma albeit the results being much more variable than those obtained under anesthetised conditions(Noreña et al., 2010).

Further evidence of AC involvement in pathologies of noise-induce auditory disorders is provided by the excellent work done by Engineer et al in rats (Engineer et al., 2011). As discussed previously, acoustic trauma is often used to induce tinnitus in animal models. In Engineer's investigation, changes in cortical properties such as tonotopic reorganisation, increased SA activity and synchronous firing was observed in animals showing behavioural correlates of tinnitus following acoustic trauma. Interestingly, diminished behavioural correlates of tinnitus were observed in these animals when they were exposed to various tones paired with brief stimulation of the vagus nerve(Engineer et al., 2011). Furthermore, changes following trauma such as, synchronisation, and BW following trauma were also reversed induction were also reversed in the animals with diminished behavioural signs of tinnitus emphasising the involvement of AC in the pathology of noise-induced disorders (Engineer et al., 2011).

Recent advances in non-invasive techniques have allowed the investigation of AC in humans suffering from auditory disorders. Imaging studies in tinnitus patients show an involvement of AI (Noreña and Farley, 2013; Schecklmann et al., 2013) confirming its contribution to the pathology of this condition. For example, Magnetic source imaging in patients suffering from tinnitus show different tonotopic organisations as compared to controls, where the extent of re-organisation was directly correlated to the perceived tinnitus strength (Muhlnickel et al., 1998; Weisz et al., 2005; Wienbruch et al., 2006). Furthermore, PET (Arnold et al., 1996) and fMRI (Leaver et al., 2011) studies have also shown hyperactivity in the AC in patients suffering from tinnitus compared to control subjects suggesting the involvement of AC in tinnitus pathologies.

As acoustic trauma often causes hearing loss, evidence of the role of AC in auditory pathology can also be derived from patients suffering from hearing loss

which may not be necessarily noise induced. PET investigation showed that metabolic activity in the AI was reduced in individuals suffering from hearing loss (Okuda et al., 2013). Also decrease in BOLD signals were observed in the AI areas contralateral to the deaf ear in unilateral deaf patients compared to control (Tschopp et al., 2000) providing further evidence of involvement of AC in hearing loss. Cochlear implants have provided new opportunities for recovery in people suffering from hearing loss (Brian C. J. Moore, 2003)and it is observed that in congenitally deaf children, cochlear implant have shown to improve AC activity highlighting the importance of AC activity in auditory processing (Shepherd et al., 2009).

The growing interest in AC to understand noise-related auditory pathologies lead to several investigations in AC following acoustic trauma, the observations of which were discussed in section 2.3.4. To summarise quickly, following acoustic trauma, changes in AC, particularly AI evoked response in the form of increased threshold and reorganisation of the spatial distribution of CF was observed (Kimura and Eggermont, 1999; Noreña et al., 2003). Increase in SA and burst-like firing were also seen following trauma induction (Kimura and Eggermont, 1999; Noreña and Eggermont, 2003a; Seki and Eggermont, 2003). However, to date, high variability in terms of extent of changes (e.g. smaller versus larger threshold shifts, increase in SA) is observed in these results making it hard to interpret them in relevance to noise induced auditory disorders (Noreña and Eggermont, 2003a; Noreña et al., 2010; Roberts et al., 2010). Differences in time frames for responses of AC are also variable; following acoustic trauma, in some instances, changes in neural activity were immediate, whereas in other instances it decreased and only increased a day after trauma inductions (Noreña et al., 2010). Furthermore, these results differ from that seen in changes due to induction of tinnitus following systemic administration of salicylates (Lobarinas et al., 2006) where no changes in firing rate were observed in AI (but observed in the AII and AAF) (Eggermont and Kenmochi, 1998). One reason for this discrepancy maybe due to the fact that salicylates possible have a direct action on AC (Wallhausser-

Franke et al., 2003) making data obtained using this model relatively hard to interpret.

One explanation for the above mentioned variability is that these investigations measure from a single point of the AI. As discussed in section 2.2.2.2.4, the AC laminar structure is complex and there is evidence that the various response parameters across the layers vary (Kanold et al., 2014; Sakata and Harris, 2009; Stolzberg et al., 2012)making it very likely that the trauma related changes will vary across layers. Indication of such possibility can be further derived from our knowledge of laminar functionalities in other sensory systems. Using electrophysiological recordings, the lamination of the somatosensory and visual cortex following peripheral deprivations such as whisker removal and visual impairment have been thoroughly investigated (Daw et al., 1992; Diamond et al., 1994; Gordon and Stryker, 1996). These studies clearly show laminar specific changes in their primary cortex and that it plays a vital role in the development of sensory related pathologies.

Furthermore, we know that the AI is connected to several components of the auditory pathway and is an essential link to higher level processing and feedback control (Lee and Sherman, 2010; Rouiller et al., 1991; Winer and Lee, 2007). The functional contribution of AI to this process in turn would depend on its laminar processing making it a crucial link in auditory processing. This fact highlights the importance for us to understand the lamination of AC to be able to fully evaluate auditory pathologies.

Several studies have investigated the role of AC in the AI using the 'gold standard' for investigating changes in neuronal activity, electrophysiology.

2.4 Electrophysiology

Neuronal cells of the brain communicate with each other via integration and propagation of neuronal activity. Thus, to understand neural and brain systems it is important to be able to quantify and measure such neuronal electrical activity. Electrophysiological techniques allow such investigations of neuronal systems

right from a single neuronal level to average changes in neuronal populations in whole systems (in vivo) or in cell/tissue preparations (in vitro). This in turn aids us in deciphering the brains natural language, making it an indispensable technique to the field of neuroscience. Electrophysiological techniques can be classified into two broad categories: Intracellular recording which can give information about factors such as 'but not limited to' membrane potentials or specific ion channels. The other category is Extracellular recordings which allow single unit, MU and field potential investigation of the electrical interactions between neural systems (discussed in further detail in the subsequent sections).

Today advances in electrophysiology are made in strides with the availability of newer nanotechnologies that allow miniaturisation of devices, newer materials which allow development of efficient and robust recording devices that can be modified to accomplish desired investigations (Berényi et al., 2014; Buzsáki, 2004; Du et al., 2009; Olsson et al., 2005). However, the foundation of this technique was rather humble, nevertheless fascinating and will be discussed in the following section.

2.4.1 History

The work done by a Dutch scientist Jam Swammerdam in the early sixteenth century (Cobb, 2002) marks the beginning of electrophysiological investigations of the nervous system. Swammerdam prepared isolated frog muscle preparations with the nerve intact which he stimulated with silver wire and measured contractions (Stillings, 1975). However it only several years later that a better understanding of the electrical excitation of nerve cells was furnished by the work done by Luigi Galvani in the late seventeenth century. Galvani too used frog muscle preparations; however he used two frog muscles with the sciatic nerves attached and showed that when the nerve of one leg muscle is in contact with the other, its stimulation with a metal wire would cause a contraction in both muscles (Piccolino, 1998). This study laid the foundation for several fundamental concepts of the electrical activity of nerves such as action potential propagation and the possible role of positive and negative charges in neural electrical activity

propagation (Verkhratsky et al., 2006).Since then, for most of the eighteenth century several other investigators used the muscle-nerve preparation to investigate nerve electrical activity using the electromagnetic galvanometer (the first instrument used to measure electrical activity), further enhancing the knowledge of the field and establishing principles for electrophysiological measurements (Du Bois-Reymond, 1848; Nobili, 1828; Piccolino, 2003).

In 1926 the pioneering work of Nobel laureate Edgar Adrian (Adrian, 1933, 1926; Chapleau, 2007) contributed immensely to the field of neuronal electrophysiology by providing vital information about neuronal communication. By amplifying and measuring small action potentials from an isolated muscle spindle of a frog attached to a single nerve fibre he showed that muscle contraction by nerve stimulation could be increased only by increasing the frequency of the stimulus produced and that the strength of stimulus did not make a difference. Adrian was thus able to establish the fact that varied neuronal communication is achieved by varying frequency of discharge. It was Adrian's work that inspired another Nobel laureate Haldan Keffer Hartline(1930). Hartline (Hartline, 1967), through his investigation on horseshoe crabs and frogs provided information about the retina in the eye understands visual information and passes it via the optic nerve to the brain. Knowledge about the ionic mechanism of neuronal action potential came from the Hodgkin and Huxley giant squid axon (Hodgkin and Huxley, 1952) investigation. This was a major milestone in the field of neurophysiology. Since then, significant strides have been made in our knowledge about neuronal electrophysiology. Another landmark in the field of neurophysiology in the early 1950's was the identification of the columnar organisation in the cat somatosensory cortex (Mountcastle, 1957) which was revolutionary in the field of neuroscience. In 1960, the accomplished work of two scientists David Hubel and Torsten Wiesel set the platform for in vivo recording. Through their work they established the link between neuronal firing and visual stimulus presentation in cats (Hubel and Wiesel, 1962). A few years later, Edwart Evarts pioneered single-unit recording by measuring activities from single neurons of the motor cortex in awake monkeys (Evarts, 1968; Thach, 1986). Finally, it was in the early 1980's that

the patch clamp was developed by Erwin Neher and Bert Sakmann. This technique allowed investigation of single ion channels which is of immense value in understanding ion mechanisms in neuronal activity(Neher, 1992).

2.4.2 In vivo extracellular recording

In in vivo extracellular recording the recording electrode is placed outside the cell if the intention is to measure the spiking activity of a single neuron, or within a small population of the neurons if the purpose to study population activity. Furthermore, this form of recording enables estimation of synaptic activity which would be useful for investigating neuronal interactions (Chung et al., 2002; Hasenstaub et al., 2005). Extracellular recording is technically much easier than Intracellular recordings and can be used in freely moving animals (Barthó et al., 2004). In recent times significant developments have been made in the recording devices used for extracellular recordings allowing us to easily evaluate a range of neuronal activities (Buzsáki, 2004).

2.4.2.1 Single unit recording

To measure single unit action potential the electrode is placed close to the neuron. This technique can efficiently detect single neuron activity (Evarts, 1968). The recording electrodes traditionally used for this purpose are glass micropipettes filled with electrolyte solutions or metal (tungsten, steel, platinum-iridium) wire electrodes. These electrodes have low mechanical stability, high impedance which can result in the generation of large artifacts (Neuman, 1999).)

Recently newly available multi-channel devices (discussed in the next section) enable the detection and extraction of single units from multi-unit activity.

2.4.2.2 Large-scale extracellular recording

To understand concepts such as cognition and perception, and how individual neurons contribute to such brain functions (Hampson et al., 2001)it is essential to understand how large neuronal networks within neuronal circuits interact with

each other(Buzsáki, 2004; Douglas and Martin, 1991). To achieve such a purpose would require recording techniques that could simultaneously record from large ensembles of neurons while preserving spatial and temporal resolution and causing minimal damage. Optical imaging techniques such as calcium two-photon imaging could achieve this goal. However, due to the poor penetration abilities of imaging techniques, they cannot be used for deeper structures (Deisseroth and Schnitzer, 2013).

The development of multiple-wire electrodes and the new generation silicon probes (discussed in detail in subsequent sections) have enabled simultaneous measurements of vast neuronal networks in both anesthetised (Sakata and Harris, 2012; Stolzberg et al., 2012)and awake (Niell and Stryker, 2010; Sakata and Harris, 2009), freely behaving animals. Investigations carried out using these recording devices have provided invaluable information regarding complex brain functions.

2.4.2.2.1 Multiple-wire electrodes

Multiple wire electrodes overcame the limitations of the single glass and wire electrodes in recording simultaneous neuronal activities. The measured neuronal amplitude is a function of the distance from the recording site i.e. as the distance from the recording site increases the measured amplitude at that site decreases.

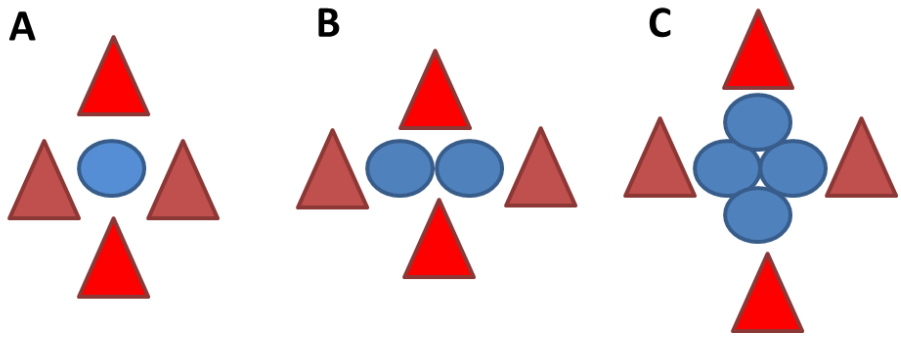

Figure 2.8 Schematic representation of recording sites (blue circles) of **A**. Sharp wire electrode with single recording point **B**. stereotrodes and **C**. tetrodes surrounded by pyramidal cell (dark and bright red triangles)

In the case of single electrodes it is hard to extract single unit activity as the surrounding neurons are equidistant from the single recording site (Figure 2.8A).

To improve the efficiency in isolating multiple wires were placed closed to each other allowing two recording sites; stereotrodes (Figure 2.8B) (McNaughton et al., 1983). As there were two recording sites the amplitude to the signal ratio for a neuron would be different at the two recording sites allowing efficient separation. However the limitation with stereotrodes was that in certain circumstances, successful isolation of single neuronal activity was not possible (Figure 2.8B, bright red triangles). An improvisation of the stereotrodes led to the development of tetrodes which are extremely efficient in isolating single-unit activity from multi-unit recordings (Gray et al., 1995; Harris et al., 2000; O'Keefe and Recce, 1989).

Tetrodes (Figure 2.8C) provide an advantage over single wire or glass electrodes and stereotetrodes. Apart from the improved abilities to isolate single neuron activity from multiple-unit activity with relatively less tissue damage, other advantages include easy fabrication, low impedance tip and improved mechanical stability (Buzsáki, 2004b; Csicsvari et al., 2003). Also due to the high spatial resolution of tetrodes they do not need to be placed in close vicinity of neurons allowing their chronic use in freely behaving animals (Buzsáki, 2004).

In spite of all the advances, wire electrodes still have a few limitations. The most significant limitation is the requirement of several wires and drives that not only increase the total mass (which would be an issue chronic implantation in behavioural studies (Bragin et al., 2000)) but also cause significant tissue damage (Csicsvari et al., 2003).

2.4.2.2.2 Silicon-based electrodes

The new generation silicon probes have all the benefits of wire tetrodes with the added advantage of having small recording tip volume which minimises tissue damage. Furthermore, as it is a micro-machine based electrode, the use of bulky wires and connectors as in the case of wire electrodes is eliminated making it practical for use in chronic implantation of freely moving animals (Bragin et al., 2000).

Silicon probes are a derivative of silicon microtechnolgy in which recording channels are lithographically assigned using integrated circuits (Wise and Najafi, 1991). This allows the assignment of several channels along the length of the recording probe providing high yield to tissue damage ratio (Csicsvari et al., 2003).

Another highlight of silicon based probes is the geometrically precise distribution of the recording channels which provides excellent spatiotemporal resolution a characteristic essential to understanding the functional dynamics of neuronal networks (Atencio and Schreiner, 2010b; Buzsáki, 2004).

Depending on the desired outcome of the experiment, these silicon probes can be customised in terms of the desired two dimensional shape of the recording probe (e.g. linear probe), number of channels (16, 32) or number of shanks, etc. making their use applicable to a wide range of areas.

Another important component that is fundamental to large scale extracellular recording is an efficient spike sorting technique (discussed in the next section) (Lewicki, 1998). Several algorithms have been suggested to enable efficient extraction of single unit activity from multi-unit recordings using multichannel probes. Further details of these spike sorting techniques are discussed in the following section.

2.4.2.2.3 Spike-sorting

Visualisation and extraction of relevant data from electrophysiological recordings is vital to understand and interpret function of neuronal activity. However, due to the large amount and type of data generated by modern recording devices (multi-channel electrodes) ,spike sorting is technically very challenging (Hazan et al., 2006) as the data generated is a complex mix of background noise and the simultaneous electrical activity of several neurons close to the recording site. Spike sorting in simple terms can be defined as identifying spikes over a noisy background and grouping them into clusters based on their waveform features. Recently, significant advances have been made in developing efficient spike

sorting techniques making the procedure more efficient and less biased (Hazan et al., 2006; Lewicki, 1998; Takekawa et al., 2010; Wood et al., 2004).

One of the major advantages of spike sorting techniques is that it allows the simultaneous measurements off several neurons which we know is essential to understand brain functions (Buzsáki, 2004). It also provides the opportunity to measure the activity of neurons anatomically very close each other which would otherwise be technically not impossible to achieve using separate recording devices (Lewicki, 1998).

Spike sorting can be classified into four main inter-related steps: 1) Filtering,

2) Spike detection, 3) Feature extraction and 4) Clustering (manual/automated). Each of these steps is discussed in further detail.

1) Filtering: This is essential to reduce background noise and improve the quality of the collected data. This step involves efficient detection and extraction of action potentials from the recorded data (Hazan et al., 2006).

2) Spike detection: The second step would involve setting a threshold criterion that would allow reliable isolation of action potentials from filtered data. The selection is a trade-off between setting the threshold criterion too low resulting in false positives (type II error) where the noise amplitude maybe high or setting it too high and missing the spike against a noisy background (type I error)(Delescluse and Pouzat, 2006; Lewicki, 1998; Quiroga et al., 2005).

   Once the spike is detected, the waveform is extracted and the next important step is alignment of the waveform to reduce temporal jitter. This is achieved by utilising in addition to the threshold a feature of the extracted waveform (Letelier and Weber, 2000) for accurate alignment.

3) Feature Extraction: the next critical step in spike sorting is to extract relevant features of the waveform using several established methods such as principal component analysis (PCA) (Csicsvari et al., 2003; Gerstein and Clark, 1964; Harris et al., 2000), reduced feature set (RFS) (Salganicoff et al., 1988), Wavelet

based spike classifier method (WSC)(Letelier and Weber, 2000; Takekawa et al., 2010). The priority of these techniques is to select dimensions that allow efficient separation of spikes and eliminate those dimensions that are influenced by background noise.

4) Clustering: The final step in spike sorting is assigning the spike waveforms to the neurons that generated them a process termed as 'cluster cutting' (Harris et al., 2000). This process can be performed manually and/or automatically. Manual clustering involves visual identification of clusters in a two dimensional plot of spike features (Gray et al., 1995). However, this method is extremely time consuming and introduces human bias (Harris et al., 2000).

   Several automated parametric (Harris et al., 2000; Lewicki, 1998)and non-parametric (Fee et al., 1996) techniques have been developed allow automation and reduce human bias in clustering analysis. These algorithms are efficient, however it is necessary to visualise the clusters after the automated cluster cutting to confirm efficient separation. Furthermore, there is always a risk of over clustering (false positive) or under clustering (false negative) using automated spike sorting techniques making it utmost important to confirm appropriate separation.

Today there are several available software packages that allow automation of all the above mentioned steps and are also equipped with a graphical user interface to allow the visualisation and further modification of these separated clusters on the basis of the different extracted features (Harris et al., 2000; Hazan et al., 2006).

2.4.3 Local Field Potential (LFP)

LFP is the measure of the extracellular potential. The generation of this measure is quasi-stationery and unlike spiking activity which are influenced by action potentials, depends mainly on postsynaptic potentials (Buzsáki, 2004; Buzsáki et al., 2003a; Mitzdorf, 1985). For a long time neurophysiological information has been dominated by the measurement of spiking activity. However in recent times

LFP measurements have gained importance in evaluating brain functions especially cortical functions (Henrie and Shapley, 2005)by giving vital information about integrated synaptic potentials (Buzsáki et al., 2012; Einevoll et al., 2013; Lewis, 2012). Such information is vital to deciphering the complete picture of circuit mechanisms which cannot be provided by measurements of spike potentials alone.

Unlike electroencephalogram which is measured from the scalp or electro-corticogram LFP is measured by the insertion of the electrodes into the brain tissue using micro-electrodes. The LFP is then extracted by low pass filtering (cut-off set at 100 -300 Hz frequency) the recorded extracellular potential in a suitable time window. LFP measurements can be used for casual yet reliable investigation in awake animals (Liu and Newsome, 2006), it can also to some extent give an indication (at a subthreshold level) about the possibility of generation of actions potentials (Rasch et al., 2009, 2008). The most valuable information that can be extracted from LFPs are synaptic potentials (Mitzdorf, 1985)after potentials of somatodendritic spikes (Gustafsson, 1984) and membrane potentials (Harada and Takahashi, 1983) , which give a good understanding about intracortical processing. Such information cannot be derived by measuring only spiking activity. However, in spite of the local nature of this measure, the spatial resolution of this measurement compared to spiking events is relatively limited. For example, measurements in macaque AC using linear multi-channel electrodes (Kajikawa and Schroeder, 2011) showed that LFP measurements spread were over areas much greater than the believed ~ 300 µm diameter (Katzner et al., 2009)and additional parameters such as CSD values (second order derivative of LFP) (Mitzdorf, 1985) are needed to improve spatial resolution (Kajikawa and Schroeder, 2011).

2.4.4 Silicon-based electrodes in Acoustic trauma related pathologies

The ability of multichannel probes to record simultaneously from large neuronal networks can be extremely advantageous in the investigation of the laminar

dynamics of AI in normal and abnormal auditory processing. Also, these multichannel probes are able to span the entire length of the AI allowing relative measurements of tone evoked and spontaneous responses in all six layers by causing minimal tissue damage. Furthermore the geometrically accurate location of the recording channels would allow the accurate determination of the different auditory cortical areas which has been difficult to achieve with traditional recording devices. Previous investigations using multichannel linear silicon probes have provided invaluable information regarding the layer specific dynamics of tone evoked (Atencio and Schreiner, 2010a)and spontaneous (Sakata and Harris, 2009) responses.

Changes in tuning properties (Kimura and Eggermont, 1999)and SA (Noreña and Eggermont, 2003a)have been observed in AI following acoustic trauma using in vivo electrophysiology in anesthetised and awake animals. However, a large variability is seen in the observed results (Noreña et al., 2010). One explanation for this could be that the variability may arise due to the fact that in different experiments the measurements were made at different cortical depths. This observation maybe further complicated by the fact that layer specific changes may occur in the AI following acoustic trauma; for e.g, layers receiving the thalamic input (layer III/IV) may show changes in trauma related evoked response such as increase in threshold. These changes maybe subsequently buffered via cortico-cortical connections and not observed in layers involved in the next stages of intralaminar processing. Both these assumptions can be answered using silicon probes. The geometric precision of the recording channels on these probes would allow accurate cortical depth estimation across experiments and also provide details about layer specific AI changes following trauma.

2.5 Hypothesis

It is evident from data obtained from animal studies and human subjects that the AC is very likely involved in the development and progression of acoustic trauma related pathophysiology. Of the several electrophysiological investigations carried

out to measure changes in AC physiology following acoustic trauma, no studies to the best of our knowledge have investigated the trauma affected lamination of AC. Furthermore laminar investigation in other sensory core areas such as the primary visual cortex following visual deprivation (Maffei et al., 2004; Shatz and Stryker, 1978) or barrel cortex following peripheral deprivation (Bender et al., 2006; Petersen, 2007; Stern et al., 2001) show layer specific effects suggesting such mechanisms very likely exist in the AC especially the AI.

Recent development of large-scale extracellular recording techniques such as silicon probe recording now enables us to study the functional connectivity of large neuronal ensembles. This recording technique would allow the investigation of the laminar functionality of the AI in auditory processing. Furthermore, with clear evidence that the pathophysiology of auditory trauma related disorders such as hearing loss and tinnitus have a strong neural component, understanding the circuit mechanisms involved in the pathology of these conditions seems vital to help develop novel treatments.

In the present research which involves the acute electrophysiological investigation of the laminar profile of evoked and SA in rat AI following acoustic trauma using multi-channel silicon probes we tested the following hypothesis:

1) Normal auditory processing involves layer specific tone evoked responses in the AI. Based on evidence from the visual and barrel cortex it is very likely that the layers receiving primary thalamic input (layer III/IV and possibly layer V) show different response patterns (evoked and SA) compared to the layers not receiving major thalamic inputs.

2) Following trauma induction laminar specific changes will occur in the AI. These changes in tuning parameters such as threshold, CF would be observed mainly in regions receiving major thalamic inputs.

3) Following trauma, layer specific changes occur in SA and temporal properties of AI. Mainly, increase in SA would be observed in layers similar

to those showing changes in evoked patterns i.e. the thalamorecipient layers.

Identification of such layer specific changes in the AC cortex would help determine neural correlates of trauma related disorders allowing the development of potential treatments of this disorder.

2.6 Conclusion

The general background relevant to the current investigation is discussed in this chapter which lays the foundation for the proposed hypothesis of the current study.

The set-up of the experiments and the measurements of the different parameters quantified from the investigation will be discussed in the next chapter.

Chapter 3

Materials and Method

3.1 Summary

In this chapter Section 3.2, Section 3.3 and Section 3.4 explain the requirements and considerations for the present research. Section 3.5 explains the experimental set-up and procedure of silicon probe recording. Finally, details of the analysis and different parameters established to measure evoked and SA response are explained in Section 3.6.

3.2 Subjects

Ninety nine, eight to ten weeks old male Sprague Dawley (SD) rats (Inbred, University of Strathclyde) weighing 290 g-430 g (349 ± 31.47 g, mean ± SD) were used in the acute, urethane anesthetised studies. All procedures were carried out in accordance to the UK home office regulations.

Animal Housing: The animals were housed in groups of four to five in an enriched environment with a 12 hour light/dark cycle. Food and water provided ad libitum.

3.3. Materials

3.3.1. Solutions

Table 3.1 Details of solutions used during surgical preparations for in vivo electrophysiology

Name	Supplier	Procedure	Other details
Phosphate Buffered Saline (PBS)	Sigma	-	-
Urethane	*Acros*	20% w/v solution in 0.1 M PBS	97% strength, Ethyl carbamate, $C_3H_7NO_2$
Agar	Fisher Scientific	-	Granular powder

3.3.2. Multichannel Silicon probe

Either a sixteen or a thirty two channel NeuroNexus, linear, single shank, acute iridium probes (A1x16-5mm-100-177-A16, A1x32-6mm-50-177-A32) was used for in vivo electrophysiology recordings. The complete assembly for acute recording is as shown in Figure 3.1A. 'A' series package was used to connect the electrode array (Figure 3.1B) to the head-stage (Figure3.4). Further specifications of the electrode array for each of the probes are as shown in Table 3.2.

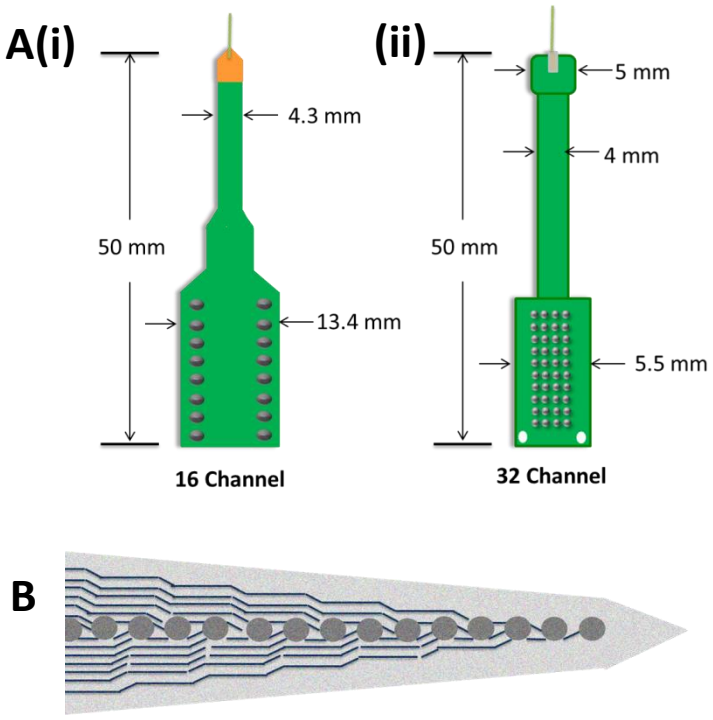

Figure 3.1A. Shows the 'A' series package for 16 and 32 channel linear probe ((i)and (ii)respectively). **B**.Linear electrode array for 16 and 32 channel linear probes .

Table 3.2 Specifications of recording channels

Number of channels	Distance between channels	Distance covered by recording channels	Diameter of recording channel	Area of recording channel
16	100 µm	1550 µm	15 µm	177µm^2
32	50 µm	1550 µm	15 µm	177µm^2

3.4. Auditory Stimulation

3.4.1 System set-up

Auditory stimuli were generated digitally using System 3 Tucker-Davis Technologies (TDT) system (Figure 3.2) and presented free-field through an electrostatic speaker (ESI, Tucker Davis Technology). Another speaker was used to present loud noise (acoustic trauma). The speakers were calibrated using a microphone (ACOpacific).

Calibration: The microphone was placed directly facing the speaker, approximately at the midpoint of the speaker. Sounds at different intensity were presented via the Tucker-Davis system and measured (recorded) using LabVIEW software.

The calibration system (Figure 3.4) was set up in a single walled acoustic chamber (MAC-3, Industrial Acoustic Company, NY)(Figure 3.3); the interiors covered with three inches of acoustic absorption foam.

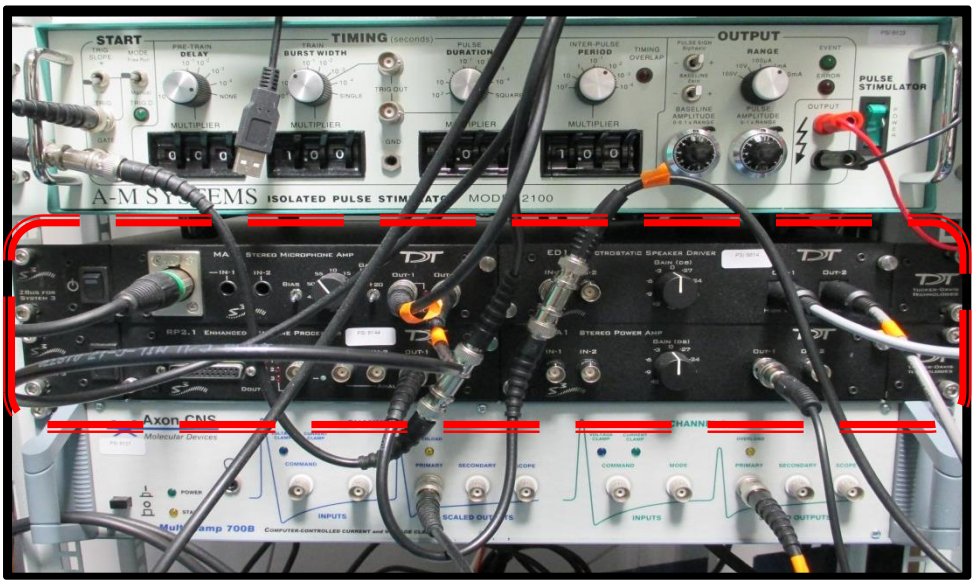

Figure 3.2. System set-up for sound presentation using TDT system (encapsulated in red box)

Figure 3.3 Acoustic chamber (MAC-3, Industrial Acoustic Company, NY)

3.4.2. Sound Presentation

Auditory stimuli for in vivo electrophysiology: Short pips and long tones at various frequency intensity combinations were presented before and after trauma (see Figure 3.9).

3.4.2.1 Short pips

Short pips were 50 milliseconds long with 5 milliseconds cosine ramps; 1/6th octave steps, frequencies 2-32 kHz; intensity 0-80 dB SPL in 10 dB steps; at a rate of 2.5 Hz (350 msec interval between consecutive stimuli). Each frequency/intensity (225) combination was repeated 20 times, equalling a total of 4500 short pip stimuli presented during each time point of recording (see Figure 3.9).

3.4.2.2 Acoustic trauma

An octave band noise centred at frequency 16 kHz and intensity 110 dB SPL was

presented for an hour. The selection of parameters for trauma induction was based on findings from previous literature (Table2.2). Based on behavioural audiograms or ABR recordings frequencies at which maximum hearing sensitivity can be determined e.g. humans is 4 kHz (Heffner and Heffner, 1991), and rats is 16 kHz (Syka and Rybalko, 2000). Also, as seen in studies involving induction of acoustic trauma in rats, threshold shifts are usually observed at the maximal hearing frequency in rats making it the frequency of choice for trauma induction (Bauer et al., 2007; Zhang and Kaltenbach, 1998). Furthermore, it is seen that effects of acoustic trauma in rats last longer when an octave noise is used instead of pure tones (Llano et al., 2012; Norman et al., 2012).In these studies, rats exposed to the above mentioned parameters (intensity, frequency, time) showed both neural and behavioural signs of hearing loss and pathologies like tinnitus (Table 2.2 ,Bauer et al., 2007; Scholl and Wehr, 2008; Sun et al., 2012) . In control groups, the trauma period was replaced by an hour of silence.

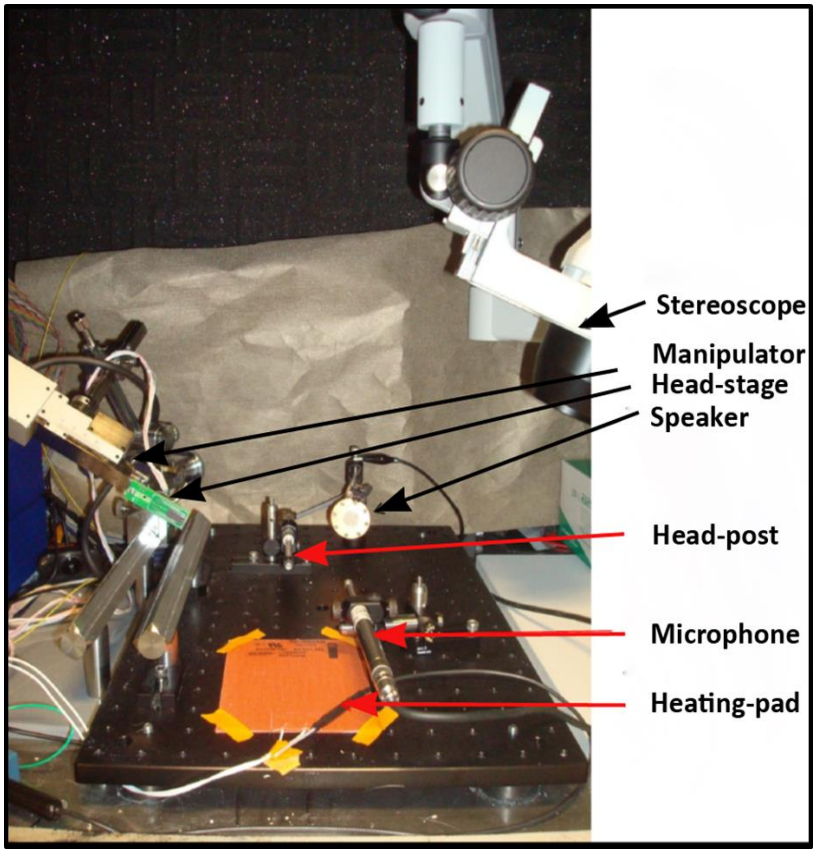

Figure 3.4 System set-up for in vivo electrophysiology investigation

3.4.2.3 Long tones:

Long tone presentations were 500 msec long with 10 millisecond cosine ramps; ½ octave steps, frequencies 2-32 kHz; intensity 30 and 60 dB SPL at a rate of 1.2 Hz (350 msec interval between stimuli). Each frequency/intensity (eighteen) combination was repeated a 100 times, equalling a total of 1800 long tone stimuli presented during each time point of recording (see Figure 3.9). Long tones allow accurate measurements of onset and offset of response and that is why they were measured. However, this data could not be used analysed due to sparse sampling.

3.5. In vivo electrophysiology

3.5.1. Experimental set-up

Animal preparation: The animals were anesthetized with urethane anaesthesia intraperitoneal (i.p) 1.5 g/Kg or 1.6 g/Kg) and placed on a heating pad (120 V, 100 Watts) (Figure 3.4) and body temperature maintained (at 37 C) using a DC temperature controller (FHC) and recorded throughout the experiment. The depth of anaesthesia was confirmed throughout the experiment by measuring the tail-pinch and foot-withdrawal reflexes.

Surgery and insertion of probe: Once absence of above mentioned reflexes were confirmed, the head was shaved and skull exposed by cutting the skin. Two holes were drilled into the skill anterior to bregma (Figure 3.6A) and two bone screws (F.S.T, 4 mm length, shaft diameter 0.85 mm) inserted (Figure 3.5) in this location for anchoring.

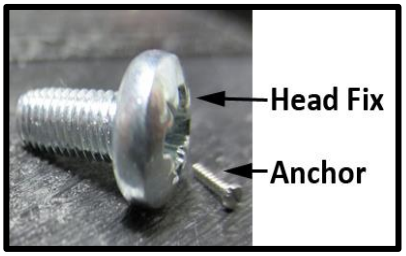

.

Figure 3.5 Screws used for anchoring and fixing the head.

A similar screw attached to the connector was inserted at a location posterior to lambda (Figure 3.6A) as ground. Once the ground screw was inserted, the large screw (Cap type or pan head) for head-fix (Figure 3.5) was placed anterior to the anchor screws using dental cement (Simplex Rapid Powder mixed with Simplex Rapid Liquid)(Figure 3.6B).

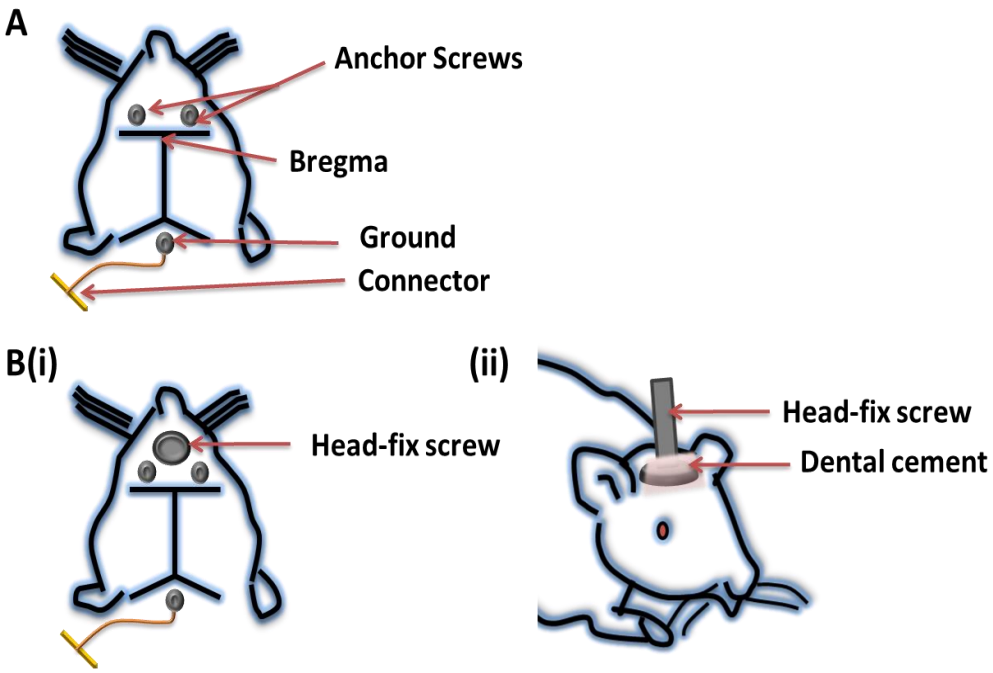

Figure 3.6 Procedure for electrophysiological recording. **A.** Location of anchor and ground screws. **B** Location of head-fix (i) top view (ii) side view, using dental cement. Screws used for anchoring and fixing the head.

Once the head-fix was securely attached to the skull, the head screw was attached to the head-post (Figure 3.4). The left AI was exposed by first removing the temporal muscle, followed by craniotomy and duratomy between 5 mm and 6 mm posterior to bregma. Following duratomy, the area was kept moist with saline maintained at 37 degrees.

The major blood vessel that passes through the region and the stereotaxic co-ordinates for the frequency organisation was used as an indication for AI (Doron et al., 2002; Rutkowski et al., 2003; Sally and Kelly, 1988) and the probe was

inserted perpendicular to the cortical surface at a rate of 3 µm per second using a motorised micro-manipulator (NARISHIGE, Japan). The 16 kHz frequency region was targeted as changes in tuning properties is usually observed around the region of presented trauma frequency which in this case was centred at the 16 kHz frequency region. However, as later discussed in Chapters 4 & 5 recordings were invariably made from different frequency regions. This is possibly due to the fact that the weights of rats used in the study varied from one experiment to the other which may have affected the specificity of the co-ordinates used to determine the desired frequency region. At a depth of 600 µm from the cortical surface, evoked response to short pips were visualised in the raw trace to further confirm location in AI. If a response similar to the one indicated in Figure 3.7 was not seen (which is the usual response to tone presentation seen in the AI), the probe was retrieved and inserted at another location till the expected response was seen. Once location was confirmed the probe was further inserted to the desired depth (~ 1600 µm) and the area covered with 1% agar solution (Table 3.1) to keep the cortical surface moist and to reduce pulsation. After that, the acoustic chamber was closed and the set-up was allowed to stabilise for a period of ninety minutes.

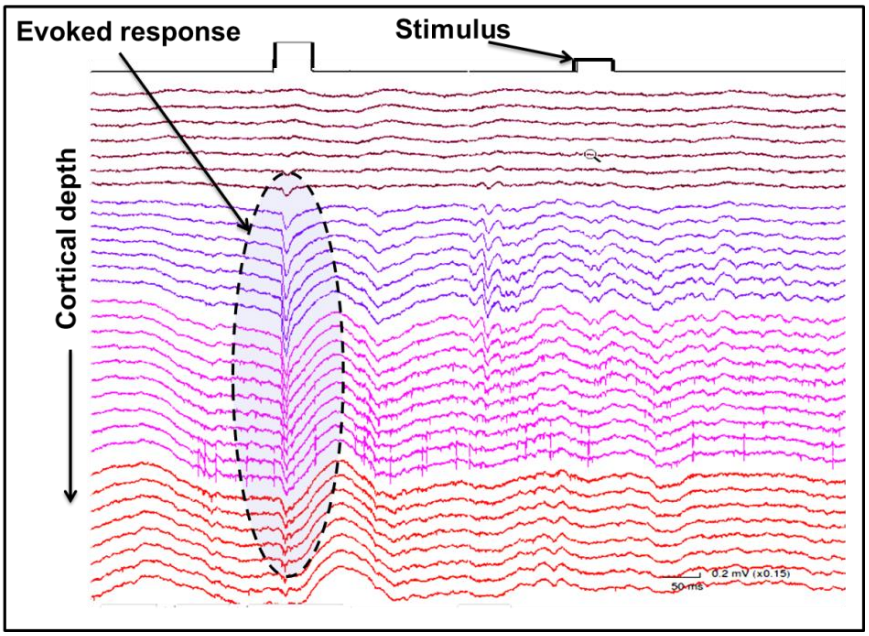

Figure 3.7 Expected auditory evoked response in AC

3.5.2. Sound presentation

Following stabilisation of recording, five minutes of SA was measured after which short pips followed by long tones were presented (pre) through a speaker directly facing the animal at a distance of 10 cm (Figure 3.4, and Figure 3.8). On completion of tone presentation another five minutes of SA activity was measured. This set of sound presentation was followed by an hour of trauma induction. Trauma intensity was delivered via a second speaker placed at a distance of 2 cm from the right ear and 2 cm from the floor of the experimental stage (Figure 3.8). The trauma speaker was kept closer to one ear than the other to achieve the high intensity sound which was otherwise not technically possible using the available hardware. Following trauma a similar set of sound presentation as discussed in 'pre' were repeated twice i.e. 10 minutes after trauma for (post1) and 10 minutes after post 1 (post 2). The details of sound presentation are summarised in Figure 3.9. The various steps involved in silicon probe recording is summarised in Figure 3.10. On completion of the experiment, the animal was sacrificed with an overdose of urethane anaesthesia.

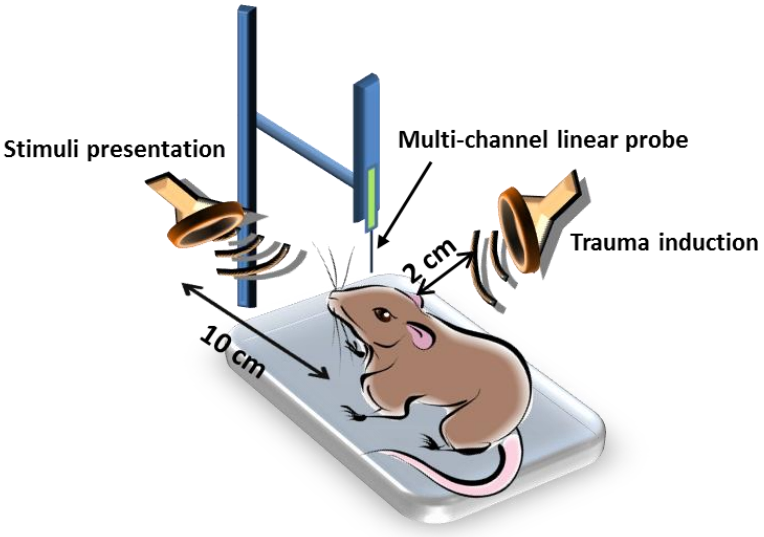

Figure 3.8 Experimental set-up showing location of speaker for trauma induction and stimuli delivery

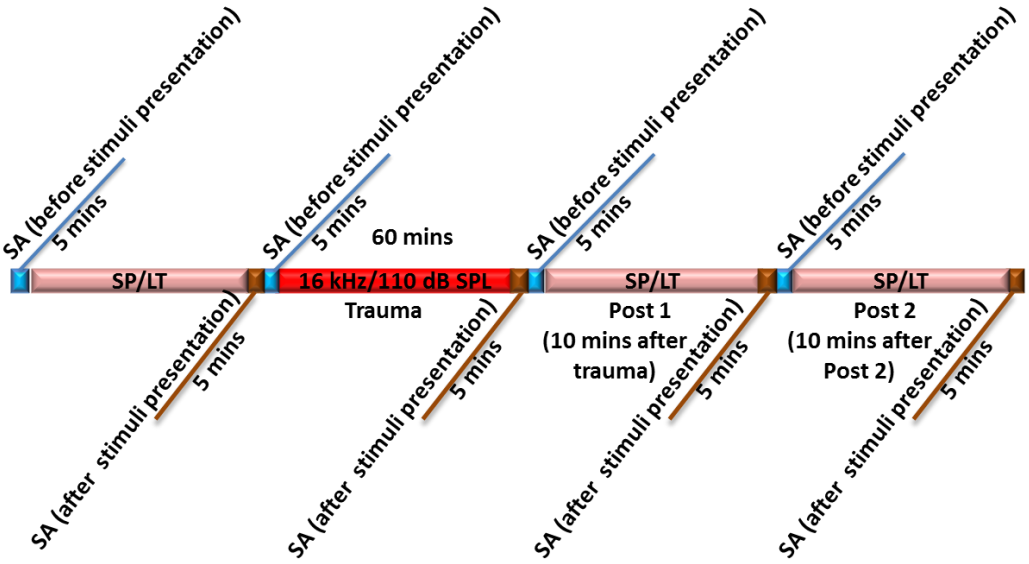

Figure 3.9 Summary of various time points for recording of evoked response (pre, post 1; where recording was started 10 mins after the completion trauma presentation and post 2; where recording was started 10 mins after completion of post 2) and SA before (light blue) and after (maroon) stimuli presentation during in vivo recording of neuronal

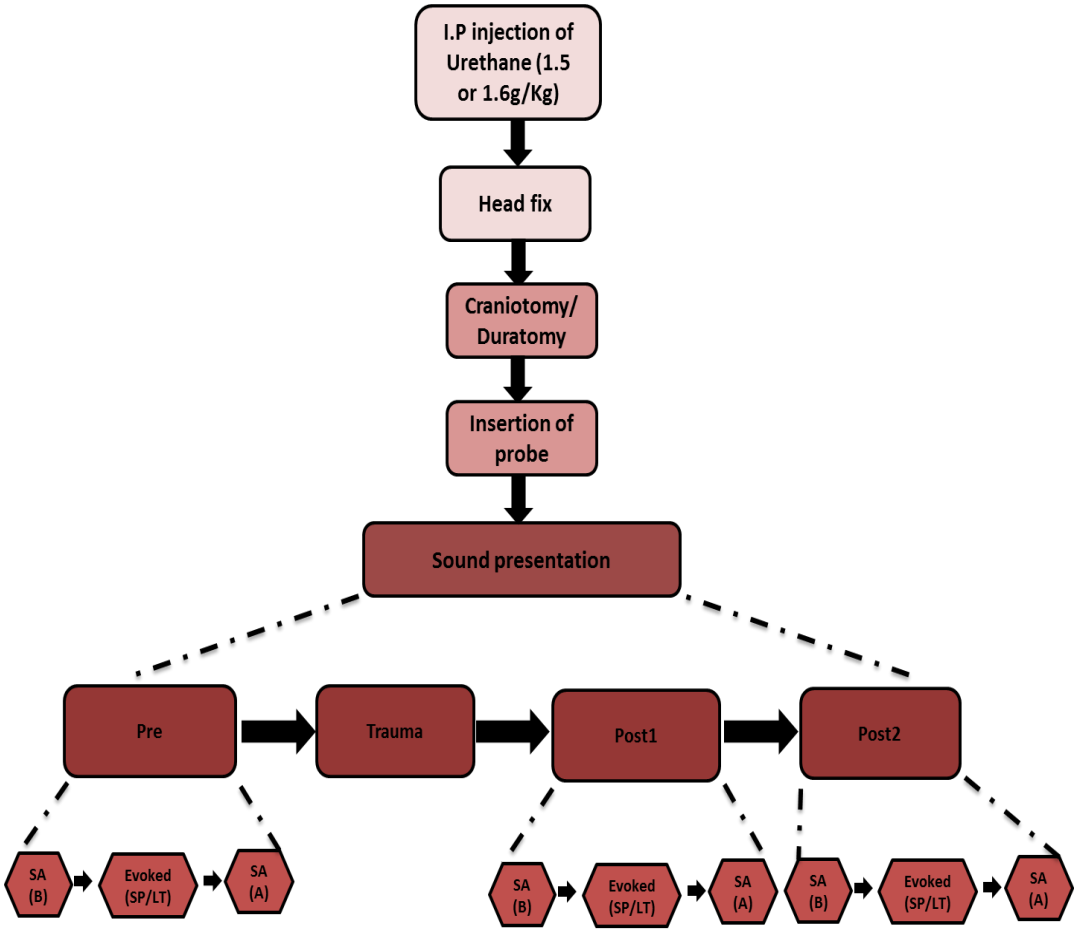

Figure 3.10 Summary of the various steps involved in silicon probe recording starting at anaesthesia induction and finishing with the various recordings of evoked and SA obtained for further analysis. B- Before, A- After. SP-Short pips, LT-Long tones.

3.6. Offline data processing

3.6.1 Spike Sorting

On completion of silicon probe recording, the raw traces were visualised offline for visual inspection (confirmation of evoked response, quality of recording) using the freely available online software NeuroScope (http://neurosuite.sourceforge.net/)(Hazan et al., 2006). Information about spiking response was then extracted from the raw data using the spike sorting system 'EToS' (Efficient technology of spike sorting)(Takekawa et al., 2010), the steps involved in this process are summarised in Figure 3.11. The sampling frequency was 20 kHz and sampling window set to 50 µsec. The raw data was first passed through a band -pass filter set at 800 Hz – 3000Hz, filter order 50, and window 'Hamming type'. This step was essential to eliminate low frequency fluctuations (Local filed potential (LFP)) on the lower end and higher frequency fluctuations (artefacts) on the other. The spike candidates were then detected by amplitude thresholding where the threshold was set to -5*Robust estimation of Standard deviations (RSD)(Quiroga et al., 2004; Takekawa et al., 2010, 2012)

$$RSD = (median|x - MED|)/0.6745$$

Where x is filtered signal, MED is the overall median of x). The features of the waveforms were then extracted using the Wavelet transform method (WT). Finally spikes for each channel were clustered automatically using a mixture model of students *t*-distribution (robust variational Bayes model (RVB) (Takekawa et al., 2010, 2012)). The clusters were further evaluated visually to eliminate artefacts using the freely available software Kluster (http://neurosuite.sourceforge.net/). Further manual clustering was not performed and only multi-unit activities (MUAs) were analysed in this study as at this stage of the project the aim was to determine laminar specific changes which could be quantified using MUA. Only if changes were observed SUA would be required to for further investigation of cell types involved in these changes.

However, such investigations involved the next stage of the project which was beyond the scope of the present investigation.

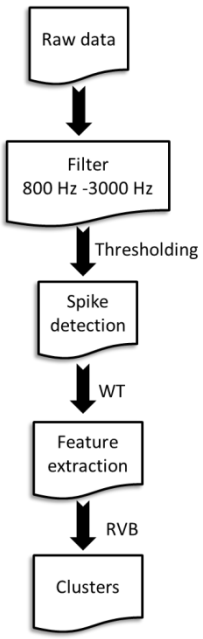

Figure 3.11 Steps in involved in spike sorting using EToS

3.6.2 Data analysis

3.6.2.1 MUA

After manual clustering in Klusters, all further analysis was performed in MATLAB (MathWorks). To establish the cut-off line for auditory evoked responses above baseline firing, several criteria used in previous literature were evaluated for the present data set. Table 3.3 summarises the different criteria that were used to set the cut-off line. Based on the results obtained using all of these parameters, by visual interpretation as shown in Figure 3.12A, we found that mean spontaneous firing rate plus 20% of peak firing rate (Sutter and Schreiner, 1991) was the most reliable (See Figure 3.12A). Reliable interpretation indicates that after elimination of background (Figure 3.12A, far right) using the cut-off criterion (Figure 3.12A, middle), a clear tuning curve was obtained, that allowed true measurements of tuning parameters. For e.g. if in this instance the 2SD criteria was used (Table 3.3),

the criteria was extremely conservative and would not be truly representative of the data set (Figure 3.12B).

Table 3.3 Different threshold criteria

Criteria for threshold response	**Reference**
Mean SA+ 2 SD (also evaluated Mean SA+ 1SD and Mean SA +1.96 SD)	(Zhang et al., 2011)
Mean SA+20% peak firing rate (also evaluated Mean SA +15% peak firing rate)	(Moshitch et al., 2006)
Mean SA+20% (Max(evoked response)-mean SA)	(Sutter and Schreiner, 1991)

Computing the cut-off line, tuning curves (frequency responsive areas) (plot of intensity versus frequency) were plotted to quantify the following features of evoked response (where response to a stimulus shows number of spikes were greater than or equal to 2) (Figure 3.12A). These were measured in 50 msec time windows following stimulus onset.

Threshold- Minimum intensity at which an evoked response (number of spikes were greater than or equal to 2) is measured.

Characteristic frequency (CF) -Is the stimulus frequency at threshold requires to elicit a neuronal response (number of spikes greater than or equal to 2).

Bandwidth (BW) – Is the difference between highest frequency and the lowest intensity stimulus eliciting a neuronal response at 10 dB above threshold intensity. Another parameter 'Q10' is often used as a criteria to measure sharpness in tuning curves (Noreña et al., 2003; Wallace and Palmer, 2008). However, because lifetime sparseness (see below) is another measure for tuning sharpness and generalizable

even for non-U/V-shape tuning curves (Sakata and Harris, 2009), we took lifetime sparseness to measure sharpness in tuning curves.

Sparseness- Was calculated using the a non-parametric statistic (Vinje, 2000), where Sparseness (S) is

$$S = (1 - \frac{A}{B})/(1 - \frac{1}{n})$$

Where A= $(\sum(r/n))^2$, B= $\sum(r^2/n)$, r= Response to a particular stimulus, averaged across trials and n= Total number of presented stimuli.

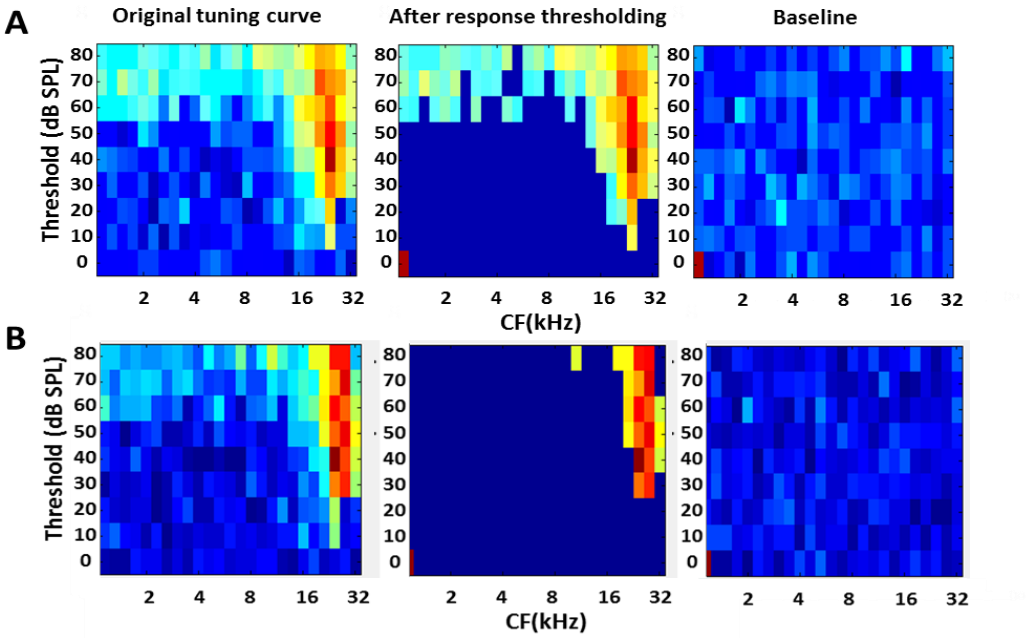

Figure 3.12 A. Example of tuning curve after eliminating baseline using the set threshold criteria and **B.** Example of tuning curve after eliminating baseline when Mean SA+2SD criteria is used

SA- As discussed in Section 3.5.2 (Figure 3.9 and 3.10), SA activity was recorded before and after sound presentation for a period of five minutes each during each set of recording (pre, post1, post2). SA was also measure just before each stimuli presentation (Background activity) in a 50 msec time window (further details discussed in Chapter 4, Section 4.3.5 and Chapter 5, Section 5.2). SA was measured as the number of spikes per second. This value was averaged over time (five minutes for SA before and after stimuli presentations).

The above parameters were calculated for each channel (i.e. every 50 µm depth for a 32 channel silicon probe and every 100 µm for a 16 channel silicon probe). However to enhance visual and statistical interpretation of the results (Chapter 4 and Chapter 5) the values across every 200 µm of cortical depths were averaged for further analysis (200 µm resolution). Initial analysis confirmed that such averaging did not alter the results from that seen in the non-averaged data.

A summary of the various evoked response and SA response data obtained from the silicon probe recording is provided in the Figure 3.13 and Figure 3.14 respectively.

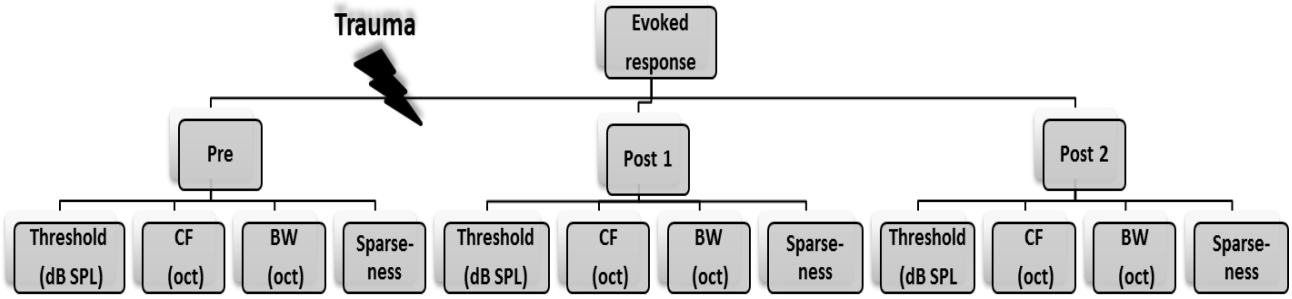

Figure 3.13 Summary of the various tuning curve parameters quantified from silicon probe

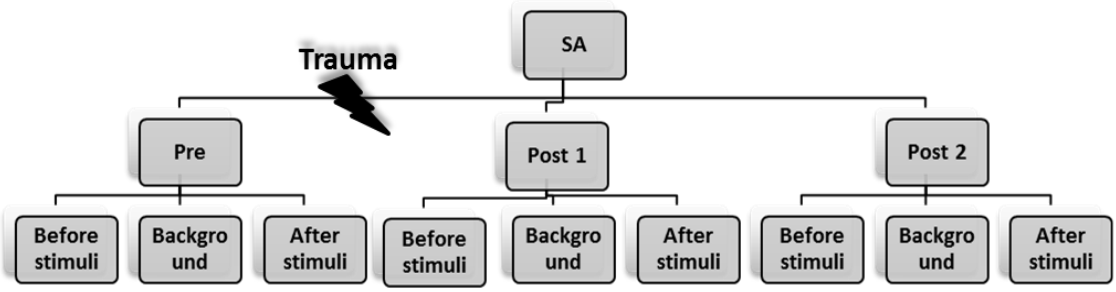

Figure 3.14 Summary of the various SA quantified from silicon probe. Background is measured 50 msec before stimuli presentation.

3.6.2.2 Local Field Potential (LFP) and Current-source Density (CSD)

For LFP measurements, the data sets were passed through a low pass filter set at 30 Hz. Following filtering, LFP data was extracted in a time window of 400 msec (100 msec before stimulus onset).

CSD analysis allows the estimation of current entering and leaving a certain region (Mitzdorf, 1985). One dimensional CSD analysis was applied to measurements post-stimulus (only 80 dB SPL) bandpassed filtered data (between 1 Hz to 300 Hz).

$$CSD = (V_i + V_{i+2} - 2 * V_{i+1})/dX^2$$

Where 'i' is the channel, 'V' is the filtered data and X- inter-electrode spacing (50 µm for 32 channel probes and 100 µm for 16 channel probes.

CSD analysis allows estimation of sources (current leaving a region) and sinks (current entering the region). The channel showing the largest sink measurement (max CSD value) via CSD analysis is in agreement with thalamic recipient layers (layer III/IV) in rat AI (Kaur et al., 2005; Sakata and Harris, 2009)and was used as an alignment point (indicated as 0 µm cortical depth to align layers across experiments). This measurement was vital to allow the accurate estimation of different cortical layers as the probe insertion depth would vary from one experiment to the other.

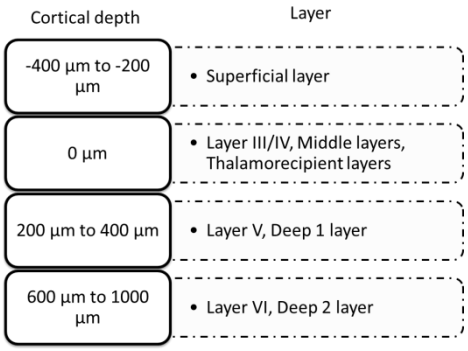

Figure 3.15 Estimation of different layers based on CSD analysis

Application of CSD analysis to the current data set is discussed in further detail in Chapter 4 and Chapter 6).

3.6.2.3 Statistical analysis

All statistical analysis was performed in MATLAB and GraphPad Prism software (version 5.00 for Windows, San Diego California USA, www.graphpad.com). One-way ANOVA and Bonferroni posthoc analysis were used to statistically evaluate baseline data and overall cortical shifts, where p values greater than 0.05 were considered to be significant. For laminar shifts following acoustic trauma the data were subjected to two-way ANOVA (ANOVAN function in MATLAB) and Bonferronis posttest comparisons, where p values greater than 0.05 were considered to be significant.

3.7 Conclusion

The first half of the chapter provides a summary of the steps involved in silicon probe recording protocol and the selection criteria for the different protocol parameters were discussed. The other half of the chapter provides details of the method used for spike clustering. MUA was evaluated from spike data by quantifying various tuning curve parameters. SA was also measured at various time points. Finally a detail of CSD analysis, the parameter used to align layers across different experiments is discussed.

Chapter 4

Results 1- Database and laminar profile of neural population activity in AI before acoustic trauma (Baseline)

4.1 Summary

This chapter provides the summary of the entire data set used for analysis and the baseline laminar profile of sensory evoked response (four tuning curve parameters) and SA in the AI. Section 4.2 summarises the entire data set and provides various details of the different evaluation criteria used to determine the validity of data sets for further analysis. Section 4.3 shows the distribution of the data at various depths and the normalised response in the primary AC in response to 50 millisecond (msec) long short pips which are then summarised in Section 4.4.

4.2 Selection of Data

As seen in column 1 of Table 4.1 a total of ninety-nine in vivo electrophysiology experiments using 32 or 16 channel linear probes were carried out. Of these, twenty five experiments were conducted for optimisation of experimental set-up; which included the technique for head fix, establishing technique for insertion of probe, location of speakers for sound delivery, and time protocol for the study. As mentioned in Chapter 3, Section 3.5.1, location in AI was targeted using the rat frequency map stereotaxic co-ordinates (Doron et al., 2002). Such a response would not be seen in PAF and AAF. Furthermore, even though the 16 kHz frequency region was targeted during each experiment, recordings were invariably made from different frequency regions. This may be due to the fact that a range of weights were used across experiments which would have affected the specificity of the co-ordinates used to map the frequency map in AC. Once the experimental set-up was established 74 experiments were performed of which 66 experiments (trauma) involved exposure to acoustic trauma and 8 experiments for which there was no trauma (control) presented (Appendix 2 (A,B) and 3(A,B)).

Of these 74 experiments, several data sets could not be completed due to several surgical or technical issues (Figure 4.1 A, Table 4.1 column 2). Twenty-two animals were lost due to surgical complications such as, anaesthesia, excessive bleeding during craniotomy or duratomy. Fifteen of the remaining experiments had several

technical issues such as, no auditory evoked response, no spikes, or issues with the tone presentation.

Table 4.1 Outline for the entire data-set and evaluation of suitable experiments for evaluation of laminar changes in AI following acoustic trauma acoustic trauma. The first column represents the total number of experiments and the overall aim of the studies. As we move from left to right of the table, the different columns indicate the various evaluation criteria for suitable experiments.

Total number of experiments (n=99)	Total number of Successful experiments (n=37)	Total number of successful experiments after laminar profiling (n=25)	Experiments in each frequency band (n=25)
Optimisation (n=25)			
Control Experiments (n=8)	**Control Experiments** (n=6)		
Acoustic trauma Experiments 32 channel linear probe (n=59) 16 channel linear probe (n=6) 4x2 tetrode (n=1)	**Acoustic trauma Experiments** 32 channel linear probe (n=26) 16 channel linear probe (n=4) 4x2 tetrode (n=1)	**Acoustic trauma Experiments** 32 channel linear probe (n=23) 16 channel linear probe (n=2)	**2-8 kHz** (n=9) **8-16 kHz** (n=10) **16-32 kHz** (n=6)

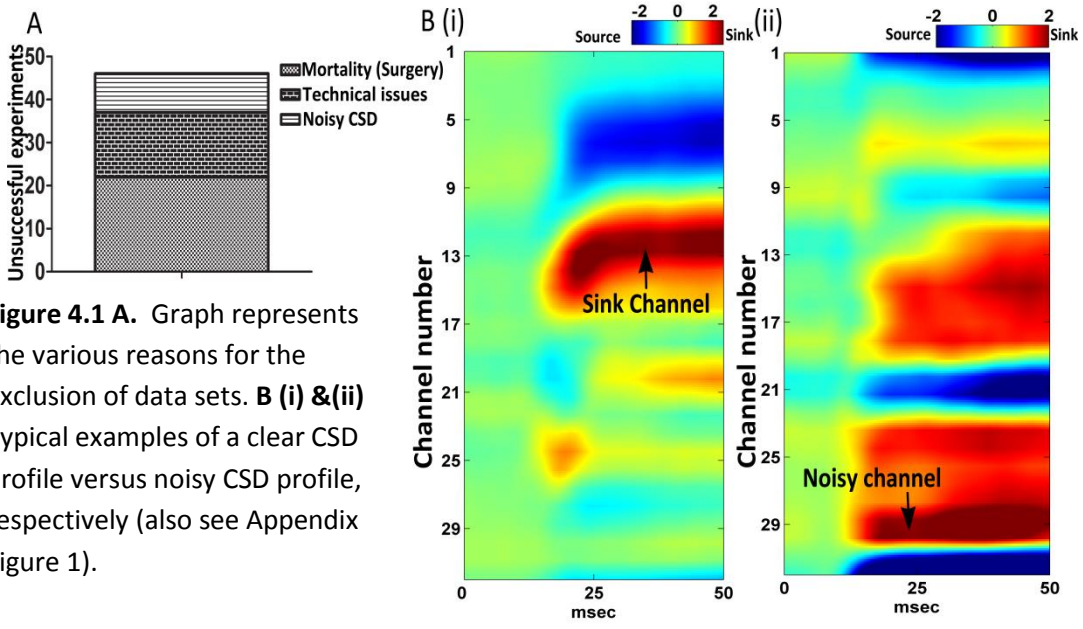

Figure 4.1 A. Graph represents the various reasons for the exclusion of data sets. **B (i) &(ii)** Typical examples of a clear CSD profile versus noisy CSD profile, respectively (also see Appendix Figure 1).

Figure 4.2 represents the scatter plot of baseline threshold versus characteristic frequency for the remaining thirty seven data sets. A locally weighted regression 'loess curve' was used to measure the trend in the scatter plot (smooth the scatter plot) and was and was found to be a good fit to the data set. This plot was used to confirm the location of the recording in the AI (Kimura and Eggermont, 1999; Noreña and Eggermont, 2003a)

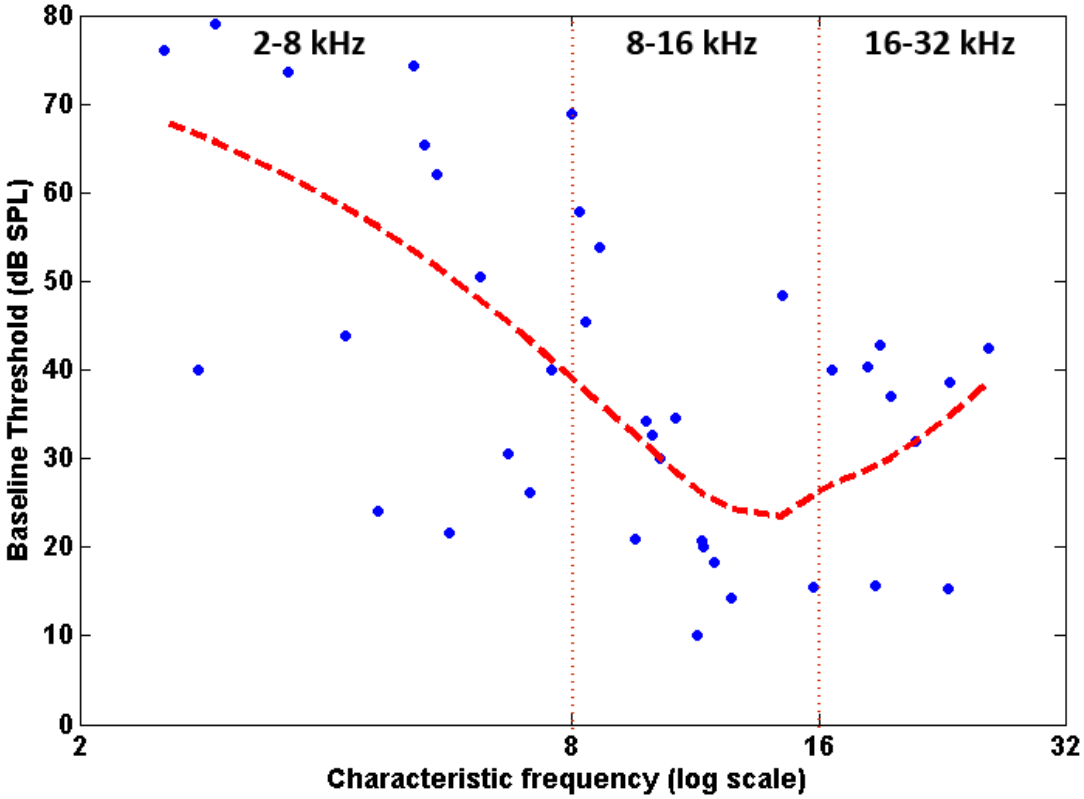

Figure 4.2 Scatter plot of mean baseline threshold value against mean CF on a log scale. Line represents loess curve. The above plot illustrates the distribution of CF in the AI. The dotted vertical lines show the division of data sets based on CF for further evaluation in Chapter 5. Red dashed line represents a moving average (loess curve)

Once the location was confirmed, the laminar profiles of all the data sets were determined using CSD analysis. CSD analysis was used to determine the largest sink channel (Figure 4.1 B (i)) to determine the channel for alignment across all data sets (see Chapter 3 Materials and Methods). In a few experiments due to repeated use of the silicon probe, some of the channels in the linear probe were unstable and caused large fluctuations in the recording (See Appendix Figure 1).

This could have generated a false interpretation of the sink channel (Figure 1B (ii)) and were not used for further analysis (Table 4.1 column 3, n=9).

The remaining data sets were then used to determine the laminar profile of tuning curve parameters in AI during normal auditory processing.

Based on CSD analysis and the fact that the calculated value represented a 200 µm resolution of cortical depth (see Chapter 3 Materials and Methods) the layers were classified based on previous investigations (Kaur et al., 2005) into: -400 to -200 µm as superficial layers (presumptive L2/3), 0 µm as middle layers or thalamorecipient layers (L4), 200 µm to 400 µm as Deep 1 (LV) and 600 µm to 1000 µm as Deep 2 (L VI).

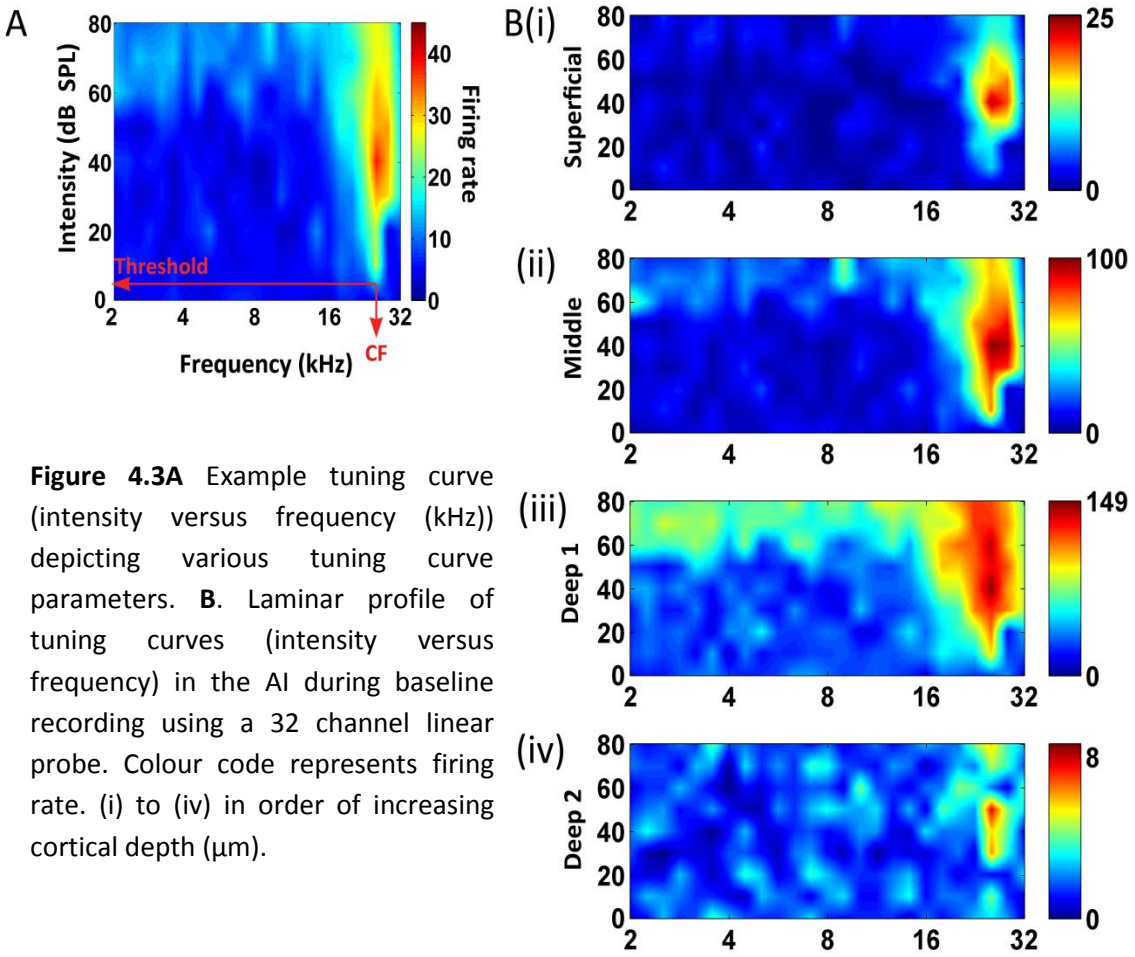

Figure 4.3A Example tuning curve (intensity versus frequency (kHz)) depicting various tuning curve parameters. **B**. Laminar profile of tuning curves (intensity versus frequency) in the AI during baseline recording using a 32 channel linear probe. Colour code represents firing rate. (i) to (iv) in order of increasing cortical depth (µm).

4.3 Laminar profile of tuning parameters before acoustic trauma

4.3.1 Characteristic frequency (CF)

Figure 4.4 shows the laminar profile of CF in AI. Figure 4.4A shows the distribution of CF values across different cortical layers in AI (n=25) on an octave scale (spanning four octaves; 2 kHz to 32 kHz). Figure 4.4B shows the normalised mean across the different layers (n=25). For normalising, the data points at each cortical depth were normalised against the mean value of that layer. As seen in Figure 4.4B, even though a tendency for a difference in CF values across the different cortical layers is observed (between -400 µm and -200 µm, this may be partly due to the nosier measurements of tuning parameters in layers I/II) no statistically significant difference was found in the CF values between the different cortical layers (one way ANOVA, p=0.3622, n=25) indicating a similar functional organisation of CF within cortical columns (Abeles and Goldstein, 1970).

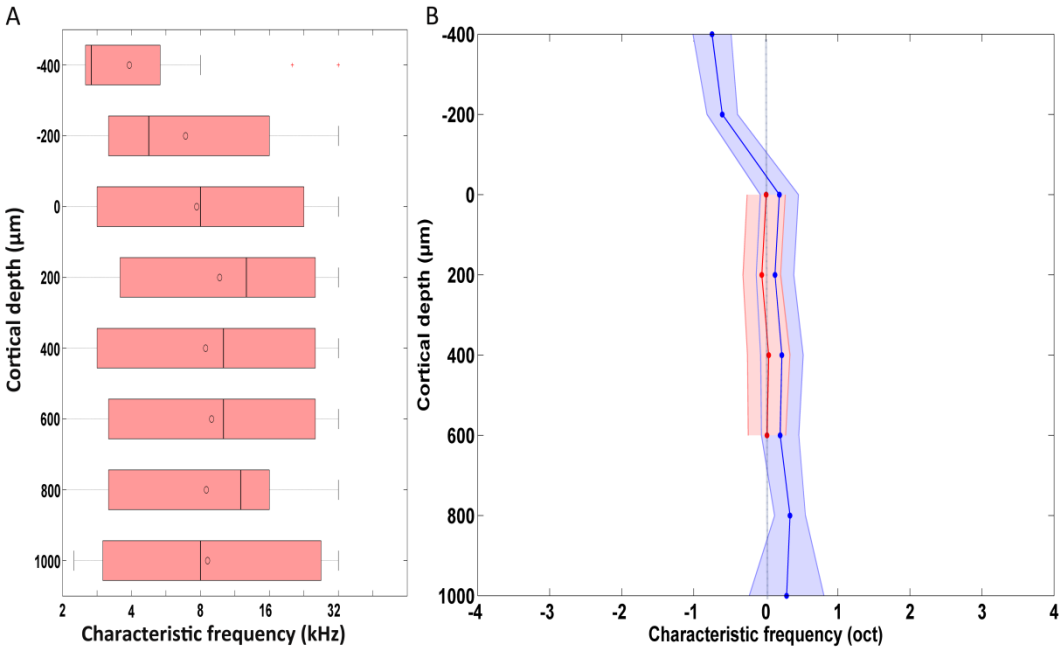

Figure 4.4 Depth profile of characteristic frequency (CF) during baseline sound presentation (n=25). **A.** Box and whisker plots on an octave scale. Circles represent mean value and lines represent median **B.** Depth profile across all cortical layers (blue) overlapped by depth profile for layers III, IV & V 1 layer(red) on an octave scale. Solid coloured lines represent mean values; shaded region represents SEM. No significant difference in CF was seen across any of the layers.

To confirm this evaluation, CF values were re-plotted by eliminating layers I,II & V (Figure 4.4 B, shaded red) and a similar functional organisation of CF across depths was observed.

4.3.2 Threshold

Figure 4.5 shows the baseline laminar distribution of threshold (dB SPL) in the AI. Figure 4.4.A shows the distribution of the threshold values across the different cortical depths as box and whisker plots. Figure 4.5B shows normalized mean across different layers. For normalising, the data points at each cortical depth were normalised against the mean value of that layer. Once again as seen in the CF distribution, even though a tendency for a difference in laminar profile across the different cortical depths is observed (layers I, II & VI layer compared to layers III,IV & V), no statistical difference was observed across the different cortical layers (one way ANOVA, p=0.0847).

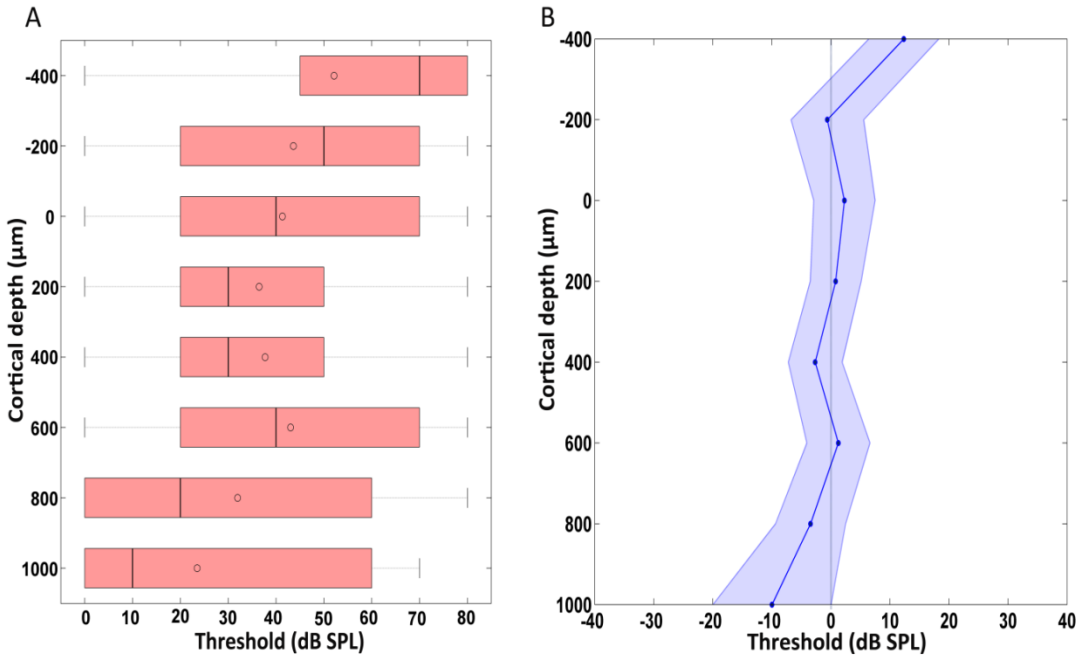

Figure 4.5 Depth profile of threshold (dB SPL) during baseline sound presentation (n=25) **A.** Box and whisker plots. Circles represent mean value and lines represent median **B.** Depth profile across all cortical layers (blue).Solid coloured lines represent mean values; shaded region represents SEM. No significant difference in threshold was seen across any of the layers.

4.3.3 Sparseness

Another useful tuning parameter is sparseness which is often used to measure neuronal population activity (Olshausen and Field, 2004) in the visual cortex (Vinje, 2000). There are several ways to measure sparseness (Willmore and Tolhurst, 2001; Willmore et al., 2011). However, in this investigation we reported only 'Lifetime Sparseness'. In this measurement values would tend to zero when neurons respond to most stimuli (dense) and tend towards one when responses were observed only against selected stimuli (sparse) (Vinje, 2000). For example if evoked response as represented by the tuning curve in Figure 4.6A were to shift to Figure 4.6B, the value of sparseness would shift from a more dense representation to a sparser representation. Figure 4.7 represents the laminar profile for sparseness in the primary auditory cortex in response to 50 msec short pips. Figure 4.7A shows the distribution of sparseness values across the different cortical layers as box and whisker plots. The mean and SEM values are visualised in Figure 4.7B. As seen in previous literature (Sakata and Harris, 2009) layers I/II (-400 µm to -200 µm) and layer VI (800 µm to 1000 µm) show a sparser response compared to the layers II,IV & V (0 to 600 µm) with the layer V being the most dense (see Table 4.2) (n=25, one way ANOVA, $p<0.0001$) .

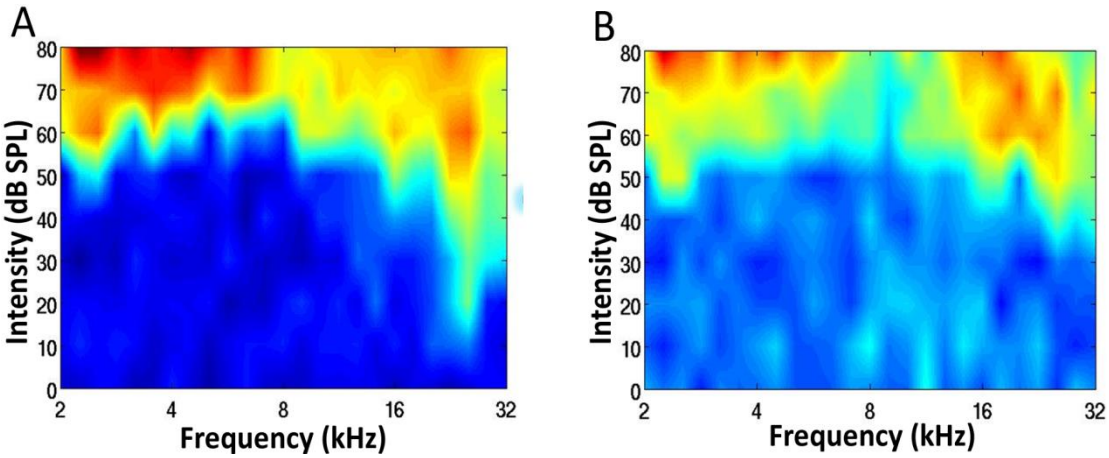

Figure 4.6 Example of tuning curves representing sparse versus dense response. **A.** Neurons respond to a large fraction of presented stimuli. **B.** Neurons respond relatively to a smaller set of presented stimuli (as compared to A).

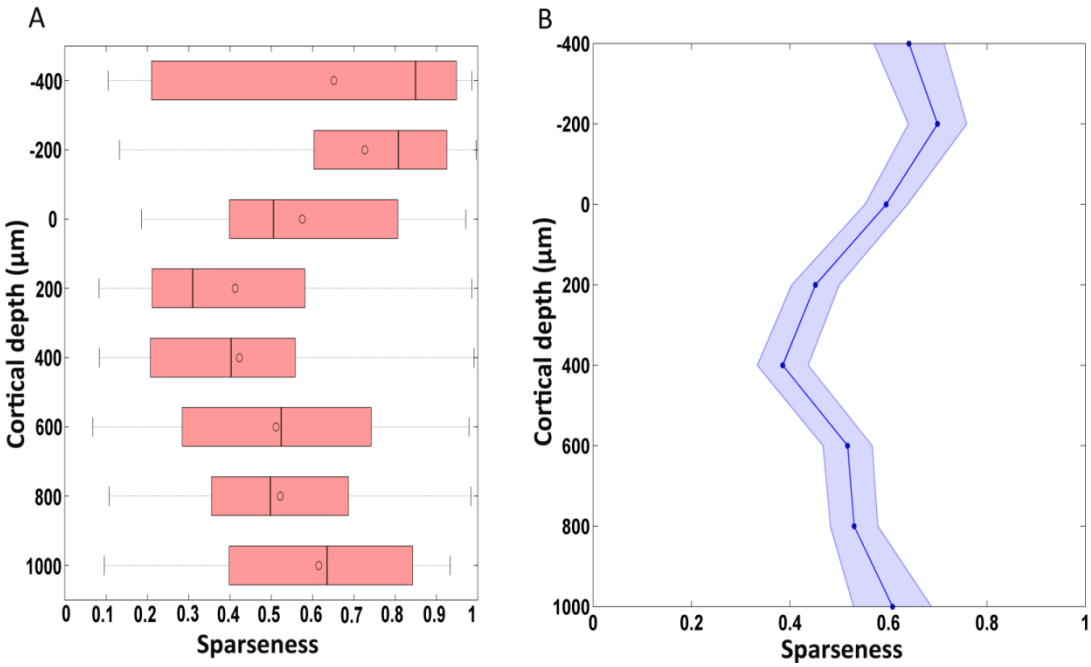

Figure 4.7 Depth profile of sparseness during baseline sound presentation (n=25) A. Box and whisker plots, Circles represent mean value and lines represent median B. Depth profile across all cortical layers (blue). Solid coloured lines represent mean values; shaded region represents SEM. One way ANOVA, bonferroni post-hoc comparison shows significant difference between different layers and is summarised in Table 4.2.

Table 4.2 Summary of statistical difference observed for sparseness in different cortical layers

Parameter	Depth	Versus					
		-400	-200	0	200	400	1000
Sparseness	0	ns	**				
	200	***	***	***		ns	*
	400	***	***	***	ns		*
	600	ns	***	ns	ns	ns	ns
	1000	ns	***	ns	ns	ns	ns

One way ANOVA, bonferroni post-hoc comparison, (n=25) *p<0.05, **p<0.005, ***p<0.0005, ns- not significant. A statistical significance (*) indicates a more dense representation as compared to (column indicated as 'versus') the other cortical layers. Only that depth at which significant difference was observed is shown in the table.

4.3.4 Bandwidth (BW)

The BW was calculated on an octave scale at 10 dB above the threshold intensity at all the cortical depths. BW at this intensity can give some indication about the differences in the shape of the tuning curve at the various depths. i.e. 'V' shaped

versus multi-peak for example (Sugimoto et al., 1997). As seen in Figure 4.8 A & B, no difference in the BW across the different cortical layers was observed in the AI during normal auditory processing indicating no laminar differences in BW across layers (n=25, one way ANOVA, p= 0.6316).

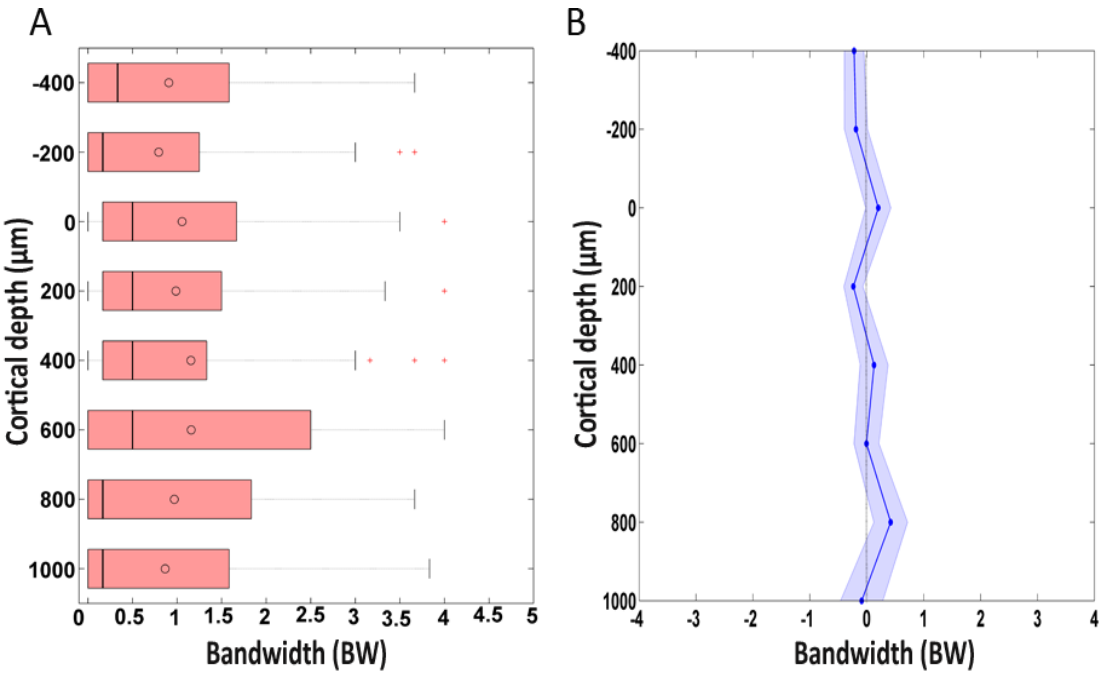

Figure 4.8 Depth profile of BW during baseline sound presentation (n=25) A. Box and whisker plots, Circles represent mean value and lines represent median B. Depth profile across all cortical layers (blue). Solid coloured lines represent mean values; shaded region represents SEM. No significant difference in threshold was seen across any of the layers.

4.3.5 Spontaneous activity (SA)

SA was measured five minutes before the entire set of stimulus presentation, and five minutes after the last short pip stimuli was presented (see Figure 4.9). Another measurement 'Background activity' was made to measure SA just before each individual stimulus onset during the short pip representation (see Figure 4.9).

Figure 4.10 (A, B, C) summarises the laminar profile of SA as spikes per second (spikes/sec) observed before stimuli presentation, after stimuli presentation and just before onset of stimulus (background activity) respectively. In all three instances the Deep layer 1 (presumptive layer V, cortical depths 200 µm to 400

µm) show higher SA as compared to layers I,II,III,IV & VI, similar to results observed in previous literature (Sakata and Harris, 2009). Statistical changes across different layers are summarised in Table 4.3. Statistical significance indicated higher SA; for example row one in table indicates that before tone presentation, SA activity at cortical depths 200 µm was statistically greater (to slightly varying degrees) compared to all other cortical depths except 400 µm.

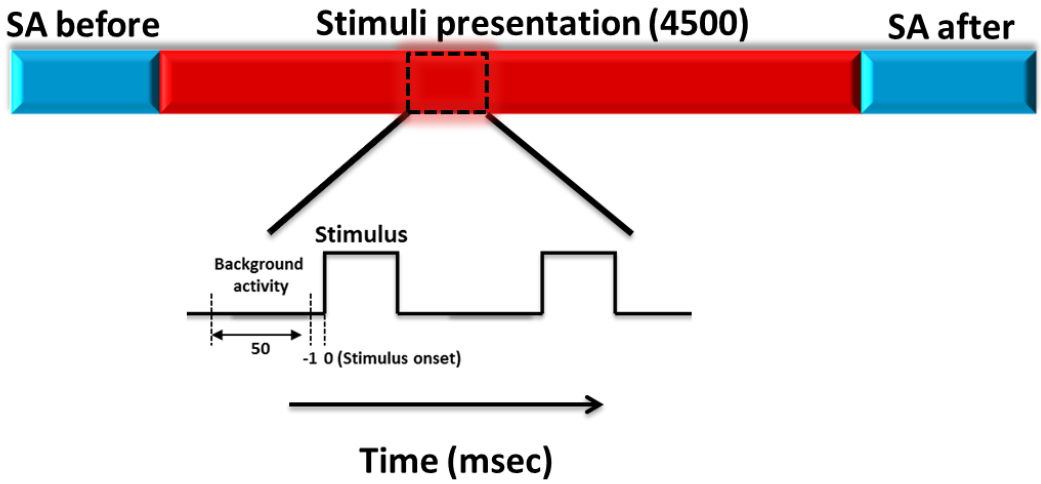

Figure 4.9 Schematic representation of the different time-points for measurement of SA. Blue bars represent the two time points of silence (5 minutes each) during which SA activity was measured. Red bar represents the time during which the different combinations of short pips were presented. Background activity was measured just before each stimulus onset.

Furthermore, as seen in Figure 4.10 SA in layer V increases following stimuli measurements (Figure 4.10 (B, C)) as compared to values before tone presentation (Figure 4.10 A) indicating some sort of a stimuli induced increase in SA. Quantifications comparing these changes are discussed in further details in Chapter 5, section 5.3.

4.4 Summary of laminar changes observed in AI during normal auditory processing

The observed laminar profiles of sensory evoked and SA during normal auditory processing are summarised in Table 4.4. Each measured parameter for sensory

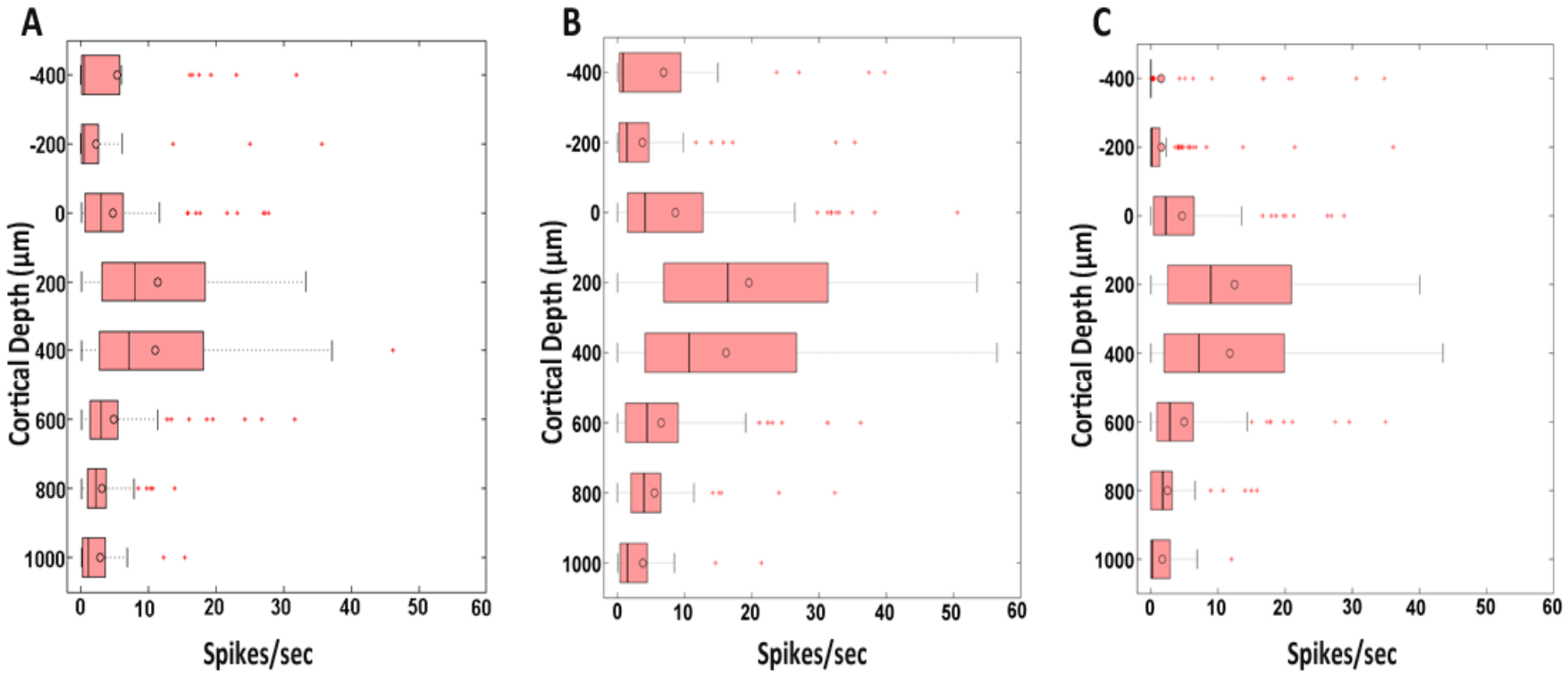

Figure 4.10 Depth profile of SA during baseline sound presentation (n=25) **A.** before stimuli presentation **B.** after stimuli presentation **C.** during stimuli presentation just before stimuli onset. Higher SA was seen in Deep 1 layer (layerV, 200 µm to 400 µm cortical depths) in all three instances compared to the other layers. However, the SA measured after (Figure 4.9B) stimuli presentation was greater compared to SA before stimuli presentation (Figure 4.9A). One way ANOVA, bonferroni post-hoc comparison shows significant difference between different layers **A.** $p<0.0001$, **B.** $p<0.0001$, **C.** $p<0.0001$ and is summarised in Table 4.3.

Table 4.3 Summary of statistical difference observed for SA in different cortical layers

Parameter	Depth	Versus							
		-400	-200	0	200	400	600	800	1000
SA Before tone presentation	200	**	***	***		ns	***	***	***
	400	**	***	***	ns		***	***	***
SA After tone presentation	200	***	***	***		***	***	***	***
	400	**	***	***	ns		***	***	***
Background activity	200	***	***	***		ns	***	***	***
	400	***	***	***	ns		***	***	***
	600	*	*	ns	ns	ns		ns	ns

One way ANOVA, bonferroni post-hoc comparison, (n=25) *p<0.05, **p<0.005, ***p<0.0005, ns- not significant. A statistical significance (*) indicates an increased SA as compared to (column indicated as 'versus') the other cortical layers. Only that depth at which significant difference was observed is shown in the table.

Table 4.4 Summary of laminar profile of sensory evoked (tuning curve parameters) and SA in AI during normal auditory processing. For sensory evoked response the various tuning curve parameters were extracted from the tuning curve, each parameter given a different colour code. All SA activity was presented by a similar colour code. Within each column the different colour shades represent laminar differences; where lighter shades present comparatively lower values and darker shades represent relatively higher values

Depth	Threshold (dB SPL)	CF (oct)	BW	Sparseness	Background	SA before stimuli	SA after stimuli
-400							
-200							
0							
200							
400							
600							
800							
1000							

evoked response is given a different colour code. SA at all time-points is represented by the same colour. Within each column the laminar differences are represented by varying colour shades with the lowest measurement represented by the lightest shade.

For sensory evoked responses, the threshold and CF parameters extracted from the tuning curves (Figure 4.3A) showed a tendency for different values across cortical layers (Figure 4.5 and Figure 4.4 respectively) however no statistical difference was observed. BW on the other hand showed no tendency or statistical difference in cortical layers (Figure 4.8). Sparseness showed a dense representation in layer V as compared to other cortical layers (Figure 4.7, table 4.2).

SA activity measured at all time-points (Figure 4.9) showed higher activity in layer V (200 µm to 400 µm) compared to all other cortical layers (Figure 4.10, Table 4.3). Furthermore an increase in SA was also observed in layer V following stimuli presentation (Figure 4.10 (B, C)).

4.5 Conclusion

The two main evaluation criteria for the validity of experiments for assessing laminar specific auditory evoked and SA was confirmation of location in the AI and laminar profile of the recording using CSD analysis. The data sets were then analysed to evaluate the baseline laminar profile of tuning curve parameters such as CF, threshold, sparseness and BW followed by SA and compared to observations made in previous literature. Confirmation of similar observations seen in previous literature for parameters such as sparseness and SA validated the evaluation and analysis protocol justifying further measurements as discussed below.

Following the baseline analysis as discussed in this chapter, the next step was to evaluate laminar specific changes in AI sensory evoked and SA responses following acoustic trauma. To minimise variations and represent such observations in different regions of the AI tonotopic map, the data sets were further divided into

three categories (Table 4.1 column 4, Figure 4.2) based on their CF:2-8 kHz (n = 9), 8-16 kHz (n = 10) and 16-32 kHz (n = 6). In the lower frequency band (2-8 kHz) data sets across two octaves were combined as compared to one octave in the other frequency band regions (8-16 kHz, and 16-32 kHz). This was essential as there were only three data sets in the 2-4 kHz region making any statistical quantification unreliable if the data sets in this frequency band were analysed separately.

The measurements for the various parameters in these three frequency band areas are discussed in details in the next chapter (Chapter 5).

Chapter 5

Results 2- Laminar specific changes in neural population activity in AI after acoustic trauma

5.1 Summary

Following baseline measurements of evoked response and SA, the data set (n=25 was divided into three sections depending on the frequency band, 2- 8 kHz, 8-16 kHz and 16-32 kHz.Section 5.2 provides the summary of laminar specific and average changes in tuning curve parameters : threshold, CF, BW and sparseness one (post 1) and two hours (post 2) post trauma. Section 5.3 provides details of changes following acoustic trauma in SA measured five minutes before and after stimuli (short pip) presentation. Details about effects of acoustic trauma on temporal properties of auditory processing is provided in Section 5.4. A summary of observed laminar specific changes in AI auditory evoked and SA responses following acoustic trauma is provided in section 5.5. Finally section 5.6 gives details of changes in cortical states before and one, two hours after acoustic trauma.

5.2 Laminar changes in tuning curve parameters following acoustic trauma

5.2.1 Threshold

After exposure to an hour of acoustic trauma (110 dB, centred at 16 kHz), the changes in threshold across all the depths in the AI were evaluated before trauma and then one and two hour time-points after the acoustic trauma (Figure 5.1). For the 2-8 kHz frequency band (Figure 5.1A) due to the noisy nature of tuning curves at the depth of 1000 µm, it was not possible to compute tuning parameters at this depth. On computing shifts in thresholds compared to baseline (Figure 5.2 (A, B, C)) increase in threshold values of 20 to 40 dB SPL were observed only in the 16-32 kHz frequency region. In this frequency band region, layers I/II showed a tendency for a decrease in threshold following acoustic trauma (post 1, p= 0.0791; post 2, p= 0.1129). However, these changes were not statistically significant. On the other hand, at cortical depths of 200 µm to 400 µm (Layer V) an increase in

threshold as compared to baseline was observed (Figure 5.1C, Figure 5.2C).

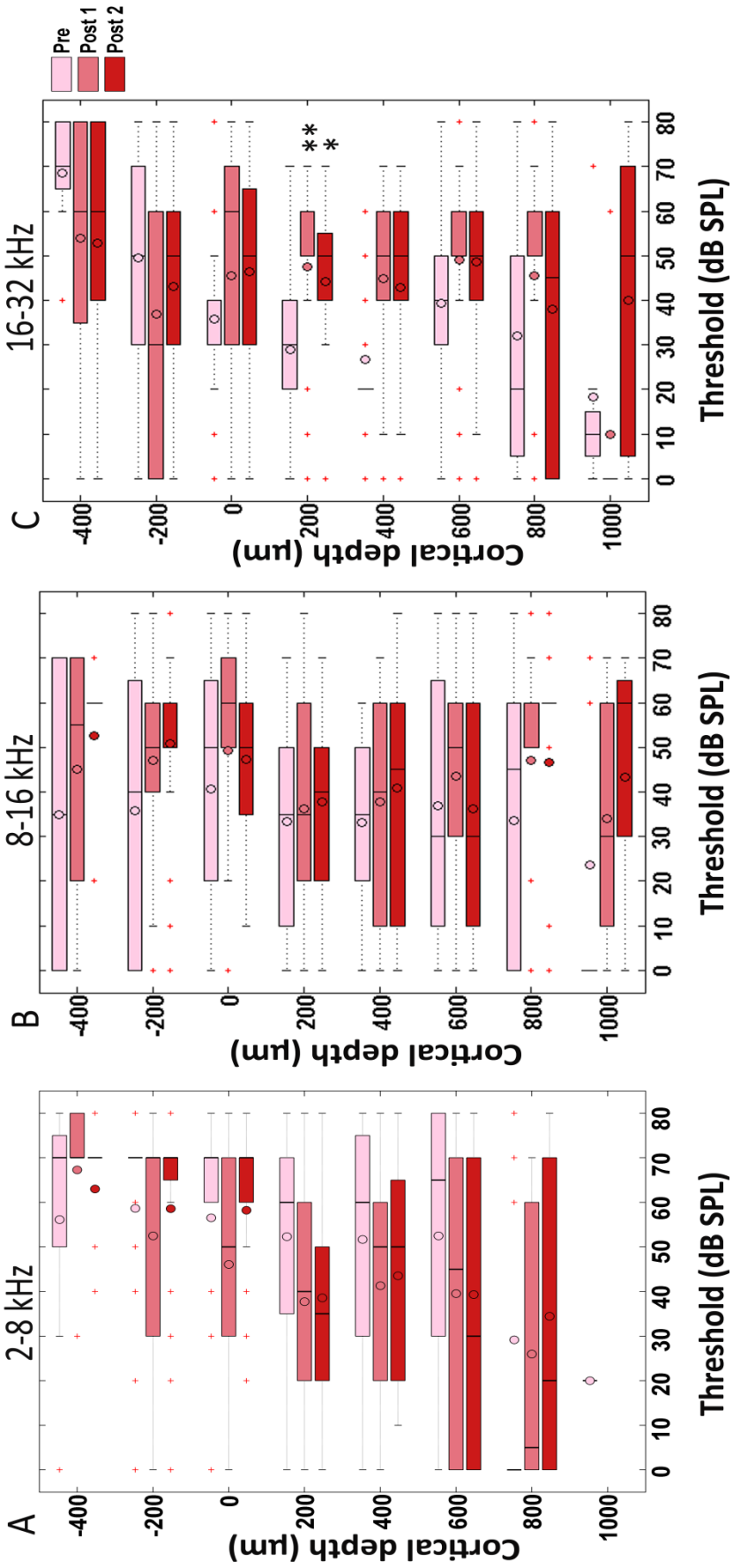

Figure 5.1. Box and whisker plots representing threshold (dB SPL) across all cortical depths before (light red box), post 1 (middle red box) and post 2(dark red bar) in different regions of the tonotopic map **A.** 2-8 kHz (n=9), **B.** 8-16 kHz (n=10) and **C.** 16-32 kHz (n=6). The overlapping circles in the box represent the mean threshold. Bonferroni posttest on two way ANOVA show statistical changes in the 16-32 kHz region (*p<0.05, **p,0.005). 2-8 kHz, p= 0.8499 ; 8-16 kHz p=0.9728)

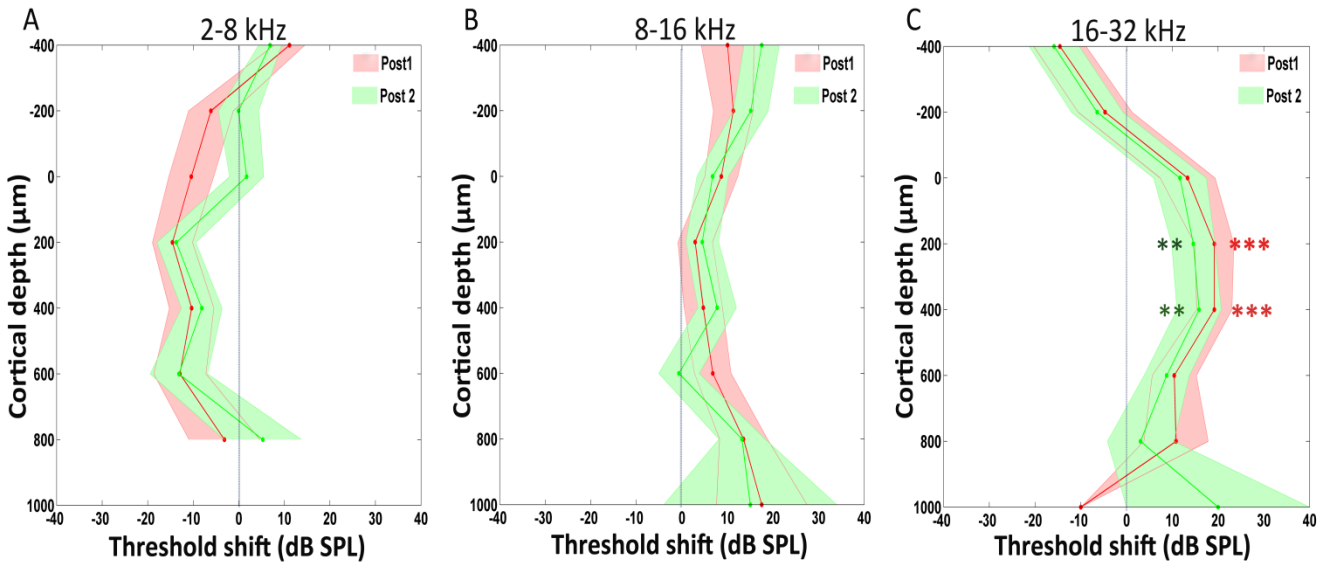

Figure 5.2. Threshold shift(dB SPL) one hour after i.e. Post 1(red) and two hours after i.e. Post 2 (green) acoustic trauma across all cortical layers in different frequency bands (A) 2-8 kHz (n=9, 0.3839),(B) 8-16 kHz (n=10, p=0.397) and (C) 16-32 kHz (n=6,p= 0.0007). Solid colour lines represent mean values whereas shaded region represent SEM. Significant shifts in threshold were observed only in the 16-32 kHz frequency band (C) at 200 µm (Post 1: p<0.0005 , n=7), (Post 2: p< 0.005, n=7)and 400 µm (Post 1:p<0.0005 , n=7, Post 2: p<0.005 , n=7) cortical depth after trauma. Statistics: Laminar graphs (A-C) Bonferroni posttest on two way ANOVA, box and whisker plots.

Furthermore, the observed increase in threshold observed one hour after trauma (post 1) was comparatively smaller (~ 10 dB) when measured two hours post trauma (post 2) (Figure 5.2C) indicating some form of recovery in sensory evoked responses over time.

The average change in threshold across the different cortical layers showed a similar tendency to that seen in the laminar profiles (Appendix Figure 6 (A, B, C)). However, the shifts in the 2-8 kHz (n=9, p=0.2170) (Appendix Figure 6A) and 16-32 kHz (n=6, p= 0.0791) (Appendix Figure 6C) were not statistically significant. Significant change in average threshold shift compared to baseline was seen in the 8-16 kHz (Appendix Figure 6B) frequency region for both time points after trauma.

5.2.2 Characteristic frequency (CF)

After exposure to an hour of acoustic trauma (110 dB, centred at 16 kHz), the changes in CF across all the depths in the AI were evaluated one and two hours

after trauma on an octave scale (Figure 5.3). For the 2-8 kHz frequency band (Figure 5.3A) due to the noisy nature of tuning curves at the depth of 1000 µm, it was not possible to compute tuning parameters at this depth.

A laminar specific shift in CF compared to baseline was seen in all frequency bands (Figure 5.4 (A, B, C)). Shifts towards a lower octave at both time points post trauma, at depths similar to those at which increase in threshold (Figure 5.2C) were seen (Figure 5. 3C, Figure 5.4C). In the 2-8 kHz frequency band, a shift from baseline towards a higher octave is seen only at the 400 µm depth (Figure 5.3A, Figure 5. 4A). Unlike no laminar specificity in threshold changes post trauma in the 8-16 kHz frequency band, a time delayed significant shift in CF from baseline towards the lower octave was observed (Figure 5.4B).

Time specific laminar shifts in CF in the different frequency bands seem to be a bit more varied as compared to observed threshold shifts. In the 2-8 kHz and 8-16 kHz frequency bands shift in CF is mostly delayed i.e. two hours after trauma (Figures 5.4A B)). In the 16-32 kHz frequency band region a similar delayed response is seen at 0 µm depth. However, the change in CF from baseline shows a tendency for a time specific reversal at cortical depths 200 µm and 800 µm (Figure 5.4C).

Average shifts in CF across all cortical layers at both time points after trauma show a similar tendency to that seen in the laminar profile in the different frequency bands (Appendix Figures (A ,B,C)). However, none of these changes at either of the time points after trauma were statistically different compared to baseline (16-32 kHz, n=6, p= 0.1656; 8-16 kHz, n= 10, p= 0.0355, 16-32 kHz, n=9, p=0.3708).

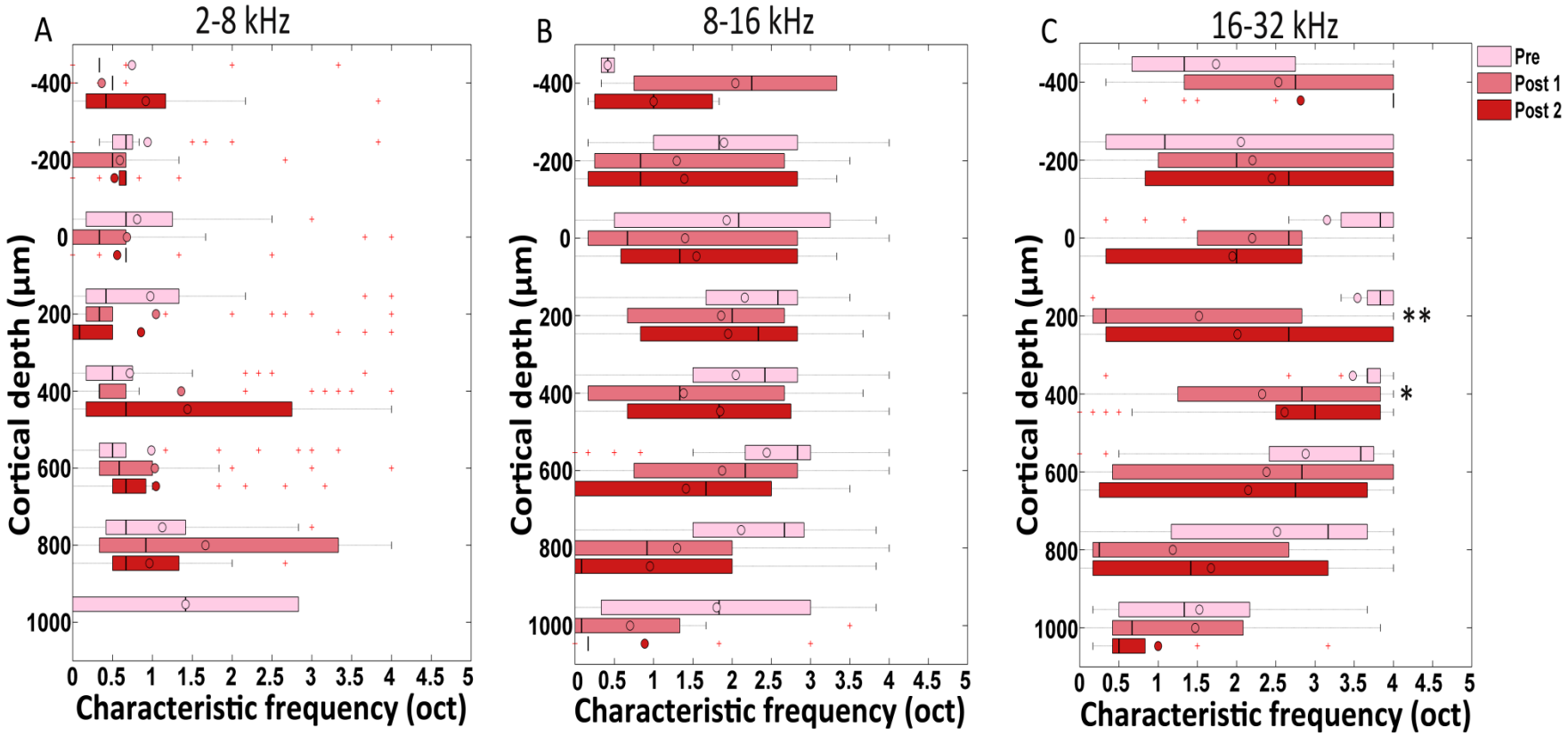

Figure 5.3. Box and whisker plots representing characteristic frequency(octave) across all cortical depths before (light red box), post 1 (middle red box) and post 2(dark red bar) in different regions of the tonotopic map **A.** 2-8 kHz (n=9), **B.** 8-16 kHz (n=10) and **C.** 16-32 kHz (n=6). The overlapping circles in the box represent the mean CF . Bonferroni posttest on two way ANOVA show statistical changes in the 16-32 kHz region (*p<0.05, **p.0.005). For 8-16 kHz, n=10, p= 0.3946; 2-8 kHz, n=9, p=0.9977.

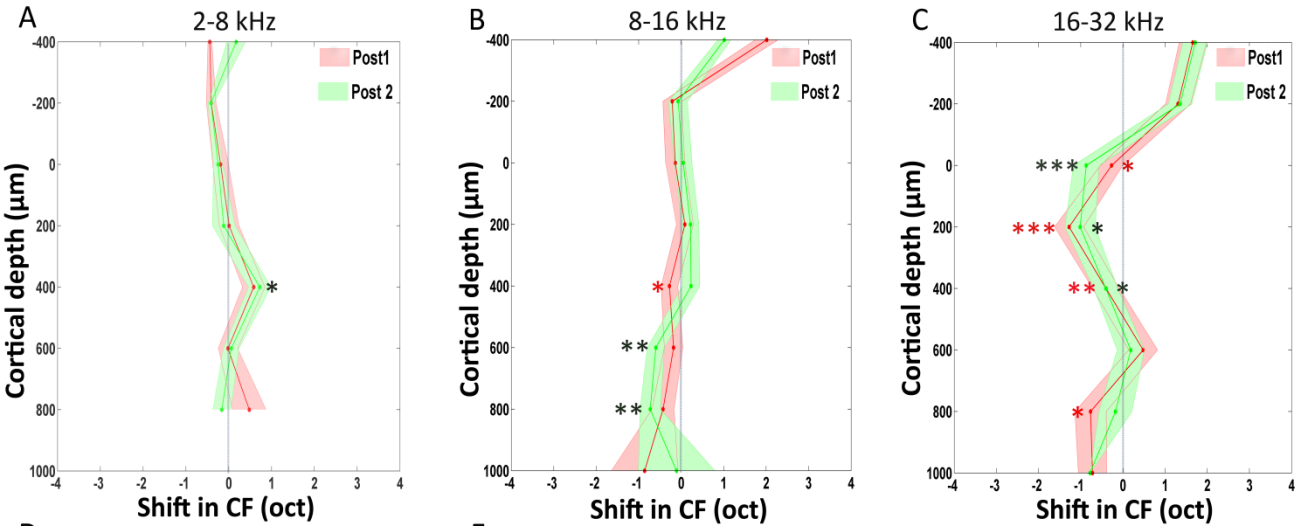

Figure 5.4. Shift in CF (octave)one hour after i.e. Post 1(red) and two hours after i.e. Post 2 (green) acoustic trauma across all cortical layers in different frequency bands (A) 2-8 kHz (n=9, 0.0637),(B) 8-16 kHz (n=10, 0.0191) and (C) 16-32 kHz (n=6, 0.0008). Solid colour lines represent mean values whereas shaded region represent SEM. Significant shifts in threshold (n= 9) were observed in all the frequency bands (A-C). Statistics: Laminar graphs (A-C) Bonferroni posttest on two way ANOVA.

5.2.3 Bandwidth (BW)

After exposure to an hour of acoustic trauma (110 dB, centred at 16 kHz), the changes in BW across all the depths in the AI were evaluated one and two hours after trauma on an octave scale (Figure 5.5).

Laminar specific changes in BW post trauma were observed only in the 16-32 kHz frequency band (Figure 5.6C). The increase in BW post trauma was observed at

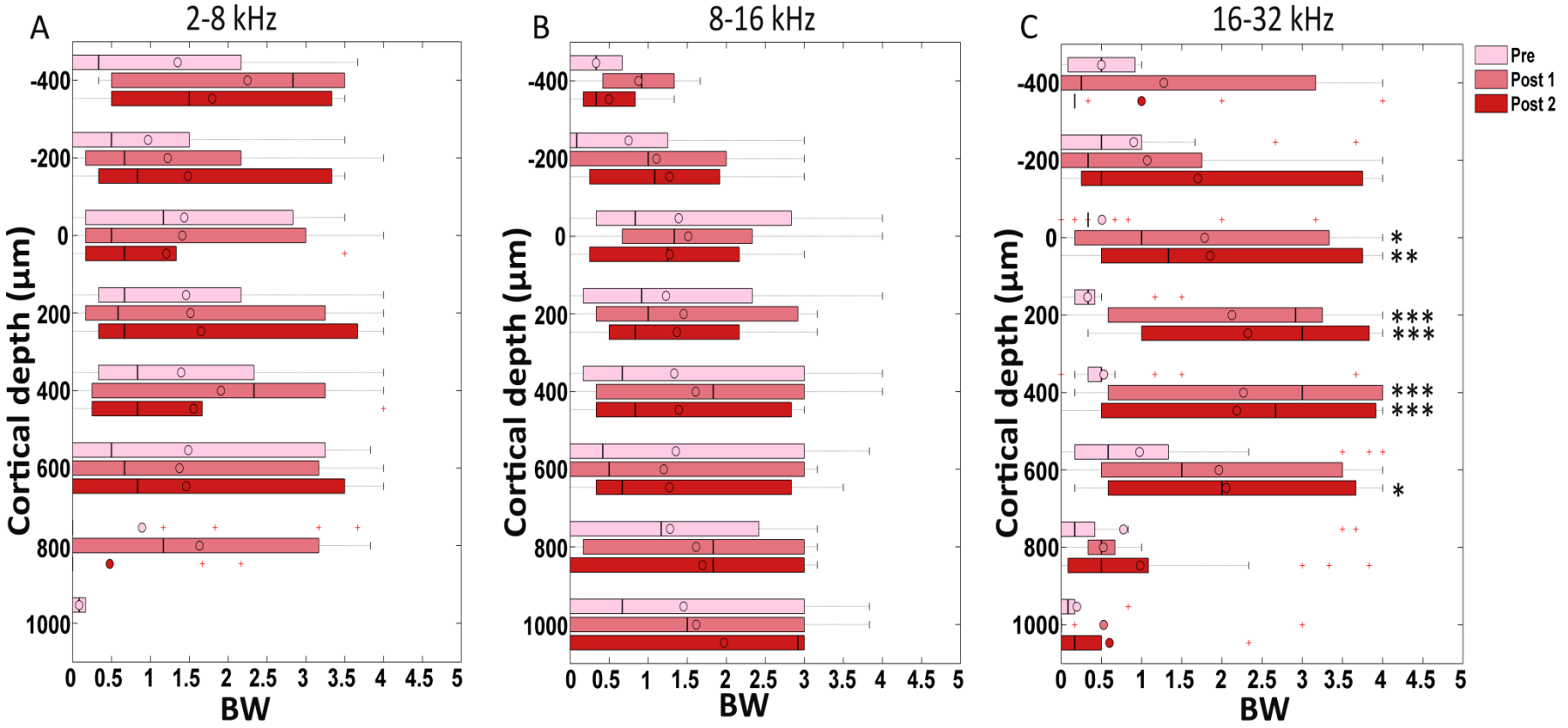

Figure 5.5. Box and whisker plots representing BW at 10 dB SPL above threshold across all cortical depths before (light red box), post 1 (middle red box) and post 2(dark red bar) in different regions of the tonotopic map **A.** 2-8 kHz (n=9), **B.** 8-16 kHz (n=10) and **C.** 16-32 kHz (n=6). The overlapping circles in the box represent the average BW .Bonferroni posttest on two way ANOVA show statistical changes in the 16-32 kHz region (*p<0.05, **p,0.005,***p<0.0005)). For 8-16 kHz, n=10, p= 0.9968; 2-8 kHz, n=9, p= 0.9581.

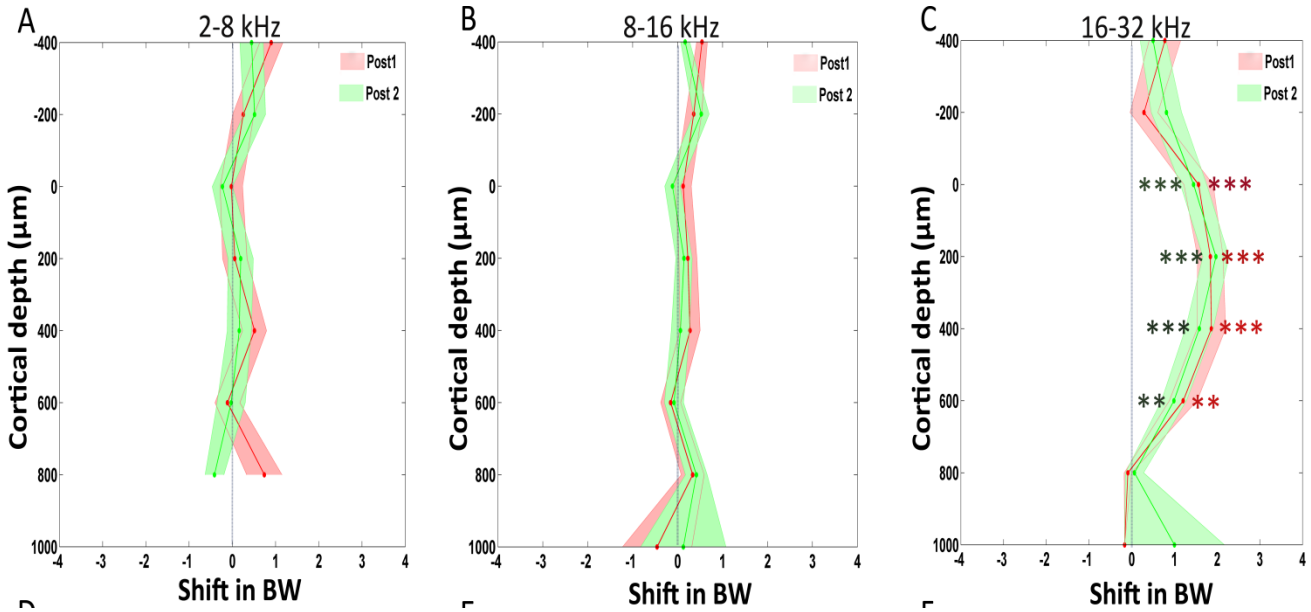

Figure 5.6. Shift in BW 10 dB above threshold (SPL) one hour after i.e. Post 1(red) and two hours after i.e. Post 2 (green) acoustic trauma across all cortical layers in different frequency bands (A) 2-8 kHz (n=9, 0.5745),(B) 8-16 kHz (n=10, 0.9001) and (C) 16-32 kHz (n=6, p=0.00065). Solid colour lines represent mean values whereas shaded region represent SEM. Significant shifts in BW were observed only in the 16-32 kHz frequency band (C) at 0,200,400,800 µm cortical depth after trauma. Statistics: Laminar graphs (A-C) Bonferroni posttest on two way ANOVA.

depths at which an increase in threshold, or decreased in the CF was observed in this frequency region. This is possibly due to the loss in the sharpness of the 'V' tuning curve following trauma induction.

Unlike time-specific laminar shifts from baseline in threshold and CF in the 16-32 kHz frequency region, shift in BW following trauma is preserved over time after acoustic trauma (Figure 5.2C, Figure 5.4C, and Figure 5.6C).

Average shifts in BW across all cortical layers at both time points after trauma were calculated in the three different frequency bands (Appendix Figure 8 (A, B, C)). Statistical increase in BW following acoustic trauma was observed one and two hours post trauma in the 16-32 kHz frequency region (Appendix Figure 8C) and one hour post trauma in the 2-8 kHz frequency band (Appendix Figure 8B). No change was observed in the 8-16 kHz frequency region (n=10, p= 0.2390).

5.2.4 Sparseness

After exposure to an hour of acoustic trauma (110 dB, centred at 16 kHz), the changes in sparseness across all the depths in the AI were evaluated ten mins after trauma (post 1) and then ten mins after post 1 (post 2) on an octave scale (Figure 5.7). As mentioned previously, life time sparseness was measured this study where a response of the given population across a set of stimuli was evaluated.

Laminar specific changes in sparseness were observed in the 2-8 kHz (Figure 5.7A, Figure 5.8A) and the 16-32 kHz (Figure 5.7C, Figure 5.8C) frequency bands. In the 16-32 kHz frequency an increase in sparseness compared to baseline was observed in layers I/II (Figure 5.8C) during post 2. A similar increase in sparseness and a statistical decrease in sparseness during post 2 was observed also in the 2-8 kHz frequency band region (Figure 5.8A).

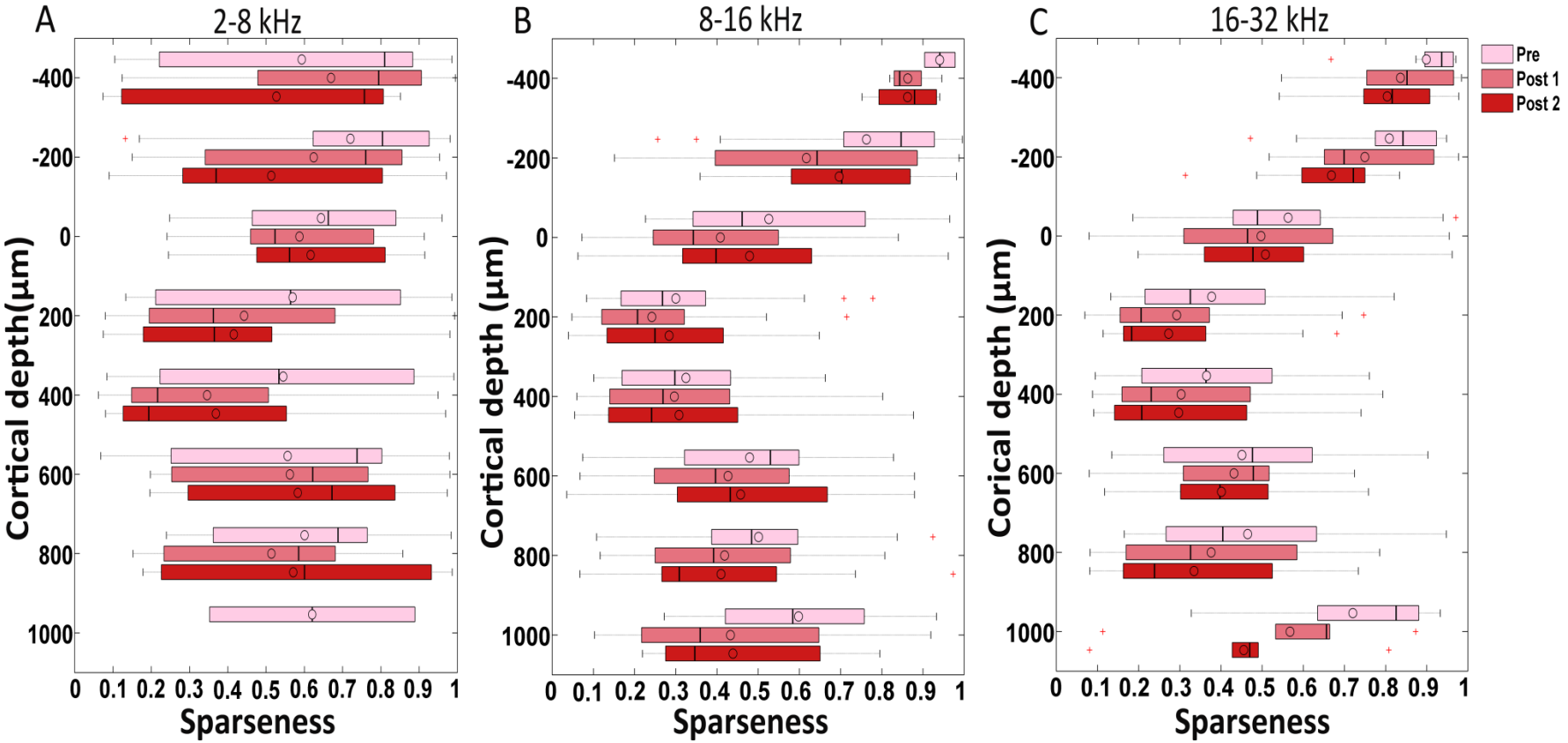

Figure 5.7. Box and whisker plots representing sparseness across all cortical depths before (light red box), post 1 (middle red box) and post 2(dark red bar) in different regions of the tonotopic map **A.** 2-8 kHz (n=9), **B.** 8-16 kHz (n=10) and **C.** 16-32 kHz (n=6). The overlapping circles in the box represent the average sparseness.

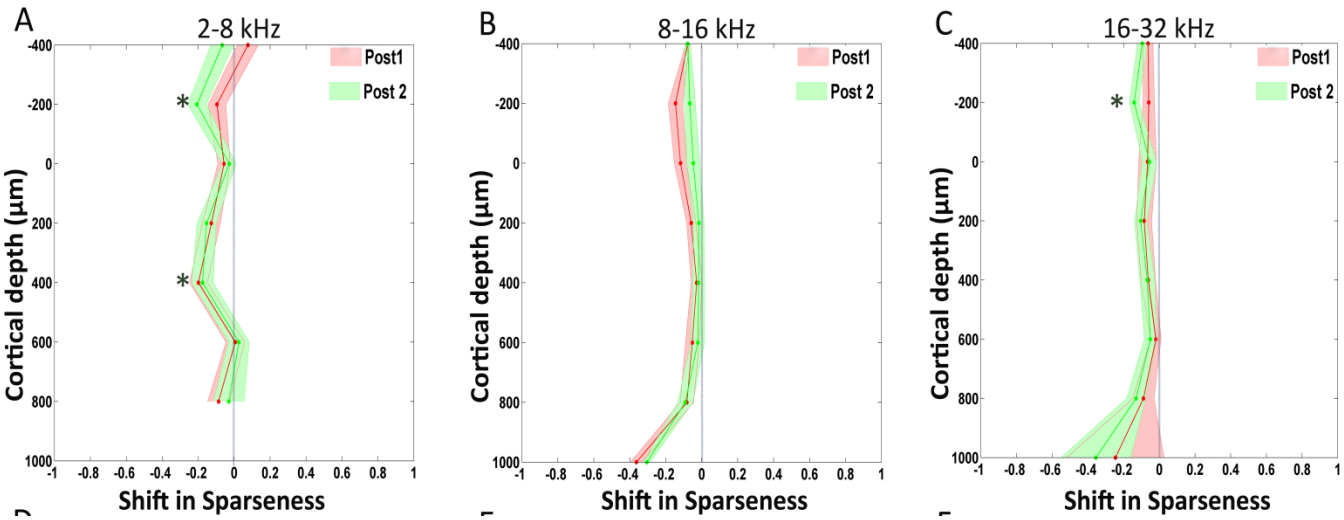

Figure 5.8. Shift in Sparseness one hour after i.e. Post 1(red) and two hours after i.e. Post 2 (green) acoustic trauma, across all cortical layers in different frequency bands (A) 2-8 kHz (n=9, 0.0545),(B) 8-16 kHz (n=10, 0.0595) and (C) 16-32 kHz (n=6, 0.05). Solid color lines represent mean values whereas shaded region represent SEM.. Significant shifts in sparseness were observed only in the 2-8 kHz and 16-32 kHz frequency band (A &C). Statistics: Laminar graphs (A-C) Bonferroni posttest on two way ANOVA.

Average shifts in sparseness across all cortical layers show a decrease in sparseness following acoustic trauma in all the three frequency bands (Appendix Figure 9 (A, B, C)). In the 2-8 kHz frequency band the overall shift show a similar delayed response as that seen in layer I/II in this region (Figure 5.8A and Appendix Figure 9A). However this was not the case in the 8-16 kHz (Figure 5.8B, Appendix Figure 9B) and the 16-32 kHz (Figure 5.8 (C, Appendix Figure 9C) frequency bands.

5.3 Changes in Background activity (SA during stimuli interval)

To investigate how spontaneous firing was changed across cortical layers after acoustic trauma, we measured changes in background activity (see above) and SA in 5 min silent periods. Background activity is SA (measured before the start and at the end of pre, post 1 & post 2) measured at a different time point i.e. intervals between the presented stimuli. Here we analyse background activity during baseline (pre), 10 mins after trauma (post 1) and 10 mins after post 1 (post 2) trauma (Figure 5.10). These responses were measured 50 milliseconds (Figure 5.9) prior to stimulus (short pips) onset. Figure 5.10 B and C shows that laminar specific

changes were seen only in the 8-16 kHz (n=10, p=0.0055) and in the 16-32 kHz (n=6, p=0.0017) frequency regions, respectively (for 2-8 kHz, p=9, p=0.9607).

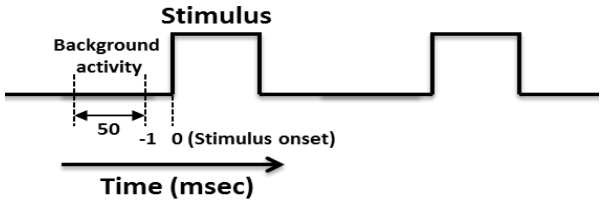

Figure 5.9 Diagram portraying the time frame from which background activity was extracted.

In the 8-16 kHz frequency band increased statistical increase in background activity post trauma were seen in at 0 µm and 200 µm cortical depths (Figure 5.10B). However, these changes were observed only two hours post trauma (post 2). Laminar specific changes in the 16-32 kHz frequency region were observed only at 200 µm and 400 µm (layer V) cortical depths (Figure 5.10C). Once again similar to results obtained in the 8-16 kHz frequency region these changes were seen only two hours post trauma.

Overall changes in background activity compared to baseline across cortical depths are visualised in Figure 5.10 (D, E, and F). A moderate increase in background activity was observed in all frequency regions at both time points (post1 and post 2) following acoustic trauma. However, contrary to laminar specific changes where increase in background activity was seen in both the 8-16 kHz and 16-32 kHz frequency bands (Figure 5.10 (B, C)), statistical increase in

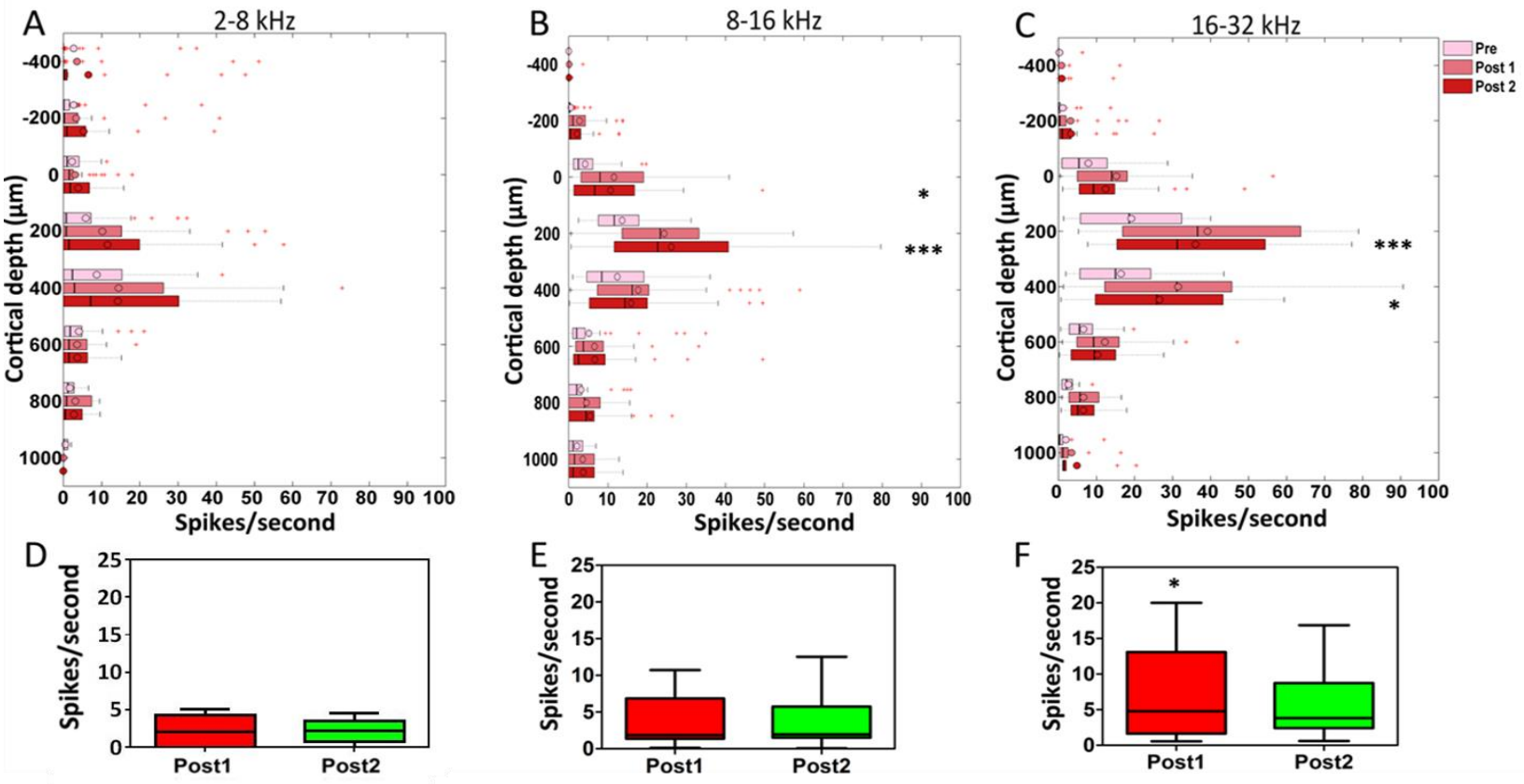

Figure 5.10. Box and whisker plots representing changes in background activity for different frequency bands (A) 2-8 kHz (n=9),(B) 8-16 kHz (n=10) and (C) 16-32 kHz (n=6) before (light red),ten minutes after (middle) trauma and one hour after (dark red)post 1. Figure 10 (D,E,F) are box and whisker plots indicating average change in background across all cortical layers during post1 (red) and post 2 (green). Statistically significant shifts in background activity were seen in the 8-16 (B), 16-32 (C) frequency bands at specific cortical depths. Statistically significant shifts were only observed in overall changes 16-32 kHz (F) frequency regions. Statistics: Laminar profiles (A-C) Bonferroni posttest on two way ANOVA, box and whisker plots (D-F) Bonferroni posttest on one way ANOVA

overall background activity was only observed in the 16-32 kHz (n=6, p=0.0277) frequency band region (Figure 5.10F) (for 8-16 kHz, p=0.0429, for 2-8 kHz, p=0.0561).

Furthermore, the time profile seen in overall changes in background activity in the 16-32 kHz region was not similar to that seen in laminar specific changes in background activity in this frequency region. Laminar specific changes were seen as a delayed response i.e. two hours post trauma (post 2) (Figure 5.10C), whereas overall changes in background activity showed a statistical increase immediately after trauma induction i.e. in post 1 (Figure 5.10F).

5.3 Changes in SA

SA (spontaneous activity) was recorded five minutes before stimuli presentation during baseline recording, post 1, post 2 and before acoustic trauma. SA was also recorded immediately following stimuli presentation or acoustic trauma for a period of five minutes (Chapter 3 Figure 3.9). Figure 5.11 shows SA measured before stimuli (short pip) presentation during baseline, one hour after (post1) and two hours after (post 2) acoustic trauma in the 2-8 kHz (A, D), 8-16 kHz (B, E) and 16-32 kHz (C, F) frequency band regions. Laminar specific changes in SA following acoustic trauma was only seen in the 8-16 kHz (n=10, p=0.0053) (Figure 5.11B) and the 16-32 kHz (n=6, p=0.0022) (Figure 5.11C) frequency regions (for 2-8 kHz, n=9,p= 0.7871). Furthermore the laminar specific increases in spontaneous firing were seen immediately after acoustic trauma and were preserved even two hours after trauma.

Statistically significant increase in average spontaneous firing across all cortical depths was observed in all frequency regions at both time points post trauma with the exception of 2-8 kHz frequency region (n=9, p= 0.0064) (Figure 5.11 (D, E, F)).

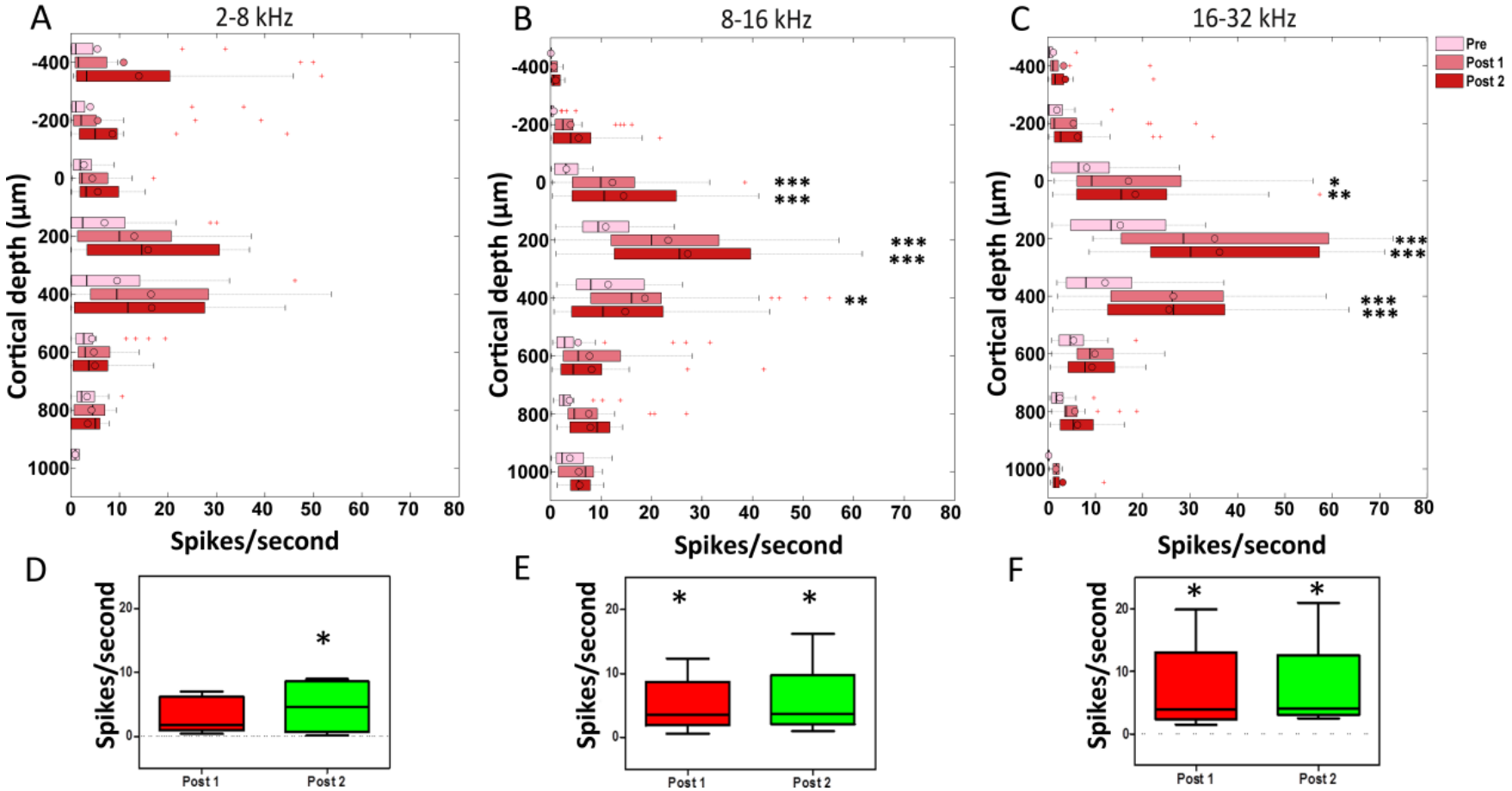

Figure 5.11. Box and whisker plots representing changes in spontaneous (spikes/sec) activity for different frequency bands (A) 2-8 kHz (n=9),(B) 8-16 kHz (n=10) and (C) 16-32 kHz (n=6) before (light red), ten mins after trauma (middle) and one hour after post 1(dark red) measured before tone presentation. Figure 11 (D,E,F) are box and whisker plots indicating average change in spontaneous activity across all cortical layers during post 1 (red) and post 2 (green). Statistically significant shifts in spontaneous activity was seen in the 8-16 kHz (B) and 16-32 kHz(C) frequency band during post 1 and post 2. Statistically significant shifts in average spontaneous activity across all cortical layers was observed in all frequency regions (D,E,F). Statistics: Laminar profiles (A-C) Bonferroni posttest on two way ANOVA, box and whisker plots (D-F) Bonferroni posttest on one way ANOVA

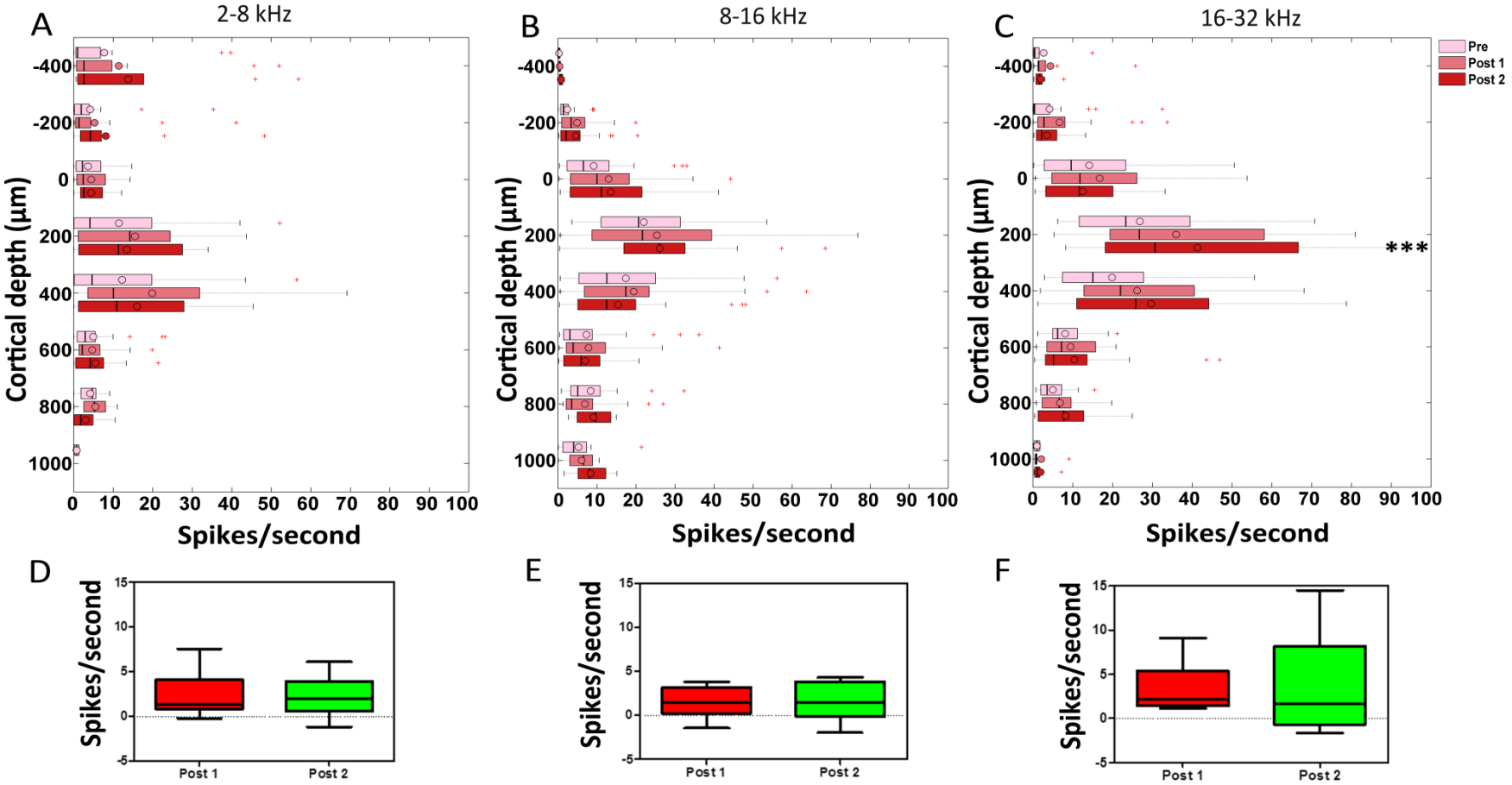

Figure 5.12. Box and whisker plots representing changes in spontaneous (spikes/sec) activity for different frequency bands (A) 2-8 kHz (n=9),(B) 8-16 kHz (n=10) and (C) 16-32 kHz (n=6) before (light red), ten mins after (middle) trauma and one hour after post 1(dark red) measured after tone presentation. Figure 12 (D,E,F) are box and whisker plots indicating average change in spontaneous activity across all cortical layers during post 1(red) and post 2 (green). Statistically significant shifts in spontaneous activity was seen in the 8-16 kHz (B) and 16-32 kHz(C) frequency band during post 2. No statistically significant shifts in average spontaneous activity across cortical layers was in any of the frequency regions (D,E,F). Statistics: Laminar profiles (A-C) Bonferroni posttest on two way ANOVA, box and whisker plots (D-F) Bonferroni posttest on one way ANOVA

Laminar specific changes in spontaneous firing after stimuli presentation (Figure 5.12 (A, B, C)) showed only a moderate increase in SA compared to baseline. Furthermore, these changes were limited to the 16-32 kHz frequency region (Figure 5.12C) (8-16 kHz, n=10, p= 0.9871; 2-8 kHz, n=9, p= 0.9514). Average changes in SA following tone presentation showed no significant changes compared to baseline in any of the frequency regions (Figure 5.12 (D, E, F)) (16-32 kHz, p=6, p=0.1285; 8-16 kHz, n=10, p =0.1241; 2-8 kHz, n=9, p= 0.0450). As discussed in Chapter 4, Figure 4.10, the SA increases following stimuli presentation. To further investigate the differences in spontaneous firing we compared the baseline SA before stimuli presentation to baseline SA after tone presentation (Figure 5.13). As summarised in Table 5.1 in the 8-16 kHz and the 16-32 kHz frequency band a statistical increase in SA was observed following stimuli presentation (short pips). To account for this fact we concluded that the appropriate way to quantify SA activity following acoustic trauma would be compare changes post acoustic trauma to the elevated baseline activity (i.e. SA in baseline recorded after tone presentation).

Table 5.1 Statistical comparison of baseline spontaneous activity before and after tone presentation, at different cortical depths (μm).

Frequency Band	Cortical depth (μm)	Onset baseline versus Finish baseline
8-16 kHz	0	*
	200	***
	400	*
16-32 kHz	0	ns
	200	***
	400	*

Bonferonni posttest on two way ANOVA .
*p<0.05, **p<0.005, ***p<0.0005.

Figure 5.14(A,B,C) show the laminar specific changes in SA following acoustic trauma (post1, post2) as compared to the elevated baseline (i.e. baseline after tone presentation). Laminar specific increase in SA was only observed in the 16-32

frequency region (Figure 5.14C) at 200 µm cortical depth (8-16 kHz, n=10, p= 0.9147, 2-8 kHz, p= 0.9957).

Furthermore, the increase in SA was seen as a delayed response (two hours post acoustic trauma).

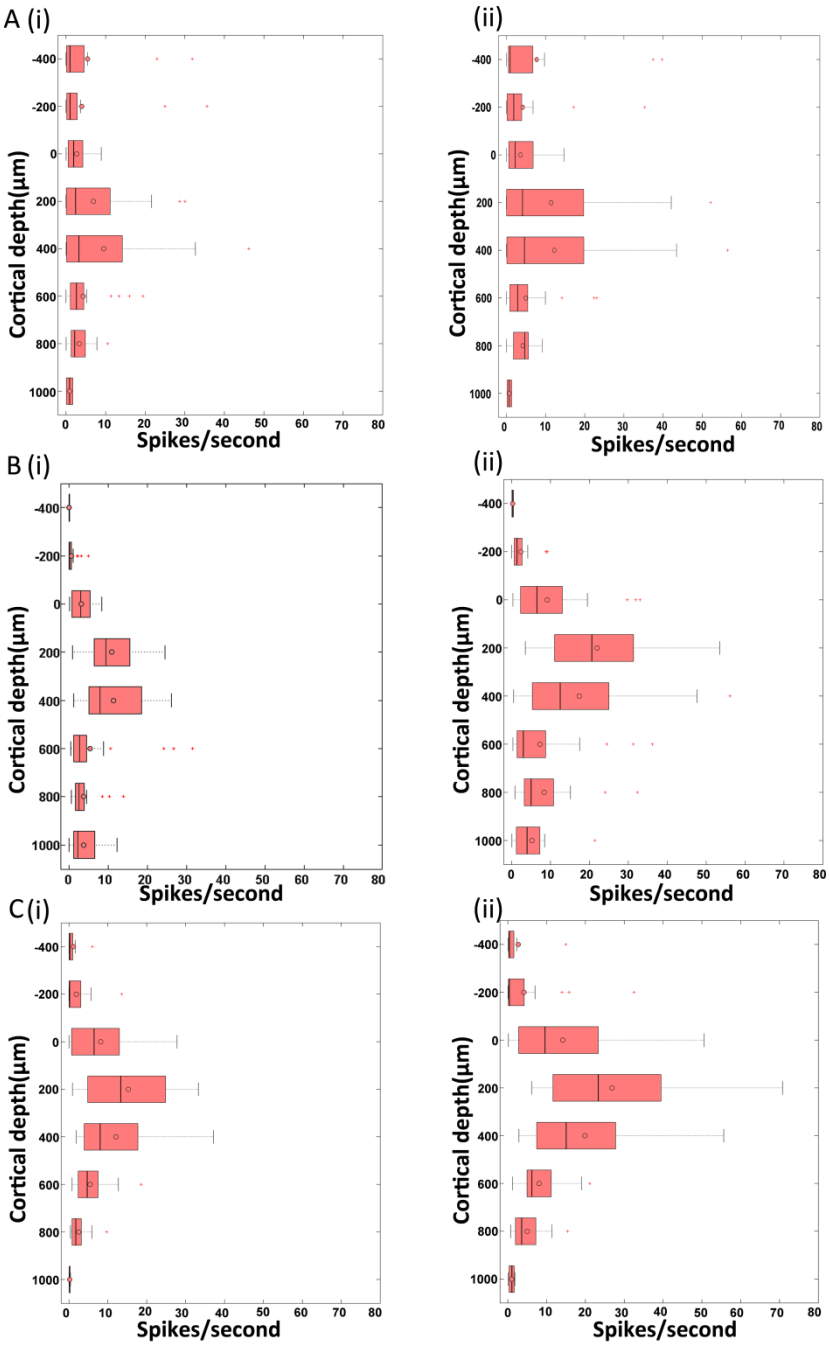

Figure 5.13 Laminar profiles comparing changes in spontaneous firing in the 2-8 kHz (n=9) (A), 8-16 kHz (n=10) (B) and 16-32 kHz (n=6) (C) frequency region before (i) and after (ii) tone presentation.

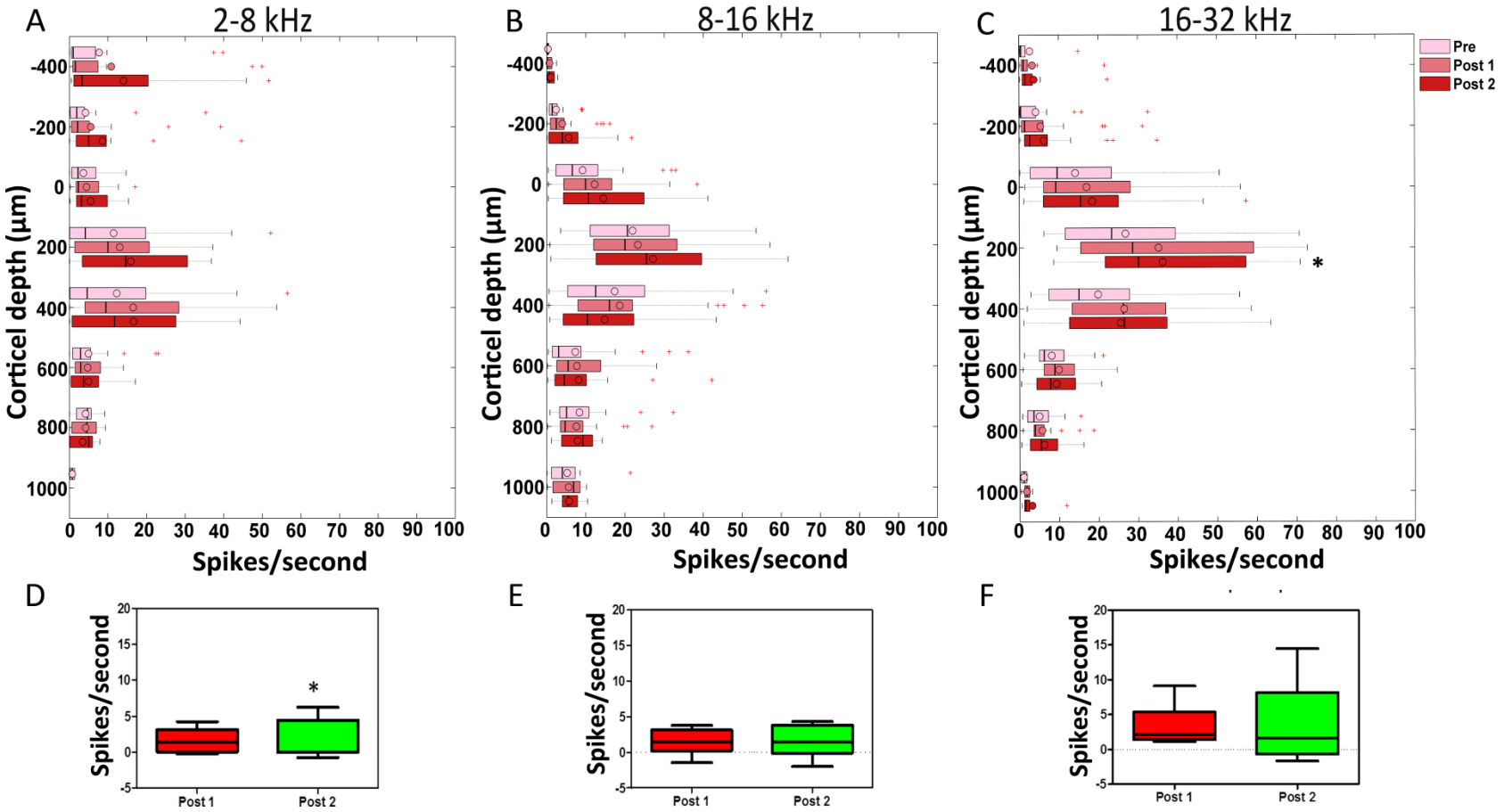

Figure 5.14 Box and whisker plots representing changes in spontaneous (spikes/sec) activity for different frequency bands (A) 2-8 kHz (n=9),(B) 8-16 kHz (n=10) and (C) 16-32 kHz (n=6) before (elevated)(light red ten mins after trauma (middle) and one hour after post 1(dark red). Figure 14 (D,E,F) are box and whisker plots indicating average change in spontaneous activity across all cortical layers during post 1 (red) and post 2(green). Statistically significant shifts in spontaneous activity was seen only in the 16-32 (C) frequency band at 200 µm cortical depth one hour after trauma. Statistically significant shifts were only observed in overall changes 2-8 kHz (D) frequency region. Statistics: Laminar profiles (A-C) Bonferroni posttest on two way ANOVA, box and whisker plots (D-F) Bonferroni posttest on one way ANOVA

5.4 Changes in inter-spike interval following acoustic trauma

To gauge temporal structure of multi-unit SA following acoustic trauma, inter-spike intervals (ISIs) across all cortical depths during SA before and after tone presentation were estimated.

Figure 5.15 (A, B, C) represents the laminar distribution of the fraction of MUA having an ISI less than 10 msec measured before stimuli presentation in three different frequency regions. Laminar specific increase in fraction of ISI less than 10 msec were seen only in the 8-16 kHz (Figure 5.15B) and 16-32 kHz (Figure 5.15C) frequency regions (2-8 kHz, p=9 , p= 0.08772). These laminar specific changes in the 8-16 kHz frequency region were immediate following trauma whereas in layers I/II of the 16-32 kHz frequency region were seen at a later time point (post 2). Average change in ISI across all cortical layers was seen in the 2-8 kHz frequency region two hours post trauma (Figure 5.15D) and in the 16-32 kHz frequency region one and two hours post trauma (Figure 5.15 (E, F)) (8-16 kHz, p= 0.2977).

Table 5.2 Estimation of time window for ISI measurements during SA before tone presentation. Table provides a summary of laminar specific changes in ISI following acoustic trauma in different frequency bands; 2-8 kHz (1), 8-16 kHz (2), 16-32 kHz (3).

Cortical depth (µm)	Time point	ISI (< 6 msec)			ISI (< 8 msec)			ISI (< 10 msec)			ISI (< 12 msec)			ISI (< 15 msec)		
		1	2	3	1	2	3	1	2	3	1	2	3	1	2	3
-200	Post 1								*			*			*	*
	Post 2		**			***			***	*		***	*		***	
0	Post 1														*	
	Post 2		*						*			*			*	
200	Post 1						*						*			**
	Post 2															
400	Post 1			**			**			**			**			*
	Post 2															

Bonferonni posttest on two way ANOVA . *p<0.05, **p<0.005, ***p<0.0005.

Once again, as seen in laminar specific changes in SA (Figure 5.12 (A, B, C)), fewer trauma induced laminar specific increase in fraction of ISI were seen in measurements after stimuli presentation (Figure 5.16 (A, B, C)). Average change across cortical depths in these measurements within all frequency regions showed no statistical shift from baseline (Figure 5.16 (D, E, F)) (16-32 kHz, n=6, p=0.4041; 8-16 kHz, n=10, p= 0.3139; 2-8 kHz, n=9, p= 0.1939)).

Figure 5.17 (A, B, C) shows laminar specific shifts in fraction of ISI less than 10 msec ten mins after trauma (post 1) and one hour after post 1 (post 2) compared to elevated baseline (i.e. baseline recorded after tone presentation). Increase in ISI less than 10 msec post trauma was only seen in the 16-32 kHz frequency region post trauma in the II cortical layers (-200 µm) (8-16 kHz, n= 10, p= 0.7102, 2-8 kHz, n=9, p= 0.9707). Furthermore, this increase in burst like activity was observed two hours after trauma (Figure 5.17C).

Table 5.3 Estimation of time window for ISI measurements during SA after tone presentation. Table provides a summary of laminar specific changes in ISI following acoustic trauma in different frequency bands; 2-8 kHz (1), 8-16 kHz (2),16-32 kHz (3).

Cortical depth (µm)	Time point	ISI (< 6 msec)			ISI (< 8 msec)			ISI (< 10 msec)			ISI (< 12 msec)			ISI (< 15 msec)		
		1	2	3	1	2	3	1	2	3	1	2	3	1	2	3
-200	Post 1															
	Post 2									*			*			*

Bonferonni posttest on two way ANOVA. *p<0.05.

Overall changes in this parameter showed statistical increase compared to elevated baseline only in the 16-32 kHz frequency region (Figure 5.17 F)(8-16 kHz, n=10, p= 0.2317; 2-8 kHz, p=9, p=0.0722). Unlike laminar specific changes, average shift in ISI fraction compared to baseline was seen during post1 and post 2.

To measure robustness of the selected time window of ISI interval (10 msec),

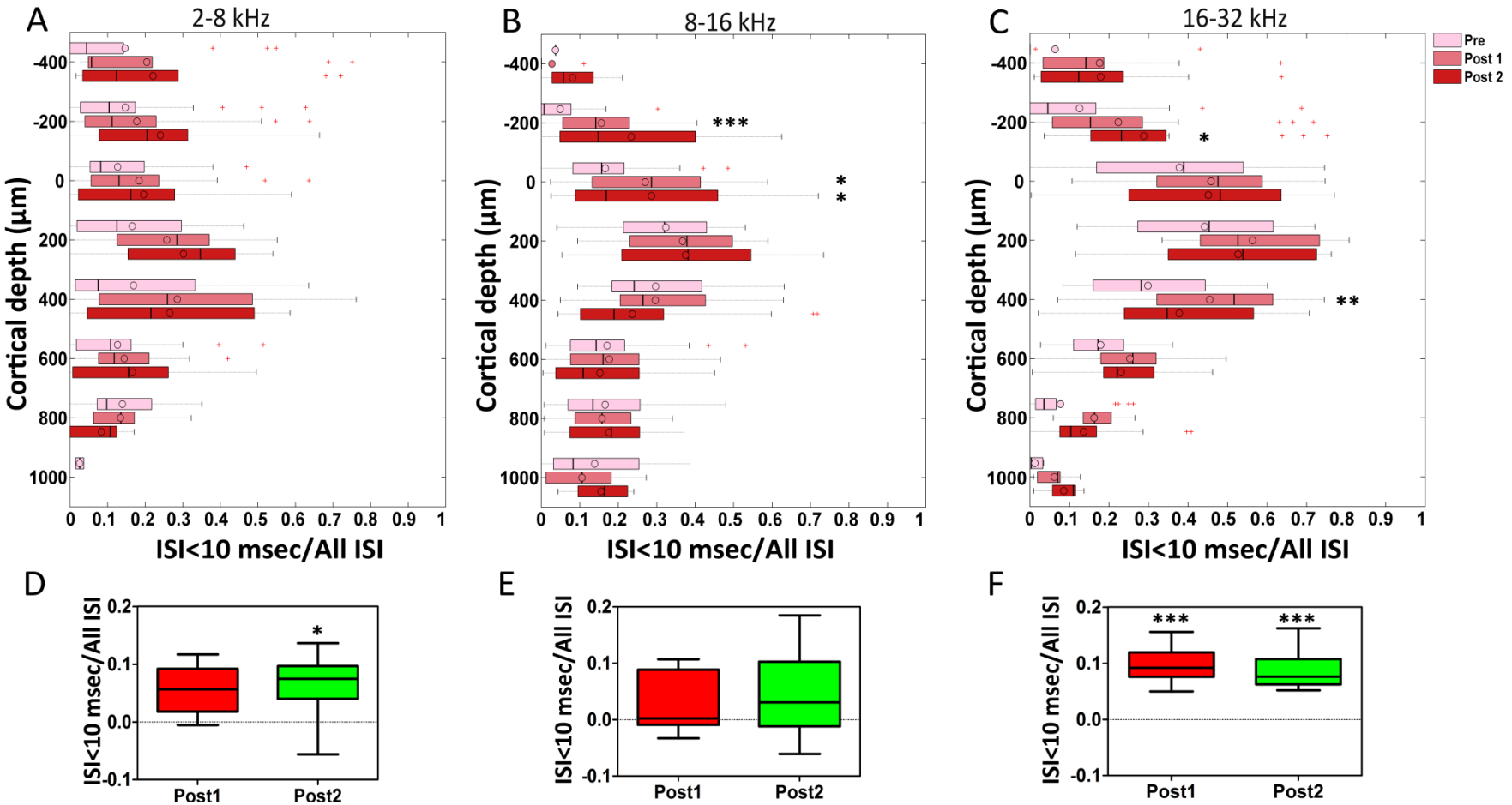

Figure 5.15 Box and whisker plots representing changes in bursting activity for different frequency bands (A) 2-8 kHz (n=9),(B) 8-16 kHz (n=10) and (C) 16-32 kHz (n=6) before (light red), ten mins after trauma (middle) and one hour after post 1(dark red) before tone presentation. Figure 15 (D,E,F) are box and whisker plots indicating average change in bursting activity across all cortical layers during post 1 (red) and post 2 (green). Statistically significant shifts in bursting activity was seen in the 8-16 kHz (B) and 16-32 (C) frequency band regions following acoustic trauma. Average statistical increase in ISI were observed in the 2-8 kHz (D) and 16-32 kHz (F) frequency region. Statistics: Laminar profiles (A-C) Bonferroni posttest on two way ANOVA, box and whisker plots (D-F) Bonferroni posttest on one way ANOVA

laminar changes at the fraction of ISI values <6 msec, <8 msec, <10 msec, <12 msec and <15 msec in different frequency bands were calculated. Table 5.2 and Table 5.3 summarises laminar specific increase in ISI following acoustic trauma before and after tone presentation respectively. This evaluation indicated that 10 msec was a suitable time window for ISI evaluation.

5.5 Summary of changes seen following acoustic trauma

Table 5.4 summarises the laminar specific changes seen at various cortical depths following acoustic trauma. Sensory-evoked responses and SA showed laminar specific changes in AI to varying degrees at one and two hours post trauma. Following acoustic trauma, increase in threshold (Figure 5.2) and BW (Figure 5.6) compared to baseline was confined to the 16-32 kHz frequency region mainly in the layer V (cortical depth 200 µm to 400 µm, layer V). For threshold, the increase was smaller at a later time point (post 2) compared to measurements immediately after trauma (post 1) indicating some sort of a reversal in changes.

Changes in CF post trauma were seen across all frequency bands mainly in layers III, IV & V (Figure 5.4). Interestingly, decrease in sparseness was seen only in layers I/II and not in the layers where increase in threshold shift was observed (Figure 5. 8). This may be due to the simultaneous increase in background activity in the 8-16 kHz and 16-32 kHz frequency region increased following acoustic trauma (Figure 5.10).

Laminar specific changes in SA was confined to the 16-32 kHz frequency region and observed only two hours post trauma (post 2) at 200 µm cortical depth (Figure 5.14) (delayed response). Similarly, increase in fraction of ISI less than 10 msec in the 16-32 kHz was seen in layers I/II during post 2 (Figure 5.17C).

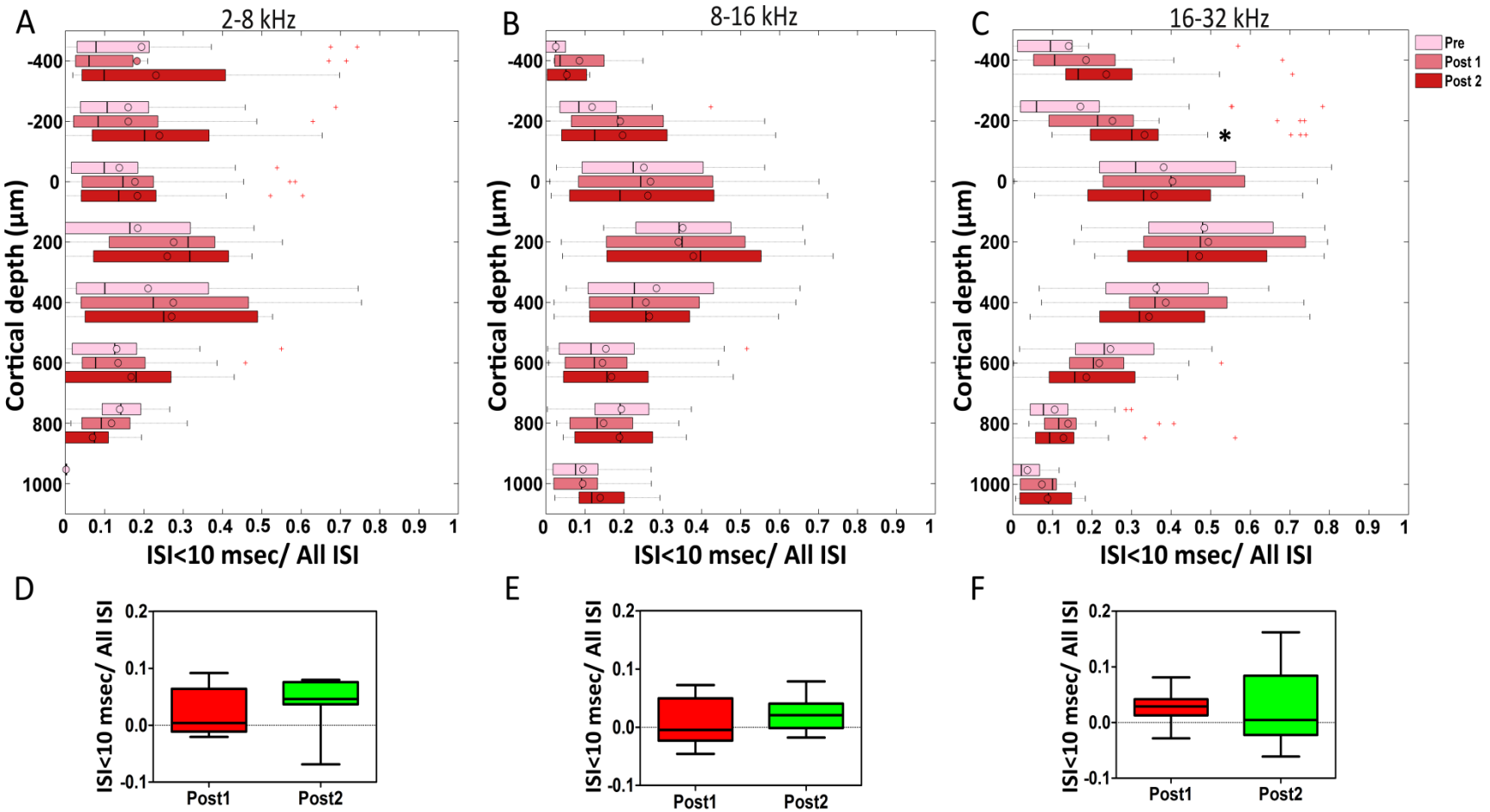

Figure 5.16. Box and whisker plots representing changes in bursting activity for different frequency bands (A) 2-8 kHz (n=9),(B) 8-16 kHz (n=10) and (C) 16-32 kHz (n=6) before (light red), ten mins after trauma (middle) and one hour after post 1(dark red) after tone presentation. Figure 16(D,E,F) are box and whisker plots indicating average change in bursting activity across all cortical layers during post 1 (red) and post 2 (green) Statistically significant shifts in bursting activity was seen in the 8-16 kHz (B) and 16-32 (C) frequency band regions following acoustic trauma. Average s tatistical increase in ISI were observed in the 2-8 kHz (D) and 16-32 kHz (F) frequency region. Statistics: Laminar profiles (A-C) Bonferroni posttest on two way ANOVA, box and whisker plots (D-F) Bonferroni posttest on one way ANOVA

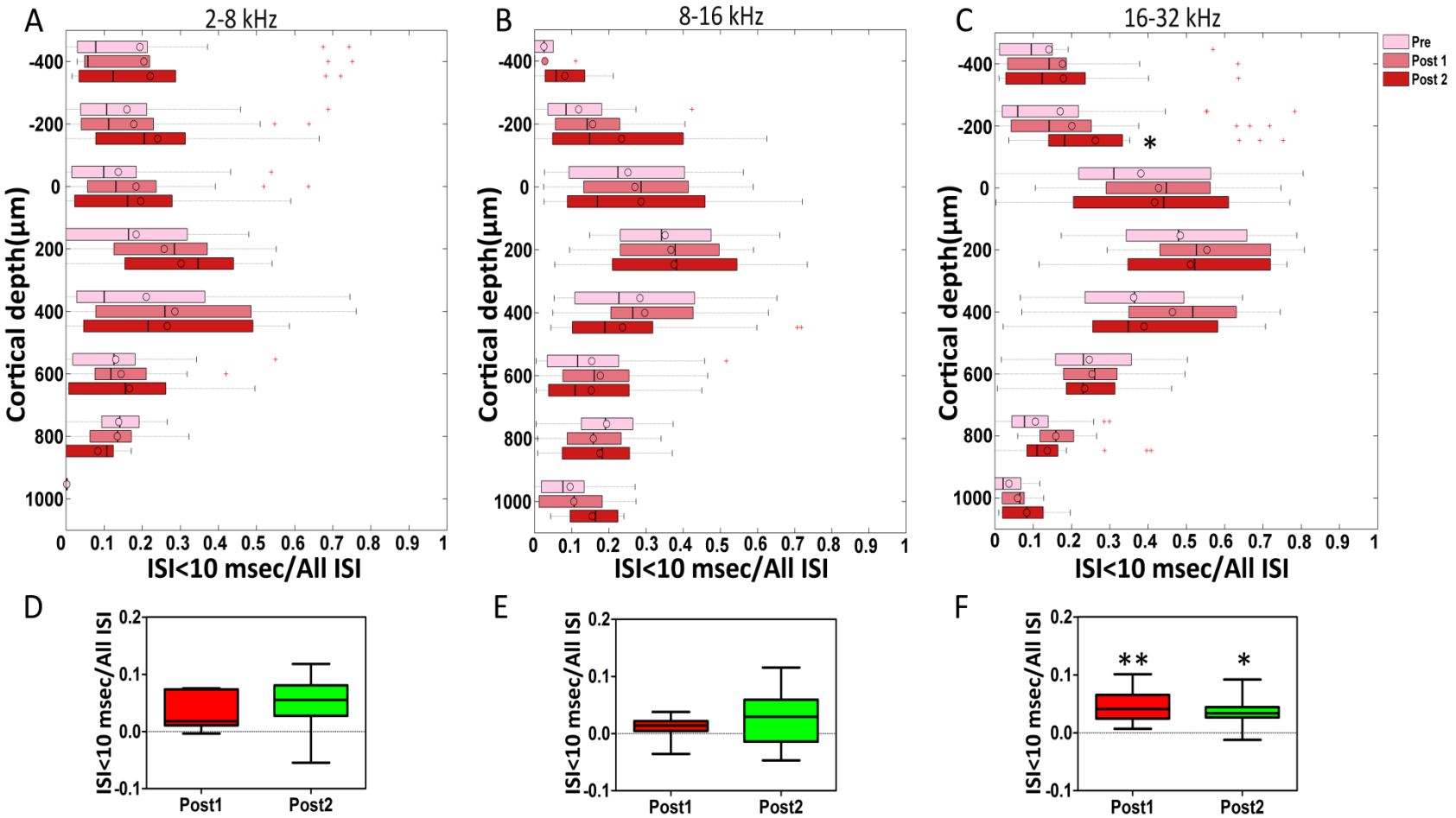

Figure 5.17 Box and whisker plots representing changes in bursting activity for different frequency bands (A) 2-8 kHz (n=9),(B) 8-16 kHz (n=10) and (C) 16-32 kHz (n=6) before (elevated) (light red), ten mins after trauma(middle) and one after post 1 (dark red) . Figure 5.17 (D,E,F) are box and whisker plots indicating average change in bursting activity across all cortical layers during post 1 (red) and post 2 (green). Statistically significant shifts in bursting activity was seen only in the 16-32 (C) frequency band at -200 µm cortical depth during post 2. Statistically significant shifts were only observed in overall changes 16-32 kHz (D) frequency region. Statistics: Laminar profiles (A-C) Bonferroni posttest on two way ANOVA, box and whisker plots (D-F) Bonferroni posttest on one way ANOVA

Table 5.4 Summary of laminar specific changes in evoked response and SA in 2-8 kHz(1), 8-16 kHz (2), 16-32 kHz(3) frequency regions one (post 1) and two hours (post 2) following acoustic trauma. Red coloured box indicate increase and blue coloured show decrease in response compared to baseline.

Pre vs	Depth	Threshold (dB SPL)			CF (oct)			BW			Sparseness			Background			SA before stimuli			SA after stimuli			SA (elevated Baseline)			Bursting (elevated baseline)		
		1	2	3	1	2	3	1	2	3	1	2	3	1	2	3	1	2	3	1	2	3	1	2	3	1	2	3
Post 1	-400																											
Post 2																												
Post 1	-200																											
Post 2																												
Post 1	0																											
Post 2																												
Post 1	200																											
Post 2																												
Post 1	400																											
Post 2																												
Post 1	600																											
Post 2																												
Post 1	800																											
Post 2																												
Post 1	1000																											
Post 2																												

5.6 Changes in cortical state

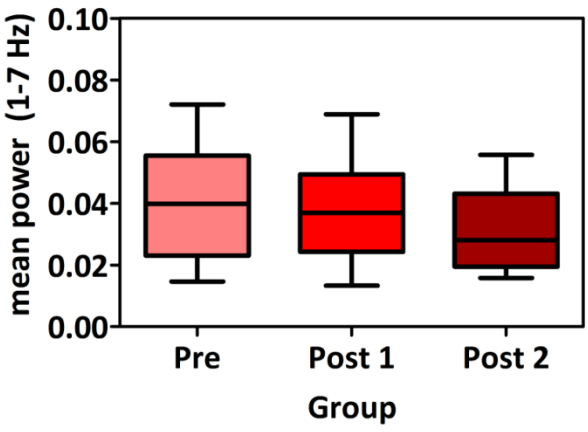

Figure 5.18 Box and whisker plot showing mean power at 1-7 Hz before, one hour after (post 1) and two hours after (post 2) acoustic trauma. No statistically significant changes were observed in across the experiment. Statistics: Bonferroni posttest on one way ANOVA

As most of the laminar specific changes were observed in between the cortical layers of 0 µm and 600 µm, measurements of changes in cortical state were limited to these depths (n=25) before and after acoustic trauma. This evaluation was necessary to exclude the possibility that any changes were observed due to fluctuations in cortical states on account of changes in level of urethane anaesthesia over time. As seen in Figure 5.18 no significant change in cortical state was seen throughout the experiment confirming that the above mentioned laminar changes were due to trauma induction alone and not because of changes in level of anaesthesia.

5.4 Conclusion

Laminar specific shifts in auditory evoked response and SA were observed in AI following acoustic trauma. Changes in auditory evoked responses were observed immediately after trauma and were more or less preserved over time (post 2). Furthermore, changes in threshold, CF and BW were mainly confined to layer V.

Unlike immediate changes observed in sensory evoked response, changes in SA activity and ISI following trauma showed a more delayed increase in activity compared to baseline. A change in SA was seen mainly in layer V and ISI were seen only in layers I/II.

Chapter 6

Discussion and Conclusions

6.1 Summary

In this chapter a comparison of current results to previous literature is made. Furthermore, the interpretation of the results and its relevance to the proposed hypothesis and its limitations are summarised, reviewed and discussed. In Section 6.2, the current results are summarised followed by their comparison to previous literature is provided in Section 6.3. The results are then interpreted in Section 6.4 and their limitations and possible future work highlighted in Section 6.5. Finally, Section 6.6. concludes the data obtained from the current investigation.

6.2 Overview of Results

To understand the role of the AI during normal auditory processing and the changes that occur following induction of acoustic trauma, it is of paramount importance that we understand the laminar specific properties of auditory evoked responses and SA in the AI before and after induction of acoustic trauma. To achieve this understanding in the present investigation we simultaneously evaluated laminar changes in AI before and after trauma induction via large-scale extracellular recording using multi-channel linear silicon probes in urethane anesthetised male, Sprague Dawley (SD) rats. Only male rats were used to avoid any variability that could be introduced due to gender differences. The individual experiments were first evaluated based on location within AC (auditory evoked response and location within the threshold/frequency map see Figure 4.2.) Any experiment where the value was outside the typical distribution observed in the AI was not included in the final analysis. Furthermore, the laminar evaluation was carried out using CSD analysis. The appropriate data-sets were then further analysed to measure auditory evoked multi-unit activity (MUA) in response to short pips and SA before (pre) trauma presentation; one hour after (post 1) and two hours (post 2) after trauma presentation. After measurements of laminar profile during baseline activity (normal auditory processing), the data-sets were further divided into three frequency bands to measure laminar changes following acoustic trauma. As mentioned in Chapter 3, the lower two frequency bands (2-4

kHz and 4-8 kHz) were combined into one (2-8 kHz) as there were very few experiments recorded in the 2-4 kHz region and the data would not have been statistically relevant on their own. In the following sections, I will briefly summarise the results from this project.

6.2.1 Criteria for data evaluation

The animals were anesthetised with a 20% w/v solution of urethane anaesthesia via the intraperitoneal route. A total of ninety-nine experiments were conducted of which twenty-five experiments were used for optimisation of the procedure. This involved selection of the position of the speaker for trauma presentation and short pip presentation, angle of insertion of the silicon probe and head fix protocols.

The remaining seventy-five experiments were conducted to investigate effect of acoustic trauma on laminar profile of the AI. However, there were a few unavoidable technical issue associated with the procedure, mainly, with the mortality associated with urethane anaesthesia. Urethane anaesthesia was a suitable choice for these recordings due to its ability to induce and maintain steady states of anaesthesia for long periods of time (Field et al., 1993). Furthermore, urethane anaesthesia is shown to maintain brain activity similar to that seen during natural slow wave sleep which is composed of alternating up (depolarising) and down (hyperpolarising) states (Clement et al., 2008; Frederick et al., 2014; Sharma et al., 2010; Steriade et al., 1993), providing an oscillation-permissive state for the measurement of evoked and SA activity in the AI. However, urethane anaesthetics have a relatively narrow therapeutic window showing about 20-25% mortality at 1.5 g/kg concentration in rats (Field et al., 1993) similar to that observed in the present investigation (Figure 4.1A).

The first data evaluation criterion was based on the MUA tuning profile of the data sets. In spite of using the co-ordinates as mentioned in Dorn et al (Doron et al., 2002) to locate AI, some experiments were wrongly recorded from the non-primary areas of the AC as it was difficult to estimate the boundaries of AI. This

issue was further magnified due to the restricted spatial diameter covered by the linear probe. Previous studies have shown that within the rat AI, typical 'V' shaped tuning curves are observed (Sally and Kelly, 1988). Data sets in which the tuning curves showed not even the slightest resemblance to the 'V' shape indicated that the recording was very likely obtained from the non-primary areas of the AC and were excluded from the final step of data interpretation.

The second step criterion for data evaluation was based on the laminar profile of the recording. As each data set is a unique recording, an alignment criterion was required to average layer specific details across data sets. The alignment criterion was determined using CSD analysis. CSD analysis on LFP (Chapter 3, Section 3.6.2.2) helps determine the spatial description of the net flow of current into and out of region allowing the estimation of activated regions in the cortical layers (Mitzdorf, 1985). The laminar CSD profile of AI is in good agreement with anatomical investigations with the major sink channel correlating to the middle layers (L III/IV) of AI (Kaur et al., 2005) and could be used as an alignment point for layers across experiments. However, in investigations where the CSD profiles were distorted due to interference of external electrical noise or noisy channels it was hard to determine the sink channel accurately (Figure 4.1B, Appendix Figure 1) and these data sets were not included for further analysis. Following evaluation based on CSD analysis and alignment across the different data-sets, values across 200 µm cortical depths were averaged providing a 200 µm resolution. Assuming that the cortical thickness is approximately 1600 µm (from pia to end of L6) (Paxinos and Watson, 1998), and that L5 is between 695 to 1100 µm (Sakata and Harris, 2012), based on the location of the alignment point (categorised as 0 µm)and the above mentioned calculation (200 µm resolution) the various layers were then determined as shown in Figure 3.15.

Finally, only when evaluating the effects of acoustic trauma the data sets were divided into three categories on the basis of their baseline mean CF: 2-8 kHz (n=9), 8-16 kHz (n=10) and 16-32 kHz (n=6) to measure laminar changes in different tonotopic areas of AI (Figure 4.2) following trauma induction.

6.2.2 Baseline profile of auditory-evoked response

Baseline profile of sensory-evoked responses was evaluated by quantifying various tuning curve parameters such as threshold, CF, BW and sparseness across different cortical layers. The scatter plot of the baseline average threshold versus the baseline CF for all the recordings showed a typical 'V' shape as represented by the moving average(loess curve), characteristic of that seen in the AI of different species (Kimura and Eggermont, 1999; Noreña and Eggermont, 2003a; Sally and Kelly, 1988).

The average tuning curve profiles for layers I, II, III, IV, V & VI were determined. Typical example of the tuning curve profile across cortical depths is shown in Figure 4.3B, showing a sharper frequency tuning in the middle layers compared to the deeper (Figure 4.3D) and superficial layers (Figure 4.3A).

The distribution of baseline evoked response across different cortical layers was determined for all data sets, (n=25). Following laminar specific profiles of the various tuning parameters were observed (Table 4.4).

CF (Figure 4.4 (A, B) - The box and whisker plots (Figure 4.4A) showed data sets spanning the entire range of presented frequencies (four octaves). The limited range of CF distribution observed at the -400 μm cortical depth is likely due to the noisy tuning curves observed at this depth. Normalised mean CF of each layer (Figure 4.4B) showed a tendency for laminar difference. However, these differences were not statistically significant.

Threshold (Figure 4.5 (A, B))-On normalising the observed threshold to the mean threshold of the particular layer, similar findings to CF were observed. Even though a tendency for laminar difference was observed, these apparent differences were not statistically significant.

Sparseness (Figure 4.7 (A, B)) - Laminar specific sparse activity was observed in the AI. Superficial and Deep 2 layers showed greater tone-evoked sparse activity as compared to the layers III, IV and V, with layer V being most dense.

BW (Figure 4.8 (A, B)) - No laminar specific changes in BW was observed in AI.

6.2.3 Laminar profile of auditory-evoked response following acoustic trauma

Following baseline measurements the data sets were further divided into three categories on the basis of their average baseline CF. Overall and laminar specific shifts in tone-evoked responses in the three different frequency bands following acoustic trauma were measured and analysed. Presented trauma intensity was centred at 16 kHz frequency and at 110 dB SPL intensity for a period of sixty minutes. For a small set of control experiments, noise trauma was replaced by an hour of silence (see Appendix Figure 3 (A, B), and Figure 4 (A, B)).

Laminar specific changes in threshold (Figure 5.1and Figure 5.2) and BW (Figure 5.5 and Figure 5.6) were only seen in the 16-32 kHz frequency region. Statistically significant increase in threshold following trauma was observed only in layerV following trauma induction. However a decrease in the threshold shift was observed at the post 2 time point. Shifts in BW were also seen immediately after trauma at both time points i.e. post 1 and post 2. However, the layer-specific shifts were observed not only in layer V but all in the middle layers as compared to control.

Some tendency of a threshold gain was observed in the 2-8 kHz frequency region in layer V). However no statistical difference in threshold shift compared to baseline was observed at this depth.

Unlike observed laminar shifts in threshold and BW, shifts in CF following trauma induction were observed in all frequency band regions (Figure 5.3 and Figure 5.4). In the 16-32 kHz frequency regions, shifts were observed immediately after trauma mainly in the cortical layers III, IV & V; mainly a shift towards a lower octave. However the shifts in CF towards a lower octave in the 8-16 kHz region were observed in much deeper layers (cortical layer VI).

On account of increase in threshold in layer V of AI following acoustic trauma in the 16-32 kHz frequency region, we expected to observe a decrease in sparseness (Figure 5.7 and Figure 5.8) in similar layers. Interestingly, no changes in sparseness were observed in layer V following acoustic trauma in the 16-32 kHz frequency region On the contrary a decrease in sparseness was observed in the superficial layers. No change in sparseness at the expected cortical depths in the 16-32 kHz was partly due to the increase in background activity observed in these layers post trauma (Figure 5.10C).

Interestingly, for all the above mentioned tuning parameters, the overall changes in any of the frequency band did not correlate statistically with the observed laminar changes.

As most of the changes associated with tone-evoked responses are confined to the layers III, IV & V (Table 5.4) and to ensure that the observed changes were not a consequence of changes in cortical state, average mean power (1-7 Hz) was evaluated at the different time points (pre, post 1 and post2). No statistical differences were seen in the cortical states across the three time points indicating that the observed changes are due to trauma induction.

6.2.4 Laminar specific change in SA before and after trauma induction

Changes in SA were observed before and after stimuli presentation (Chapter 3, Figure 3.9) during baseline recording (Figure 4.10). Laminar specific SA was observed in AI during normal auditory processing in which the cortical layer V showed highest SA activity. Furthermore, the SA activity increased even after normal stimuli presentation (short pips). Hence, to evaluate true SA changes following acoustic trauma, additional analysis was carried out in which laminar specific changes in SA following acoustic trauma were evaluated against both the true and elevated baselines.

Comparison of SA recorded before stimuli presentation and compared at time points one and two hours after acoustic trauma, showed an immediate layer

specific and overall increase in SA in the 8-16 kHz and 16-32 kHz frequency band region (Figure 5.11). These changes were confined to layers III, IV & V. However, when these shifts were compared against the elevated baseline SA (Figure 5.14), a delayed increase in SA compared to baseline only in layer V was observed in the 16-32 kHz region, which was similar to observations of SA measured after tone presentation (Figure 5.12). Unlike an increase in SA compared to baseline observed when SA was measured prior to stimuli presentation, no changes in overall SA was observed when measured against the elevated baseline or after the stimuli presentation.

Previous studies have shown an increase in synchronous firing following acoustic trauma (Seki and Eggermont, 2003). As in this investigation only MUA is evaluated, in this instance one of the means to measure possible synchronous firing was to evaluate layer specific changes in ISI representing burst like activity during SA measurements before and after acoustic trauma. Various ISI parameters were evaluated across all frequency regions (Table 5.2 and Table 5.3) and 10 msec was selected to be the ideal ISI time window. As in the case of SA activity significant differences were seen in the baseline ISI measure before and after tone presentation (Figure 5.15, Figure 5.16). When changes in burst-like activity compared to elevated baseline an increase in activity is observed two hours post trauma only in the superficial cortical layers in the16-32 kHz frequency region (Figure 5.17).

6.3 Comparison to previous literature

Laminar structure of the AI has been investigated previously in different species under anesthetised and awake conditions. However, most studies involved the comparisons of laminar information from different data sets inducing possible variations and discrepancies in the observed results. Recently, relative laminar changes have been investigated using large scale extracellular recordings in normal (Atencio and Schreiner, 2010b; Sakata and Harris, 2009, 2012) and abnormal auditory processing (Stolzberg et al., 2012). In this section, the observed

results in this investigation will be compared to previous findings regarding laminar specificity in normal and abnormal auditory processing.

6.3.1 Laminar specific auditory evoked response during normal auditory processing

To evaluate how the AI microcircuit contributes as a whole towards auditory processing it is vital to understand the laminar specific response of AI. Evidence about the laminar differences in evoked response properties of the AI has been contradictory. Several studies have shown that that in terms of CF, threshold, BW no laminar difference in AI microcircuits is observed (Abeles and Goldstein, 1970; Clarey et al., 1994; Foeller et al., 2001; Phillips and Irvine, 1981). However other studies show laminar specific differences in these properties during normal auditory processing (Dear et al., 1993; Eggermont, 1996; Reser et al., 2000; Stolzberg et al., 2012; Sugimoto et al., 1997; Wallace and Palmer, 2008). Furthermore, evidence from other sensory modalities such as the somatosensory (Brumberg et al., 1999) and visual cortex (Hubel and Wiesel, 1962) which show strong laminar specific sensory responses (Linden and Schreiner, 2003) indicate a high likelihood of laminar specific organisations in the AI. By simultaneous measurements of evoked responses to auditory stimuli using multi-channel silicon probes we aimed to address some of these discrepancies.

The laminar profile of the observed tuning curves is in agreement with previous studies where the layer III/IV), Figure 4.3B show sharper tuning curves compared to the layer V where the tuning curves are relatively broader, Figure 4.3D (Atencio and Schreiner, 2010a; Sakata and Harris, 2009). This is possibly because these layers receive direct input (Huang and Winer, 2000; Lee and Imaizumi, 2013; Winer and Lee, 2007)from the sharply tuned vMGB neurons (Anderson et al., 2007; Calford, 1983) influencing their tuning properties.

In the present investigation, we measured BW at thresholds 10 dB above the actual threshold. No laminar specific changes in BW (See Figure 4.8B) were observed in AI during normal auditory processing. This observation is not in

agreement with previous reported studies(Sakata and Harris, 2009; Sugimoto et al., 1997; Wallace and Palmer, 2008) which report a difference in BW between the middle and deep layers. It is crucial to point out that several of these investigations (Sugimoto et al., 1997; Wallace and Palmer, 2008)do not directly report BW but a Q 10 value which is inversely proportional to BW; Q10 is CF/BW(Kiang, 1965). One possible explanation for the observed discrepancies between the current and previous literature may be due the fact that the present study reports MUA versus single unit activity (better resolution) reported in comparable literature. Also, as BW at 10 dB is dependent on the threshold, which in turn depends on the threshold response criterion (Chapter 3 Section 3.6.2.1), dissimilarities in the selected criterion for estimation of threshold could have possibly given rise to the discrepancies.

The laminar properties of other tuning curve parameters such as threshold, CF and sparseness have been previously investigated (Abeles and Goldstein, 1970; Atencio and Schreiner, 2010a, 2010b; Sakata and Harris, 2009; Stolzberg et al., 2012; Sugimoto et al., 1997; Wallace and Palmer, 2008). The present investigation is on par with several previous studies that show that the CF is generally preserved across layers in the AI (Figure 4.4 B) (Abeles and Goldstein, 1970; Atencio and Schreiner, 2010b; Foeller et al., 2001; Phillips and Irvine, 1981). This however is not in agreement with other investigations that show laminar difference in CF properties in AI (Stolzberg et al., 2012; Sugimoto et al., 1997). Furthermore, recent imaging studies claim the possibility of laminar specific tonotopic organisations (Rothschild et al., 2010; Winkowski and Kanold, 2013). These discrepancies could be contributed to a few factors. Apart from variations observed in species (Kanold et al., 2014) differences in the resolution offered by measuring techniques could contribute to these differences. It has been suggested imaging techniques such as in vivo two photon Ca^{2+} imaging provide better resolution compared to electrophysiological recording techniques (Kanold et al., 2014). However, the fractured tonotopy observed in the two photon imaging studies have been contradicted by investigations using two photon Ca^{2+} imaging studies in Cre Lox system controlled GCaMP3 transgenic mice which reconfirm

electrophysiological findings of possible smooth laminar distributions of CF in AI (Issa et al., 2014). Thus, this issue needs to be solved by further investigations.

Indications of a variation in threshold across cortical depths has been seen in the AI of mouse (Shen et al., 1999), gerbils (Sugimoto et al., 1997),and guinea pigs (Wallace and Palmer, 2008) indicating a layer specific organisation of threshold values. Furthermore, in these studies an increase in threshold parameters were observed with depth, with deeper layers (V/VI) showing statistically higher threshold values compared to the superficial layers (Sugimoto et al., 1997; Wallace and Palmer, 2008). In the current investigation even though a tendency for differences in threshold values across layers I, II, III, IV, V & VI was seen, no statistically significant differences were observed (Figure 4.5 A, B) indicating no laminar specific differences in AI which is in agreement with observations in cat AI (Clarey et al., 1994).

Further analysis would be required to measure single unit activity instead of MUA reported here which may provide better resolution and confirm whether the observed tendencies for laminar CF and threshold are real or unreal. Another factor that could influence the observed laminar profile is in the estimation of evoked response criterion. As discussed in Chapter 3, Section 3.6.2.1, in the present investigation, several response criterions were evaluated and the ability to detect threshold over background SA varied. Hence, different response criterions could introduce variations in the final observation.

Another parameter of interest for understanding principles of evoked response is sparseness (Barlow, 1972; Olshausen and Field, 2004; Willmore and Tolhurst, 2001). As previously mentioned, in the present research, field sparseness was investigated. In such a measurement, the response distribution of neurons to a range of stimuli is measured (Willmore and Tolhurst, 2001). At one end of the spectrum the measurement is considered sparse when a response is measured only during certain stimuli whereas the other end is dense where strong responses are measured throughout (Olshausen and Field, 1996). This type of evaluation has been successfully used in several sensory modalities across various species such as

rodents(Davison and Katz, 2007), cats (Haider et al., 2010), ferrets (Tolhurst et al., 2009) and non-human primates (Vinje, 2000)..

The observations regarding the laminar profile of sparseness in the AI auditory evoked response is in good agreement with previous investigations in anesthetised and awake rodents (Sakata and Harris, 2009) where layer V showed a denser response as compared to the other cortical layers, where the encoding of the auditory evoked signals is sparse (Figure 4.7 (A,B)).

To summarise, the laminar profile of auditory evoked response (MUA) such as threshold, BW and CF in the AI obtained in the present study was in good agreement with previous observations where no laminar difference in these parameters were observed within cortical columns (Abeles and Goldstein, 1970; Clarey et al., 1994; Phillips and Irvine, 1981). Furthermore, as seen in previous literature, sparseness in AI showed laminar specific response (Sakata and Harris, 2009).

6.3.2 Laminar specific SA during normal auditory processing

In the absence of sensory evoked response, the sensory cortex shows spontaneous spiking activity. In the visual cortex for example it is seen that these responses are not entirely random but show patterns similar to those seen in visually evoked responses (Arieli et al., 1996). Furthermore, these patterned SA observed in the sensory cortex are similar to sensory evoked responses (Arieli et al., 1996; Hoffman and McNaughton, 2002; Luczak et al., 2009; Saitoh et al., 2010) and are believed to play a vital role in normal functions such as memory consolidation, variability in behaviour (Fox and Raichle, 2007; Hoffman et al., 2007) and pathological conditions such as auditory hallucinations (Dierks et al., 1999).

In the current investigation (Figure 4.10) layer V showed greater SA activity as compared to the layer I, II, III, IV & VI. These observations are similar to findings

seen in previous investigation of the laminar profile of SA in the rat AI (Sakata and Harris, 2009; Stolzberg et al., 2012).

6.3.3 Laminar specific auditory evoked response and SA in AC following acoustic trauma

Evidence of effects of acoustic trauma on sub cortical structures in various species is abundant (Basta and Ernest, 2004; Bruce et al., 2003; Chen et al., 2003; Kaltenbach et al., 2004; Mulders and Robertson, 2009; Salvi et al., 1990; Zhang and Kaltenbach, 1998). On the contrary, investigations exploring the effects of acoustic trauma on AC are very limited (Eggermont and Komiya, 2000; Engineer et al., 2011; Kimura and Eggermont, 1999; Noreña et al., 2003; Seki and Eggermont, 2002, 2003). However, all of these studies report changes mostly in the middle layers of AI following acoustic trauma and not in other cortical layers. One commonly reported acute change in AI following trauma inductions is changes in tuning curve parameters. One such tuning curve parameter commonly indicated is changes in distribution of CF (tonotopic modification) following trauma induction . Unlike tonotopic reorganisation, tonotopic modification shows a change in receptive fields where higher frequency neurons respond to lower frequency stimulus. These changes have been observed in cats(Noreña et al., 2003), rats (Engineer et al., 2011)and guinea pigs (Huetz et al., 2014). Figure 5.4 (A,B,C) show that in the frequency band region above the trauma frequency as observed by Norena et al and Engineer et al a shift in CF to the lower frequency region is observed. Such shifts were not seen in the 2-8 kHz region. Similar to previous investigations in rats following acoustic trauma (Engineer et al., 2011)in the present study shifts to the lower frequency area were also observed in the 8-16 kHz region. However, unlike the 16-32 kHz region where shifts were seen in the layers III/IV & V (Figure 5.3 C and Figure 5.4 C), in the 8-16 kHz region the shifts post trauma were observed only in the layer VI (Figure 5.3 B and Figure 5.4 B). As in previous literature, the changes in CF following acoustic trauma are reported as an average shift, the layer specific effects may have been masked and not reported. These changes in CF are in some but not all instances associated with a

shift in threshold at that frequency (Engineer et al., 2011; Kimura and Eggermont, 1999; Noreña and Eggermont, 2003b). The threshold changes observed in the present investigation following acoustic trauma in the middle layers showed no change in any of the frequency band regions as seen in previous literature (Noreña et al., 2003). On the contrary, the observed threshold shift was confined to layer V at both time points post trauma (Figure 5.2 C).

Contrary to previous literature which reported a decrease in tuning curve BW 10 dB above threshold (Kimura and Eggermont, 1999) we noticed an increase in BW at both time points post trauma in the frequency region 16-32 kHz in layers III, IV & V. One possible explanation for this is that the loss in the lower intensity regions can result in a loss in the 'V' shape of the tuning curve post trauma reflecting an increase in the BW in that region.

Another neural parameter often acutely altered in AC following acoustic trauma is spontaneous firing. Following acoustic trauma we noticed an overall increase in SA in the 2-8 kHz frequency region as a slightly delayed response (post 2) (Figure 5.14 D) which is similar to observations made in cats (Noreña et al., 2003). However, even though there is a tendency for increase in the higher frequency region, there was no statistical difference (Figure 5.14 F). Laminar specific changes were confined to the higher frequency regions in layer V (5.14C). In the present study we investigated changes in SA before (Figure 5.11) and after (Figure 5.12) trauma presentation and did notice some discrepancies at the two time points. Where the SA after tone presentation was similar to what was observed previously, the SA before tone presentation was seen in all tonotopic regions and immediately after trauma presentation (Figure 5.11 A-F). Interestingly, we also observed increase in SA in the control experiments (Appendix 3B, 4B) implying that the invasive nature of the procedure may play a role in the noted increased SA. To determine changes in temporal MUA properties following acoustic trauma i.e. enhanced burst-like property, we measured changes in ISI intervals during SA (Figure 5.17). A similar trend to that observed in SA with the difference in measurements observed before and after tone presentation was seen for ISI activity (Figure 5.15 and Figure 5.16). An increase in ISI was observed in the 16-32 kHz region which is not on par

with investigations in cats where no changes in ISI was observed following trauma(Noreña and Eggermont, 2003a). One possible explanation for this is that, the MUA response measure in this study measure average ISI changes versus specific single unit investigations reported in previous literature.

6.4 Interpretation of Results

To understand pathologies of noise induced auditory disorders, it is vital to investigate the laminar profiles of auditory evoked response and SA during normal auditory processing and evaluate the laminar specific changes following acoustic trauma. In the present investigation we measured auditory evoked and spontaneous activity before and after trauma by simultaneously recording from different cortical layers using multi-channel silicon probes. During normal auditory processing, we did not observe any laminar specific responses in threshold, CF, BW. However, laminar specific sparseness and SA response as seen in previous investigations was observed. Following acoustic trauma, changes in evoked response in layers III, IV & V immediately after trauma were observed. Changes in SA responses varied depending on whether they were measured before or after stimuli presentation. Details about these changes and the possible relevance to changes in auditory processing post trauma are discussed in the subsequent sections.

6.4.1 Novelty and Relevance to Hypothesis

6.4.1.1 Laminar structure of population activity during normal auditory processing

Compared to the visual and somatosensory system, our knowledge about the laminar profile of the vertical microcircuits in the auditory system is still limited (Linden and Schreiner, 2003). To understand auditory cortical processing, it is vital to understand how the different cortical layers process information in the presence and absence of external stimuli. Using multi-channels silicon probes we were able to determine layer specific differences in AI in terms of tuning curve

parameters. Based on findings from previous investigations which showed laminar specific auditory evoked response (Anderson et al., 2007; Sakata and Harris, 2009; Stolzberg et al., 2012; Sugimoto et al., 1997)and by drawing inspiration from other sensory modalities such as the barrel (Brumberg et al., 1999) and visual (Hubel and Wiesel, 1962)cortex , we had hypothesised that the different layers of AI would show laminar specific tuning properties. However, in the current investigation as discussed previously, even though we saw a tendency for differential lamination of these properties, they could not be statistically quantified. This observation is in good agreement with other investigations that showed similar tuning profiles of the tuning properties of the AI (Abeles and Goldstein, 1970; Phillips and Irvine, 1981).

However, based on the current level of investigation neither of the possibilities (laminar specific or non-specific) can be confirmed. The resolution offered by MUA measurements in this study may not be sufficient to tease out laminar differences if any and further analysis to determine single unit activity will be required. If these results are confirmed following single unit activity measurements, it would indicate the possibility that unlike other sensory modalities auditory processing in the AI influences functional organisation in such a way that it masks any laminar differences by confining response variability's to certain layers rather than across cortical layers(Linden and Schreiner, 2003). However, this is very unlikely to be the case. Laminar specific profiles such as higher inhibitory inputs in the superficial layers compared to the other cortical layers (van Brederode and Spain, 1995), layer specific sparse activity (Sakata and Harris, 2009) also observed in this investigation, strongly suggest the existence of laminar specific responses in AI. In the current investigation, sparseness was measured over a larger frequency area compared to previous investigations (Sakata and Harris, 2009). Once again, as reported in previous investigation, layer specific differences in sparse activity were observed, with layer V being the least sparse.

Further evidence for such assumptions of layer specific processing can be derived from studies in which the auditory thalamocortical circuit is modified by directing retinal inputs to the auditory thalamus. These studies have shown that AI is

capable of developing laminar specific responses similar to those seen in the primary visual cortex, strongly suggesting the possibilities of similar columnar organisations across the different sensory modalities.

6.4.1.2 Laminar specific changes in the auditory evoked responses following acoustic trauma

To the best of our knowledge, no other studies have investigated laminar changes in AI in rats following acoustic trauma by simultaneously recording from the different cortical layers before and after trauma presentation. The MUA activity recorded showed laminar specific effects in the commonly observed changes in neural activity following acoustic trauma (Noreña et al., 2003).

One of the major issues with interpretations regarding the neural correlates of acoustic trauma is the high variability in the results using animal models (Noreña et al., 2010). Apart from the species and anaesthesia/awake induced variability, the present research indicates that the discrepancies can also arise depending on the layer from which the recordings were measured. Shift in CF (Figure 5.3 (A,B,C, Figure 5.4 (A,B,C) and BW(Figure 5.5(A,B,C) and Figure 5.6 (A,B,C)) following acoustic trauma were immediate and confined mainly to middle layers III, IV & V), indicating that the changes in CF distribution are confined mainly to these layers. In the AI, apart from the major thalamic afferents received by layer III/IV cortical layers, another major thalamic input is observed in the V/VI boundary of rat AI (Constantinople and Bruno, 2013; Kimura et al., 2003; Romanski and LeDoux; Sakata and Harris, 2009). This may explain the possible observed immediate changes in these layers following acoustic trauma as through direct inputs from the thalamic afferents these layers mirror changes that are occurring in the peripheral and sub cortical auditory structures. Furthermore, these changes could possibly be due to the rapid unmasking of fine tuning in these areas (Noreña et al., 2003). As discussed earlier (Chapter 2), the cortical neurons are fine-tuned by maintaining a fine balance between excitatory and inhibitory inputs. Following acoustic trauma, a reduction of this inhibitory mechanism which masks the excitatory thalamic inputs from nerve fibres tuned to CF different from the

expected CF is observed. This unmasking can then change the tuning properties of the neuron explaining the observed changes in tuning parameters following acoustic trauma(Noreña et al., 2003; Salvi et al., 2000).

Interestingly, unlike CF and BW, the threshold values seem to increase only in the Deep layer 1 (Figure 5.1 (A, B, C) and Figure 5.2 (A, B, C)). Further, investigation would probably be required to understand these discrepancies fully. However, inspiration can be taken from findings from the Barrel cortex where sensory deprivations in the form of whisker deprivation caused experience induced plasticity in layer V (Diamond et al., 1994; Fox, 2009; Jacob et al., 2012) with minimal changes in layer IV of the thalamorecipient layers (Glazewski and Fox, 1996) indicating that layer V is possibly more susceptible to changes post trauma compared to the middle layers.

No studies previously have reported changes in laminar profile of sparseness following acoustic trauma. Based on previous observations that layer V show dense auditory evoked responses (Sakata and Harris, 2009) one would expect an increase in sparseness in regions following acoustic trauma associated with increase in threshold intensity. Interestingly increase in sparseness was observed only in layers I /II (Figure 5.7 and Figure 5.8). On measuring background activity in the different cortical layers we noticed that the increase in sparseness was not observed in this layer due to enhanced background activity in this region (Figure 5.10), suggesting that the signal-to-noise ratio also decreased after trauma.

The above findings suggest that the acute effects of trauma on auditory evoked responses with the exception of sparseness is confined mainly to layer III, IV & V which receives a direct imprint of the peripheral changes occurring on account of exposure to trauma intensities. However, this change in information in the middle layers is not carried forward and possibly buffered by intracortical innervations (van Brederode and Spain, 1995)during the feed forward process to the superficial and then deeper layers. Similar observations can be applicable to the trauma related shifts observed in layer V, that they are a direct imprint of changes

occurring peripherally. However, these changes are buffered as they are processed in the further downstream targets (Constantinople and Bruno, 2013).

6.4.1.2 Laminar specific changes in the SA following acoustic trauma

Increase in SA in the AI is believed to be a consequence of reduced peripheral input due to trauma induction (Noreña, 2011). However, based on previous literature, increase SA activity is seen as a more delayed response compared to the immediate shifts in auditory evoked parameters (Noreña and Eggermont, 2003a). Unlike sensory evoked responses which have their origin mainly from the thalamic input, the SA activity in the cortical areas have their origin mainly in the cortico-cortical connections (Timofeev et al., 2000). This might partly explain why the SA activity is seen as a delayed response. Furthermore, the increase in SA post trauma was only seen in layer V in the frequency region one octave higher than the trauma frequency. At a similar time point an increase in the fraction of neurons having an ISI less than 10 msec indicating a burst like activity was observed in the superficial layers. Although it is not clear what are the potential mechanisms, one possible explanation is that following the initial changes in the auditory evoked response after trauma induction, the deeper layers receive feedback projections from higher cortical areas (Rouiller et al., 1991) which influence SA activity which in turn increase the burst like activity observed in the superficial layers.

6.4.2 Limitation and Future work for current study

6.4.2.1 Data Analysis

One possible limitation of the current study is the partly subjective nature of clustering of different MU spikes. After the initial clustering using EToS, the clusters were visually inspected, to eliminate extremely noisy clusters. Even though extreme caution was taken while determining the fate of such noisy clusters some level of operator bias is unavoidable. Improvised algorithms for

spike separation could be used in the future which could allow complete automation in detection of noisy clusters minimising need of manual detection and human bias.

Another limitation of the study is the subjective nature of the criteria to choose evoked response over background activity (cut-off). Even though different parameters were tested to optimise the choice of the cut-off (Chapter 3, Section 3.6.2.1), there is a possibility that the final result could slightly vary depending on the selected choice of cut-off determination method. One issue with conventional cut-off detection techniques assume a Gaussian distribution of background activity. This assumption may not always be true and more resilient estimations of evoked response criterion which do not assume Gaussian distribution may offer better; more robust option.

Further analysis of the current research would involve determination of neuronal correlations such as signal correlation and noise correlation (Averbeck et al., 2006). Signal correlations would quantify the similarity in evoked response to a stimulus between neurons and would provide additional analysis for the measurement of observed homogeneity of evoked response in layers III, IV & V during normal auditory processing. Noise correlations provide information about trial to trial variability (Cohen and Kohn, 2011)and can be used to measure responses such as correlated firing between neurons.

The current research represents layer specific MUA response in auditory evoked and SA activity in the AI following acoustic trauma. Owing to the laminar specific variations in cell type and density in the AC (Section 2.2.1.3.1, Table 2.1) the next step would be to carry out further analysis to determine layer specific single unit activity following acoustic trauma using spike sorting methods similar to that outlined in Section 2.4.2.2.3. Single unit activity would help determine the above explained changes in better detail e.g. which neurons are involved in the unmasking of stimulus evoked response in layers III, IV & V. It would also help determine factors such as drifting which is a common occurrence in electrophysiological recordings.

As increase in SA is often considered as a neural correlate of acoustic trauma, it would be important to further understand the variability in SA responses e.g. increase SA in control experiments (Appendix 3B and Appendix 4B). To achieve this, it would be critical to perform and quantify SA observations from additional control experiments in the different frequency bands.

6.4.2.2 Technical refinements

The silicon probes offer an excellent platform for large-scale extracellular recordings. However they are fragile and on very rare occasions can bend within the cortex. To determine such factors and to confirm the anatomical location of the probe, the silicon probes can be previously stained with fluorescent dyes (Buzsáki et al., 2003b; Prox et al., 2013; Sakata and Harris, 2009)and post-mortem histological evidence of paraformaldehyde fixed brains can be carried out (Sakata and Harris, 2009).

In the current investigation, the layer specific changes following acoustic trauma was simultaneously measured using multi-channel linear probes. However, changes in the different areas of the tonotopy of the AI were calculated by combining results from different rats. Such interpretations can induce variability in the final result. One alternative to reduce such variability would be to using multi-shank probes to simultaneously determine laminar changes in different tonotopic areas of the AI in the same rat following acoustic trauma.

6.5 Long term objectives of the project

6.5.1 Changes in thalamocortical functioning in response to acoustic trauma under anaesthesia

Following interpretation of the laminar profile changes in AC following acoustic trauma, simultaneous recording in the auditory thalamus and AI would allow characterisation of auditory thalamacortical interactions under anaesthesia

following acoustic trauma (explained in details in Chapter 2). This would provide details of circuit mechanisms involved in the pathology of acoustic trauma.

6.5.2 Neural correlates of acoustic trauma in awake animals

Acoustic trauma is one of the main causes of phantom auditory perception; tinnitus (Eggermont and Roberts, 2004). Animal models following trauma induction has been often recognised as an animal model of tinnitus (Eggermont, 2008; Kaltenbach, 2011; Moody, 2004; Noreña et al., 2010). Observations such as increased SA, burst-like activity and tonotopic modifications have been implicated in neural correlates of tinnitus (Eggermont and Roberts, 2004; Noreña et al., 2010; Stolzberg et al., 2012).Further investigations would involve measurements of behavioural correlates of tinnitus (Turner et al., 2006) following trauma induction using similar parameters as that used for the acute studies. After which electrophysiological recording mentioned in the acute study in the Section 1.3.2 would be repeated in head restrained, awake animals showing behavioural correlates of tinnitus. This would provide further in detail investigation of the neural correlates of tinnitus.

6.5.3 Reversal of the tinnitus like symptoms using techniques such as optogenetics or pharmacogenetics

Once the neural mechanisms of tinnitus are confirmed in the head restrained studies (Section 1.3.3), the next step would be to test whether correction of observed abnormal thalamocortical circuit would reverse the behavioural symptoms associated with tinnitus. Expressing light sensitive proteins locally into the desired region would allow optogenetic manipulation of the affected neuralcircuits and eliminate behavioural correlates of tinnitus.

Single-unit analysis could help recognise neuronal cell types involved in pathologies related to acoustic trauma. This in turn could identify novel gene targets that could be further assessed using pharmacogenetic manipulation.

6.6 Conclusion

In the current investigation we simultaneously measured layer specific auditory evoked MUA responses and SA in AI of urethane anesthetised rats before and after acoustic trauma. During normal auditory processing, we observed no laminar specific evoked response properties such as threshold or CF in the AI. However, following acoustic trauma mainly in the layer V immediate shifts in these response properties were observed. This suggests the possibility that laminar specific evoked responses in the AI do exist and are possible exacerbated following trauma. Furthermore, we observed that changes in evoked response following acoustic trauma were measured predominantly in the layer V, suggesting greater abilities for plasticity in this layer compared to other cortical layers.

Laminar-specific SA responses were observed during normal auditory processing and following acoustic trauma. Interestingly, changes following acoustic trauma unlike evoked responses were more delayed. This is possibly due to the fact that SA activities have their origin in cortico-cortical circuits which are not directly influenced by thalamic afferents. These changes in SA following acoustic trauma further altered temporal properties of spontaneous spiking such as burst-like firing in the more superficial layers of the AI suggesting feedback modification in the superficial layers by deeper layers via intra cortical processing.

This study suggests that laminar specific changes in evoked response and SA is observed in rat AC following acoustic trauma predominantly in layer V of the AI. Thus the current research shows that similar to that seen in the visual and the barrel cortex, layer specific changes exist in the auditory cortex, suggesting a similar pattern of cortical processing across the various sensory modalities. Further investigation would shed light on the pathophysiology of acoustic trauma

related disorders and the contribution of such layer specific changes to the development of such pathologies.

Appendix A

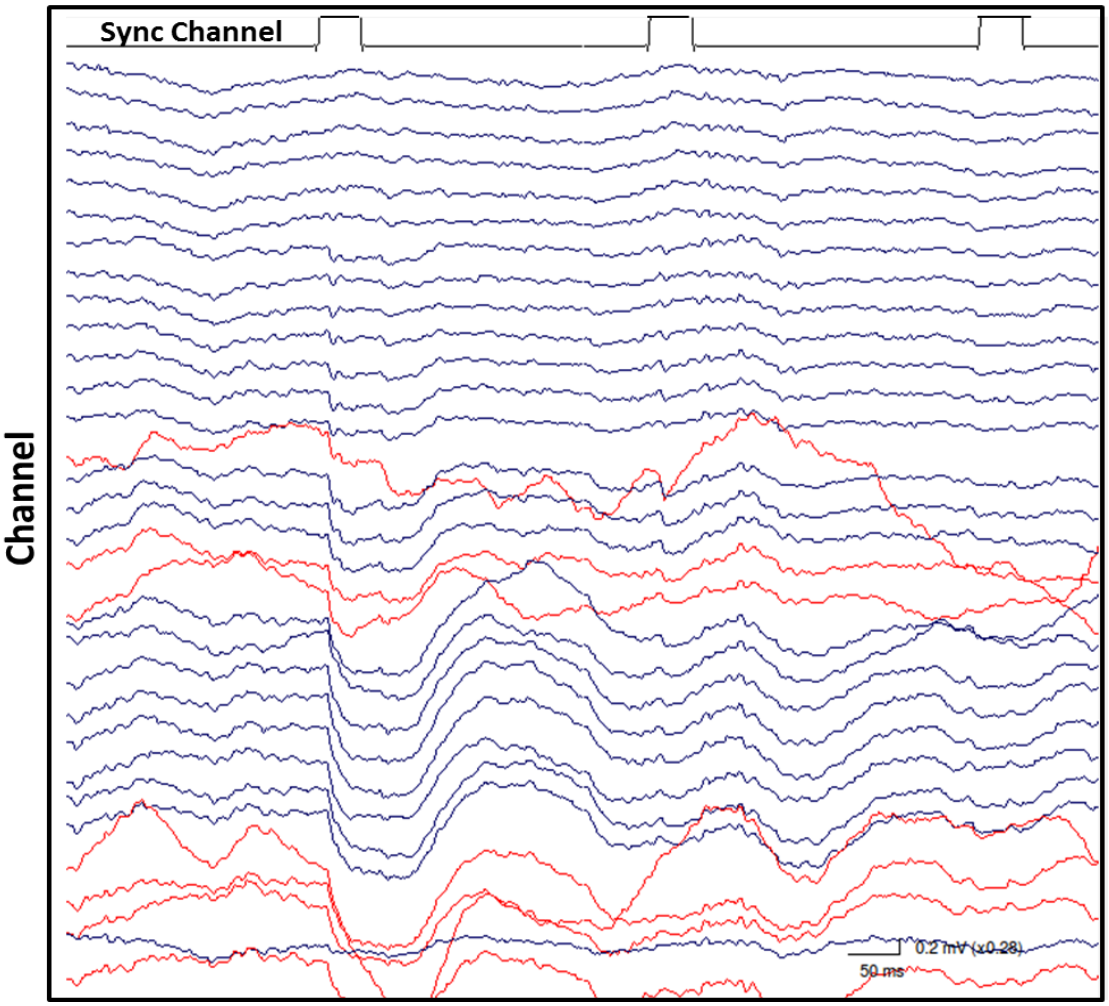

Appendix Figure 1. Typical example of raw LFP trace resulting in unclear CSD profiles The noisy channels (red colour) showing large fluctuations can make it hard to interpret accurate sink cannels.

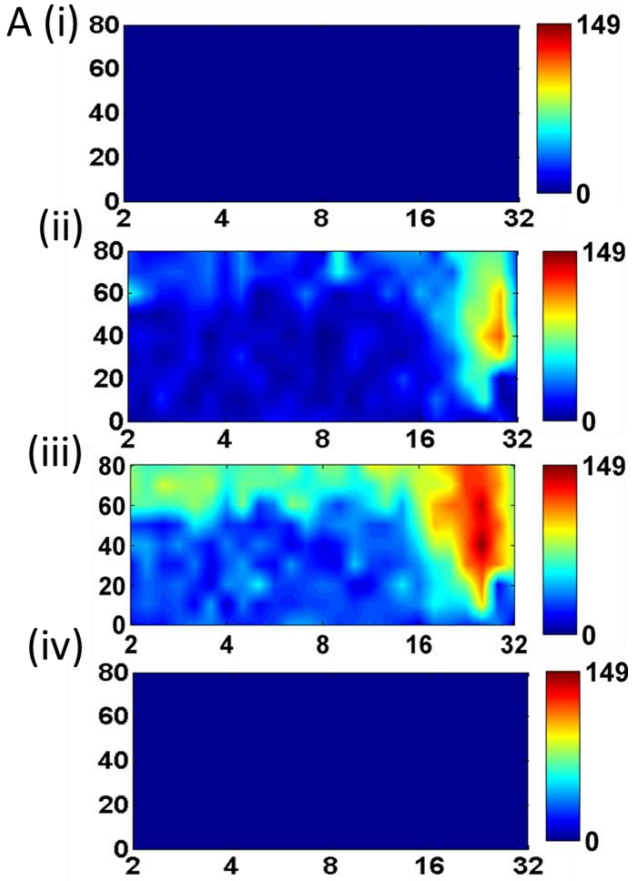

Appendix Figure 2.3A, **Laminar profile of tuning curves (intensity versus frequency) in the AI during baseline recording using a 32 channel linear probe**; Colour code represents firing rate. (i) to (iv) in order of increasing cortical depth (µm).

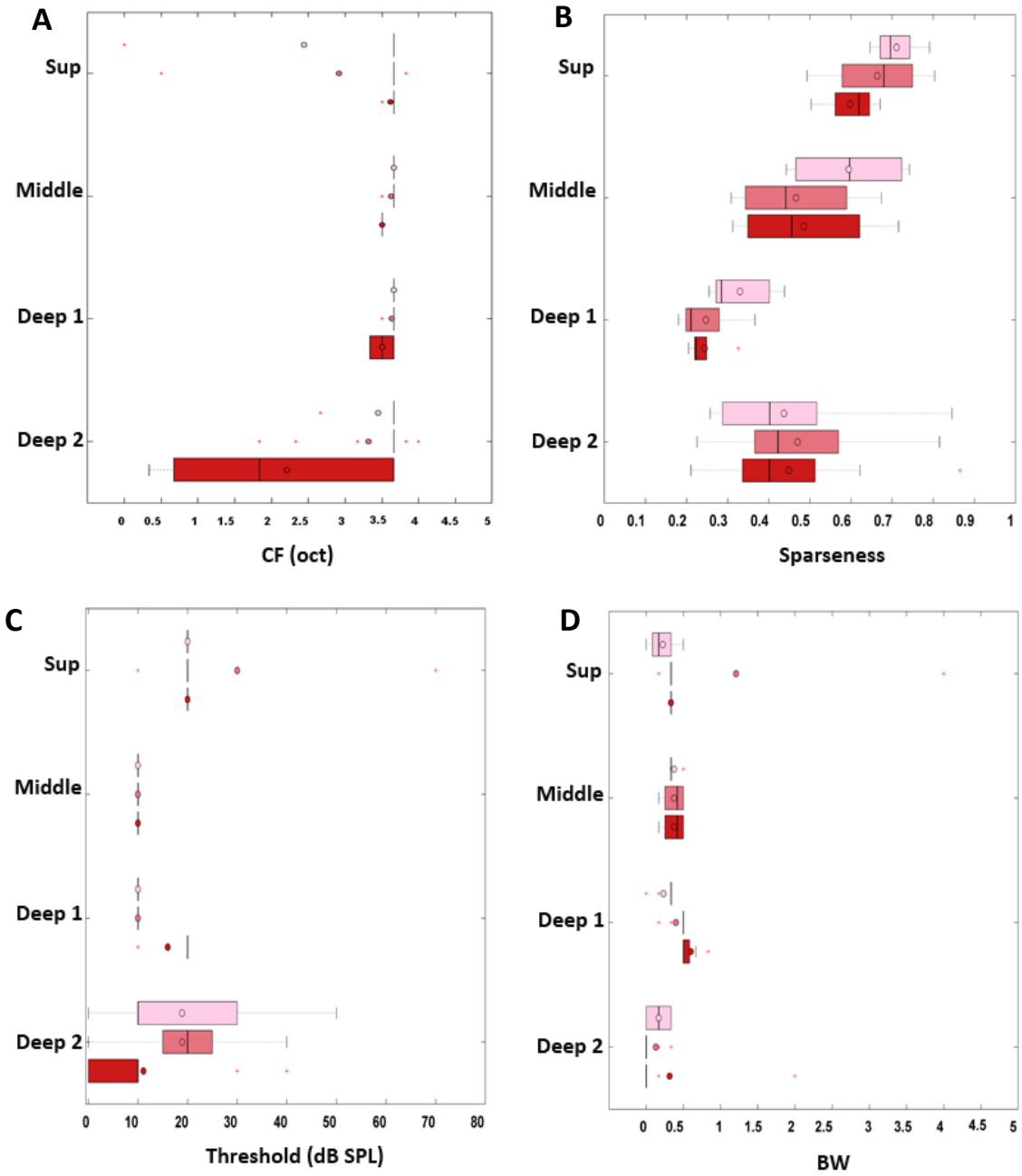

Appendix Figure 3A, Control Experiment 1; Hour of trauma was replaced by silence. **1**. Laminar profile of AI tuning curve parameters from a single control experiment: **A-**CF**, B-**Sparseness, **C-**Threshold and **D-**BW, before (light red bar), one hour after (middle red bar) and two hours after (dark red bar) silence. Sup- Superficial, Mid-Middle, Deep1 (Layer V), Deep 2 (Layer VI). No significant difference was seen during between the different time points at any of the cortical depths.

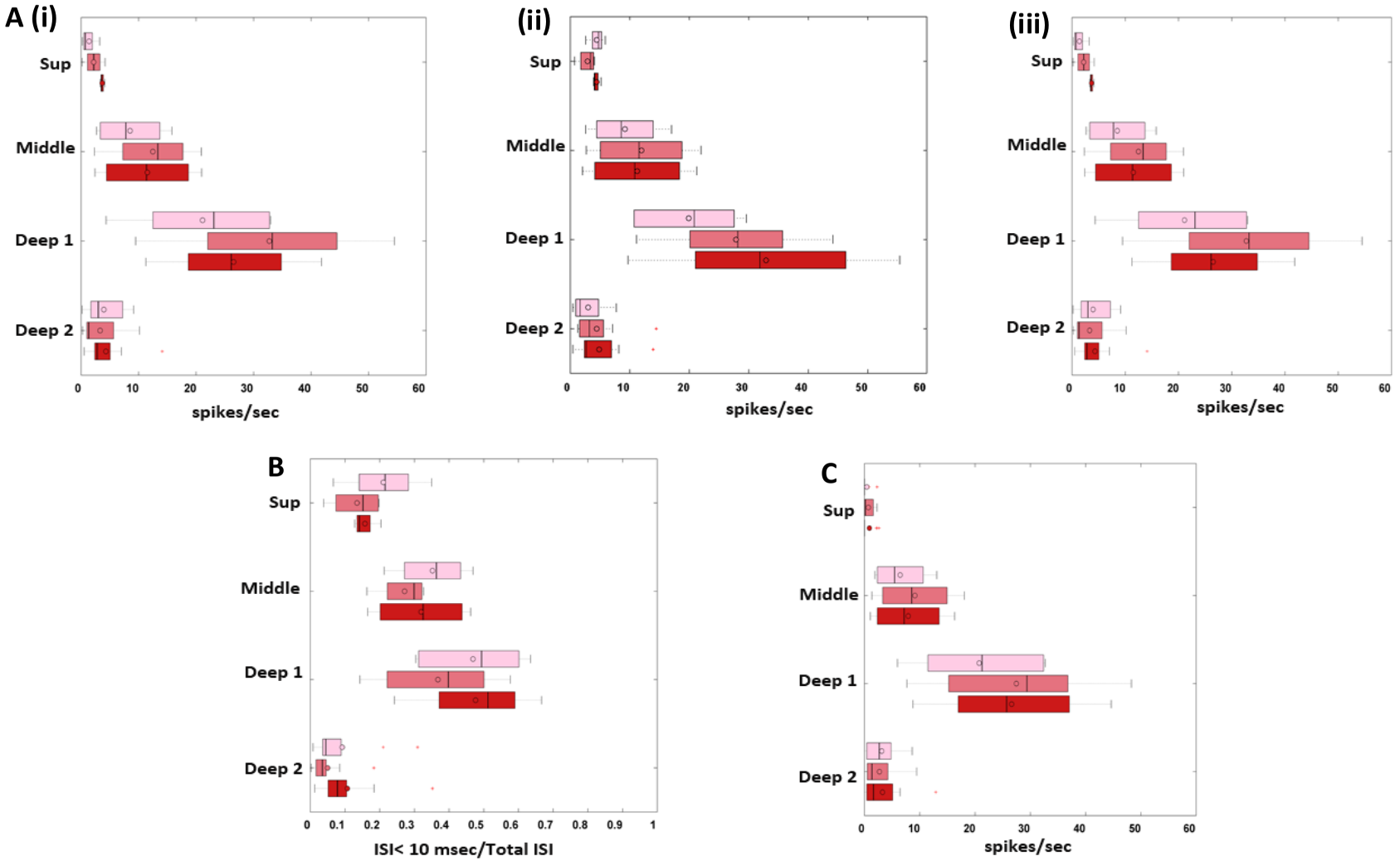

Appendix Figure 3B, Control Experiment 1; Hour of trauma was replaced by silence. **1**. Laminar profile of AI SA from a single control experiment: **A-**(i) SA before stimuli presentation, (ii) SA after stimuli presentation, (iii) SA with elevated baseline.**, B-**fraction of MUA with ISI < 10 msec, and **C-**Background activity, before (light red bar), one hour after (middle red bar) and two hours after (dark red bar) silence. Sup- Superficial, Mid- Middle, Deep1 (Layer V), Deep 2 (Layer VI). No significant difference was seen during between the different time points at any of the cortical depths.

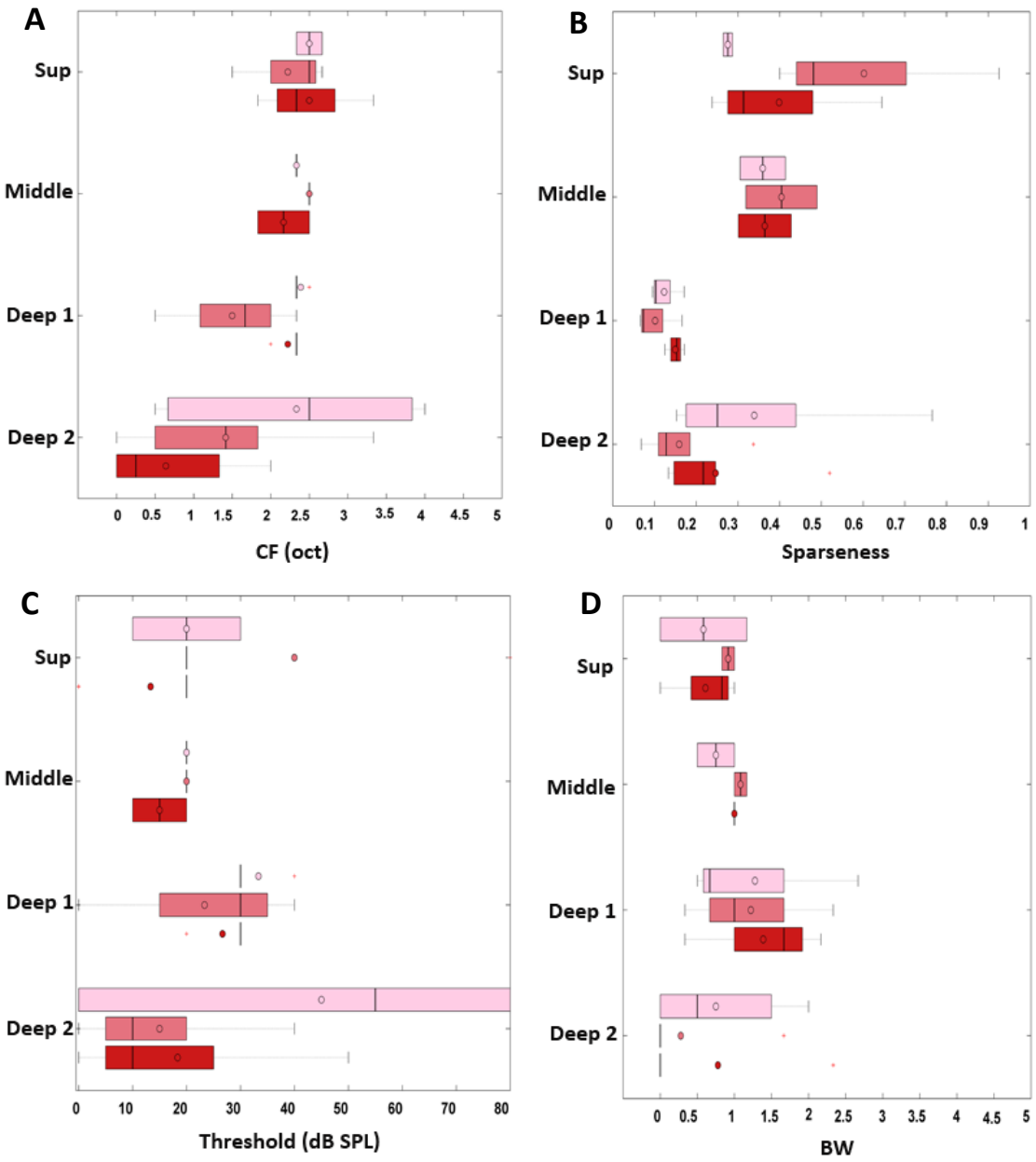

Appendix Figure 4A, Control Experiment 2; Hour of trauma was replaced by silence. **1**. Laminar profile of AI tuning curve parameters from a single control experiment: **A**-CF**, B**-Sparseness, **C**-Threshold and **D**-BW, before (light red bar), one hour after (middle red bar) and two hours after (dark red bar) silence. Sup- Superficial, Mid- Middle, Deep1 (Layer V), Deep 2 (Layer VI). No significant difference was seen during between the different time points at any of the cortical depths.

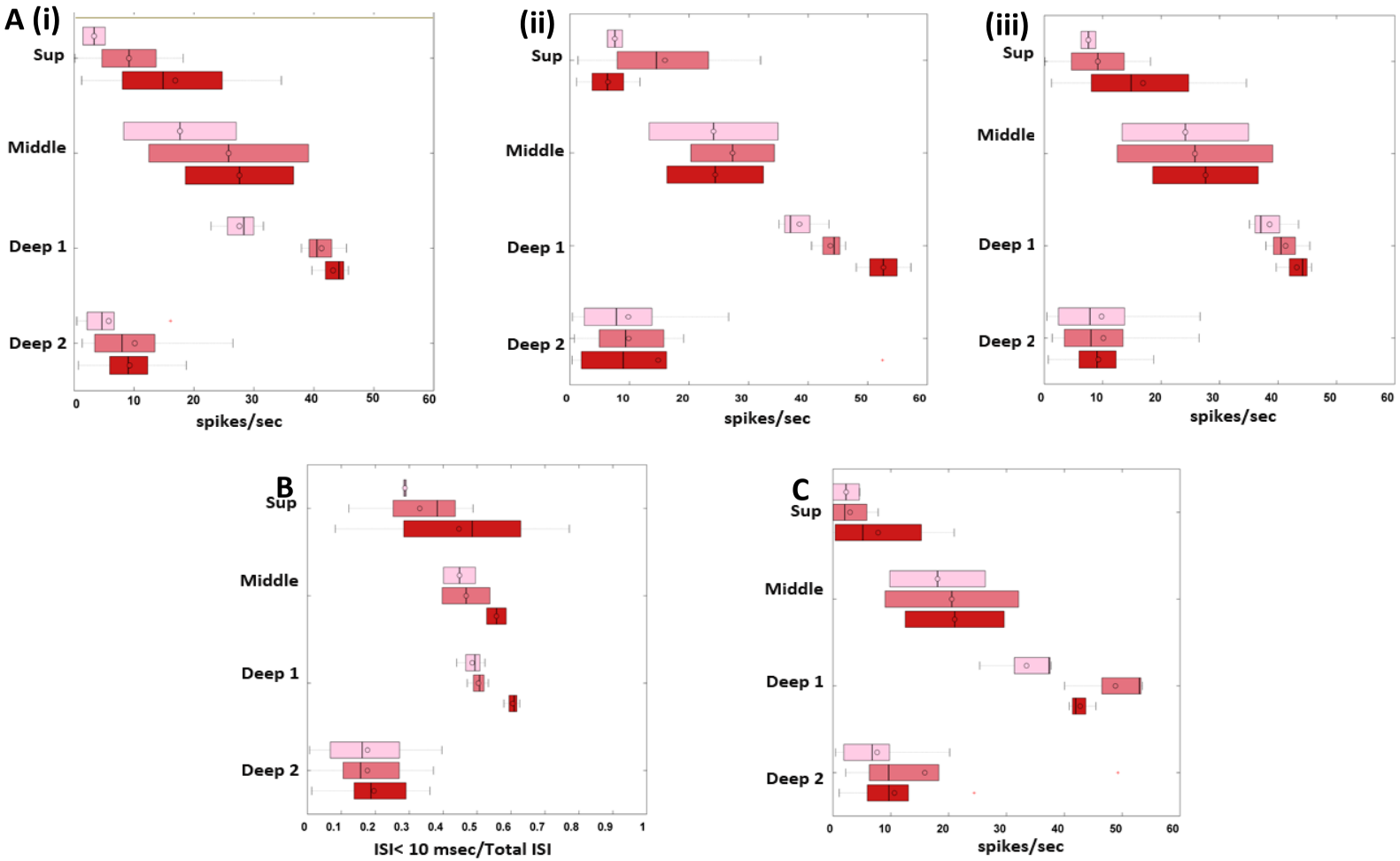

Appendix Figure 4B, Control Experiment 2; Hour of trauma was replaced by silence. **1**. Laminar profile of AI SA from a single control experiment: **A-**(i) SA before stimuli presentation, (ii) SA after stimuli presentation, (iii) SA with elevated baseline.**, B-**fraction of MUA with ISI < 10 msec, and **C-**Background activity, before (light red bar), one hour after (middle red bar) and two hours after (dark red bar) silence. Sup- Superficial, Mid- Middle, Deep1 (Layer V), Deep 2 (Layer VI). No significant difference was seen during between the different time points at any of the cortical depths.

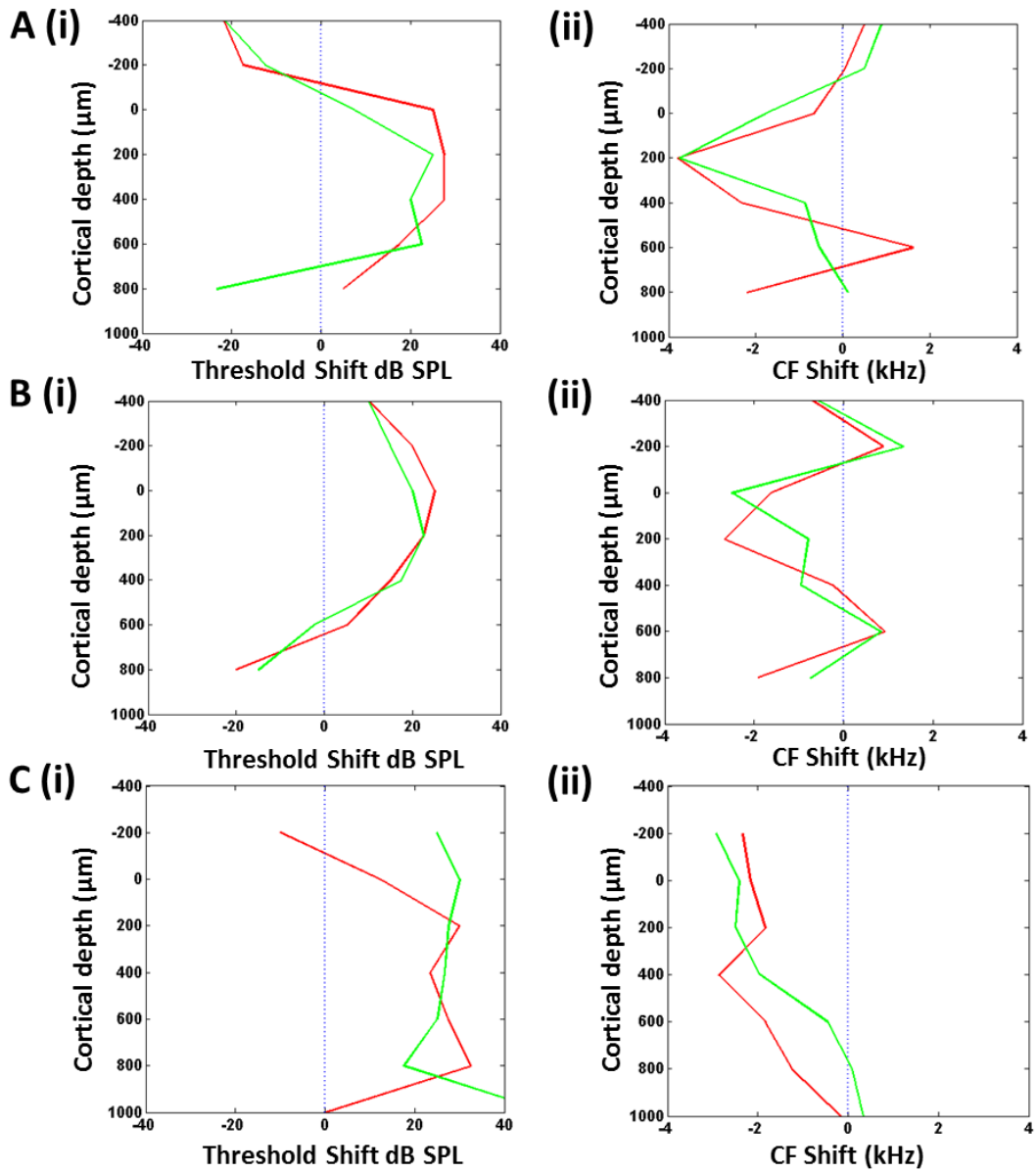

Appendix Figure 5, Shift in tuning curve parameters; Threshold (i) and CF (ii) during post 1 (red)and post 2 (green) across different cortical layers for three individual experiments (A,B,C)

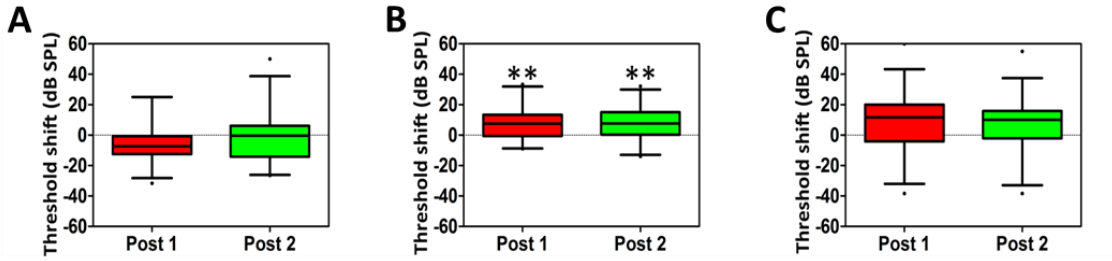

Appendix Figure 6 (A,B,C); Box and whisker plots indicating average change in threshold across all cortical layers during post 1 (red) and post 2 (green). ** p< 0.005, Bonferroni posttest on one way ANOVA.

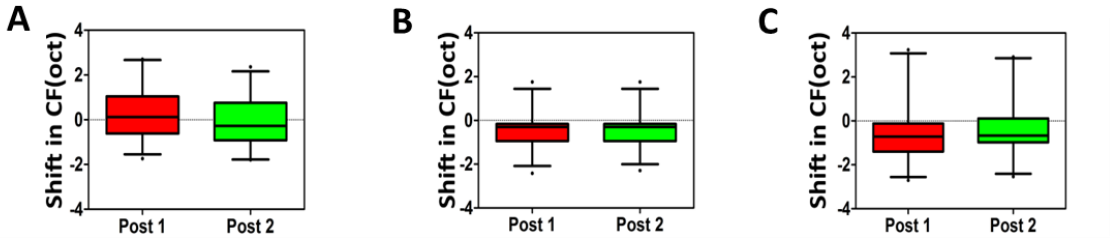

Appendix Figure 7(A,B,C); Box and whisker plots indicating average change in characteristic frequency across all cortical layers during post 1 (red) and post 2 (green). Bonferroni posttest on one way ANOVA.

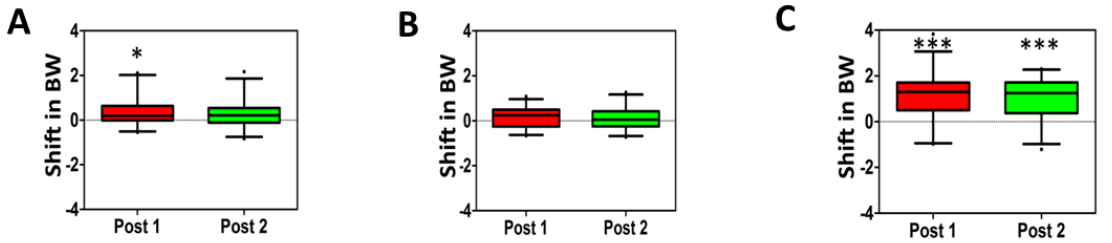

Appendix Figure 8(A,B,C); Box and whisker plots indicating average change in Q 10 across all cortical layers during post 1 (red) and post 2 (green). *p<0.05, ***p<0.0005, Bonferroni posttest on one way ANOVA.

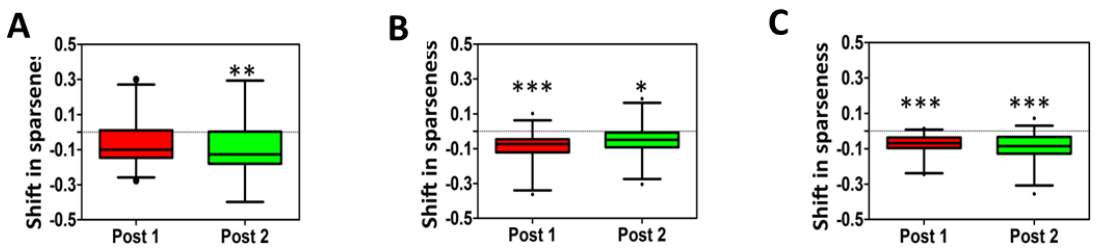

Appendix Figure 9(A,B,C); Box and whisker plots indicating average change in sparseness across all cortical layers during post 1 (red) and post 2(green). *p<0.05, **p<0.005, *p<0.0005 Bonferroni posttest on one way ANOVA

Appendix B

Script 1: Extract relevant spike activity before and after tone presentation

```
cd('\\sipbssrv\sakata_disk\Tansi\Experiments\E phys\data');
DirList=dir;
DirList(1:2,:)=[]; % exclude '.' & '..'
nData=size(DirList,1);
a=[29 30 34 39 46 48 57 59 61 62 63 64 66 67 70 71 73 74 76 77 78 79 81 82 83 84
85 86 88 89 93 97 98 99];
Exp16=[29];
OnsetSpikes=[];
finishSpikes=[];
   for d=1:nData
   MyID=str2double(DirList(d).name); % from ID25
   if MyID==a

MyPath=['\\sipbssrv\sakata_disk\Tansi\Experiments\E
phys\data\',num2str(MyID)];
fprintf(['expID=',num2str(MyID),':']);

  cd(MyPath)
      if Exp16==MyPath
         channel=16
      else
         channel=32
        end
cd pre

Mat1pre=zeros(channel,1); %avg SA/sec before sound presentation
Mat2pre=zeros(channel,1); %avg SA/sec after sound presntation

Evt=load([Filebase,'pre','.tc.syn.evt']);
onset=Evt(1,1);
if fopen([Filebase,'pre','.tcl.syn.evt'])~=-1
   EvtTCL=load([Filebase,'pre','.tcl.syn.evt']);
   finish=EvtTCL(end,1)+500; % PLEASE CONSIDER OFFSET RESPONSE.
else
   finish=Evt(end,1)+500;
end

for n=1:channel
   %%%%%%%%%%%%load relevant channels
   Clu=load([Filebase,'pre','.clu.',num2str(n)]);
   Res0=load([Filebase,'pre','.res.',num2str(n)]);%data points
   Res1=Res0/20; %Convert to time points,sampling rate is 20kS
```

```
   Clu(1)=[]; %first row menions total number of clusters so delete.
   idx=find(Clu>=2); %find relevant clusters

   if ~isempty(idx)
      Res=Res1(idx); %find relevant spike time
      nspikes1=length(find(Res<onset));

      %%%%%%%%Sponatenous activity after sound presentation
      Duration2=Res1(end)-finish; % THIS IS AN APPROXIMATION
      nspikes2=length(find(Res>finish));

      %%%%%%Load the matrix
      Mat1pre(n)=nspikes1;
      Mat2pre(n)=nspikes2;
   else
      Mat1pre(n)=NaN;
      Mat2pre(n)=NaN;
   end
end
cd ..

 cd post 1

Mat1post=zeros(channel,1); %avg SA/sec before sound presentation
Mat2post=zeros(channel,1); %avg SA/sec after sound presntation

Evt=load([Filebase,'post','.tc.syn.evt']);
onset=Evt(1,1);
if fopen([Filebase,'post','.tcl.syn.evt'])~=-1
   EvtTCL=load([Filebase,'post','.tcl.syn.evt']);
   finish=EvtTCL(end,1)+500; % PLEASE CONSIDER OFFSET RESPONSE.
else
   finish=Evt(end,1)+500;
end

for n=1:channel
   %%%%%%%%%%%%load relevant channels
   Clu=load([Filebase,'post','.clu.',num2str(n)]);
   Res0=load([Filebase,'post','.res.',num2str(n)]);%data points
   Res1=Res0/20; %Convert to time points,sampling rate is 20kS

   Clu(1)=[]; %first row menions total number of clusters so delete.
   idx=find(Clu>=2); %find relevant clusters

   if ~isempty(idx)
      Res=Res1(idx); %find relevant spike time
      nspikes1=length(find(Res<onset));
```

```
%%%%%%%%Sponatenous activity after sound presentation
      Duration2=Res1(end)-finish; % THIS IS AN APPROXIMATION
      nspikes2=length(find(Res>finish));

      %%%%%%Load the matrix
      Mat1post(n)=nspikes1;
      Mat2post(n)=nspikes2;
   else
      Mat1post(n)=NaN;
      Mat2post(n)=NaN;
   end
end
cd ..

cd post 2

Mat1aft=zeros(channel,1); %avg SA/sec before sound presentation
Mat2aft=zeros(channel,1); %avg SA/sec after sound presntation

Evt=load([Filebase,'aft','.tc.syn.evt']);
onset=Evt(1,1);
if fopen([Filebase,'aft','.tcl.syn.evt'])~=-1
   EvtTCL=load([Filebase,'aft','.tcl.syn.evt']);
   finish=EvtTCL(end,1)+500; % PLEASE CONSIDER OFFSET RESPONSE.
else
   finish=Evt(end,1)+500;
end

for n=1:channel
   %%%%%%%%%%%%load relevant channels
   Clu=load([Filebase,'aft','.clu.',num2str(n)]);
   Res0=load([Filebase,'aft','.res.',num2str(n)]);%data points
   Res1=Res0/20; %Convert to time points,sampling rate is 20kS

   Clu(1)=[]; %first row menions total number of clusters so delete.
   idx=find(Clu>=2); %find relevant clusters

   if ~isempty(idx)
      Res=Res1(idx); %find relevant spike time
      nspikes1=length(find(Res<onset));

%%%%%%%%Sponatenous activity after sound presentation
      Duration2=Res1(end)-finish; % THIS IS AN APPROXIMATION
      nspikes2=length(find(Res>finish));

      %%%%%%Load the matrix
      Mat1aft(n)=nspikes1;
```

```
      Mat2aft(n)=nspikes2;
   else
      Mat1aft(n)=NaN;
      Mat2aft(n)=NaN;
   end
end
   else
      fprintf('no data, skip \n');
        OnsetSpikes=NaN*ones(1,3);
        finishSpikes=NaN*ones(1,3)

 %%%%%%%%%%%%%%Summarise data%%%%%%%%%%%%%%

OnsetSpikess=[Mat1pre Mat1post Mat1aft]
finishSpikess=[Mat2pre Mat2post Mat2aft]
   end
OnsetSpikes=[OnsetSpikes;OnsetSpikess];
finishSpikes=[finishSpikes;finishSpikess]

end
```

Script 2: Box and whisker plots for group and average of various tuning curve parameters, spontaneous activity for the different frequency bands

```
load ('ModifiedTC','MyTC'); % Load relevant file containing all the runing curve
data
a=[30 61 64 74 78 97 98 77 85]; % Load relevant experiments in the frequency
band group
 Data=ModifiedTC;

BigExp=[];
for i=1:length(a)
   TmpExp=Data(Data(:,1)==a(i),:);
   BigExp=[BigExp;TmpExp];
end

% %%%Combine in one matrix
Exp= BigExp(:,[2,3:5]); %Load relevant TC data
%[Exp1;Exp2;Exp3;Exp4;Exp5;Exp6;Exp7;Exp8;Exp9;Exp10;Exp11;Exp12;Exp13;Exp
14;Exp15];

x=size(a,2);
%%%Align the data and calculate mean
Alignedvalue=[];
for Depth=-400:50:1200
   idx=find(Exp(:,1)==Depth);
   value=Exp(idx,:);

 Alignedvalue=[Alignedvalue;value];
end

idx1=find(Alignedvalue(:,1)>=-400&(Alignedvalue(:,1)<-200));
Data1=Alignedvalue(idx1,2:4);
% Data1=(log(Data1)/log(2)-1); When Calculating CF

idx2=find(Alignedvalue(:,1)>=-200&(Alignedvalue(:,1)<0));
Data2=Alignedvalue(idx2,2:4);
% Data2=(log(Data2)/log(2)-1); When Calculating CF

idx3=find(Alignedvalue(:,1)>=0&(Alignedvalue(:,1)<200));
Data3=Alignedvalue(idx3,2:4);
% Data3=(log(Data3)/log(2)-1); When Calculating CF

 idx4=find(Alignedvalue(:,1)>=200&(Alignedvalue(:,1)<400));
Data4=Alignedvalue(idx4,2:4);
```

```
% Data4=(log(Data4)/log(2)-1); When Calculating CF

idx5=find(Alignedvalue(:,1)>=400&(Alignedvalue(:,1)<600));
Data5=Alignedvalue(idx5,2:4);
% Data5=(log(Data5)/log(2)-1); When Calculating CF

idx6=find(Alignedvalue(:,1)>=600&(Alignedvalue(:,1)<800));
Data6=Alignedvalue(idx6,2:4);
% Data6=(log(Data6)/log(2)-1); When Calculating CF

idx7=find(Alignedvalue(:,1)>=800&(Alignedvalue(:,1)<1000));
Data7=Alignedvalue(idx7,2:4);
% Data7=(log(Data7)/log(2)-1); When Calculating CF

idx8=find(Alignedvalue(:,1)>=1000&(Alignedvalue(:,1)<1200));
Data8=Alignedvalue(idx8,2:4);
% Data8=(log(Data8)/log(2)-1); When Calculating CF

%%%%%%%%%%%%%%%%%%%%Pre%%%%%%%%%%%%%%%%%%%%
Datapre={Data1(:,1)', Data2(:,1)', Data3(:,1)', Data4(:,1)', Data5(:,1)', Data6(:,1)',
Data7(:,1)', Data8(:,1)'};

maxSize = max(cellfun(@numel,Datapre));   %# Get the maximum vector size
 fcn = @(x) [x nan(1,maxSize-numel(x))];  %# Create an anonymous function
 rmat = cellfun(fcn,Datapre,'UniformOutput',false);  %# Pad each cell with NaNs
  rmatp = vertcat(rmat{:});
 rmatpre = vertcat(rmat{:})' ;%# Vertically concatenate cells

 rmat1pre = nanmean(rmatpre);

%%%%%%%%%%%%%%%%%%%%Trauma%%%%%%%%%%%%%%%%%%%%

% Datatrauma={Data1(:,2)' Data2(:,2)' Data3(:,2)' Data4(:,2)' Data5(:,2)' Data6(:,2)'
Data7(:,2)' Data8(:,2)'};
% maxSize = max(cellfun(@numel,Datatrauma));    %# Get the maximum vector
size
%  fcn = @(x) [x nan(1,maxSize-numel(x))];  %# Create an anonymous function
%  rmat = cellfun(fcn,Datatrauma,'UniformOutput',false);  %# Pad each cell with
NaNs
%   rmatt = vertcat(rmat{:});
%  rmattrauma = vertcat(rmat{:})'  ;            %# Vertically concatenate cells

%%%%%%%%%%%%%%%%%%%%Post1%%%%%%%%%%%%%%%%%%%%

% Datapost={Data1(:,2)' Data2(:,2)' Data3(:,2)' Data4(:,2)' Data5(:,2)' Data6(:,2)'
Data7(:,2)' Data8(:,2)'};
% maxSize = max(cellfun(@numel,Datapost));    %# Get the maximum vector size
```

```
%  fcn = @(x) [x nan(1,maxSize-numel(x))];  %# Create an anonymous function
%  rmat = cellfun(fcn,Datapost,'UniformOutput',false);  %# Pad each cell with NaNs
%   rmatpo = vertcat(rmat{:});
%  rmatpost = vertcat(rmat{:})';           %# Vertically concatenate cells
%  rmat1post = nanmean(rmatpost);
%
%
%%%%%%%%%%%%%%%%%%%%%%Post2%%%%%%%%%%%%%%%%%%%%
%  Dataaft={Data1(:,3)' Data2(:,3)' Data3(:,3)' Data4(:,3)' Data5(:,3)' Data6(:,3)'
Data7(:,3)' Data8(:,3)'};
% maxSize = max(cellfun(@numel,Dataaft));    %# Get the maximum vector size
%  fcn = @(x) [x nan(1,maxSize-numel(x))];  %# Create an anonymous function
%  rmat = cellfun(fcn,Dataaft,'UniformOutput',false);  %# Pad each cell with NaNs
%   rmata = vertcat(rmat{:});
%  rmataft = vertcat(rmat{:})'  ;           %# Vertically concatenate cells
%  rmat1aft = nanmean(rmataft);

figure(1)
MATRIX={rmatpre};
aboxplot(MATRIX,'Colorgrad','red_up')

s=get(gca,'XTickLabel');
set(gca, 'XTickLabel',{'-400','-200','0','200','400','600','800','1000'})
% get the currrent axis
ax1 = gca;

set(ax1, 'YAxisLocation', 'right')
xesPosition = get(gca,'YAxis');        %# Get the current axes position
  %#   ... located on the right

%%%%%%%%%%%%%%%%%%Tick properties%%%%%%%%%%%

ylim([-2 80])
% set(gca, 'YTickLabel',[0:5:60])
yticklabel_rotate
%rotate text
%get current tick labels
d=get(gca,'YTickLabel');
%erase current tick labels from figure
set(gca,'YTickLabel',[]);
%get tick label positions
e=get(gca,'YTick');
f=get(gca,'XTick');
rot=90;
%make new tick labels
if rot<180
```

```
   text(e,repmat(f(1)-.2*(f(2)-
f(1)),length(e),1),d,'VerticalAlignment','bottom','rotation',rot,'FontSize', 16,
'FontWeight', 'Bold');
else
   text(e,repmat(f(1)-.2*(f(2)-
f(1)),length(e),1),d,'VerticalAlignment','bottom','rotation',rot, 'FontSize', 16,
'FontWeight', 'Bold');
end

d=get(gca,'XTickLabel');
%erase current tick labels from figure
set(gca,'XTickLabel',[]);
%get tick label positions
e=get(gca,'XTick');
f=get(gca,'YTick');
rot=90;
%make new tick labels
if rot<180
   text(e,repmat(f(1)-.4*(f(2)-
f(1)),length(e),1),d,'HorizontalAlignment','left','rotation',rot,'FontSize', 16,
'FontWeight', 'Bold');
else
   text(e,repmat(f(1)-.4*(f(2)-
f(1)),length(e),1),d,'HorizontalAlignment','left','rotation',rot, 'FontSize', 16,
'FontWeight', 'Bold');
end

%  figure(2)
% MAT= {rmat1pre(:);rmat1post(:);rmat1aft(:)}
%
% aboxplot(MAT)%%Function is available as a function

% figure(3)
% MAT1={(MAT{2}-MAT{1});(MAT{3}-MAT{1})};
% aboxplot(MAT1,'Colorgrad','pink_down')

%%%%%%%%%%%Analysis%%%%%%%%%%%%%%%%%%%%%%%%%%%
%%%%%

Datapre={Data1(:,1)', Data2(:,1)', Data3(:,1)', Data4(:,1)', Data5(:,1)', Data6(:,1)',
Data7(:,1)', Data8(:,1)'};

Group=[(ones(size(Data1(:,1)',2),1));2*(ones(size(Data2(:,1)',2),1));3*(ones(size(Da
ta3(:,1)',2),1));4*(ones(size(Data4(:,1)',2),1));5*(ones(size(Data5(:,1)',2),1));6*(one
s(size(Data6(:,1)',2),1));7*(ones(size(Data7(:,1)',2),1));8*(ones(size(Data8(:,1)',2),1)
);];
```

```
DATA=[Data1(:,1);Data2(:,1);Data3(:,1);Data4(:,1);Data5(:,1);Data6(:,1);Data7(:,1);
Data8(:,1);];
% size(DATA)
% d=size(Group)

[p Table stats]=anova1(DATA,Group)
 [c,m,h,nms]= multcompare(stats,'alpha',0.05,'ctype','bonferroni')
```

Script 3: Group and average shift in the various tuning curve parameters, spontaneous activity for the different frequency bands

```
%%%%%%%%%%%%%%%%%%%%%%%%%%%%%%%%%%%%%%%%%%%%
% This function is used to measure shift in the various tuning curve
% parameters in the different frequency band areas
% Requires the various tuning curve parameters (Modified TC in this instance)
% summarised into one summary sheet to allow easy extraction of different
parameters

%%%%%%%%%%%%%Relevant frequency band %%%%%%%%%%%%%%%%%%

load ('ModifiedTC', 'ModifiedTC');%%% %%
mid=[70 73 76 82 83 86]; % relevant experiments

 NewData=ModifiedTC(:,[1,2,32:34]); % relevant column of tuning curve
parameters
%  PP=NewData(:,3);
%  threshidx=find(PP>80); %Maximum intensity
 P=NewData(:,[3,4,5]);
 idx=find(P<0);
P(idx)=NaN;
% P(threshidx)=NaN;

DataP=[NewData(:,(1:2)) P];

BigExpP=[];
for m=1:length(mid);
    TmpExpP=DataP(DataP(:,1)==mid(m),:);
    BigExpP=[BigExpP;TmpExpP];

end
ExpP=BigExpP;
AlignedvaluePmid=[];%%%%% Align data set as per depth
SEMP=[]; SEMPost=[]; SEMAft=[]; AlignedvaluePP=[];
for Depth=-400:50:1000
   fprintf(['Depth',num2str(Depth)])

    idxdp=find(ExpP(:,2)==Depth);
    valueP=ExpP(idxdp,:);
     STDP=nanstd(valueP(:,3));
     STDPost=nanstd(valueP(:,4));
     STDAft=nanstd(valueP(:,5));
    SEMFP=STDP/sqrt(length(valueP(:,3)));
```

```
    SEMFPost=STDPost/sqrt(length(valueP(:,4)));
     SEMFAft=STDAft/sqrt(length(valueP(:,5)));
   valueep=nanmean(valueP,1);

AlignedvaluePP=[AlignedvaluePP;valueP];
 AlignedvaluePmid(end+1,:)=[valueep];
 SEMP=[SEMP;SEMFP];
 SEMPost=[SEMPost;SEMFPost];
 SEMAft=[SEMAft;SEMFAft];

end

ThreshP=AlignedvaluePmid(:,3);
WholemeanP=nanmean(ThreshP);
CFocttP=ThreshP-WholemeanP;

%%%%%Post1 Shift%%%%%
ThreshPPost1=AlignedvaluePmid(:,4);
WholemeanPPost1=nanmean(ThreshPPost1);
CFocttPPost1=ThreshPPost1-WholemeanPPost1;

%%%%%%%Post2 Shift%%%%%
ThreshPAft=AlignedvaluePmid(:,5);
WholemeanPPost2=nanmean(ThreshPPost2);
CFocttPPost2=ThreshPPost2-WholemeanPPost2;

%%%%%%%%%%%%%Measure Shift%%%%%%%%%%%%%%%%%%%%%%%%%
Post1shiftmid=CFocttPPost1-CFocttP;
Post2shiftmid=CFocttPPost2-CFocttP;

% % AlignedvaluePPmid=[AlignedvalueP(:,1) AlignedvalueP(:,2)  CFocttP
CFocttPPost  CFocttPAft];

%%%%%%%%%%%%%%Depth resolution %%%%%%%%%%%%%%

% Summarise data sets at relevant depths (200 µm in this instance)

% idx1=find(AlignedvaluePP(:,2)>=-400&(AlignedvaluePP(:,2)<-200));
% Data1=AlignedvaluePP(idx1,3:5);
% Data1m=nanmean(Data1);
% STDP1=nanstd(Data1(:,1));
%     STDPost1=nanstd(Data1(:,2));
%     STDAft1=nanstd(Data1(:,3));
%    SEMFP1=STDP1/sqrt(length(Data1(:,1)));
%     SEMFPost1=STDPost1/sqrt(length(Data1(:,2)));
%      SEMFAft1=STDAft1/sqrt(length(Data1(:,3)));
% % idx2=find(AlignedvaluePP(:,2)>=-200&(AlignedvaluePP(:,2)<0));
```

```
% Data2=AlignedvaluePP(idx2,3:5);
% Data2m=nanmean(Data2);
%
% STDP2=nanstd(Data2(:,1));
%     STDPost2=nanstd(Data2(:,2));
%     STDAft2=nanstd(Data2(:,3));
%    SEMFP2=STDP2/sqrt(length(Data2(:,1)));
%     SEMFPost2=STDPost2/sqrt(length(Data2(:,2)));
%      SEMFAft2=STDAft2/sqrt(length(Data2(:,3)));
%
%
% idx3=find(AlignedvaluePP(:,2)>=0&(AlignedvaluePP(:,2)<200));
% Data3=AlignedvaluePP(idx3,3:5);
% Data3m=nanmean(Data3);
% STDP3=nanstd(Data3(:,1));
%     STDPost3=nanstd(Data3(:,2));
%     STDAft3=nanstd(Data3(:,3));
%    SEMFP3=STDP3/sqrt(length(Data3(:,1)));
%     SEMFPost3=STDPost3/sqrt(length(Data3(:,2)));
%      SEMFAft3=STDAft3/sqrt(length(Data3(:,3)));
%
%  idx4=find(AlignedvaluePP(:,2)>=200&(AlignedvaluePP(:,2)<400));
% Data4=AlignedvaluePP(idx4,3:5);
% Data4m=nanmean(Data4);
% STDP4=nanstd(Data4(:,1));
%     STDPost4=nanstd(Data4(:,2));
%     STDAft4=nanstd(Data4(:,3));
%    SEMFP4=STDP4/sqrt(length(Data4(:,1)));
%     SEMFPost4=STDPost4/sqrt(length(Data4(:,2)));
%      SEMFAft4=STDAft4/sqrt(length(Data4(:,3)));
%
% idx5=find(AlignedvaluePP(:,2)>=400&(AlignedvaluePP(:,2)<600));
% Data5=AlignedvaluePP(idx5,3:5);
% Data5m=nanmean(Data5);
%
% STDP5=nanstd(Data5(:,1));
%     STDPost5=nanstd(Data5(:,2));
%     STDAft5=nanstd(Data5(:,3));
%    SEMFP5=STDP5/sqrt(length(Data5(:,1)));
%     SEMFPost5=STDPost5/sqrt(length(Data5(:,2)));
%      SEMFAft5=STDAft5/sqrt(length(Data5(:,3)));
%
%  idx6=find(AlignedvaluePP(:,2)>=600&(AlignedvaluePP(:,2)<800));
% Data6=AlignedvaluePP(idx6,3:5);
% Data6m=nanmean(Data6);
%
% STDP6=nanstd(Data6(:,1));
```

```
%     STDPost6=nanstd(Data6(:,2));
%     STDAft6=nanstd(Data6(:,3));
%    SEMFP6=STDP6/sqrt(length(Data6(:,1)));
%     SEMFPost6=STDPost6/sqrt(length(Data6(:,2)));
%      SEMFAft6=STDAft6/sqrt(length(Data6(:,3)));
%
% idx7=find(AlignedvaluePP(:,2)>=800&(AlignedvaluePP(:,2)<1000));
% Data7=AlignedvaluePP(idx7,3:5);
% Data7m=nanmean(Data7);
%
% STDP7=nanstd(Data7(:,1));
%     STDPost7=nanstd(Data7(:,2));
%     STDAft7=nanstd(Data7(:,3));
%    SEMFP7=STDP7/sqrt(length(Data7(:,1)));
%     SEMFPost7=STDPost7/sqrt(length(Data7(:,2)));
%      SEMFAft7=STDAft7/sqrt(length(Data7(:,3)));
%
%   idx8=find(AlignedvaluePP(:,2)>=1000&(AlignedvaluePP(:,2)<1200));
% Data8=AlignedvaluePP(idx8,3:5);
% Data8m=nanmean(Data8);
%
% STDP8=nanstd(Data8(:,1));
%     STDPost8=nanstd(Data8(:,2));
%     STDAft8=nanstd(Data8(:,3));
%    SEMFP8=STDP8/sqrt(length(Data8(:,1)));
%     SEMFPost8=STDPost8/sqrt(length(Data8(:,2)));
%      SEMFAft8=STDAft8/sqrt(length(Data8(:,3)));
%
%      idx9=find(AlignedvaluePP(:,2)>=400&(AlignedvaluePP(:,2)<500));
% Data9=AlignedvaluePP(idx9,3:5);
% Data9m=nanmean(Data9);
%
% STDP9=nanstd(Data9(:,1));
%     STDPost9=nanstd(Data9(:,2));
%     STDAft9=nanstd(Data9(:,3));
%    SEMFP9=STDP9/sqrt(length(Data9(:,1)));
%     SEMFPost9=STDPost9/sqrt(length(Data9(:,2)));
%      SEMFAft9=STDAft9/sqrt(length(Data9(:,3)));

% %%% %%%%%Summarise data%%%%%%%
PRE200=[Data1m(:,1);Data2m(:,1);Data3m(:,1);Data4m(:,1);Data5m(:,1);Data6m(:,
1);Data7m(:,1);Data8m(:,1);Data9m(:,1)]

% %      Depth200=[-400:100:900];
SEMPre200=[SEMFP1;SEMFP2;SEMFP3;SEMFP4;SEMFP5;SEMFP6;SEMFP7;SEMFP8
;SEMFP9]POST1200=[Data1m(:,2);Data2m(:,2);Data3m(:,2);Data4m(:,2);Data5m(:,
2);Data6m(:,2);Data7m(:,2);Data8m(:,2);Data9m(:,2)]
```

```
% %      Depth200=[-400:100:900];
SEMPOST1200=[SEMFPost1;SEMFPost2;SEMFPost3;SEMFPost4;SEMFPost5;SEMFP
ost6;SEMFPost7;SEMFPost8;SEMFPost9]
POST2200=[Data1m(:,3);Data2m(:,3);Data3m(:,3);Data4m(:,3);Data5m(:,3);Data6
m(:,3);Data7m(:,3);Data8m(:,3);Data9m(:,3)]
% %      Depth200=[-400:100:900];
SEMPOST2200=[SEMFAft1;SEMFAft2;SEMFAft3;SEMFAft4;SEMFAft5;SEMFAft6;SE
MFAft7;SEMFAft8;SEMFAft9]

% % %%%% Summarise Shift %%%%%%%
% % Post1shiftmidd=POST1200-PRE200;
% % Post2shiftmidd=POST2200-PRE200;

%%%%%%%%%%%%%%%%%%%Figure%%%%%%%%%%%%%%%%%%%%%%%%
figure(x)%%%% Plots the shit in diffrent layers at 200 depth resolution
subplot(1,3,1)
shadedErrorBar(Depth200',PRE200,SEMPre200,'b')
subplot(1,3,2)
shadedErrorBar(Depth200',POST1200,SEMPOST1200,'r')
subplot(1,3,3)
shadedErrorBar(Depth200',POST2200,SEMPOST2200,'g')
```

References

Abbott, S.D., Hughes, L.F., Bauer, C.A., Salvi, R., and Caspary, D.M. (1999). Detection of glutamate decarboxylase isoforms in rat inferior colliculus following acoustic exposure. Neuroscience *93*, 1375–1381.

Abeles, M., and Goldstein, M.H.. J. (1970). Functional architecture in cat primary auditory cortex: columnar organization and organization according to depth. J Neurophysiol *33*, 172–187.

Ades, H.W., and Engström, H. (1974). Anatomy of the Inner Ear. In Handbook of Sensory Physiology Auditory System, W.D. Keidel, and W.D. Neff, eds. (Berlin, Heidelberg: Springer Berlin Heidelberg), pp. 125–158.

Adrian, E. (1933). The activity of the nerve fibres. : Nobel lecture delivered at Stockholm, 12th December 1932. (Stockholm).

Adrian, E.D. (1926). The impulses produced by sensory nerve endings: Part I. J. Physiol. *61*, 49–72.

Aitkin, L.M., and Phillips, S.C. (1984a). Is the inferior colliculus an obligatory relay in the cat auditory system? Neurosci. Lett. *44*, 259–264.

Aitkin, L.M., and Phillips, S.C. (1984b). The interconnections of the inferior colliculi through their commissure. J. Comp. Neurol. *228*, 210–216.

Aitkin, L.M., Anderson, D.J., and Brugge, J.F. (1970). Tonotopic organization and discharge characteristics of single neurons in nuclei of the lateral lemniscus of the cat. J. Neurophysiol. *33*, 421–440.

Allon, N., Yeshurun, Y., and Wollberg, Z. (1981). Responses of single cells in the medial geniculate body of awake squirrel monkeys. Exp. Brain Res. *41*, 222–232.

Andersen, R.A., Knight, P.L., and Merzenich, M.M. (1980). The thalamocortical and corticothalamic conections of AI, AII, and the anteriior auditory field (AFF) in the cat: Evidence ofr two largely sergregarted systems of connections. J. Comp. Neurol. *194.3*, 663–701.

Anderson, H., and Wedenberg, E. (1968). Audiometric identification of normal hearing carriers of genes for deafness. Acta Otolaryngol. *65*, 535–554.

Anderson, L.A., Wallace, M.N., and Palmer, A.R. (2007). Identification of subdivisions in the medial geniculate body of the guinea pig. Hear. Res. *228*, 156–167.

Arieli, A., Sterkin, A., Grinvald, A., and Aertsen, A. (1996). Dynamics of Ongoing Activity: Explanation of the Large Variability in Evoked Cortical Responses. Science. *273*, 1868–1871.

Arnold, W., Bartenstein, P., Oestreicher, E., Römer, W., and Schwaiger, M. (1996). Focal metabolic activation in the predominant left auditory cortex in patients suffering from tinnitus: a PET study with [18F]deoxyglucose. ORL. J. Otorhinolaryngol. Relat. Spec. *58*, 195–199.

Ascoli, G.A., Alonso-Nanclares, L., Anderson, Stewart A; Barrionuevo, G.B.-P., and Al, R. et (2008). Petilla terminology: nomenclature of features of GABAergic interneurons of the cerebral cortex. Nat. Rev. Neurosci. *9*, 557–568.

Atencio, C.A., and Schreiner, C.E. (2010a). Columnar connectivity and laminar processing in cat primary auditory cortex. PLoS One *5*, 1-18.

Atencio, C.A., and Schreiner, C.E. (2010b). Laminar diversity of dynamic sound processing in cat primary auditory cortex. J. Neurophysiol. *103*, 192–205.

Averbeck, B.B., Latham, P.E., and Pouget, A. (2006). Neural correlations, population coding and computation. Nat. Rev. Neurosci. *7*, 358–366.

Bajo, V., Rouiller, E., Welker, E., Clarke, S., Ribaupierre, F., Villa, A., and Ribaupierre, Y. (1995). Morphology and spatial distribution of corticothalamic terminals originating from the cat auditory cortex. Hear. Res. *83,* 161-174.

Bajo, V.M., Nodal, F.R., Bizley, J.K., Moore, D.R., and King, A.J. (2007). The ferret auditory cortex: descending projections to the inferior colliculus. Cereb. Cortex *17*, 475–491.

Barlow, H.B. (1972). Single units and sensation: a neuron doctrine for perceptual psychology? Perception *1*, 371–394.

Barth, D.S., and Di, S. (1990). Three-dimensional analysis of auditory-evoked potentials in rat neocortex. J Neurophysiol *64*, 1527–1536.

Barthó, P., Hirase, H., Monconduit, L., Zugaro, M., Harris, K.D., and Buzsáki, G. (2004). Characterization of neocortical principal cells and interneurons by network interactions and extracellular features. J. Neurophysiol *92*, 600–608.

Bartlett, E.L., and Smith, P.H. (1999). Anatomic, Intrinsic, and Synaptic Properties of Dorsal and Ventral Division Neurons in Rat Medial Geniculate Body. J Neurophysiol *81*, 1999–2016.

Basta, D., and Ernest, A. (2004). Noise-induced changes of neuronal spontaneous activity in mice inferior colliculus brain slices. Neurosci. Lett. *368*, 297–302.

Bauer, C.A., and Brozoski, T.J. (2008). Tinnitus: Theories Mechanisms and Treatments. In Auditory Trauma, Protection, and Repair, J. Schacht, A.N. Popper, and R.R. Fay, eds. (Boston, MA: Springer US), pp. 101–129.

Bauer, C.A., Brozoski, T.J., and Myers, K. (2007). Primary afferent dendrite degeneration as a cause of tinnitus. J. Neurosci. Res. *85*, 1489–1498.

Bayraktar, T., Staiger, J.F., Acsady, L., Cozzari, C., and Freund, T. (1997). Co-localization of vasoactive intestinal polypeptide, γ-aminobutyric acid and choline acetyltransferase in neocortical interneurons of the adult rat. Brain Res. *757*, 209–217.

Behrens, W. von der (2014). Animal Models of Subjective Tinnitus. Neural Plast. 13 pages.

Von Békésy, G. (1960). Experiments in hearing. E. G. Wever ,eds. (New York: McGraw-Hill).

Bender, K.J., Allen, C.B., Bender, V.A., and Feldman, D.E. (2006). Synaptic basis for whisker deprivation-induced synaptic depression in rat somatosensory cortex. J. Neurosci. *26*, 4155–4165.

Berényi, A., Somogyvári, Z., Nagy, A.J., Roux, L., Long, J.D., Fujisawa, S., Stark, E., Leonardo, A., Harris, T.D., and Buzsáki, G. (2014). Large-scale, high-density (up to 512 channels) recording of local circuits in behaving animals. J. Neurophysiol. *111*, 1132–1149.

Berger, J.I., Coomber, B., Shackleton, T.M., Palmer, A.R., and Wallace, M.N. (2012). A novel behavioural approach to detecting tinnitus in the guinea pig. J Neurosci Methods. *213*, 188–195.

Blackburn, C.C., and Sachs, M.B. (1990). The representations of the steady-state vowel sound /e/ in the discharge patterns of cat anteroventral cochlear nucleus neurons. J Neurophysiol *63*, 1191–1212.

Bohmer, A. (1988). The Preyer reflex – an easy estimate of hearing function in guinea pigs. Acta Otolaryngol. *106.*, 368–372.

Du Bois-Reymond, E. (1848). Untersuchungen über thierische Elektricität, von Emil Du Bois-Reymond. (Berlin: G. Reimer).

Borg, E. (1973). On the neuronal organization of the acoustic middle ear reflex. A physiological and anatomical study. Brain Res. *49*, 101–123.

Bourk, T.R. (1976). Electrical reponses of neural units in the Anteroventral Cochlear Nucleus of Cat . PhD. dissertation. MIT, Cambridge MA.

Bragin, A., Hetke, J., Wilson, C.L., Anderson, D.J., Engel, J., and Buzsáki, G. (2000). Multiple site silicon-based probes for chronic recordings in freely moving rats: implantation, recording and histological verification. J. Neurosci. Methods *98*, 77–82.

Brawer, J.R., Morest, D.K., and Kane, E.C. (1974). The neuronal architecture of the cochlear nucleus of the cat. J. Comp. Neurol. *155*, 251–300.

Bredberg, G. (1977). The innervation of the organ of Corti. A scanning electron microscopic study. Acta Otolaryngol. *83*, 71–78.

Van Brederode, J.F., and Spain, W.J. (1995). Differences in inhibitory synaptic input between layer II-III and layer V neurons of the cat neocortex. J. Neurophysiol. *74*, 1149–1166.

Brian C. J. Moore (2003). Coding of Sounds in the Auditory System and Its Relevance to Signal Processing and Coding in Cochlear Implants. Otol. Neurotol. *24*, 243–254.

Brigande, J. V, and Heller, S. (2009). Quo vadis, hair cell regeneration? Nat. Neurosci. *12*, 679–685.

Brown, J.J., Vernon, J.A., and Fenwick, J.A. (2009). Reduction of Acoustically-Induced Auditory Impairment by Inhalation of Carbogen Gas. Permanent Noise-induced Cochlear Damage. Acta oto-laryngologica. *93,* 319-28

Brown, M.C., de Venecia, R.K., and Guinan, J.J. (2003). Responses of medial olivocochlear neurons. Specifying the central pathways of the medial olivocochlear reflex. Exp. Brain Res. *153*, 491–498.

Brozoski, T., Odintsov, B., and Bauer, C. (2012a). Gamma-aminobutyric acid and glutamic acid levels in the auditory pathway of rats with chronic tinnitus: a direct determination using high resolution point-resolved proton magnetic resonance spectroscopy (H-MRS). Front. Syst. Neurosci. *6*, 9.

Brozoski, T.J., Bauer, C.A., and Caspary, D.M. (2002). Elevated fusiform cell activity in the dorsal cochlear nucleus of chinchillas with psychophysical evidence of tinnitus. J. Neurosci. *22*, 2383–2390.

Brozoski, T.J., Wisner, K.W., Sybert, L.T., and Bauer, C.A. (2012b). Bilateral dorsal cochlear nucleus lesions prevent acoustic-trauma induced tinnitus in an animal model. J. Assoc. Res. Otolaryngol. *13*, 55–66.

Bruce, I.C., Sachs, M.B., and Young, E.D. (2003). An auditory-periphery model of the effects of acoustic trauma on auditory nerve responses. J. Acoust. Soc. Am. *113*, 369–388.

Brumberg, J.C., Pinto, D.J., and Simons, D.J. (1999). Cortical Columnar Processing in the Rat Whisker-to-Barrel System. J Neurophysiol *82*, 1808–1817.

Butler, B.E., and Lomber, S.G. (2013). Functional and structural changes throughout the auditory system following congenital and early-onset deafness: implications for hearing restoration. Front. Syst. Neurosci. *7*, 92.

Buzsáki, G. (2004). Large-scale recording of neuronal ensembles. Nat. Neurosci. *7*, 446–451.

Buzsáki, G., Traub, R.D., and Pedley, T. (2003a). The cellular synaptic generation of EEG. In Current Practice of Clinical Encephalography, J.S. Ebersole, and T.A. Pedley, eds. (Philadelphia: Lippincott Williams & Wilkins.), pp. 1–11.

Buzsáki, G., Buhl, D.L., Harris, K.D., Csicsvari, J., Czéh, B., and Morozov, A. (2003b). Hippocampal network patterns of activity in the mouse. Neuroscience *116*, 201–211.

Buzsáki, G., Anastassiou, C.A., and Koch, C. (2012). The origin of extracellular fields and currents--EEG, ECoG, LFP and spikes. Nat. Rev. Neurosci. *13*, 407–420.

Byers, B., Lee, H., and Reijo Pera, R. (2012). Modeling Parkinson's disease using induced pluripotent stem cells. Curr. Neurol. Neurosci. Rep. *12*, 237–242.

Calford, M. (1983). The parcellation of the medial geniculate body of the cat defined by the auditory response properties of single units. J. Neurosci. *3*, 2350–2364.

Calford, M.B., and Aitkin, L.M. (1983). Ascending projections to the medial geniculate body of the cat: evidence for multiple, parallel auditory pathways through thalamus. J. Neurosci. *3*, 2365–2380.

Cant, N.B. (1992). The cochlear nucleus: neuronal types and their synaptic organization. In Springer Handbook of Auditory Research, Vol. 1, The Mammalian Auditory Pathway: Neuroanatomy, D. B. Webster, A.N. Popper, and R.R. Fay, eds. (New York: Springer), pp. 66–116.

Cetas, J.S., Price, R.O., Velenovsky, D.S., Sinex, D.G., and McMullen, N.T. (2001). Frequency organization and cellular lamination in the medial geniculate body of the rabbit. Hear. Res. *155*, 113–123.

Chapleau, M.W. (2007). Exciting times in sensory transduction from A(drian) to Z. J. Physiol. *582*, 13–14.

Chau, J.K., Lin, J.R.J., Atashband, S., Irvine, R.A., and Westerberg, B.D. (2010). Systematic review of the evidence for the etiology of adult sudden sensorineural hearing loss. Laryngoscope *120*, 1011–1021.

Chen, Y.-S., Liu, T.-C., Cheng, C.-H., Yeh, T.-H., Lee, S.-Y., and Hsu, C.-J. (2003). Changes of hair cell stereocilia and threshold shift after acoustic trauma in guinea pigs: comparison between inner and outer hair cells. ORL. J. Otorhinolaryngol. Relat. Spec. *65*, 266–274.

Chung, J.W., Ahn, J.H., Kim, J.Y., Lee, H.J., Kang, H.H., Lee, Y.K., Kim, J.U., and Koo, S.-W. (2007). The effect of isoflurane, halothane and pentobarbital on noise-induced hearing loss in mice. Anesth. Analg. *104*, 1404–1408, table of contents.

Chung, S., Li, X., and Nelson, S.B. (2002). Short-Term Depression at Thalamocortical Synapses Contributes to Rapid Adaptation of Cortical Sensory Responses In Vivo. Neuron *34*, 437–446.

Ciuman, R.R. (2010). The efferent system or olivocochlear function bundle - fine regulator and protector of hearing perception. Int. J. Biomed. Sci. *6*, 276–288.

Clarey, J.C., Barone, P., and Imig, T.J. (1994). Functional organization of sound direction and sound pressure level in primary auditory cortex of the cat. J Neurophysiol *72*, 2383–2405.

Clark, J.A., and Pickles, J.O. (1996). The effects of moderate and low levels of acoustic overstimulation on stereocilia and their tip links in the guinea pig. Hear. Res. *99*, 119–128.

Clement, E.A., Richard, A., Thwaites, M., Ailon, J., Peters, S., and Dickson, C.T. (2008). Cyclic and sleep-like spontaneous alternations of brain state under urethane anaesthesia. PLoS One *3*, e2004.

Clerici, W.J., and Coleman, J.R. (1990). Anatomy of the rat medial geniculate body: I. Cytoarchitecture, myeloarchitecture, and neocortical connectivity. J. Comp. Neurol. *297*, 14–31.

Cobb, M. (2002). Timeline: exorcizing the animal spirits: Jan Swammerdam on nerve function. Nat. Rev. Neurosci. *3*, 395–400.

Cohen, M.R., and Kohn, A. (2011). Measuring and interpreting neuronal correlations. Nat. Neurosci. *14*, 811–819.

Colletti, V., Shannon, R., Carner, M., Sacchetto, L., and Turazzi, S. (2007). The first successful case of hearing produced by electrical stimulation of the human midbrain. Otol. Neurotol. *28*, 39–43.

Constantinople, C.M., and Bruno, R.M. (2013). Deep cortical layers are activated directly by thalamus. Science *340*, 1591–1594.

Cronin, T., and Bennett, J. (2011). Switching on the lights: the use of optogenetics to advance retinal gene therapy. Mol. Ther. *19*, 1190–1192.

Csicsvari, J., Henze, D. a, Jamieson, B., Harris, K.D., Sirota, A., Barthó, P., Wise, K.D., and Buzsáki, G. (2003). Massively parallel recording of unit and local field potentials with silicon-based electrodes. J. Neurophysiol. *90*, 1314–1323.

D'Aldin, C., Cherny, L., Devriere, F., and Dancer, A. (1999). Treatment of Acoustic Trauma. Ann. N. Y. Acad. Sci. *884*, 328–344.

Dallos, P. (1976). Production of cochlear potentials by inner and outer hair cells. J. Acoust. Soc. Am. *60*, 510.

Dallos, P., and Harris, D. (1978). Properties of auditory nerve responses in absence of outer hair cells. J. Neurophysiol. *41*, 365–383.

Daniel, E. (2007). Noise and hearing loss: a review. J. Sch. Health *77*, 225–231.

Dannhof, B.J., and Bruns, V. (1993). The innervation of the organ of Corti in the rat. Hear. Res. *66*, 8–22.

David, A.S., Woodruff, P.W., Howard, R., Mellers, J.D., Brammer, M., Bullmore, E., Wright, I., Andrew, C., and Williams, S.C. (1996). Auditory hallucinations inhibit exogenous activation of auditory association cortex. Neuroreport *7*, 932–936.

Davison, I.G., and Katz, L.C. (2007). Sparse and selective odor coding by mitral/tufted neurons in the main olfactory bulb. J. Neurosci. *27*, 2091–2101.

Daw, N.W., Fox, K., Sato, H., and Czepita, D. (1992). Critical period for monocular deprivation in the cat visual cortex. J Neurophysiol *67*, 197–202.

Dear, S.P., Fritz, J., Haresign, T., Ferragamo, M., and Simmons, J.A. (1993). Tonotopic and functional organization in the auditory cortex of the big brown bat, Eptesicus fuscus. J. Neurophysiol. *70*, 1988–2009.

DeFelipe J. (1993). Neocortical neuronal diversity: chemical heterogeneity revealed by colocalization studies of classic neurotransmitters, neuropeptides, calcium binding proteins, and cell surface molecules. Cereb. Cortex *3*, 273–289.

Dehmel, S., Eisinger, D., and Shore, S.E. (2012). Gap prepulse inhibition and auditory brainstem-evoked potentials as objective measures for tinnitus in guinea pigs. Front. Syst. Neurosci. *6*, 42.

Deisseroth, K., and Schnitzer, M.J. (2013). Engineering approaches to illuminating brain structure and dynamics. Neuron *80*, 568–577.

Delescluse, M., and Pouzat, C. (2006). Efficient spike-sorting of multi-state neurons using inter-spike intervals information. J. Neurosci. Methods *150.1*, 16–21.

Diamond, I.T., Powell, T.P.., and Jones, E.G. (1969). The projection of the auditory cortex upon the diencephalon and brain stem in the cat. Brain Res. *15*, 305–340.

Diamond, M., Huang, W., and Ebner, F. (1994). Laminar comparison of somatosensory cortical plasticity. Science (80-.). *265*, 1885–1888.

Dierks, T., Linden, D.E., Jandl, M., Formisano, E., Goebel, R., Lanfermann, H., and Singer, W. (1999). Activation of Heschl's gyrus during auditory hallucinations. Neuron *22*, 615–621.

Doron, N.N., Ledoux, J.E., and Semple, M.N. (2002). Redefining the tonotopic core of rat auditory cortex: physiological evidence for a posterior field. J. Comp. Neurol. *453*, 345–360.

Douglas, R.J., and Martin, K.A.C. (1991). Opening the grey box. Trends Neurosci. *14*, 286–293.

Druga, R., Syka, J., and Rajkowska, G. (1997). Projections of auditory cortex onto the inferior colliculus in the rat. Physiol. Res. *46*, 215–222.

Du, J., Riedel-Kruse, I.H., Nawroth, J.C., Roukes, M.L., Laurent, G., and Masmanidis, S.C. (2009). High-resolution three-dimensional extracellular recording of neuronal activity with microfabricated electrode arrays. J. Neurophysiol. *101*, 1671–1678.

Du, Y., Wu, X., and Li, L. (2011). Differentially organized top-down modulation of prepulse inhibition of startle. J. Neurosci. *31*, 13644–13653.

E Mugnaini, W.W. and K.O. (1980). Distribution and light microscopic features of granule cells in the cochlear nuclei of cat, rat, and mouse. J Comp Neurol *191*, 581–606.

E. Borg and J. E. Zakrisson (1974). Stapedius Reflex and Monaural Masking. Acta Otolaryngol. *78*, 155–161.

Eggermont, J.J. (1996). How homogeneous is cat primary auditory cortex? Evidence from simultaneous single-unit recordings. Audit. Neurosci. *2*, 79.

Eggermont, J.J. (2008). Role of auditory cortex in noise- and drug-induced tinnitus. Am. J. Audiol. *17*, S162–S169.

Eggermont, J.J. (2013). Hearing loss, hyperacusis, or tinnitus: what is modeled in animal research? Hear. Res. *295*, 140–149.

Eggermont, J.J., and Kenmochi, M. (1998). Salicylate and quinine selectively increase spontaneous firing rates in secondary auditory cortex. Hear. Res. *117*, 149–160.

Eggermont, J.J., and Komiya, H. (2000). Moderate noise trauma in juvenile cats results in profound cortical topographic map changes in adulthood. Hear. Res. *142*, 89–101.

Eggermont, J.J., and Roberts, L.E. (2004). The neuroscience of tinnitus. Trends Neurosci. *27*, 676–682.

Einevoll, G.T., Kayser, C., Logothetis, N.K., and Panzeri, S. (2013). Modelling and analysis of local field potentials for studying the function of cortical circuits. Nat. Rev. Neurosci. *14*, 770–785.

Engineer, N.D., Riley, J.R., Seale, J.D., Vrana, W. a, Shetake, J. a, Sudanagunta, S.P., Borland, M.S., and Kilgard, M.P. (2011). Reversing pathological neural activity using targeted plasticity. Nature *470*, 101–104.

Epstein, S., and Reilly, J. (1989). Sensorineural hearing loss. Pediatr. Clin. North Am. *36*, 1501–1520.

Escera, D.C., Althen, H., and Grimm, D.S. (2014). Auditory Evoked Brainstem Responses In Encyclopedia of Computational Neuroscience. D. Jaeger and R. Jung, eds. (New York: Springer), pp.1–3.

Van Essen, D.C., and Maunsell., J.H. (1983). Hierarchical organization and functional streams in the visual cortex. Trends Neurosci. *6*, 370–375.

Estes, W.K., and Skinner, B.F. (1941). Some quantitative properties of anxiety. J. Exp. Psychol. *29*, 390–400.

Evans, E.F. (1972). The frequency response and other properties of single fibres in the guinea-pig cochlear nerve. J. Physiol. *226*, 263–287.

Evans, S., Perkins, R.E., and Disterhoft, J.F. (1980). Neuronal morphology of the rabbit cochlear nucleus. J. Comp. Neurol. *192*, 687–702.

Evarts, E. V (1968). A technique for recording activity of subcortical neurons in moving animals. Electroencephalogr. Clin. Neurophysiol. *24*, 83–86.

Faye-Lund, H., and Osen, K.K. (1985). Anatomy of the inferior colliculus in rat. Anat. Embryol. (Berl). *171*, 1–20.

Fee, M.S., Mitra, P.P., and Kleinfeld., D. (1996). Automatic sorting of multiple unit neuronal signals in the presence of anisotropic and non-Gaussian variability. J. Neurosci. Methods *69*, 175–18.

Feldman, M.L., and Harrison, J.M. (1969). The projection of the acoustic nerve to the ventral cochlear nucleus of the rat. A Golgi study. J. Comp. Neurol. *137*, 267–294.

Feliciano, M., Saldana, E., and Mugnaini., E. (1995). Direct projections from the rat primary auditory neocortex to nucleus sagulum, paralemniscal regions, superior olivary complex and cochlear nuclei. Aud Neurosci *1*, 287–308.

Felleman, D.J., and Van Essen, D.C. (1991). Distributed hierarchical processing in the primate cerebral cortex. Cereb. Cortex *1*, 1–47.

Field, K.J., White, W.J., and Lang, C.M. (1993). Anaesthetic effects of chloral hydrate, pentobarbitone and urethane in adult male rats. Lab. Anim. *27*, 258–269.

Foeller, E., Vater, M., and Kössl, M. (2001). Laminar analysis of inhibition in the gerbil primary auditory cortex. J. Assoc. Res. Otolaryngol. *2*, 279–296.

Fox, K. (2009). Experience-dependent plasticity mechanisms for neural rehabilitation in somatosensory cortex. Philos. Trans. R. Soc. Lond. B. Biol. Sci. *364*, 369–381.

Fox, M.D., and Raichle, M.E. (2007). Spontaneous fluctuations in brain activity observed with functional magnetic resonance imaging. Nat. Rev. Neurosci. *8*, 700–711.

Frederick, A., Bourget-Murray, J., Chapman, C.A., Amir, S., and Courtemanche, R. (2014). Diurnal influences on electrophysiological oscillations and coupling in the dorsal striatum and cerebellar cortex of the anesthetized rat. Front. Syst. Neurosci. *8*.

Friauf, E., and Lohmann, C. (1999). Development of auditory brainstem circuitry. Cell Tissue Res. *297*, 187–195.

Gaese, B.H., and Ostwald, J. (2001). Anesthesia changes frequency tuning of neurons in the rat primary auditory cortex. J. Neurophysiol. *86*, 1062–1066.

Gardner, M.B. and Gardner, R.S. (1973). . J.Acous, Soc,Am. *53*, 400–408.

Geniec, P., and Morest, D.K. (1971). The neuronal architecture of the human posterior colliculus. A study with the Golgi method. Acta Otolaryngol Suppl. *295*, 1–33.

Genis, E.D., Serkov, F.N., and Maiskii, V.A. (1974). Morphology of the cat auditory cortex. Neurophysiology *5*, 399–407.

Geocze, L., Mucci, S., Abranches, D.C., Marco, M.A. de, and Penido, N. de O. (2013). Systematic review on the evidences of an association between tinnitus and depression. Braz. J. Otorhinolaryngol. *79*, 106–111.

Gerstein, G.L., and Clark, W.A. (1964). Simultaneous Studies of Firing Patterns in Several Neurons. Science *143*, 1325–1327.

Giraudet, F., Horner, K.C., and Cazals, Y. (2002). Similar half-octave TTS protection of the cochlea by xylazine/ketamine or sympathectomy. Hear. Res. *174*, 239–248.

Glazewski, S., and Fox, K. (1996). Time course of experience-dependent synaptic potentiation and depression in barrel cortex of adolescent rats. J. Neurophysiol. *75*, 1714–1729.

Godfrey, D.A., Kiang, N.Y., and Norris, B.E. (1975). Single unit activity in the posteroventral cochlear nucleus of the cat. J. Comp. Neurol. *162*, 247–268.

Gold, J.R., and Bajo, V.M. (2014). Insult-induced adaptive plasticity of the auditory system. Front. Neurosci. *8*, 110.

Gordon, J.A., and Stryker, M.P. (1996). Experience-Dependent Plasticity of Binocular Responses in the Primary Visual Cortex of the Mouse. J. Neurosci. *16*, 3274–3286.

Gray, C.M., Maldonado, P.E., Wilson, M., and McNaughton, B. (1995). Tetrodes markedly improve the reliability and yield of multiple single-unit isolation from multi-unit recordings in cat striate cortex. J. Neurosci. Methods *63*, 43–54.

Gustafsson B (1984). Afterpotentials and transduction properties in different types of central neurones. Arch. Ital. Biol. *122*, 17–30.

Hackett, T.A. (2011). Information flow in the auditory cortical network. Hear. Res. *271*, 133–146.

Haider, B., Krause, M.R., Duque, A., Yu, Y., Touryan, J., Mazer, J.A., and McCormick, D.A. (2010). Synaptic and network mechanisms of sparse and reliable visual cortical activity during nonclassical receptive field stimulation. Neuron *65*, 107–121.

Hakuba, N., Koga, K., Gyo, K., Usami, S., and Tanaka, K. (2000). Exacerbation of Noise-Induced Hearing Loss in Mice Lacking the Glutamate Transporter GLAST. J. Neurosci. *20*, 8750–8753.

Hampson, R.E., Simeral, J.D., and Deadwyler, S.A. (2001). The evolution of population and modular neural coding ideas. In Advances in Neural Population Coding, M.A.L. Nicolelis, ed.(Elsevier).

Harada, Y., and Takahashi, T. (1983). The calcium component of the action potential in spinal motoneurones of the rat. J. Physiol. Lond. *335*, 89–100.

Harris, K.D., Henze, D.A., Csicsvari, J., Hirase, H., and Buzsaki, G. (2000). Accuracy of Tetrode Spike Separation as Determined by Simultaneous Intracellular and Extracellular Measurements. J Neurophysiol *84*, 401–414.

Harris, K.D., Bartho, P., Chadderton, P., Curto, C., de la Rocha, J., Hollender, L., Itskov, V., Luczak, A., Marguet, S.L., Renart, A., et al. (2011). How do neurons work together? Lessons from auditory cortex. Hear. Res. *271*, 37–53.

Hartline, H.K. (1967). Visual receptors and retinal interaction. Les Prix Nobel en 1967. 242–259. (online).

Hasenstaub, A., Shu, Y., Haider, B., Kraushaar, U., Duque, A., and McCormick, D.A. (2005). Inhibitory postsynaptic potentials carry synchronized frequency information in active cortical networks. Neuron *47*, 423–435.

Hatch, M., Tsai, M., LaRouere, M.J., Nuttall, A.L., and Miller, J.M. (1991). The effects of Carbogen, carbon dioxide, and oxygen on noise-induced hearing loss. Hear. Res. *56*, 265–272.

Hawkins, J.E. (2004). Sketches of otohistory. Part 3: Alfonso Corti. Audiol. Neurootol. *9*, 259–264.

Hawkins, J.E. (2005). Sketches of otohistory. Part 6: Gustaf Retzius. Audiol. Neurootol. *10*, 65–68.

Hawkins, J.E., and Schacht, J. (2005). Sketches of Otohistory Part 10: Noise-Induced Hearing Loss. Audiol Neurotol *10*, 305–309.

Hazan, L., Zugaro, M., and Buzsáki, G. (2006). Klusters, NeuroScope, NDManager: a free software suite for neurophysiological data processing and visualization. J. Neurosci. Methods *155*, 207–216.

Heffner, H.E. The neurobehavioral study of auditory cortex. In Auditory Cortex - Towards a Synthesis of Human and Animal Research., Budinger, and H. Scheich, eds. (Mahwah NJ: Lawrence Erlbaum Associates), pp. 111–126.

Heffner, H.E., and Heffner, R.S. (2003). Audition. In Handbook of Research Methods in Experimental Psychology, S.Davis, ed. (Blackwell), pp. 413–440.

Heffner, H.E., and Heffner, R.S. (2007). Hearing ranges of laboratory animals. J. Am. Assoc. Lab. Anim. Sci. *46*, 20–22.

Heffner, R.S., and Heffner, H.E. (1991). Behavioral hearing range of the chinchilla. Hear. Res. *52*, 13–16.

Heffner, H.E., Koay, G., and Heffner, R.S. (2006). Behavioral assessment of hearing in mice--conditioned suppression. Curr. Protoc. Neurosci. *Chapter 8*, Unit8.21D.

Heffner, H.E., Koay, G., and Heffner, R.S. (2008). Comparison of behavioral and auditory brainstem response measures of threshold shift in rats exposed to loud sound. J. Acoust. Soc. Am. *124*, 1093–1104.

Heffner, R., Heffner, H., and Masterton, B. (1971). Behavioral measurements of absolute and frequency-difference thresholds in guinea pig. J. Acoust. Soc. Am. *49*, 1888–1895.

Heffner, R.S., Koay, G., and Heffner, H.E. (2001). Audiograms of five species of rodents: implications for the evolution of hearing and the perception of pitch. Hear. Res. *157*, 138–152.

Heinz, M.G., Colburn, H.S., and Carney, L.H. (2001). Rate and timing cues associated with the cochlear amplifier: level discrimination based on monaural cross-frequency coincidence detection. J. Acoust. Soc. Am. *110*, 2065–2084.

Henrie, J.A., and Shapley, R. (2005). LFP power spectra in V1 cortex: the graded effect of stimulus contrast. J. Neurophysiol. *94*, 479–490.

Henson.O.W (1974). Comparative Anatomy of the Middle Ear. In Handbook of Sensory Physiology Auditory System, W.D. Keidel, and W.D. Neff, eds. (Berlin: Springer Berlin Heidelberg), pp. 39–110.

Hernandez, V.H., Gehrt, A., Reuter, K., Jing, Z., Jeschke, M., Schulz, A.M., Hoch, G., Bartels, M., Vogt, G., Garnham, C.W., et al. (2014). Optogenetic stimulation of the auditory pathway. J. Clin. Invest *124*, 1114-1129.

Hill, E.M. (2011). A Comparison of Behavioral and Auditory Brainstem Response Measures of Hearing in the Laboratory Rat (Rattus norvegicus). PhD. dissertation. Univ. Toledo, Spain.

Hind, J.E., Goldberg, J.M., Greenwood, D.D., and ROSE, J.E. (1963). Some discharge characteristics of single neurons in the inferior colliculus of the cat. II. Timing of the discharges and observations on binaural stimulation. J. Neurophysiol. *26*, 321–341.

Hodgkin, A.L., and Huxley, A.F. (1952). A quantitative description of membrane current and its application to conduction and excitation in nerve. J. Physiol. *117*, 500–544.

Hoffman, K.L., and McNaughton, B.L. (2002). Coordinated reactivation of distributed memory traces in primate neocortex. Science *297*, 2070–2073.

Hoffman, K.L., Battaglia, F.P., Harris, K., MacLean, J.N., Marshall, L., and Mehta, M.R. (2007). The upshot of up states in the neocortex: from slow oscillations to memory formation. J. Neurosci. *27*, 11838–11841.

Horikawa, J., Ito, S., Hosokawa, Y., Homma, T., and Murata, K. (1988). Tonotopic representation in the rat auditory cortex. Proc. Japan Acad. Ser. B Phys. Biol. Sci. *64*, 260–263.

Hu, Z., Ulfendahl, M., and Olivius, N.P. (2004). Central migration of neuronal tissue and embryonic stem cells following transplantation along the adult auditory nerve. Brain Res. *1026*, 68–73.

Huang, T. (2007). Age-related hearing loss. Minn. Med. *90*, 48–50.

Huang, C.L., and Winer, J. a (2000). Auditory thalamocortical projections in the cat: laminar and areal patterns of input. J. Comp. Neurol. *427*, 302–331.

Hubel, D.H., and Wiesel, T.N. (1962). Receptive fields, binocular interaction and functional architecture in the cat's visual cortex. J. Physiol. *160*, 106–154.

Huetz, C., Guedin, M., and Edeline, J.-M. (2014). Neural correlates of moderate hearing loss: time course of response changes in the primary auditory cortex of awake guinea-pigs. Front. Syst. Neurosci. *8*, 65.

Humphries, C., Liebenthal, E., and Binder, J.R. (2010). Tonotopic organization of human auditory cortex. Neuroimage *50*, 1202–1211.

Imaizumi, K., and Lee, C.C. (2014). Frequency transformation in the auditory lemniscal thalamocortical system. Front. Neural Circuits *8*, 1–9.

Imig, T.J., and Morel, A. (1985). Tonotopic organization in ventral nucleus of medial geniculate body in the cat. J. Neurophysiol. *53*, 309–340.

Imig, T.J., and Reale, R.A. (1980). Patterns of cortico-cortical connections related to tonotopic maps in cat auditory cortex. J. Comp. Neurol. *192*, 293–332.

Irvine, D.R. (1986). A review of the structure and fuction of auditory brainstem processing mechanisms. In Sensory Physiology, Vol 7, D.Ottoson, ed. (Berlin: Springer- Verlag), pp. 1–279.

Issa, J.B., Haeffele, B.D., Agarwal, A., Bergles, D.E., Young, E.D., and Yue, D.T. (2014). Multiscale Optical Ca2+ Imaging of Tonal Organization in Mouse Auditory Cortex. Neuron *83*, 944–959.

Jacob, V., Petreanu, L., Wright, N., Svoboda, K., and Fox, K. (2012). Regular spiking and intrinsic bursting pyramidal cells show orthogonal forms of experience-dependent plasticity in layer V of barrel cortex. Neuron *73*, 391–404.

Jastreboff, P.J., Brennan, J.F., and Sasaki, C.T. (1988a). An animal model for tinnitus. Laryngoscope *98*, 280–286.

Jastreboff, P.J., Brennan, J.F., Coleman, J.K., and Sasaki, C.T. (1988b). Phantom auditory sensation in rats: an animal model for tinnitus. Behav. Neurosci. *102*, 811–822.

Jewett, D.L., and Willinston, J.S. (1971). Auditory-Evoked Far Fields Averaged From The Scalp Of Humans. Brain *94*, 681–696.

Jones, E.G. (2011). The Historical Development of Ideas About the Auditory Cortex. In The Auditory Cortex, J.A. Winer, and C.E. Schreiner, eds. (New York: Springer), pp. 1–40.

KA., F. (1975). Cellular architecture and topographic organization of the inferior colliculus of the squirrel monkey. J Comp Neurol *164*, 185–207.

Kaas, J.H., and Hackett, T. a (2000). Subdivisions of auditory cortex and processing streams in primates. Proc. Natl. Acad. Sci. U. S. A. *97*, 11793–11799.

Kaas, J.H., Hackett, T.A., and Tramo, M.J. (1999). Auditory processing in primate cerebral cortex. Curr. Opin. Neurobiol. *9*, 164–170.

Kajikawa, Y., and Schroeder, C.E. (2011). How local is the local field potential? Neuron *72*, 847–858.

Kalatsky, V.A., Polley, D.B., Merzenich, M.M., Schreiner, C.E., and Stryker, M.P. (2005). Fine functional organization of auditory cortex revealed by Fourier optical imaging. Proc. Natl. Acad. Sci. U. S. A. *102*, 13325–13330.

Kaltenbach, J.A. (2011). Tinnitus: Models and mechanisms. Hear. Res. *276*, 52–60.

Kaltenbach, J.A., and Zhang, J. (2007). Intense sound-induced plasticity in the dorsal cochlear nucleus of rats: evidence for cholinergic receptor upregulation. Hear. Res. *226*, 232–243.

Kaltenbach, J.A., Zacharek, M.A., Zhang, J., and Frederick, S. (2004). Activity in the dorsal cochlear nucleus of hamsters previously tested for tinnitus following intense tone exposure. Neurosci. Lett. *355*, 121–125.

Kanold, P.O., Nelken, I., and Polley, D.B. (2014). Local versus global scales of organization in auditory cortex. Trends Neurosci 37, 502-10.

Katzner, S., Nauhaus, I., Benucci, A., Bonin, V., Ringach, D.L., and Carandini, M. (2009). Local origin of field potentials in visual cortex. Neuron *61*, 35–41.

Kaur, S., Rose, H.J., Lazar, R., Liang, K., and Metherate, R. (2005). Spectral integration in primary auditory cortex: laminar processing of afferent input, in vivo and in vitro. Neuroscience *134*, 1033–1045.

Kawamoto, K., Sha, S.-H., Minoda, R., Izumikawa, M., Kuriyama, H., Schacht, J., and Raphael, Y. (2004). Antioxidant gene therapy can protect hearing and hair cells from ototoxicity. Mol. Ther. *9*, 173–181.

Kazuhiro Iida, M.Y. and M.M. (1998). Role of pinna cavities in median plane localization. J. Acoust. Soc. Am. *103*, 845–846.

Kelly, J.B., Judge, P.W., and Phillips, D.P. (1986). Representation of the cochlea in primary auditory cortex of the ferret (Mustela putorius). Hear. Res. *24*, 111–115.

Kiang, N.Y.-S. (1965). DISCHARGE PATTERNS OF SINGLE FIBERS IN THE CAT'S AUDITORY NERVE. MIT Press. Cambridge MA.

Kiang, N.Y., Pfeiffer, R.R., Warr, W.B., and Backus, A.S. (1965). Stimulus coding in the cochlear nucleus. Trans. Am. Otol. Soc. *53*, 35–58.

Kiang, N.Y., Rho, J.M., Northrop, C.C., Liberman, M.C., and Ryugo, D.K. (1982). Hair-cell innervation by spiral ganglion cells in adult cats. Science *217*, 175–177.

Kiang, N.Y.S., Moxon, E.C., and Levine, R.A. (1970). Auditory-nerve activity in cats with normal and abnormal cochleas. In Sensorineural Hearing Loss, G.E.W. Wolstenholme, and J. Knight, eds. (J and A Churchill), pp. 241–273.

Kimura, M., and Eggermont, J.J. (1999). Effects of acute pure tone induced hearing loss on response properties in three auditory cortical fields in cat. *135*, 146–162.

Kimura, A., Donishi, T., Sakoda, T., Hazama, M., and Tamai, Y. (2003). Auditory thalamic nuclei projections to the temporal cortex in the rat. Neuroscience *117*, 1003–1016.

Knipper, M., Van Dijk, P., Nunes, I., Rüttiger, L., and Zimmermann, U. (2013). Advances in the neurobiology of hearing disorders: recent developments regarding the basis of tinnitus and hyperacusis. Prog. Neurobiol. *111*, 17–33.

Koehler, K.R., Mikosz, A.M., Molosh, A.I., Patel, D., and Hashino, E. (2013). Generation of inner ear sensory epithelia from pluripotent stem cells in 3D culture. Nature *500*, 217–221.

Koerber, K.C., Pfeiffer, R.R., Warr, W.B., and Kiang, N.Y.S. (1966). Spontaneous spike discharges from single units in the cochlear nucleus after destruction of the cochlea. Exp. Neurol. *16*, 119–130.

Kuypers, H.G., and Lawrence, D.G. (1967). Cortical projections to the red nucleus and the brain stem in the Rhesus monkey. Brain Res. *4*, 151–188.

LaLumiere, R.T. (2011). A new technique for controlling the brain: optogenetics and its potential for use in research and the clinic. Brain Stimul. *4*, 1–6.

Lasak, J.M., Allen, P., McVay, T., and Lewis, D. (2014). Hearing loss: diagnosis and management. Prim. Care *41*, 19–31.

Lavine, R.A. (1971). Phase-locking in response of single neurons in cochlear nucler complex of the cat to low-frequency tonal stimuli. J. Neurophysiol. *34*, 467–483.

Leao, R.N., Sun, H., Svahn, K., Berntson, A., Youssoufian, M., Paolini, A.G., Fyffe, R.E.W., and Walmsley, B. (2006). Topographic organization in the auditory brainstem of juvenile mice is disrupted in congenital deafness. J. Physiol. *571*, 563–578.

Leaver, A.M., Renier, L., Chevillet, M.A., Morgan, S., Kim, H.J., and Rauschecker, J.P. (2011). Dysregulation of limbic and auditory networks in tinnitus. Neuron *69*, 33–43.

Lee, C. (2014). Two types of auditory glutamatergic synapses and their implications for repairing damaged central auditory pathways. Neural Regen. Res. *9*, 2002–2004.

Lee, C.C., and Imaizumi, K. (2013). Functional convergence of thalamic and intrinsic projections to cortical layers 4 and 6. Neurophysiology *45*, 396–406.

Lee, C.C., and Sherman, S.M. (2010). Drivers and modulators in the central auditory pathways. Front. Neurosci. *4*, 79.

Lee, C.C., and Sherman, S.M. (2011). On the classification of pathways in the auditory midbrain, thalamus, and cortex. Hear. Res. *276*, 79–87.

Lee, C.C., Imaizumi, K., Schreiner, C.E., and Winer, J.A. (2004). Concurrent tonotopic processing streams in auditory cortex. Cereb. Cortex *14*, 441–451.

Lesoine, W. (1983). [Acoustic trauma--new viewpoints in therapy]. Laryngol. Rhinol. Otol. (Stuttg). *62*, 555–557.

Letelier, J.C., and Weber, P.P. (2000). Spike sorting based on discrete wavelet transform coefficients. J. Neurosci. Methods *101*, 93–106.

Lewicki, M.S. (1998). A review of methods for spike sorting: the detection and classification of neural action potentials. Network *9*, R53–R78.

Lewis, S. (2012). Neuronal circuits: Mapping the local field potential. Nat. Rev. Neurosci. *13*, 75.

Li, H., Roblin, G., Liu, H., and Heller, S. (2003a). Generation of hair cells by stepwise differentiation of embryonic stem cells. Proc. Natl. Acad. Sci. U. S. A. *100*, 13495–13500.

Li, H., Liu, H., and Heller, S. (2003b). Pluripotent stem cells from the adult mouse inner ear. Nat. Med. *9*, 1293–1299.

Li, L., Du, Y., Li, N., Wu, X., and Wu, Y. (2009). Top-down modulation of prepulse inhibition of the startle reflex in humans and rats. Neurosci. Biobehav. Rev. *33*, 1157–1167.

Liberman, M.C. (1980). Efferent synapses in the inner hair cell area of the cat cochlea: an electron microscopic study of serial sections. Hear. Res. *3*, 189–204.

Liberman, M.C. (1991). Central projections of auditory-nerve fibers of differing spontaneous rate. I. Anteroventral cochlear nucleus. J. Comp. Neurol. *313*, 240–258.

Liberman, M.C. (1993). Central projections of auditory nerve fibers of differing spontaneous rate, II: Posteroventral and dorsal cochlear nuclei. J. Comp. Neurol. *327*, 17–36.

Liberman, U. (1988). External stability and ESS: criteria for initial increase of new mutant allele. J. Math. Biol. *26*, 477–485.

Liberman, M.C., and Kiang, N.Y. (1984). Single-neuron labeling and chronic cochlear pathology. IV. Stereocilia damage and alterations in rate- and phase-level functions. Hear. Res. *16*, 75–90.

Lim, H., Lenarz, T., Joseph, G., Battmer, R., Patrick, J., and Lenarz, M. (2008). Effects of phase duration and pulse rate on loudness and pitch percepts in the first auditory midbrain implant patients: Comparison to cochlear implant and auditory brainstem implant results. Neuroscience *154*, 370–380.

Linden, J.F., and Schreiner, C.E. (2003). Columnar transformations in auditory cortex? A comparison to visual and somatosensory cortices. Cereb. Cortex *13*, 83–89.

Lindvall, O., and Kokaia, Z. (2010). Stem cells in human neurodegenerative disorders--time for clinical translation? J. Clin. Invest. *120*, 29–40.

Liu, J., and Newsome, W.T. (2006). Local field potential in cortical area MT: stimulus tuning and behavioral correlations. J. Neurosci. *26*, 7779–7790.

Llano, D.A., Turner, J., and Caspary, D.M. (2012). Diminished cortical inhibition in an aging mouse model of chronic tinnitus. J. Neurosci. *32*, 16141–16148.

Lobarinas, E., Yang, G., and Sun, W. (2006). Salicylate- and quinine-induced tinnitus and effects of memantine. Acta Otolaryngol. *556*, 13–19.

Lobarinas, E., Hayes, S.H., and Allman, B.L. (2013). The gap-startle paradigm for tinnitus screening in animal models : Limitations and optimization. Hear. Res. *295*, 150–160.

Luczak, A., Barthó, P., and Harris, K.D. (2009). Spontaneous events outline the realm of possible sensory responses in neocortical populations. Neuron *62*, 413–425.

Luethke, L.E., Krubitzer, L.A., and Kaas, J.H. (1989). Connections of primary auditory cortex in the New World monkey, Saguinus. J. Comp. Neurol. *285*, 487–513.

Martinez, L.M., Alonso, J.M., Reid,C.R., and Hirsch J.A. (2002). Laminar processing of stimulus orientation in cat visual cortex. J. Physiol. *540*, 321–333.

Maffei, A., Nelson, S.B., and Turrigiano, G.G. (2004). Selective reconfiguration of layer 4 visual cortical circuitry by visual deprivation. Nat. Neurosci. *7*, 1353–1359.

Malmeirca, M.S., and Ryugo, D.K. (2011). Descending Connections of Auditory Cortex to the Midbrain and the Brain Stem. In The Auditory Cortex, J.A. Winer, and C.E. Schreiner, eds. (New York: Springer), pp. 189–204.

Malmierca, M.S., Saint Marie, R.L., Merchan, M.A., and Oliver, D.L. (2005). Laminar inputs from dorsal cochlear nucleus and ventral cochlear nucleus to the central nucleus of the inferior colliculus: two patterns of convergence. Neuroscience *136*, 883–894.

Malmierca, M.S., Izquierdo, M.A., Cristaudo, S., Hernández, O., Pérez-González, D., Covey, E., and Oliver, D.L. (2008). A discontinuous tonotopic organization in the inferior colliculus of the rat. J. Neurosci. *28*, 4767–4776.

Mao, J.C., Pace, E., Pierozynski, P., Kou, Z., Shen, Y., VandeVord, P., Haacke, E.M., Zhang, X., and Zhang, J. (2012). Blast-induced tinnitus and hearing loss in rats: behavioral and imaging assays. J. Neurotrauma *29*, 430–444.

Mathers, C., Fat, D.M., and Boerma, J.T. (2008). World Health Organization.The global burden of disease: 2004 update. (Geneva).

McNaughton, B.L., O'Keefe, J., and Barnes, C.A. (1983). The stereotrode: a new technique for simultaneous isolation of several single units in the central nervous system from multiple unit records. J. Neurosci. Methods *8*, 391–397.

Meltzer, N.E., and Ryugo, D.K. (2006). Projections from auditory cortex to cochlear nucleus: A comparative analysis of rat and mouse. Anat. Rec. A. Discov. Mol. Cell. Evol. Biol. *288*, 397–408.

Mendelson, J.R., and Cynader, M.S. (1985). Sensitivity of cat primary auditory cortex (Al) neurons to the direction and rate of frequency modulation. Brain Res. *327*, 331–335.

Merzenich, M.M., and Reid, M.D. (1974). Representation of the cochlea within the inferior colliculus of the cat. Brain Res. *77*, 397–415.

Merzenich, M.M., Knight, P.L., and Roth, G.L. (1975). Representation of cochlea within primary auditory cortex in the cat. J Neurophysiol *38*, 231–249.

Milbrandt, J.., Holder, T.., Wilson, M.., Salvi, R.., and Caspary, D.. (2000). GAD levels and muscimol binding in rat inferior colliculus following acoustic trauma. Hear. Res. *147*, 251–260.

Mitzdorf, U. (1985). Current source-density method and application in cat cerebral cortex: investigation of evoked potentials and EEG phenomena. Physiol Rev *65*, 37–100.

Moller, A. (1982). Anatomy and general function of the auditory nervous system. In Auditory Physiology, (New York: Academic Press Inc), pp. 109–115.

Moller, A.R. (1975). The acoustic middle ear reflex. In Handbook of Sensory Physiology Auditory System Vol. V/1, W.D. Keidel, and D.L. Neff, eds. (Berlin: Springer- Verlag), pp. 519–548.

Moller, A.R. (2006). Anatomy of the auditory nervous system. In Hearing: Anatomy, Physiology, and Disorders of the Auditory System, (Elsevier), pp. 75–90.

Møller.A.R (1974). Function of the Middle Ear. In Handbook of Sensory Physiology Auditory Pathway, W.D.N. Keidel, Wolf D., ed. (Springer Berlin Heidelberg), pp. 491–517.

Moody, D.. (2004). Tinnitus: Theory and Management. In Tinnitus, J.B. Snow, ed. (PMPH-USA), pp. 81–95.

Moore, D.R., and Shannon, R. V (2009). Beyond cochlear implants: awakening the deafened brain. Nat. Neurosci. *12*, 686–691.

Moore, D., Palmer, A., Hall, D., and Sumner, C. (2007). Auditory Cortex 2006: the listening brain. Hear. Res. *229*, 1–2.

Morel, A., and Imig, T.J. (1987). Thalamic projections to fields A, AI, P, and VP in the cat auditory cortex. J. Comp. Neurol. *265*, 119–144.

Morest, D.K. (1965). The lateral tegmental system of the midbrain and the medial geniculate body: Study with Golgi and Nauta methods in cat. J. Anat. *99*, 611–634.

Morest, D.K., and Oliver, D.L. (1984). The neuronal architecture of the inferior colliculus in the cat: defining the functional anatomy of the auditory midbrain. J. Comp. Neurol. *222*, 209–236.

Morosan, P., Rademacher, J., Schleicher, A., Amunts, K., Schormann, T., and Zilles, K. (2001). Human primary auditory cortex: cytoarchitectonic subdivisions and mapping into a spatial reference system. Neuroimage *13*, 684–701.

Moser, T. (2015). Optogenetic stimulation of the auditory pathway for research and future prosthetics. Curr. Opin. Neurobiol. *34C*, 29–36.

Moshitch, D., Las, L., Ulanovsky, N., Bar-Yosef, O., and Nelken, I. (2006). Responses of neurons in primary auditory cortex (A1) to pure tones in the halothane-anesthetized cat. J. Neurophysiol. *95*, 3756–3769.

Mountcastle, V.B. (1957). Modality and topographic properties of single neurons of cat's somatic sensory cortex. J. Neurophysiol. *20*, 408–434.

Mountcastle, V.B. (1997). The columnar organization of the neocortex. Brain *120*, 701–722.

Mugnaini E, Osen KK, Dahl AL, Friedrich VL, Jr, K.G. (1980). Fine structure of granule cells and related interneurons (termed Golgi cells) in the cochlear nuclear complex of cat, rat and mouse. J Neurocytol *9*, 537–570.

Muhlnickel, W., Elbert, T., Taub, E., and Flor, H. (1998). Reorganization of auditory cortex in tinnitus. Proc. Natl. Acad. Sci. *95*, 10340–10343.

Mulders, W.H.A.M., and Robertson, D. (2009). Hyperactivity in the auditory midbrain after acoustic trauma: dependence on cochlear activity. Neuroscience *164*, 733–746.

Neff, D.L. (1995). Springer Handbook of Auditory Research. Ear and Heaing *16*, 545.

Neher, E. (1992). Nobel lecture. Ion channels for communication between and within cells. Embo J. *11*, 1672–1679.

Nelson, D.I., Nelson, R.Y., Concha-Barrientos, M., and Fingerhut, M. (2005). The global burden of occupational noise-induced hearing loss. Am. J. Ind. Med. *48*, 446–458.

Neuman, M.R.. (1999). Biopotential Electrodes. In The Biomedical Engineering Handbook, D. Joseph, ed. (CRC Press).

Niell, C.M., and Stryker, M.P. (2010). Modulation of visual responses by behavioral state in mouse visual cortex. Neuron *65*, 472–479.

Nobili, L. (1828). Comparaison entre les deux galvanometres les plus sensibles, la grenouille et le moltiplicateur a deux aiguilles, suivie de quelques resultats noveaux. *7*, 267–271.

Noreña, A.J. (2011). An integrative model of tinnitus based on a central gain controlling neural sensitivity. Neurosci. Biobehav. Rev. *35*, 1089–1109.

Noreña, a. J., and Eggermont, J.J. (2003a). Changes in spontaneous neural activity immediately after an acoustic trauma: implications for neural correlates of tinnitus. Hear. Res. *183*, 137–153.

Noreña, A., and Eggermont, J.J. (2002). Comparison between local field potentials and unit cluster activity in primary auditory cortex and anterior auditory field in the cat. Hear. Res. *166*, 202–213.

Noreña, A.J., and Eggermont, J.J. (2003b). Neural correlates of an auditory afterimage in primary auditory cortex. J. Assoc. Res. Otolaryngol. *4*, 312–328.

Noreña, A.J., and Eggermont, J.J. (2005). Enriched acoustic environment after noise trauma reduces hearing loss and prevents cortical map reorganization. J. Neurosci. *25*, 699–705.

Noreña, A.J., and Farley, B.J. (2013). Tinnitus-related neural activity: theories of generation, propagation, and centralization. Hear. Res. *295*, 161–171.

Noreña, A.J., Tomita, M., and Eggermont, J.J. (2003). Neural changes in cat auditory cortex after a transient pure-tone trauma. J. Neurophysiol. *90*, 2387–2401.

Noreña, A.J., Moffat, G., Blanc, J.L., Pezard, L., and Cazals, Y. (2010). Neural changes in the auditory cortex of awake guinea pigs after two tinnitus inducers: salicylate and acoustic trauma. Neuroscience *166*, 1194–1209.

Norman, M., Tomscha, K., and Wehr, M. (2012). Isoflurane blocks temporary tinnitus. Hear. Res. *290*, 64–71.

O'Keefe, J., and Recce, M. (1989). The tetrode: a new technique for multiunit extra-cellular recording. Soc Neurosci Abstr 15 1270.

Ojima, H. (1991). Terminal morphology and distribution of corticothalamic fibers originating from layers 5 and 6 of cat primary auditory cortex. Cereb. Cortex *4*, 646–663.

Okuda, T., Nagamachi, S., Ushisako, Y., and Tono, T. (2013). Glucose metabolism in the primary auditory cortex of postlingually deaf patients: an FDG-PET study. ORL. J. Otorhinolaryngol. Relat. Spec. *75*, 342–349.

Oliver, D.L. (1987). Projections to the inferior colliculus from the anteroventral cochlear nucleus in the cat: possible substrates for binaural interaction. J. Comp. Neurol. *264*, 24–46.

Oliver, D.L., Ostapoff, E.M., and Beckius, G.E. (1999). Direct innervation of identified tectothalamic neurons in the inferior colliculus by axons from the cochlear nucleus. Neuroscience *93*, 643–658.

Olshausen, B.A., and Field, D.J. (1996). Emergence of simple-cell receptive field properties by learning a sparse code for natural images. Nature *381*, 607–609.

Olshausen, B.A., and Field, D.J. (2004). Sparse coding of sensory inputs. Curr. Opin. Neurobiol. *14*, 481–487.

Olsson, R.H., Buhl, D.L., Sirota, A.M., Buzsaki, G., and Wise, K.D. (2005). Band-tunable and multiplexed integrated circuits for simultaneous recording and stimulation with microelectrode arrays. IEEE Trans. Biomed. Eng. *52*, 1303–1311.

Osborne, M.., Comis, S.., and Pickles, J.. (1988). Further observations on the fine structure of tip links between stereocilia of the guinea pig cochlea. Hear. Res. *35*, 99–108.

Osen, K.K. (1969). Cytoarchitecture of the cochlear nuclei in the cat. J. Comp. Neurol. *136*, 453–484.

Paxinos, G., and Watson, C. (1998). The Rat Brain in Stereotaxic Coordinates. (New York, NY: Academic Press).

Peters, C., and Steward, C.G. (2003). Hematopoietic cell transplantation for inherited metabolic diseases: an overview of outcomes and practice guidelines. Bone Marrow Transplant. *31*, 229–239.

Petersen, C.C.H. (2007). The functional organization of the barrel cortex. Neuron *56*, 339–355.

Petkov, C.I., Kayser, C., Augath, M., and Logothetis, N.K. (2006). Functional imaging reveals numerous fields in the monkey auditory cortex. PLoS Biol. *4*, 215.

Phillips, D.P., and Irvine, D.R. (1981). Responses of single neurons in physiologically defined primary auditory cortex (AI) of the cat: frequency tuning and responses to intensity. J. Neurophysiol. *45*, 48–58.

Piccolino, M. (1998). Animal electricity and the birth of electrophysiology: the legacy of Luigi Galvani. Brain Res. Bull. *46*, 381–407.

Piccolino, M. (2003). A "lost time" between science and literature: the "temps perdu" from Hermann von Helmholtz to Marcel Proust. Audiol. Med. *1*, 261–270.

Piña-Crespo, J.C., Talantova, M., Cho, E.-G., Soussou, W., Dolatabadi, N., Ryan, S.D., Ambasudhan, R., McKercher, S., Deisseroth, K., and Lipton, S.A. (2012). High-frequency hippocampal oscillations activated by optogenetic stimulation of transplanted human ESC-derived neurons. J. Neurosci. *32*, 15837–15842.

Polley, D.B., Read, H.L., Storace, D. a, and Merzenich, M.M. (2007). Multiparametric auditory receptive field organization across five cortical fields in the albino rat. J. Neurophysiol. *97*, 3621–3638.

Prieto, J.J., Peterson, B.A., and Winer, J.A. (1994). Morphology and spatial distribution of GABAergic neurons in cat primary auditory cortex (AI). J. Comp. Neurol. *344*, 349–382.

Prox, J., Bernreuther, C., Altmeppen, H., Grendel, J., Glatzel, M., D'Hooge, R., Stroobants, S., Ahmed, T., Balschun, D., Willem, M., et al. (2013). Postnatal disruption of the disintegrin/metalloproteinase ADAM10 in brain causes epileptic seizures, learning deficits, altered spine morphology, and defective synaptic functions. J. Neurosci. *33*, 12915–12928.

Quiroga, R.Q., Nadasdy, Z., and Ben-Shaul, Y. (2004). Unsupervised spike detection and sorting with wavelets and superparamagnetic clustering. Neural Comput. *16*, 1661–1687.

Quiroga, R.Q., Reddy, L., Kreiman, G., Koch, C., and Fried, I. (2005). Invariant visual representation by single neurons in the human brain. Nature *435*, 1102–1107.

Raczkowski, D., Irving T., D., and Winer, J. (1976). Organization of thalamocortical auditory system in the cat studied with horseradish peroxidase. Brain Res. *101*, 345–354.

Radnikow, G., Feldmeyer, D., and Lübke, J. (2002). Axonal projection, input and output synapses, and synaptic physiology of Cajal-Retzius cells in the developing rat neocortex. J. Neurosci. *22*, 6908–6919.

Rajan, R. (1998). Receptor organ damage causes loss of cortical surround inhibition without topographic map plasticity. Nat. Neurosci. *1*, 138–143.

Raman, Y., and Cajal, S. (1955). Histologie du Systeme Nerveux de l'Homme et des Vertebris, t. ii. Madrid: Instituto Ranl6n y Cajal.

Rasch, M., Logothetis, N.K., and Kreiman, G. (2009). From neurons to circuits: linear estimation of local field potentials. J. Neurosci. *29*, 13785–13796.

Rasch, M.J., Gretton, A., Murayama, Y., Maass, W., and Logothetis, N.K. (2008). Inferring spike trains from local field potentials. J. Neurophysiol. *99*, 1461–1476.

Rauschecker, J.P. (1998). Parallel processing in the auditory cortex of primates. Audiol. Neurootol. *3*, 86–103.

Raz, Y. (2004). Conductive Hearing Loss. In Advanced Therapy Of Otitis Media, (USA: BC Decker), pp. 419–424.

Reale, R.A., and Imig, T.J. (1980). Tonotopic organization in auditory cortex of the cat. J. Comp. Neurol. *192*, 265–291.

Reser, D.H., Fishman, Y.I., Arezzo, J.C., and Steinschneider, M. (2000). Binaural interactions in primary auditory cortex of the awake macaque. Cereb. Cortex *10*, 574–584.

Ress, D., and Chandrasekaran, B. (2013). Tonotopic organization in the depth of human inferior colliculus. Front. Hum. Neurosci. *7*, 586.

Retzius, G. (1881). Retzius G: Biologische Untersuchungen, *1,2.*.

Rietze, R.L., Valcanis, H., Brooker, G.F., Thomas, T., Voss, A.K., and Bartlett, P.F. (2001). Purification of a pluripotent neural stem cell from the adult mouse brain. Nature *412*, 736–739.

Roberts, L.E., Eggermont, J.J., Caspary, D.M., Shore, S.E., Melcher, J.R., and Kaltenbach, J.A. (2010). Ringing ears: the neuroscience of tinnitus. J. Neurosci. *30*, 14972–14979.

Rodrigues-Dagaeff, C., Simm, G., De Ribaupierre, Y., Villa, A., De Ribaupierre, F., and Rouiller, E.M. (1989). Functional organization of the ventral division of the medial geniculate body of the cat: Evidence for a rostro-caudal gradient of response properties and cortical projections. Hear. Res. *39*, 103–125.

Romanski, L.M., and LeDoux, J.E. Organization of rodent auditory cortex: anterograde transport of PHA-L from MGv to temporal neocortex. Cereb. Cortex *3*, 499–514.

Rose, J.E. (1949). The cellular structure of the auditory region of the cat. J. Comp. Neurol. *91*, 409–439.

Roth, B., and Bruns, V. (1992). Postnatal development of the rat organ of Corti. Anat. Embryol. (Berl). *185*, 571–581.

Rothschild, G., Nelken, I., and Mizrahi, A. (2010). Functional organization and population dynamics in the mouse primary auditory cortex. Nat. Neurosci. *13*, 353–360.

Rouiller, E.M., Capt, M., Dolivo, M., and De Ribaupierre, F. (1986). Tensor tympani reflex pathways studied with retrograde horseradish peroxidase and transneuronal viral tracing techniques. Neurosci. Lett. *72*, 247–252.

Rouiller, E.M., Simm, G.M., Villa, A.E., de Ribaupierre, Y., and de Ribaupierre, F. (1991). Auditory corticocortical interconnections in the cat: evidence for parallel and hierarchical arrangement of the auditory cortical areas. Exp. Brain Res. *86*, 483–505.

Rouiller.E.M (1997). Functional organisation of the auditory pathway. In The Central Auditory System, Gunter Ehret, and R. Romand, eds. (Oxford: Oxford University Press), pp. 3–16.

Russell, I.J. (1987). The physiology of the organ of Corti. Br. Med. Bull. *43*, 802–820.

Rutkowski, R.G., Miasnikov, A.A., and Weinberger, N.M. (2003). Characterisation of multiple physiological fields within the anatomical core of rat auditory cortex. Hear. Res. *181*, 116–130.

Ryugo, D.K. (1992). The auditory nerve: peripheral innervation, cell body morphology, and central projections. In The Mammalian Auditory Pathway: Neuroanatomy, A.N. Popper. and R.R. Fay. D. B. Webster, ed. (New York: Springer), pp. 23–65.

Ryugo, D.K., Dodds, L.W., Benson, T.E., and Kiang, N.Y. (1991). Unmyelinated axons of the auditory nerve in cats. J. Comp. Neurol. *308*, 209–223.

Saitoh, K., Inagaki, S., Nishimura, M., Kawaguchi, H., and Song, W.-J. (2010). Spontaneous activity resembling tone-evoked activity in the primary auditory cortex of guinea pigs. Neurosci. Res. *68*, 107–113.

Sakata, S., and Harris, K.D. (2009). Laminar structure of spontaneous and sensory-evoked population activity in auditory cortex. Neuron *64*, 404–418.

Sakata, S., and Harris, K.D. (2012). Laminar-dependent effects of cortical state on auditory cortical spontaneous activity. Front. Neural Circuits *6*, 109.

Saldaña, E., Aparicio, M.-A., Fuentes-Santamaría, V., and Berrebi, A.S. (2009). Connections of the superior paraolivary nucleus of the rat: projections to the inferior colliculus. Neuroscience *163*, 372–387.

Salganicoff, M., Sarna, M., Sax, L., and Gerstein, G.L. (1988). Unsupervised waveform classification for multi-neuron recordings: a real-time, software-based system. I. Algorithms and implementation. J. Neurosci. Methods *25*, 181–187.

Sally, S.L., and Kelly, J.B. (1988). Organization of auditory cortex in the albino rat: sound frequency. J. Neurophysiol. *59*, 1627–1638.

Salvi, R.., Saunders, S.., Gratton, M.., Arehole, S., and Powers, N. (1990). Enhanced evoked response amplitudes in the inferior colliculus of the chinchilla following acoustic trauma. Hear. Res. *50*, 245–257.

Salvi, R.J., Wang, J., and Ding, D. (2000). Auditory plasticity and hyperactivity following cochlear damage. Hear. Res. *147*, 261–274.

Saunders, J.C. (1985). The anatomical consequences of acoustic injury: A review and tutorial. J. Acoust. Soc. Am. *78*, 833.

Schacht, J. (1986). Molecular mechanisms of drug-induced hearing loss. Hear. Res. *22*, 297–304.

Schecklmann, M., Lehner, A., Poeppl, T.B., Kreuzer, P.M., Rupprecht, R., Rackl, J., Burger, J., Frank, E., Hajak, G., Langguth, B., et al. (2013). Auditory cortex is implicated in tinnitus distress: a voxel-based morphometry study. Brain Struct. Funct. *218*, 1061–1070.

Schmiedt, R.A., Zwislocki, J.J., and Hamernik, R.P. (1980). Effects of hair cell lesions on responses of cochlear nerve fibers. I. Lesions, tuning curves, two-tone inhibition, and responses to trapezoidal-wave patterns. J Neurophysiol *43*, 1367–1389.

Schofield, B.R. (2001). Origins of projections from the inferior colliculus to the cochlear nucleus in guinea pigs. J. Comp. Neurol. *429*, 206–220.

Schofield, B.R., and Cant, N.B. (1999). Descending auditory pathways: projections from the inferior colliculus contact superior olivary cells that project bilaterally to the cochlear nuclei. J. Comp. Neurol. *409*, 210–223.

Scholl, B., and Wehr, M. (2008). Disruption of balanced cortical excitation and inhibition by acoustic trauma. J. Neurophysiol. *100*, 646–656.

Schwartz, I.R. (1992). The Superior Olivary Complex. In In Springer Handbook of Auditory Research, Vol. 1, The Mammalian Auditory Pathway: Neuroanatomy, D. B. Webster, A.N. Popper, and R. R. Fay, eds. (New York: Springer), pp. 117–167.

Seki, S., and Eggermont, J.J. (2002). Changes in cat primary auditory cortex after minor-to-moderate pure-tone induced hearing loss. Hear. Res. *173*, 172–186.

Seki, S., and Eggermont, J.J. (2003). Changes in spontaneous firing rate and neural synchrony in cat primary auditory cortex after localized tone-induced hearing loss. Hear. Res. *180*, 28–38.

Sharma, A. V, Wolansky, T., and Dickson, C.T. (2010). A comparison of sleeplike slow oscillations in the hippocampus under ketamine and urethane anesthesia. J. Neurophysiol. *104*, 932–939.

Shatz, C.J., and Stryker, M.P. (1978). Ocular dominance in layer IV of the cat's visual cortex and the effects of monocular deprivation. J. Physiol. *281*, 267–283.

Shaw, M.D., and Baker, R. (1983). The locations of stapedius and tensor tympani motoneurons in the cat. J. Comp. Neurol. *216*, 10–19.

Shen, J.X., Xu, Z.M., and Yao, Y.D. (1999). Evidence for columnar organization in the auditory cortex of the mouse. Hear. Res. *137*, 174–177.

Shepherd, R.K., Hartmann, R., Heid, S., Hardie, N., and Klinke, R. (2009). The Central Auditory System and Auditory Deprivation: Experience with Cochlear Implants in the Congenitally Deaf. Acta Otolaryngol. *532*, 28–38.

Skoe, E., and Kraus, N. (2010). Auditory brain stem response to complex sounds: a tutorial. Ear Hear. *31*, 302–324.

Sliwinska-Kowalska, M., and Davis, A. (2012). Noise-induced hearing loss. Noise Health *14*, 274–280.

Smith, P.H., and Populin, L.C. (2001). Fundamental differences between the thalamocortical recipient layers of the cat auditory and visual cortices. J. Comp. Neurol. *436*, 508–519.

Sousa-Pinto, A. (1973). The structure of the first auditory cortex (A I) in the cat. I.--Light microscopic observations on its organization. Arch. Ital. Biol. *111*, 112–137.

Spoendlin, H. (1969). Innervation patterns in the organ of corti of the cat. Acta Otolaryngol. *67*, 239–254.

Spoendlin, H. (1972). Innervation densities of the cochlea. Acta Otolaryngol. *73*, 235–248.

Stapells, D.R. (2011). Frequency-specific threshold assessment in young infants using the transient ABR and the brainstem ASSR. Compr. Handb. Pediatr. Audiol. 409–448.

Steriade, M., Nuñez, A., and Amzica, F. (1993). A novel slow (< 1 Hz) oscillation of neocortical neurons in vivo: depolarizing and hyperpolarizing components. J. Neurosci. *13*, 3252–3265.

Stern, E.A., Maravall, M., and Svoboda, K. (2001). Rapid development and plasticity of layer 2/3 maps in rat barrel cortex in vivo. Neuron *31*, 305–315.

Stiebler, I., Neulist, R., Fichtel, I., and Ehret, G. (1997). The auditory cortex of the house mouse: left-right differences, tonotopic organization and quantitative analysis of frequency representation. J. Comp. Physiol. A. *181*, 559–571.

Stillings, D. (1975). Did Jan Swammerdam beat Galvani by 134 years? Med. Instrum. *9*, 226.

Stolzberg, D., Chrostowski, M., Salvi, R.J., and Allman, B.L. (2012). Intracortical circuits amplify sound-evoked activity in primary auditory cortex following systemic injection of salicylate in the rat. J. Neurophysiol. *108*, 200–214.

Strominger, N.L., Nelson, L.R., and Dougherty, W.J. (1977). Second order auditory pathways in the chimpanzee. Strominger. J. Comp. Neurol. *172*, 349–365.

Stuber, G.D., Sparta, D.R., Stamatakis, A.M., Leeuwen, W.A. Van, Hardjoprajitno, J.E., Cho, S., Tye, K.M., Kempadoo, K.A., Zhang, F., Deisseroth, K., et al. (2011). Excitatory transmission from the amygdala to nucleus accumbens facilitates reward seeking. Nature *475*, 377–380.

Sugimoto, S., Sakurada, M., Horikawa, J., and Taniguchi, I. (1997). The columnar and layer-specific response properties of neurons in the primary auditory cortex of Mongolian gerbils. Hear. Res. *112*, 175–185.

Sun, W., Deng, A., Jayaram, A., and Gibson, B. (2012). Noise exposure enhances auditory cortex responses related to hyperacusis behavior. Brain Res. *1485*, 108–116.

Sutter, M.L., and Schreiner, C.E. (1991). Physiology and topography of neurons with multipeaked tuning curves in cat primary auditory cortex. J Neurophysiol *65*, 1207–1226.

Sutter, M.L., and Schreiner, C.E. (1995). Topography of intensity tuning in cat primary auditory cortex: single-neuron versus multiple-neuron recordings. J Neurophysiol *73*, 190–204.

Sutter, M.L., Morrison, J.A., Farzan, F., Fremouw, T., Sayegh, R., Covey, E., Paul, A., Nourski, K. V, Steinschneider, M., Oya, H., et al. (2014). Shapes and Level Tolerances of Frequency Tuning Curves in Primary Auditory Cortex : Quantitative Measures and Population Codes Shapes and Level Tolerances of Frequency Tuning Curves in Primary Auditory Cortex : Quantitative Measures and Population Codes. J Neurophysiol *84,* 1012–1025.

Syka, J. (2002). Plastic Changes in the Central Auditory System After Hearing Loss, Restoration of Function, and During Learning. Physiol Rev *82*, 601–636.

Syka, J., and Rybalko, N. (2000). Threshold shifts and enhancement of cortical evoked responses after noise exposure in rats. Hear. Res. *139*, 59–68.

Syka, J., Popelář, J., Kvašňák, E., and Astl, J. (2000). Response properties of neurons in the central nucleus and external and dorsal cortices of the inferior colliculus in guinea pig. Exp. Brain Res. *133*, 254–266.

Takekawa, T., Isomura, Y., and Fukai, T. (2010). Accurate spike sorting for multi-unit recordings. Eur. J. Neurosci. *31*, 263–272.

Takekawa, T., Isomura, Y., and Fukai, T. (2012). Spike sorting of heterogeneous neuron types by multimodality-weighted PCA and explicit robust variational Bayes. Front. Neuroinform. *6*, 5.

Tanji, K., Leopold, D.A., Ye, F.Q., Zhu, C., Malloy, M., Saunders, R.C., and Mishkin, M. (2010). Effect of sound intensity on tonotopic fMRI maps in the unanesthetized monkey. Neuroimage *49*, 150–157.

Thach, W.T. (1986). Edward Vaughan Evarts (1926–1985). Trends Neurosci. *9*, 397–400.

Timofeev, I., Grenier, F., Bazhenov, M., Sejnowski, T.J., and Steriade, M. (2000). Origin of slow cortical oscillations in deafferented cortical slabs. Cereb. Cortex *10*, 1185–1199.

Tolhurst, D.J., Smyth, D., and Thompson, I.D. (2009). The sparseness of neuronal responses in ferret primary visual cortex. J. Neurosci. *29*, 2355–2370.

Toma, J.G., Akhavan, M., Fernandes, K.J., Barnabé-Heider, F., Sadikot, A., Kaplan, D.R., and Miller, F.D. (2001). Isolation of multipotent adult stem cells from the dermis of mammalian skin. Nat. Cell Biol. *3*, 778–784.

Torben Brask (1978). The Noise Protection Effect of the Stapedius Reflex. Acta Otolaryngol. *86*, 116–117.

Tritsch, N.X., Yi, E., Gale, J.E., Glowatzki, E., and Bergles, D.E. (2007). The origin of spontaneous activity in the developing auditory system. Nature *450*, 50–55.

Tritsch, N.X., Rodríguez-Contreras, A., Crins, T.T.H., Wang, H.C., Borst, J.G.G., and Bergles, D.E. (2010). Calcium action potentials in hair cells pattern auditory neuron activity before hearing onset. Nat. Neurosci. *13*, 1050–1052.

Tschopp, K., Schillinger, C., Schmid, N., Rausch, M., Bilecen, D., and Scheffler, K. (2000). [Detection of central auditory compensation in unilateral deafness with functional magnetic resonance tomography]. Laryngorhinootologie. *79*, 753–757.

Tsuchitani, C. (1967). Encoding of Stimulus Frequency and Intensity by Cat Superior Olive S-Segment Cells. J. Acoust. Soc. Am. *42*, 794.

Tsuchitani, C., and Boudreau, J.C. (1966). Single unit analysis of cat superior olive S segment with tonal stimuli. J. Neurophysiol. *29*, 684–697.

Turner, J.G. (2007). Behavioral measures of tinnitus in laboratory animals. Prog. Brain Res. *166*, 147–156.

Turner, J.G., Brozoski, T.J., Bauer, C. a, Parrish, J.L., Myers, K., Hughes, L.F., and Caspary, D.M. (2006). Gap detection deficits in rats with tinnitus: a potential novel screening tool. Behav. Neurosci. *120*, 188–195.

Verkhratsky, A., Krishtal, O.A., and Petersen, O.H. (2006). From Galvani to patch clamp: the development of electrophysiology. Pflugers Arch. *453*, 233–247.

Vinje, W.E. (2000). Sparse Coding and Decorrelation in Primary Visual Cortex During Natural Vision. Science. *287*, 1273–1276.

Wallace, M.N., and Palmer, A.R. (2008). Laminar differences in the response properties of cells in the primary auditory cortex. Exp. Brain Res. *184*, 179–191.

Wallhausser-Franke, E., Mahlke, C., Oliva, R., Braun, S., Wenz, G., and Langner, G. (2003). Expression of c-fos in auditory and non-auditory brain regions of the gerbil after manipulations that induce tinnitus. Exp. Brain Res. *153*, 649–654.

Wang, H., Brozoski, T.J., and Caspary, D.M. (2011). Inhibitory neurotransmission in animal models of tinnitus: maladaptive plasticity. Hear. Res. *279*, 111–117.

Wang, J., Caspary, D., and Salvi, R.J. (2000). GABA-A antagonist causes dramatic expansion of tuning in primary auditory cortex. Neuroreport *11*, 1137–1140.

Warr, W. (1992). Organization of olivocochlear efferent systems in mammals. In The Mammalian Auditory Pathway, Neuroanatomy. Volume 2, Springer Handbook of Auditory Research, D. Webster, A. Popper, and R. Fay, eds. (Berlin: Springer), pp. 410–448.

Warr, W.B. (1975). Olivocochlear and vestibular efferent neurons of the feline brain stem: their location, morphology and number determined by retrograde axonal transport and acetylcholinesterase histochemistry. J. Comp. Neurol. *161*, 159–181.

Weick, J.P., Liu, Y., and Zhang, S.-C. (2011). Human embryonic stem cell-derived neurons adopt and regulate the activity of an established neural network. Proc. Natl. Acad. Sci. U. S. A. *108*, 20189–20194.

Weisz, N., Wienbruch, C., Dohrmann, K., and Elbert, T. (2005). Neuromagnetic indicators of auditory cortical reorganization of tinnitus. Brain *128*, 2722–2731.

Wenstrup JJ (2005). The Tectothalamic System. In The Inferior Colliculus, J.A. Winer, and C. Schreiner, eds. (New York: Springer), pp. 200–230.

Wessinger, C.M., Buonocore, M.H., Kussmaul, C.L., and Mangun, G.R. (1997). Tonotopy in human auditory cortex examined with functional magnetic resonance imaging. Hum. Brain Mapp. *5*, 18–25.

White, J.S., and Warr, W.B. (1983). The dual origins of the olivocochlear bundle in the albino rat. J. Comp. Neurol. *219*, 203–112.

WHO (2012). WHO | Estimates (World Health Organization).

Wienbruch, C., Paul, I., Weisz, N., Elbert, T., and Roberts, L.E. (2006). Frequency organization of the 40-Hz auditory steady-state response in normal hearing and in tinnitus. Neuroimage *33*, 180–194.

Willmore, B., and Tolhurst, D.J. (2001). Characterizing the sparseness of neural codes. Network *12*, 255–270.

Willmore, B.D.B., Mazer, J.A., and Gallant, J.L. (2011). Sparse coding in striate and extrastriate visual cortex. J. Neurophysiol. *105*, 2907–2919.

Willott, J.F., and Lu, S.M. (1982). Noise-induced hearing loss can alter neural coding and increase excitability in the central nervous system. Science *216*, 1331–1334.

Willott, J.F., Aitkin, L.M., and McFadden, S.L. (1993). Plasticity of auditory cortex associated with sensorineural hearing loss in adult C57BL/6J mice. J. Comp. Neurol. *329*, 402–411.

Winer, J. a (2005a). Decoding the auditory corticofugal systems. Hear. Res. *207*, 1–9.

Winer, J. a (2011). A Profile of Auditory Forebrain Connections and Circuits. In The Auditory Cortex, J.A. Winer, and C.E. Schreiner, eds. (New York: Springer), pp. 56–74.

Winer, J.A. (1984a). The pyramidal neurons in layer III of cat primary auditory cortex (AI). J. Comp. Neurol. *229*, 476–496.

Winer, J.A. (1984b). The non-pyramidal cells in layer III of cat primary auditory cortex (AI). J. Comp. Neurol. *229*, 512–530.

Winer, J.A. (1984c). Anatomy of layer IV in cat primary auditory cortex (AI). J. Comp. Neurol. *224*, 535–567.

Winer, J.A. (1985). Structure of layer II in cat primary auditory cortex (AI). J. Comp. Neurol. *238*, 10–37.

Winer, J.A. (1992). The functional architecture of the medial geniculate body and the primary auditory cortex. In The Mammalian Auditory Pathway: Neuroanatomy, A.N. Popper D. B. Webster, and R.R. Fay, eds. (New York: Springer- Verlag), pp. 222–409.

Winer, J.A. (2005b). The central auditory system: a functional analysis. In The Inferior Colliculus, J. A. Winer and C. E. Schreiner, eds. (New York: Springer- Verlag).

Winer, J.A. (2005c). Three Systems of Descending Projections to the Inferior Colliculus. In The Inferior Colliculus, J.A. Winer, and C.E. Schreiner, eds. (New York: Springer), pp. 231–247.

Winer, J. a, and Lee, C.C. (2007). The distributed auditory cortex. Hear. Res. *229*, 3–13.

Winer, J. a, Miller, L.M., Lee, C.C., and Schreiner, C.E. (2005). Auditory thalamocortical transformation: structure and function. Trends Neurosci. *28*, 255–263.

Winer, J.A., Larue, D.T., Diehl, J.J., and Hefti, B.J. (1998). Auditory cortical projections to the cat inferior colliculus. J. Comp. Neurol. *400*, 147–174.

Winer, J.A., Diehl, J.J., and Larue, D.T. (2001). Projections of auditory cortex to the medial geniculate body of the cat. J. Comp. Neurol. *430*, 27–55.

Winkowski, D.E., and Kanold, P.O. (2013). Laminar transformation of frequency organization in auditory cortex. J. Neurosci. *33*, 1498–1508.

Wise, K., and Najafi, K. (1991). Microfabrication techniques for integrated sensors and microsystems. Science (80-.). *254*, 1335–1342.

Wood, F., Black, M.J., Vargas-Irwin, C., Fellows, M., and Donoghue, J.P. (2004). On the variability of manual spike sorting. IEEE Trans. Biomed. Eng. *51*, 912–918.

Yankaskas, K. (2013). Prelude: noise-induced tinnitus and hearing loss in the military. Hear. Res. *295*, 3–8.

Young, E.D., Spirou, G.A., Rice, J.J., and Voigt, H.F. (1992). Neural organization and responses to complex stimuli in the dorsal cochlear nucleus. Philos. Trans. R. Soc. Lond. B. Biol. Sci. *336*, 407–413.

Zatorre, R.J. (2001). Spectral and Temporal Processing in Human Auditory Cortex. Cereb. Cortex *11*, 946–953.

Zdebik, A.A., Wangemann, P., and Jentsch, T.J. (2009). Potassium ion movement in the inner ear: insights from genetic disease and mouse models. Physiology (Bethesda). *24*, 307–316.

Zhang, J.S., and Kaltenbach, J.A. (1998). Increases in spontaneous activity in the dorsal cochlear nucleus of the rat following exposure to high-intensity sound. Neurosci. Lett. *250*, 197–200.

Zhang, X., Yang, P., Cao, Y., Qin, L., and Sato, Y. (2011). Salicylate induced neural changes in the primary auditory cortex of awake cats. Neuroscience *172*, 232–245.